ALUMINA SUPPORTED MANGANESE-BASED CATALYSTS FOR CATALYTIC OZONATION OF ACETONE AND TOLUENE IN AIR

A Thesis Submitted to the
College of Graduate and Postdoctoral Studies
In Partial Fulfillment of the Requirements
For the Degree of Doctor of Philosophy
In the Department of Chemical & Biological Engineering
University of Saskatchewan
Saskatoon

By

MEHRANEH GHAVAMI

Permission to Use

In presenting this thesis in partial fulfillment of the requirements for a Postgraduate degree from the University of Saskatchewan, I agree that the Libraries of this University may make it freely available for inspection. I further agree that permission for copying of this thesis in any manner, in whole or in part, for scholarly purposes may be granted by the professor or professors who supervised my thesis work or, in their absence, by the Head of the Department or the Dean of the College in which my thesis work was done. It is understood that any copying or publication or use of this thesis or parts thereof for financial gain shall not be allowed without my written permission. It is also understood that due recognition shall be given to me and to the University of Saskatchewan in any scholarly use which may be made of any material in my thesis.

Disclaimer

Reference in this thesis to any specific commercial products, process, or service by trade name, trademark, manufacturer, or otherwise, does not constitute or imply its endorsement, recommendation, or favouring by the University of Saskatchewan. The views and opinions of the author expressed herein do not state or reflect those of the University of Saskatchewan, and shall not be used for advertising or product endorsement purposes.

Requests for permission to copy or to make other uses of materials in this thesis in whole or part should be addressed to:

Head of the Department of Chemical and Biological Engineering
57 Campus Drive
University of Saskatchewan
Saskatoon, Saskatchewan S7N 5A9
Canada

OR

Dean
College of Graduate and Postdoctoral Studies
University of Saskatchewan
116 Thorvaldson Building, 110 Science Place
Saskatoon, Saskatchewan S7N 5C9
Canada

Abstract

Volatile organic compounds (VOCs) are hazardous substances produced from anthropogenic emissions and are among the main sources of air pollution. Catalytic ozonation is an efficient process for VOCs removal from indoor air at room temperature. In this Ph.D. thesis, alumina supported Mn oxides which are considered as one of the most active catalysts for ozonation of VOCs are used to oxidize acetone and toluene in air at room temperature. The primary aim of this research is to develop the catalyst for catalytic ozonation of VOCs at room temperature. Therefore, the influence of addition of second metal oxide, catalyst preparation procedure, and calcination temperature on catalytic properties and activity in ozonation of VOCs were investigated. In addition, kinetics and mechanism of the catalytic ozonation reaction were studied to clarify the role of metal oxide and support in the reaction pathway.

It was found that addition of manganese and cobalt at lower loading levels (2.5% or 5%) to single metal oxide catalysts improved the catalytic activity significantly. By changing the loading of the secondary metals, its oxidation state changed. It is suggested that lower oxidation state of the secondary metal improves ozone decomposition and oxidation of acetone.

Polyol process can produce catalysts with smaller manganese cluster size, higher surface area, and lower oxidation states than impregnation method which led to enhancing the VOC conversion. An increase in the calcination temperature increased the manganese particle size while reducing the surface area and dispersion of the catalyst. The results indicated that the oxidation state of manganese shifted to lower values by increasing the calcination temperature. An increase in the calcination temperature to 800 ºC, increased acetone oxidation, while no significant change was observed in toluene oxidation. In the binary mixture of acetone and toluene, the oxidation behaviors were different from the single component system. The toluene conversion was promoted whereas the acetone conversion was inhibited.

Kinetic modeling was conducted on catalytic ozonation of acetone using the catalysts that exhibited the best catalytic activity. The kinetic experimental data were expressed well by Langmuir-Hinshelwood dual-site (LHd) mechanism, indicating that both MnO_x and Al_2O_3 sites are essential and involved in the reaction. The cooperation of these sites on the surface of the catalysts provides the adjacent attack and migration of intermediates and enables the dual-site mechanism.

Acknowledgements

I would like to express my great appreciation to my supervisor, Dr. Jafar Soltan, for his encouragement, guidance, and support throughout my Ph.D. studies. He made my Ph.D. journey very productive, instructive, and enthusiastic even during the toughest times.

I would like to appreciate and acknowledge my advisory committee members: Dr. Ning Chen, Dr. Catherine Niu, Dr. Hui Wang, and Dr. Lifeng Zhang for their valuable comments and constructive suggestions, which greatly helped to improve the quality of this research work.

I also appreciate the help and collaborations of my group members during my Ph.D. studies who provided me great memories, support, and valuable assistance. I especially would like to thank Dr. Mostafa Aghbolaghy for the exchange of knowledge and skills during the first year of my Ph.D. program. I thank the assistance of the technical staff in the Department of Chemical and Biological Engineering, who helped me with the maintenance of the analysis instruments.

I acknowledge the College of Graduate and Postdoctoral Studies, and the Department of Chemical and Biological Engineering of the University of Saskatchewan, the Natural Sciences and Engineering Research Council of Canada, and the Government of Saskatchewan for providing financial support for this research.

Many thanks go to my lovely friends who supported me with love and encouragement during the adversity period of my life and made my time a lot more fun. I appreciate their support during the toughest time of my program.

Last but not least, I would like to deeply thank the most special people in my life; my lovely parents, sisters, and brother-in-laws for all their love, support, and encouragement. And most of all, my greatest appreciation is for my best friend, the love of my life, and my husband, Kourosh who has believed in me, supported me and encouraged me a lot to achieve my goals.

Table of Contents

List of Tables

List of Figures

List of Abbreviations

ANOVA	analysis of variance
ASHRAE	American society of heating, refrigerating, and air-conditioning Engineers
BET	Brunauer–Emmett–Teller
BN	boron nitride
CLS	Canadian light source
CN	coordination number
C.V.	Coefficient of Variation
DF	degrees of freedom
DLaTGS	deuterated l-alanine doped triglycine sulfate
DRIFTS	diffuse reflectance infrared Fourier transform spectroscopy
EDX	energy dispersive X-ray
EG	ethylene glycol
EPA	environmental protection agency
EXAFS	extended X-ray absorption fine-structure
FEG	field emission gun
FTIR	Fourier transform infrared
GC	gas chromatograph
HAADF	high-angle annular dark-field
H_2-TPR	Hydrogen temperature-programmed reduction
HXMA	hard X-ray microanalysis
ICP-MS	inductively coupled plasma mass spectrometry
LHd	Langmuir-Hinshelwood dual-site
LHs	Langmuir-Hinshelwood single-site
LCF	linear combination fitting
MCT	mercuric cadmium telluride
MS	mass spectrometer
PL	power law
PMs	particulate matters
POMs	particulate organic matters

PVC	Production of polyvinyl chloride
PVP	polyvinylpyrrolidone
RSM	response surface methodology
Std. Dev.	Standard deviation
SSQ	Sum of squared differences
STEM	scanning transmission electron microscope
SVOCs	semi-volatile organic compounds
TEM	transmission Electron Microscopy
TGA	Thermogravimetric analysis
TPD	temperature programmed desorption
TPO	temperature programmed oxidation
UV	ultraviolet
VOC	volatile organic compound
VVOC	very volatile organic compound
WHO	world health organization
WHSV	weight hour space velocity (L h^{-1} g^{-1})
XAFS	X-ray absorption fine structure
XANES	X-ray absorption near-edge structure
XPS	X-ray photoelectron spectroscopy
XRD	X-ray Diffraction

List of Nomenclature and Symbols

A	pre-exponential factor
a	Mn atom surface area
C	concentration
D	dispersion
d	mean metal particle size
E_a	apparent activation energy
ΔE_o	change in energy scale in EXAFS analyses (eV)
Fc	F value in Fisher's F-test
ΔH_{ads}	adsorption enthalpy change
k	reaction rate constant
K	adsorption equilibrium constant
M	molar mass of Mn
N	Avogadro number
r	reaction rate
R	universal gas constant
R	bond distance of the neighboring atoms
R_f	absolute percentage misfit between theory and data
R^2	coefficient of determination
ΔS_{ads}	adsorption entropy change
S_g^0	gas phase entropy
T	reaction temperature
W	catalyst weight
X	conversion

Greek letters/prefixes

α	reaction order of acetone
β	reaction order of ozone
v	total gas flow rate
σ^2	Debye–Waller factor
ρ	density of Mn
ρ^2	multiple correlation coefficients

Chapter 1:

Introduction and Thesis Outline

In this chapter, research background and motivation of this research work will be discussed. The organization of the thesis and the manuscript content are listed at the end of this chapter.

1.1. Research background and motivation

Air pollution has serious impacts on human and environmental health and is considered a global concern [1]. The World Health Organization (WHO) evaluated that air pollution was responsible for nearly seven million deaths which are one in eight of all deaths in the world [2,3]. Air pollution consists of a mixture of complex components such as particulate matters (PMs), ozone (O_3), nitrogen dioxide (NO_2), volatile organic compounds (VOCs), and sulfur dioxide (SO_2) in outdoor and indoor environments [4]. Studies estimated that people spend around 90% of their time indoors, therefore they are exposed to indoor air pollutants more than those outdoors [5]. The high exposure demonstrates the extent of the human health risk posed by indoor air pollutants [6].

VOCs are organic compounds with a high vapor pressure that include a large number of chemicals such as simple aliphatic hydrocarbon, chlorinated hydrocarbons, alcohols, aldehydes, ketones, etc. [7]. VOCs in indoor environments are emitted from human activities and a wide variety of materials such as cleaning agents, floorings, paints, surface coatings, and furniture [8]. Environmental Protection Agency (EPA) of US indicated that in general levels of VOCs in indoor air are up to ten times higher than outdoors, regardless of the building location [1,9]. The presence of VOCs in air is associated with acute and chronic health issues, such as eye, sensory and skin irritation, headaches, asthma, and cancer [10].

There are different techniques available based on physical, chemical and biological treatments to remove VOCs from the polluted air [11]. Common technologies for the VOCs elimination are

adsorption, biological treatment, plasma, photocatalysis, and so on [12]. Catalytic oxidation has been widely studied and applied for VOC degradation due to its high removal efficiency, applicability at high and low concentration, production of less secondary pollutants, and wide adaptability to VOC types. Despite the high efficiency of the catalytic oxidation process, there are some concerns in this technique including high reaction temperature and high energy consumption [12–14].

Catalytic oxidation in the presence of ozone or catalytic ozonation reduces the apparent activation energy and enhances conversion at low temperatures significantly compared to catalytic oxidation process. High efficiency of VOC catalytic degradation is strongly linked with highly effective catalysts [14]. Two categories of catalysts are promising in catalytic ozonation of VOCs: supported noble metals and transition metal oxides [15]. Noble metals such as Au, Pt, Pd, and Ru display superior catalytic activities, whereas, these catalysts have limited sources and problems of high cost, difficulty in regeneration, and inclining to sinter that limit their applications in the industry [14,16,17]. On the other hand, transition metal oxides of Mn, Co, Cu, Ni, Cr, V, and Fe have reasonable prices, variable valence states, along with high catalytic activity which make them good alternatives to be widely used in oxidation process [18].

Among the transition metal oxides, MnO_x demonstrate highest catalytic activity in catalytic oxidation of VOCs [18–20]. Superior activity of manganese-based catalysts is attributed to their ability in ozone decomposition, forming oxides with different oxidation states, and their high oxygen storage capacity [21–24]. Catalytic properties and activity of MnO_x for catalytic ozonation have been investigated over various VOCs [14,21,24–26]. It has been demonstrated that Mn-based catalysts in the catalytic ozonation process can efficiently oxidize various VOCs at relatively low temperatures. Supported MnO_x present higher catalytic activity than unsupported ones and are commonly used in catalytic ozonation process [27,28]. In addition to the metal oxide, different types of support significantly impact the final performance of the catalyst. Several studies have been performed over manganese-based catalysts with various supports such as Al_2O_3, SiO_2, TiO_2, ZrO_2, CeO_2 in catalytic ozonation of VOCs. It was found that MnO_x supported on Al_2O_3 exhibited better performance than other types of supports. It was found that MnO_x supported on Al_2O_3 exhibited better performance than other types of supports. High activity of MnO_x/Al_2O_3 was attributed to its excellent textual properties, high proportion of

surface adsorbed oxygen species, and high redox ability [14,29]. Moreover, it has been reported that lower oxidation state of Mn corresponded to the higher catalytic activity that can be obtained using alumina as a support for Mn [21].

Even though catalytic ozonation is recognized as a promising technique for VOC oxidation, some serious challenges are still in this process for its practical application. Catalyst deactivation at low temperatures due to the accumulation of intermediates and generation of CO as a byproduct of this reaction are the main concerns in this technique [30,31]. Therefore, catalyst development in catalytic ozonation process is essential to enhance catalyst activity and stability, especially at room temperature. In this thesis, some approaches have been employed to promote the catalytic activity of MnO_x/Al_2O_3 in room temperature ozonation of VOCs including addition of another active metal oxides, variation of metal loading, different preparation procedure, and effect of calcination temperature.

1.2. Organization of the thesis

This thesis consists of seven chapters. The thesis organization is listed as follows:

Chapter 1 presents a brief introduction of the research project including research background, motivation, and thesis organization.

Chapter 2 provides an extensive literature review on indoor air quality, VOCs in indoor air, recent technologies for VOC removal, and catalytic ozonation of VOCs. Moreover, knowledge gaps and objectives are discussed in this chapter.

Chapters 3 to 6 each present research papers that each address one of the objectives. Chapter 3 investigates the influence of augmenting the single Mn and Co catalysts on the performance and structure of the catalyst. In this part, Al_2O_3 supported manganese and cobalt single and mixed oxides catalysts were prepared for ozonation of acetone at room temperature.

Chapter 4 presents the synthesis and characterization of MnO_x/Al_2O_3 for catalytic ozonation of toluene. The catalysts were synthesized via polyol method, while the polyol synthesis temperature and time were optimized using response surface methodology. Results of catalyst

characterization and catalytic ozonation of toluene over MnO_x/Al_2O_3 prepared by polyol and conventional impregnation methods are also discussed.

Chapter 5 presents the impacts of preparation procedure and calcination temperature of MnO_x/Al_2O_3 catalysts in catalytic degradation of VOCs at room temperature. This research was conducted to enhance the catalytic performance by tuning characteristic properties through the synthesis technique and calcination temperature. Results of catalytic ozonation of single and mixture of toluene and acetone at room temperature are also presented and discussed.

Chapter 6 focuses on the kinetic and reaction mechanism study for the catalytic ozonation of acetone using the best catalysts obtained in the third objective in chapter 5. This chapter investigates the most suitable kinetic model for catalytic ozonation of acetone over MnO_x/Al_2O_3 catalyst. The roles of the catalyst support and metal in the reaction pathway were assessed using the Langmuir-Hinshelwood dual-site (LHd) mechanism.

Finally, conclusions and suggestions for future work are summarized in Chapter 7.

Research presented in this thesis has resulted in the following publications and conference presentations:

Journal papers:

- M. Ghavami, M. Aghbolaghy, J. Soltan, N. Chen, Room temperature oxidation of acetone by ozone over alumina-supported manganese and cobalt mixed oxides, Frontiers of Chemical Science and Engineering (2020), 14(6): 937–947. https://doi.org/10.1007/s11705-019-1900-6.
- M. Ghavami, J. Soltan, N. Chen, Synthesis of MnO_x/Al_2O_3 catalyst by polyol method and its application in room temperature ozonation of toluene in air, Catalysis Letters (2021) 151:1418–1432. https://doi.org/10.1007/s10562-020-03393-8.
- M. Ghavami, J. Soltan, N. Chen, Enhancing catalytic ozonation of acetone and toluene in air using MnO_x/Al_2O_3 catalysts at room temperature, Industrial & Engineering Chemistry Research (2021). https://doi.org/10.1021/acs.iecr.1c02288.
- M. Ghavami, J. Soltan, Kinetics and mechanism of catalytic ozonation of acetone in air over MnO_x/Al_2O_3 catalyst, Reaction Kinetics, Mechanisms and Catalysis (2021). https://doi.org/10.1007/s11144-021-02024-6.

Conference presentation:

- M. Ghavami, M. Aghbolaghy, J. Soltan and N. Chen, Catalytic oxidation of acetone by ozone over alumina supported cobalt-manganese catalysts. 67th Canadian Chemical Engineering Conference, October 22-25, 2017, Edmonton, Canada.
- M. Ghavami, M. Aghbolaghy, J. Soltan and N. Chen, Low Temperature Acetone Oxidation using Ozone over Supported Manganese-Cobalt Bimetallic Catalysts. 25th Canadian Symposium on Catalysis, May 8-11, 2018, Saskatoon, Canada.
- M. Ghavami, M. Aghbolaghy, J. Soltan and N. Chen, Low Temperature Acetone Oxidation using Ozone over Supported Manganese-Cobalt Bimetallic Catalysts. 68th Canadian Chemical Engineering Conference, October 28-31, 2018, Toronto, Canada.
- M. Ghavami and J. Soltan, Comparison between polyol and impregnation method in preparation of alumina supported Mn oxides for oxidation of volatile organic compounds

by ozone. 68th Canadian Chemical Engineering Conference, October 28-31, 2018, Toronto, Canada.

- M. Ghavami and J. Soltan, Manganese oxide catalysts for ozonation of acetone and toluene: Effect of preparation method and calcination temperature. 69th Canadian Chemical Engineering Conference, October 20-23, 2019, Halifax, Canada.
- M. Ghavami and J. Soltan, Insights into the effect of calcination temperature on catalytic properties and activity in catalytic ozonation of VOCs over $MnO_x/\gamma\text{-}Al_2O_3$. Prairie Environmental Chemistry Colloquium, June 2-3, 2020, University of Saskatchewan, Saskatoon, Canada.
- M. Ghavami, J. Soltan and N. Chen, The effect of calcination temperature on catalytic ozonation of VOCs over MnO_x/Al_2O_3. AUM & CLS 2.0 Event, October 7-8, 2020, Canadian Light Source, Saskatoon, Canada.

Chapter 2:

Literature Review

In this chapter, different types of VOCs and current technologies for VOCs elimination are discussed. Afterward, a comprehensive literature review of previous findings in catalyst ozonation of different VOCs, various types of catalysts, and their properties is provided.

2.1. Volatile organic compounds

Volatile organics are a large group of carbon-based compounds which evaporate easily at room temperature. WHO has categorized VOC into very volatile organic compounds (VVOCs), volatile organic compounds (VOCs), semi-volatile organic compounds (SVOCs), and particulate organic matters (POMs) groups. According to these categories, VVOCs, VOCs, SVOCs, and POMs are compounds with boiling points of between 0 ºC and 50-100 ºC, 50-100 ºC and 240-260 ºC, 240-260 ºC and 360-400 ºC and higher than 380 ºC, respectively [32,33].

VOCs can be found in indoor and outdoor environments; however, concentrations of most VOCs are significantly higher indoors than outdoors [34]. In indoor air, VOCs are emitted from household and consumer products, furnishing, and building materials, office equipment, air fresheners, paints, and solvents. Moreover, human activities such as cooking, cleaning, and smoking produce high levels of various VOCs. Other than indoor sources, VOCs infiltrate from attached garages, outdoor traffic, biogenic and industrial emissions contributing to the level of VOC in indoor air [32,35]. In a study, the indoor and outdoor concentrations of 193 VOCs were measured in Edmonton residences in 2010. Indoor levels of VOCs were considerably higher than outdoor levels during winter and summer. Figure 2.1 shows the average concentrations of detected VOCs in indoor and outdoor environments from various sources.

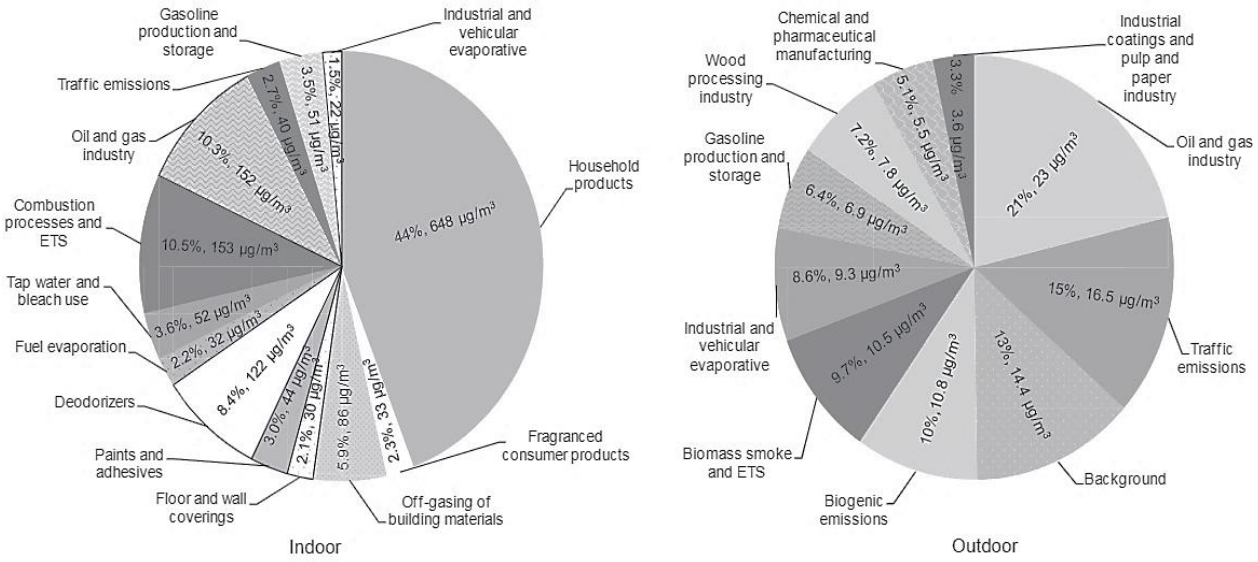

Figure 2.1. Average source of total measured VOCs in indoor and outdoor environments in residences of Edmonton, Alberta [36].

Since people spend around 80-90% of their lives in indoor environments, the risks related to poor indoor air quality are a growing concern [45]. Exposure to VOCs might cause eye, nose, and throat irritation, headache, loss of coordination, nausea, damage to liver, kidney, and central nervous system. The type of VOC, time, and level of exposure fluence the extent of a health effect [37,38]. Among all VOCs, benzene, toluene, formaldehyde, propylene, phenol, acetone, xylenes, and styrene cause the major concern and are most monitored by researchers [39,40]. Table 2.1 lists some typical VOCs, their maximum concentration, potential indoor sources, and health effects.

Table 2.1. The maximum concentration, indoor sources, and potential health effects of some VOCs [41–43].

Compound	Structural formula	Maximum concentration toluene ($\mu g/m^3$)	Indoor source	Potential health effect
Formaldehyde	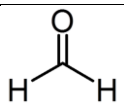	20	Wood-based materials, combustion sources, tobacco smoke, other textiles, and glues	Eye, nose, and throat irritation; asthma; lung damage, nausea, wheezing, and coughing; fatigue; and risk of cancer
Acetone	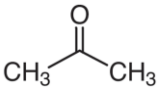	60	Nail polish remover, paint removers, waxes, resins, polishes, detergents, and cleansers	Irritation of the eyes and respiratory tract; headaches, dizziness; nervous system toxicity
1,2-Dichloroethane	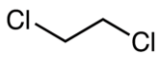	1	Adhesives, cleaning products, removers, pesticides, wallpaper/carpeting glue	Drowsiness; nausea; dizziness, and loss of consciousness; liver and kidney damage; immune and system toxicity
Trichloroethene	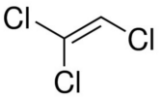	1	Paint stripper, adhesive solvent, paints, and varnishes	Narcosis; cumulative systemic toxicity; risk of reproductive and developmental health effects
Tetrachloroethene	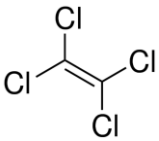	10	Fabrics, paint and spot removers, water repellents, brake and wood cleaners, and glues	Cumulative liver and CNS damage; narcosis; reproductive effects
Vinyl chloride	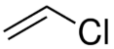	1	Production of polyvinyl chloride (PVC), waterpipes, wire and cable coatings, packaging materials, furniture automobile upholstery, housewares, and toys	Lung, liver, and kidney cancer; angiosarcoma; nervous system and immune system toxicity
Benzene	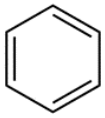	5	Tobacco smoke, fuels and paint supplies, automobile emissions in attached garages, glues, paints, furniture wax, resins, nylon, and synthetic fibers rubbers, lubricants, dyes, detergents, drugs, and pesticides	Cancer; leukemia; cumulative bone marrow damage; CNS depression; respiratory arrest; cardiovascular collapse; aplastic anemia; irritation
Toluene	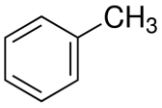	1	Tobacco smoke, paints, paint thinners, fingernail polish, lacquers, adhesives, rubber, printing, and leather tanning processes	Irritation of the eyes, respiratory tract, and skin; narcosis
Styrene	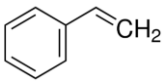	0.1-50	Tobacco smoke emissions from building materials, consumer products	Irritation of the eyes, nose, throat, skin; CNS effects; narcosis; mutagen
Dichloromethane	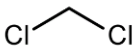	5	Paint strippers, aerosol products, adhesives, spray paints, automotive cleaners, and varnish remover	Dizziness, headache, confusion, drowsiness, risk for nervous system, liver and kidney toxicity

There are more than 300 VOCs, and based on the molecular structure, the VOCs can be classified into alkanes, alkenes, aromatic hydrocarbons, alcohols, aldehydes, ketones, etc. In addition, the polar and nonpolar VOCs are recognized based on the degree of molecular polarity [43–45]. Aromatic compounds are produced mainly from combustion, automobile exhaust, refinery products, and architectural materials. These VOCs are carcinogenic and highly toxic. Oxygenated VOCs such as alcohols, aldehydes, and ketones are generated from architectural materials, solvents, gases, and coal chemical industries [38]. BTX (benzene, toluene, xylene) belongs to aromatic group is frequently encountered in indoor air, and considered as the most hazardous pollutants among VOCs [46]. Toluene was reported to be more abundant than xylene and benzene in homes (around 60% of the total BTX compounds) [47]. In addition, toluene is among the eight indoor air VOC representatives proposed by ASHRAE (American Society of Heating, Refrigerating, and Air-Conditioning Engineers) to determine the efficiency of indoor air cleaning systems [48]. Acetone is a common compound in indoor environments with elevated levels due to its extensive use as solvent in nail polishing or many other products [49]. In this thesis, acetone and toluene were chosen as model compounds due to different structures, common presence in indoor air, and hazardous effects on humans.

2.2. Technologies for removal of VOCs from indoor air

There are many technologies available for VOC elimination in indoor air which can be classified into destruction and recovery groups. In destruction techniques, VOCs can be decomposed into CO_2, H_2O, or other non/less toxic compounds using chemical or biological methods. In recovery technologies, VOCs can be physically separated from air by transferring to another phase via changing the temperature and pressure in the process [45,50]. Adsorption is the most common technique in recovery-based group and biofiltration, photocatalytic oxidation, plasma catalysis, and catalytic ozonation are the most commonly used methods in the destruction group for removal of indoor VOCs [40].

Adsorption is regarded as one of the established methods for VOC removal due to its cost-effectiveness, flexible operation, and low energy consumption. Activated carbon, zeolites, alumina, silica gel, and other molecular sieves, which are available as granules, extruded pellets,

fibers, and powder are the commonly used adsorbents. Poor thermal stability, pore blockage, and limited adsorption capacity are considered as the main limitations of this technique. Suitable adsorbents have large surface area and highly developed porous structure. Activated carbon and zeolite are the most widely used adsorbents for indoor air treatment. Activated carbon-based adsorbents present some limitations as they are combustible, difficult to regenerate for high boiling solvents, and require control of relative humidity. Zeolite is an alternative for activated carbon since it has properties such as thermal stability and hydrophobicity. Since the cost of zeolite is higher its application is limited to cases that activated carbon that is not well suited [45,51,52].

Biological technologies are processes in which polluted air is passed through a biologically active porous medium that supports a flourishing population of microorganisms such as biofilters and biotrickling filters. The contaminants are adsorbed and then degraded biologically. The contaminants are converted to carbon dioxide, water, and biomass by oxidation process. Although biofiltration is an economical and easy technique, it has certain drawbacks due to the accumulation of biomass in the filter bed. This can cause some problems, which lead to a reduction in performance including rising pressure drop, bed channeling, and generation of anaerobic zones. Therefore, the main challenge in biofiltration is keeping the balance between excess biomass generation and optimum sustainable pollutant removal. Moreover, the acclimation period for the microbial population may take weeks or even months particularly for VOC removal [53,54].

Photocatalytic oxidation is a cost-effective and efficient method for VOC removal and it has gained research interest in the last two decades [55]. TiO_2 is the most widely used photocatalyst for VOC removal due to its low cost, simple preparation, and high stability [41]. Semiconductor catalyst such as TiO_2 and ultraviolet (UV) light in this process generate electrons and holes which react with VOC molecules [56]. The main disadvantage of this technique is formation of harmful intermediates and particularly volatile aldehydes such as formaldehyde and acetaldehyde. In addition, the intermediate species tend to accumulate on the surface and cause catalyst deactivation [51,57].

Plasma treatment is a potential technique for removal of indoor air pollutants. In non-thermal plasma technology, a strong electrical field with high discharge voltage is created to decompose

VOCs using active electrons. The high potential difference between two electrodes leads to formation of a highly reactive environment favorable to react with various compounds [58,59]. This process alone has drawbacks such as high energy consumption, incomplete oxidation, poor efficiency at low VOCs, incomplete oxidation, and harmful byproducts formation. To overcome these challenges, this method was coupled with catalyst in a process called plasma catalysis which leads to an increase in the removal efficiency. However, incomplete elimination of VOCs, unpleasant products, and low efficiency at higher humidity levels are still the unsolved challenges in this technique [41,59,60].

Thermal oxidation is the process of oxidizing combustible materials at high temperatures (>700 °C). VOCs in the presence of oxygen and at high temperatures convert to carbon dioxide and water. However, this method has high operating costs. Another concern in thermal oxidation applications is producing some acidic compounds in the vent stream. Therefore, corrosion-resistant materials should be used in the construction of equipment [44,61]. The catalytic oxidation system operates at a lower temperature than thermal oxidation due to the effect of catalysts. The VOCs are oxidized in the presence of a suitable catalyst at much lower temperatures (250-500 °C) compared to thermal oxidation. Combustion temperature can be reduced significantly by using catalysts and this leads to advantages of lowering operating temperature and less fuel cost. Catalytic oxidation system is a suitable technology for lower exhaust volumes where contaminants such as chlorine, sulfur, heavy hydrocarbons, and particulates are not present. One of the disadvantages of this method is that capital cost of the catalytic unit is relatively high [62,63].

Ozone is a strong oxidizing agent and by addition of ozone, the required reaction temperature and the apparent activation energy decrease significantly. When ozone is used with a suitable catalyst, the reaction can occur at low temperatures close to ambient temperature. Therefore, important benefits of catalytic ozonation for removal of VOCs are reduction in reaction temperature and saving energy. Another advantage of catalytic ozonation over catalytic oxidation is the possibility of using transition metal oxides instead of noble metals, which are commonly used in oxidation systems. Therefore, using low-cost catalysts for oxidation of VOCs is possible [14,31,64].

2.3. Catalytic ozonation of VOCs in air

2.3.1. Ozone properties and decomposition

Ozone is an unstable powerful oxidant with strong electrophilic and oxidizing properties which makes it useful for waste treatment processes. The molecule of ozone has three oxygen atoms at the vertices of an obtuse-angled triangle (Figure 2.3). Ozone can be generated at a short wavelength of UV radiation or in electric discharges. During the degradation of ozone to oxygen, atomic oxygens will be formed which creates very strong oxidizing effects that can be used in water treatment and air cleaning devices [65,66].

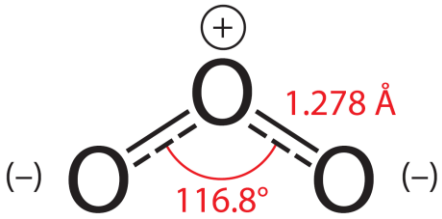

Figure 2.2. Structure of ozone molecule [66].

Electron configurations of the ozone molecule and its resonance structures are shown in Figure 2.2. The electron configuration of ozone and the four different resonance structures are ascribed to high reactivity of ozone and its thermodynamic instability. Ozone is resonance stabilized which causes its resistance against decomposition at low temperature [64,66].

The oxidation potential of ozone is 2.07 eV which is high compared with those of oxygen (0.68 eV) and hydrogen peroxide (1.78 eV) [67]. It reacts with most compounds with organic/organometallic structures. Ozone is electrophile with a dipolar structure, therefore, the reaction of ozone with compounds with electron-donating groups is faster.

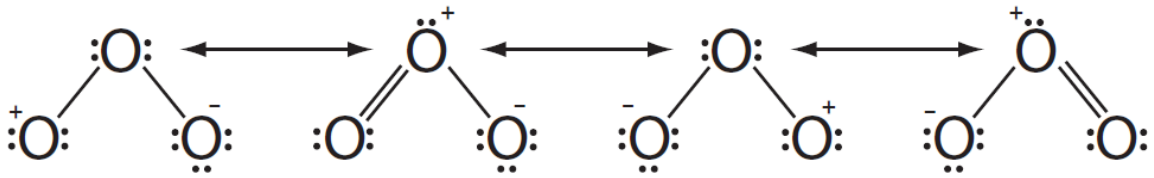

Figure 2.3. Resonance structures of ozone [66,67].

The reaction of ozone with aromatic compounds other than styrene is reported to be negligible. The reason can be attributed to the aromatic ring structure of these compounds. Oxygen-containing organic compounds that have no unsaturated carbon-carbon bonds in their structure have a slow reaction with ozone. In addition, alcohols, aldehydes, and ketones that do not contain unsaturated carbon-carbon bonds will have extremely slow reactions with ozone [68].

Natural decomposition of ozone is very low at ambient temperature and it can be enhanced with temperature. However, ozone can be easily decomposed in the presence of catalysts at low temperatures. Catalytic ozone conversion has been performed over supported and unsupported noble metals (Ag, Pd, and Pt) and transition metal oxides of Co, Ni, Fe, Mn, Ce, and Cu. Mn-based catalysts have presented the highest efficiency in decomposing ozone [67,69,70].

Oyama et al. proposed the mechanism of ozone decomposition on manganese oxides on various supports [71,72]. First, ozone is adsorbed on Mn active site and forms surface atomic oxygen (O*) and molecular oxygen O_2. Then, the generated atomic oxygen reacts with the second ozone molecule and forms a surface peroxide (O_2*) and another oxygen molecule. In the final step, the peroxide species desorb leading to a free active site and an oxygen molecule (Figure 2.4).

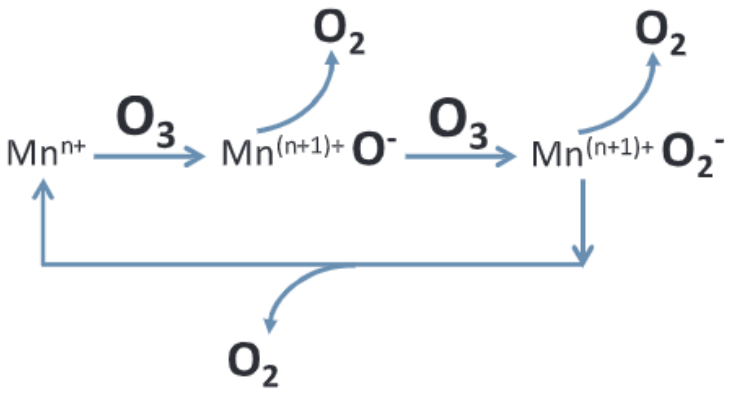

Figure 2.4. Ozone decomposition reaction mechanism on manganese oxide active sites [69].

2.3.2. Studies in catalytic systems of VOC oxidation

One of the main advantages of the catalytic ozonation technique is its capability to destroy VOCs at low temperatures. Heterogeneous catalytic ozonation has been the focus of many studies in recent years intending to improve this process to successfully eliminate VOCs at temperatures close to room temperature. Approaches such as investigating the effect of operating conditions, calcination temperature, preparation procedure, and water vapor; and comparing different transition metal oxides, noble metals, and supports have been studied extensively. The catalytic performance and reaction condition of effective catalysts on ozonation of VOCs in gas phase are summarized in Table 2.2. In these studies, some variables such as reaction conditions, catalyst loading, mixed metal oxides, different supports, calcination temperature, etc. have been investigated and the best catalyst characteristics with the highest performance are reported in Table 2.2.

Table 2.2.Catalytic ozonation of VOCs using different catalysts.

VOC	Concentration (ppmv)	Catalyst	Preparation methods	Calcination temperature (ºC)	Reaction temperature (ºC)	Conversion (%)	Ref.
Toluene	100	Ru-Mn/HZSM-5	Wet impregnation	350	25	36	[73]
Chlorobenzene	115	Fe_2O_3	Precipitation	180	150	92	[74]
Benzene	150	Cu-Mn/SiO_2	Dry impregnation	600	70	88	[25]
Benzene	150	Co-MnO_x	Evaporation-to-dryness	400	70	50	[27]
Benzene	150	Mn/SiO_2	Dry impregnation	400-600	70	54-67	[25]
Acetone	150	Co/Al_2O_3	Dry impregnation	500	25	85	[75]
Toluene	100	MgO/GAC	Sol–gel	500	100	91	[76]
Chlorobenzene	100	Mn/Al_2O_3	Precipitation	450	120	83	[14]
Toluene	120	Mn/Al_2O_3	Dry impregnation	500	22-100	60-95	[30]
Benzene	30	Mn/ZSM-5	Dry impregnation	550	25	85	[77]
Methanol	380	Pt/FeO_x	Coprecipitation	200-500	30	75-100	[78]
Acetone	144	Mn/Al_2O_3	Dry impregnation	500	25-90	54-87	[79]
Acetaldehyde	269	Ti/H-ZSM-5	Dry impregnation	350-700	25	55-72	[80]
Benzene	150	Mn_2O_3	Evaporation-to-dryness	400-900	70	20-80	[27]
Formaldehyde	45	Mn/CVC-TiO_2	Chemical vapor condensation	500	25	100	[24]
Benzene	200	α-Mn_2O_3	Nano-replication	200-500	80	50-70	[81]
Toluene	395	Co-MCM-41	Hydrothermal	400	22-50	55-70	[82]
Toluene	200	Mn/G	Hydrothermal	-	22	34	[83]
Benzene	100	Mn/AL-SBA-16	Dry impregnation	550	80	85	[84]
Toluene	20	Mn/USY	Hydrothermal	-	25	56	[12]
Toluene	80	$ZrCeO_x$	Evaporation-induced self-assembly	700-900	100	57-80	[85]

Transition metal oxides, both supported and unsupported have attracted great attention in catalytic ozonation of VOCs. It was found that manganese is the most active transition metal for oxidation of VOCs at low temperatures [86–89]. Supported manganese oxides in catalytic ozonation of benzene present higher catalytic activity than unsupported manganese oxide [27]. MnO_x supported on Al_2O_3, TiO_2, SiO_2, CeO_2, and ZrO_2 have been investigated for catalytic ozonation of chlorobenzene by Chen et al. [14]. Among the studied supports, alumina displayed the highest catalytic activity. This was attributed to its textual properties, surface adsorbed oxygen species, highest redox potential, and high surface acidity [14]. Manganese oxides on γ-alumina and MCM-41 supports were studied for catalytic ozonation of toluene and the results indicated that MCM-41 supported catalyst presents lower conversions than alumina [21].

Catalytic ability in oxidation of VOCs can be enhanced by combination of metal oxides as a bimetallic oxide type of catalysts [27]. Manganese-based mixed oxides were found to have higher catalytic ability than single oxides due to the changes in its properties such as catalysts' oxidation state and surface area [27,73,90,91]. Mn-based bimetallic catalysts supported on HZSM-5 have been prepared by addition of Fe, Cu, Ru, and Ag and tested in catalytic ozonation of toluene [73]. The catalytic performance of Mn catalyst was improved by the addition of the secondary metals. Among the mixed oxides catalysts, Ru-Mn/HZSM-5 showed the highest efficiency in toluene degradation which can be related to the increase in reducibility of Mn oxidation state. M-containing mixed oxides of Fe, Co, Ni, and Cu, have been studied for catalytic ozonation of benzene [27]. Co–Mn mixed oxide was the most effective catalyst for benzene oxidation with higher CO_2 selectivity and ozone decomposition ability [27].

The preparation method is of great importance to achieve catalysts with high activity [92]. However, most of the studies on the effect of preparation procedure have been performed on catalytic oxidation of VOCs than catalytic ozonation. Tang et al. [93] examined the influence of preparation method on manganese oxides catalyst for oxidation of benzene, toluene, and xylene. They reported that MnO_x obtained by oxalate route had better performance than NH_4HCO_3 route and NaOH route, although the surface area of the samples was slightly smaller than the other two methods. The order of catalytic activity was related to the content of surface lattice oxygen species [93]. Titanium oxides supported Pt, Pd and Rh catalysts were applied for oxidation of CO, ethanol, and toluene. The catalysts were prepared by liquid-phase reduction deposition and

incipient wetness impregnation [94]. It was found that the preparation procedure has a considerable effect on metal dispersion, and consequently on the catalytic activity. Einaga et al. [27] investigated the effect of preparation conditions of evaporation-to-dryness method and co-precipitation method on their catalytic properties of Mn-based catalysts. They reported that properties of catalyst were almost independent of preparation procedure.

The catalytic properties and performance greatly depend on the calcination temperature. The effect of calcination temperature was investigated on catalytic ozonation of methanol using Pt/FeO_x catalyst. Upon rising the calcination temperature from 200 to 500 ºC, methanol conversion increased with calcination temperature up to 400 ºC, followed a decline as the calcination temperature went up to 500 ºC. Therefore, the highest conversion was achieved at 400 ºC due to its higher dispersion and the appropriate molar ratio of Pt^0/Pt^{2+} [78]. Calcination temperature was studied on oxidation of formaldehyde using Mn-Ce mixed oxide catalysts in the range between 300 and 700 ºC [95]. By increasing the calcination temperature, the BET surface areas and pore volumes decreased substantially. Formaldehyde conversion increased with calcination temperature up to 500 ºC, followed a decline as the calcination temperature went up to 700 ºC. The highest conversion was obtained at 500 ºC due to its higher oxidation state and lattice oxygen species on the surface [95]. Catalytic ozonation of benzene was performed over MnO_x/SiO_2 catalyst calcined at 400-600 ºC [25]. Benzene oxidation rate and CO_2/CO ratio were enhanced with increase in calcination temperature. It has been reported that formation of Mn_2O_3 on SiO_2 support demonstrated higher activity than MnO_2 in oxidation of benzene which can be obtained at higher calcination temperature [25]. Yuan et al. made MnO_x catalysts with mesoporous structure using SBA-15 as a hard template at calcination temperatures of 300-500 ºC. Toluene conversion could reach up to 100% by increasing calcination temperature up to 500 ºC due to enough surface adsorbed oxygen [96].

2.3.3. Mechanism of catalytic ozonation of VOCs

Although several studies have been performed to describe catalytic ozonation of VOCs, the proposed models are limited and there are still conflicting conclusions. These studies have assumed that the reaction happens on the surface of the catalyst between atomic oxygen resulted from ozone decomposition and adsorbed VOC molecule, suggesting the Langmuir–Hinshelwood mechanism. The original suggested model was proposed by Reed et al. on catalytic ozonation of acetone using MnO_x/SiO_2 [26]. They used *in-situ* Raman spectroscopy and the transient kinetics techniques to develop the Langmuir–Hinshelwood expression in which only one site (MnO_x) was involved in the mechanism.

$$O_3 + * \rightarrow O_2 + O* \quad (2.1)$$

$$O* + O_3 \rightarrow O_2 + O_2* \quad (2.2)$$

$$O_2* \rightarrow O_2 + * \quad (2.3)$$

$$A + \square \rightleftarrows A\square \quad (2.4)$$

$$A\square + * \rightarrow A* + \square \quad (2.5)$$

$$A* + O* \rightarrow products \quad (2.6)$$

where * represents a surface Mn site, □ represents a surface SiO_2 site, and *A* represents acetone. The presented model was used by other researcher on ozonation of benzene [97] , toluene [98] and cyclohexane [99]. Reed et al.'s model was only validated experimentally by Rezaei et al. on catalytic ozonation of toluene using MnO_x/Al_2O_3. In the same study by Rezaei et al., they proposed a mechanism based on the assumption that C–H bond cleavage is the limiting step. However, experimental evidence was not performed to support and validate the proposed mechanism. In these two studies, Langmuir–Hinshelwood single site mechanism were developed, assuming that the reaction occurred only on active MnO_x sites. The support (silica or alumina) only helps to increase the dispersion of active Mn sites. Recent study by Hu et al. investigated mechanism of catalytic ozonation of toluene using MnO_x/graphene catalyst. They

suggested a dual site mechanism for catalytic ozonation of toluene in which dual roles are played by graphene and MnO_x. Mn sites are used for ozone decomposition, while graphene offers sites for toluene adsorption.

$$O_3 + * \rightarrow O_2 + O \quad (2.7)$$

$$O* + O_3 \rightarrow O_2 + O_2* \quad (2.8)$$

$$O_2* \rightarrow O_2 + * \quad (2.9)$$

$$C_7H_8 + \square \rightleftarrows C_7H_8\,\square \quad (2.10)$$

$$C_7H_8\,\square + O* \rightarrow products \quad (2.11)$$

* and □ represent surface manganese sites and surface graphene sites, respectively. The first three steps which are related to ozone decomposition are similar to the Reed et al.'s mechanism. However, it has been considered that the migration of the adsorbed VOC from support site to Mn site is not happening and the reaction occurs within dual sites. The proposed mechanism and the derived expression have not yet been assessed on VOCs other than toluene.

Based on the reaction and *in-situ* DRIFT results over pure alumina and alumina supported manganese oxide, alumina acts not only as a support for Mn dispersion, and a reservoir for adsorbed VOC, but also interacts with VOC and creates surface carboxylate. These intermediates further react with atomic oxygen [79,100]. Due to limited studies and conflicting conclusions, the mechanism of catalytic ozonation of VOCs remains unclear and needs further investigations to clarify this reaction's mechanism and kinetic steps.

2.4. Knowledge gaps and research objectives

Although many studies have been conducted on catalytic ozonation of VOCs, this technique still faces some limitations for its practical application. According to the literature and the recent reported developments, there are still knowledge gaps and challenges in catalytic ozonation of VOCs.

- One of the limitations in catalytic ozonation process is that the required temperature for this process for a stable reaction is still higher than room temperature. Key issues such as catalyst deactivation and incomplete oxidation byproducts limit the reaction at low temperatures. Many studies aimed to improve catalytic activity to remove VOCs at room temperature but this problem still needs investigation [95,101,102].
- Incomplete oxidation of VOC at room temperature and generation of lots of organic intermediates are other serious problems in this technique. Other than CO_2, CO -which is a toxic gas and should be inhibited- is generated due to partial oxidation. Nevertheless, this issue has not been addressed enough in the literature. Many researchers have been trying to improve VOC oxidation, CO production has not been addressed [22,31,103,104].
- Catalytic ozonation of mixtures of VOCs especially at various concentration ratios is still not clear. There are over 350 VOCs in indoor air, mostly found in chemical mixtures at very low concentrations. However, there are very few studies of catalytic ozonation of mixture of VOCs and catalyst application of mixture system needs further investigation [102,105].
- Another important issue is the mechanism behind catalytic ozonation of VOCs which is not completely obvious according to the limited studies conducted so far. It is considered that the reaction takes place between adsorbed atomic oxygen and VOC molecules following the Langmuir-Hinshelwood type of mechanism. Langmuir-Hinshelwood single-site and dual-site mechanisms were proposed which very few studies systematically validated them. These studies only considered one type of VOCs and the generality of the mechanism is not clear yet [26,64,98].

Based on the mentioned knowledge gaps, the main objective of this research is to consider different approaches to enhance catalytic activity and delay catalyst deactivation at room temperature. To obtain a catalytic with higher efficiency, the most promising catalyst for catalytic ozonation of VOCs according to the literature was chosen which was Alumina-supported manganese oxides catalyst. Approaches such as the addition of secondary metal oxide, change in catalyst preparation procedure, and calcination temperature which are reported to affect the properties of the catalysts and subsequently the catalyst activity were studied.

To achieve the overall main objective of this research, the following sub-objectives have been considered:

- Investigate the influence of augmenting the single Mn and Co catalysts on the performance and structure of the catalyst in catalytic ozonation of acetone at room temperature.
- Apply the novel method entitled polyol process for catalyst preparation and study the structure and activity of the new catalyst for ozonation of toluene in air at room temperature.
- Study the effect of calcination temperature on the structural properties and catalytic activity of the polyol and impregnated catalysts in ozonation of single component and binary mixtures of acetone and toluene with various concentration ratios.
- Conduct kinetic study of polyol and impregnated catalysts in catalytic ozonation of acetone.

Chapter 3:

Room Temperature Oxidation of Acetone by Ozone over Alumina-Supported Manganese and Cobalt Mixed Oxides

The content of this chapter has been published in Journal of Frontiers of Chemical Science and Engineering and presented in the following conferences:

Citation:

M. Ghavami, M. Aghbolaghy, J. Soltan, N. Chen, Room temperature oxidation of acetone by ozone over alumina-supported manganese and cobalt mixed oxides, Frontiers of Chemical Science and Engineering (2020), 14(6): 937–947.

Conference Proceedings:

M. Ghavami, M. Aghbolaghy, J. Soltan and N. Chen, Catalytic oxidation of acetone by ozone over alumina supported cobalt-manganese catalysts. 67th Canadian Chemical Engineering Conference, October 22-25, 2017, Edmonton, Canada.

M. Ghavami, M. Aghbolaghy, J. Soltan and N. Chen, Low Temperature Acetone Oxidation using Ozone over Supported Manganese-Cobalt Bimetallic Catalysts. 25th Canadian Symposium on Catalysis, May 8-11, 2018, Saskatoon, Canada.

M. Ghavami, M. Aghbolaghy, J. Soltan and N. Chen, Low Temperature Acetone Oxidation using Ozone over Supported Manganese-Cobalt Bimetallic Catalysts. 68th Canadian Chemical Engineering Conference, October 28-31, 2018, Toronto, Canada.

Contribution of the Ph.D. candidate

All the experiments were conducted by Mehraneh Ghavami in consultation with Dr. Jafar Soltan. The experimental setup had been upgraded by previous group member, Dr. Mostafa Aghbolaghy. Dr. Mostafa Aghbolaghy provided guidance and training. All the written text and data analysis were prepared by Mehraneh Ghavami. Dr. Jafar Soltan supervised and provided consultation during the experimental period and thesis preparation. XANES and XAFS data were collected at the Canadian Light Source with the assistance of Dr. Ning Chen. Dr. Ning Chen provided general guidance for analyses of the XAS data and revised the manuscript.

Contribution of this chapter to the overall Ph.D. Research

This chapter covers the first phase of the research, which is "the investigation of the influence of augmenting the single Mn and Co catalysts on the performance and structure of the catalyst in catalytic ozonation of acetone at room temperature". This section demonstrates the impact of addition of another active metal oxide to single metal oxides catalyst. In addition, the effect of variation of metal loading in mixed metal oxides catalysts was studied. The catalyst preparation, characterizations, and activity results are provided in this chapter.

3.1. Abstract

VOCs are among the major sources of air pollution. Catalytic ozonation is an efficient process for removing VOCs at lower reaction temperatures compared to catalytic oxidation. In this study, a series of alumina supported single and mixed manganese and cobalt oxides catalysts were used for ozonation of acetone at room temperature. The influence of augmenting the single Mn and Co catalysts was investigated on the performance and structure of the catalyst. The manganese and cobalt single and mixed oxides catalysts of the formula Mn10%-CoX and Co10%-MnX (where X = 0, 2.5, 5, or 10%) were prepared. Structure of the catalysts was examined by BET, XRD, XANES, and EXAFS. It was found that addition of Mn and Co at lower loading levels (2.5% or 5%) to single metal oxide catalysts enhanced the catalytic activity. The mixed oxides catalysts of (Mn10%-Co2.5%) and (Mn10%-Co5%) led to acetone conversion of about 84%. It

is concluded that lower oxidation state of the secondary metal improves ozone decomposition and oxidation of acetone.

3.2. Introduction

Air pollution by VOCs is an environmental threat that can negatively affect human health [106,107]. Ozone is considered a strong oxidant for water treatment and air cleaning [108,109]. Catalytic reaction with ozone (catalytic ozonation) is a promising method for VOC removal with distinct advantages over catalytic oxidation processes. Important advantages of catalytic ozonation are oxidation of VOCs at lower temperature, the possibility of using transition metal oxides catalysts instead of noble metals, and effectiveness of the process at low concentration levels of the VOC [31,76,85,110].

Transition metal oxides such as Mn, Co, Cu, Ni, Fe, and Ce are among the most active metals in catalytic ozonation reactions [111]. Supported manganese oxides are the most effective catalysts for oxidation of VOCs with ozone [30,102,104,112]. It has been reported that high activity of MnO_x in the oxidation of VOCs can be related to the activity of Mn in decomposition of ozone and generation of active oxygen species [113]. VOC removal rates normalized by catalyst surface area were determined to be higher for alumina-supported catalysts than titania, silica, or zirconia-supported catalysts [29]. Investigation on catalytic ozonation of acetone using supported manganese oxide catalyst on γ-alumina and silica showed that alumina-supported catalyst was more active than the silica-supported catalyst in acetone removal [112].

One method of enhancing the catalyst activity is the addition of another metal to the supported manganese oxide. It has been reported that mixed metal catalysts can offer higher catalytic performance and selectivity, and better deactivation resistance compared to monometallic catalysts [114–116]. Among transition metal oxides, cobalt oxides have been identified as promising catalysts in oxidation of VOCs [114,117–119]. Doping ceria with cobalt oxide has been reported to modify the redox properties, enhance the oxygen mobility and eventually lead to better catalyst activity [118,120]. Cobalt is a metal with different oxidation states and relatively low energy gap exists between its different oxidation states. This can be beneficial for ozone decomposition and catalytic ozonation reactions [75].

In the present study, alumina supported Mn and Co single and mixed metal catalysts with different loadings of Co or Mn were used in catalytic ozonation of acetone at room temperature. The model VOC in this work was acetone since it is a prevalent industrial solvent and common pollutant in indoor air [112]. Reed et al. examined ozonation of acetone on silica-supported manganese oxide catalysts. The effect of metal oxide loading on oxidation of acetone was investigated, and it was noted that higher Mn loadings of silica-supported catalysts are more active due to their lower oxidation state and better adsorption of intermediates and easier delivery of oxygen equivalents [113]. On the contrary, it has also been reported that lower loadings of Mn are more favorable in catalytic ozonation of VOCs due to higher dispersion of Mn as well as lower oxidation states of Mn [30,103,104].

Einaga et al.[27] investigated the effect of different metal oxides of Fe, Co, Ni, and Cu on performance of unsupported Mn catalyst based on the catalyst activity and selectivity in oxidation of benzene with ozone. They reported that Co–Mn mixed oxide was the most effective catalyst for benzene oxidation among the mixed oxide catalysts. Yao et al. [121] applied post plasma catalysis system to remove hexanal at ambient temperature and pressure from air using unsupported Co-Mn catalyst with different mole ratios. They deduced that CoMn(9/1) showed the best catalytic activity because the redox properties of Co-Mn solid solutions were promoted. Since both Mn and Co are active metals in catalytic ozonation of VOCs, catalytic ozonation of acetone over alumina supported Mn and Co mixed oxide catalysts at different levels of the primary and secondary metal loading was investigated. The catalysts were characterized by Brunauer–Emmett–Teller (BET) surface area and pore volume, X-ray diffraction (XRD), X-ray absorption near edge structure (XANES), extended X-ray absorption fine structure (EXAFS), and diffuse reflectance infrared Fourier transform spectroscopy (DRIFT) to relate the properties of the catalysts to their activities.

3.3. Material and methods

3.3.1. Catalyst preparation

Single MnO_x and CoO_x catalysts with metal loading of 10 wt% on γ-Al_2O_3 (Alfa Aesar, S_{BET} = 220 m^2 g^{-1}) were prepared by dry impregnation method using manganese (II) nitrate tetrahydrate (Sigma–Aldrich, 97%) and cobalt (II) nitrate hexahydrate (Sigma–Aldrich, 98%) precursors. After impregnation by the given amounts of the precursor solution, catalysts were dried at 100 °C for 10 h and calcined at 500 °C for 4 h. The calcined catalysts were crushed and sieved to achieve particles with diameter less than 208 μm for activity tests.

The mixed transition metal oxides catalysts were prepared via successive impregnation method. Once the single metal catalysts were prepared, Mn-Co mixed oxides catalysts were synthesized by adding 2.5%, 5%, and 10 wt% Co to the already prepared MnO_x/γ-Al_2O_3 catalyst using cobalt (II) nitrate hexahydrate solution. In the case of Co-Mn catalysts, solutions of manganese (II) nitrate tetrahydrate with appropriate content were added to the already prepared CoO_x/γ-Al_2O_3 catalyst. The catalysts were dried, calcined, and sieved again.

3.3.2. Catalyst characterization

BET surface area and pore volume of the catalysts were determined by nitrogen adsorption using ASAP 2020 (Micromeritics) instrument. The samples were degassed for 2 hours at 110 °C and 0.5 mm Hg before the surface area and pore volume measurements. Structure of the catalysts was analyzed by XRD, XANES, and EXAFS. XRD spectra were collected by Brucker diffractometer (D8 Advance, Cu Kα radiation) in the 2θ range of 10–80º with a step size of 0.04º. XANES and EXAFS spectra of Mn *K-edge* and Co *K-edge* were collected at HXMA beamline of the Canadian Light Source. Catalysts were diluted with boron nitride (BN), ground, and pressed to make thin disks. The prepared disks were protected by Kapton tape. All measurements were carried out in transmission mode using straight ion chamber detectors filled with helium gas. A Si(1 1 1) monochromator crystal used for data collection and the beamline was operated in Rh mirrors. Data processing was performed by ATHENA software [122].

3.3.3. Experimental setup and activity tests

A schematic diagram of the experimental setup is shown in Figure 3.1. An ozone generator (AZCO Industries LTD, HTU-500S) was used to generate ozone from a high purity oxygen cylinder (Praxair, 99.993%). An acetone cylinder with ppm level concentration (Praxair, accuracy of ±2%) was diluted with nitrogen (Praxair, 99.999%) to provide acetone with appropriate concentration in the system. Gas flows were controlled by mass flow controllers (Brooks, SLA 5850, accuracy of ±1%). The catalytic ozonation experiments were carried out at 25 °C and atmospheric pressure using a feed gas with 1200 ppm ozone and 150 ppm acetone.

Total feed flow rate of 250 ml/min (at STP) was set for all experiments. For each experiment, 0.065 g of the fresh catalyst was used. First, feed gas streams passed through a horizontal Pyrex tube, filled with glass beads, to enhance mixing before entering the reactor. All the reaction experiments were conducted in a reaction chamber (Harrick, HVC) at atmospheric pressure. Concentration of ozone was measured by an ozone analyzer (Teledyne API M454) in the exhaust gas stream. A long-path gas cell (PIKE, volume 0.1 l, 2.4 m optical length, KBr window) coupled with a Nicolet iS50 FTIR spectrometer equipped with a Deuterated l-alanine doped triglycine sulfate (DLaTGS) detector was used for analysis of acetone, CO, and CO_2. Based on the blank tests, homogeneous reaction between ozone and acetone in the absence of the catalyst was negligible in this system.

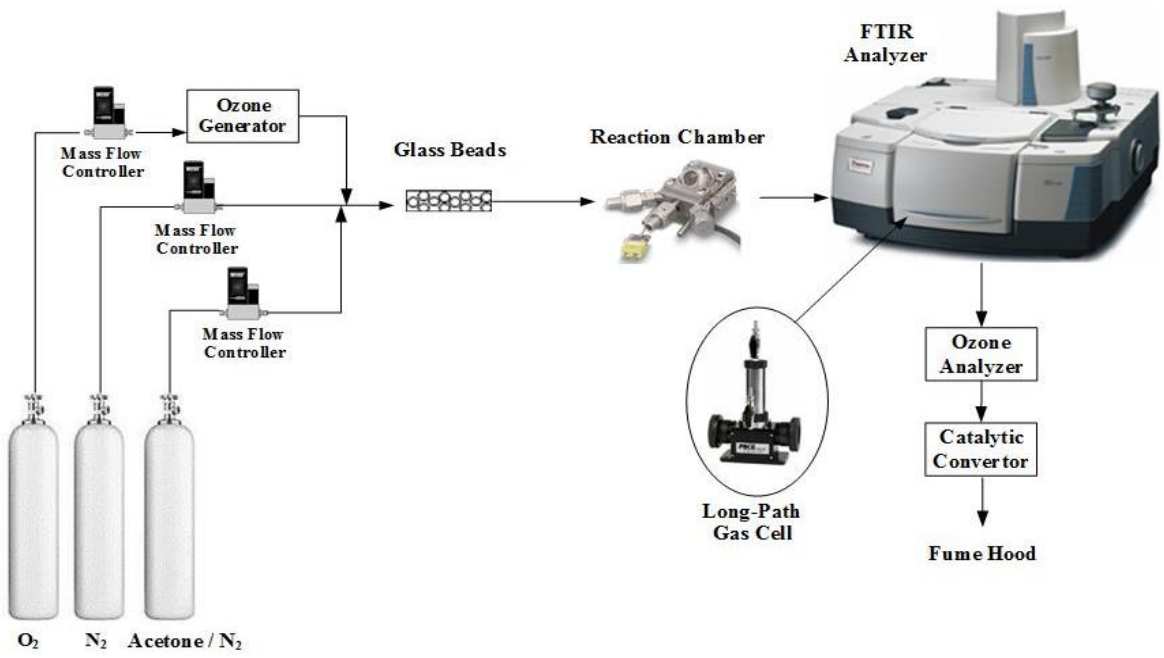

Figure 3.1. Schematic of the experimental setup.

Prior to the reaction, the catalyst was heated for 1 h under flow of 200 ml/min oxygen at 490 °C. Then, the catalyst was cooled down to the reaction temperature under 250 ml/min nitrogen flow. The catalyst was saturated by passing gas mixture containing acetone, nitrogen, and oxygen before introducing ozone to the reaction chamber. After the catalyst became saturated with acetone, the ozone generator was turned on, and the ozonation of acetone was monitored at room temperature for 150 min. Experiments were repeated, and experimental errors in terms of standard error were calculated. For calibration purposes, a gas cylinder with ppm level concentrations of carbon dioxide and carbon monoxide balanced with nitrogen (Praxair, accuracy of ±2%) was used.

DRIFTS experiments were performed in another configuration of the experimental setup in which the long-path gas cell was replaced with a DRIFTS accessory (Harrick, Praying Mantis) on the FTIR spectrometer. The reaction chamber, equipped with ZnSe windows, was installed in the DRIFTS accessory in the FTIR spectrometer. To attain higher sensitivity and faster scanning, a narrow band mercuric cadmium telluride (MCT-A) detector was used for the DRIFTS operations. Spectra were collected at a resolution of 4 cm^{-1} in the range of 3900–1300 cm^{-1} to avoid saturation of the MCT-A detector.

The acetone and ozone conversions (X_i) were calculated as follows:

$$X_i = \frac{C_{i,in} - C_{i,out}}{C_{i,in}} \times 100\% \quad (3.1)$$

where $C_{i,in}$ and $C_{i,out}$ are the inlet and outlet concentrations of acetone or ozone, respectively.

CO_x yield was calculated from the following equation:

$$CO_x\ yield\ (\%) = \frac{[CO]+[CO_2]}{(3\times[C_3H_6O]_{reacted})} \times 100 \quad (3.2)$$

3.4. Results and discussion

3.4.1. Catalyst characterization

Table 3.1 presents Mn and Co loading, BET surface area, and pore volume of all the studied catalysts and the alumina support. By adding Mn and Co on the alumina, surface area and pore volume of the samples decreased. In the mixed oxide catalysts, surface area and pore volume kept decreasing by increasing metal loading mainly due to contribution of the mass of nonporous metal components to the catalyst mass and partial plugging of alumina pores [30].

Figure 3.2 shows XRD spectra of the eight catalysts supported on alumina. According to XRD peaks, Mn_2O_3 and Co_3O_4 are the main phases of manganese and cobalt oxides in single metal oxides catalysts [79,123]. Co_3O_4 has a sharp peak at 37º, which can be observed in all catalysts containing cobalt. In CoO_x/γ-Al_2O_3, only peaks related to Co_3O_4 phase can be seen. In Co-based catalysts augmented by adding different loadings of manganese, the main phase of cobalt oxides is Co_3O_4. Whereas, in Mn-based catalysts augmented by adding cobalt, an overlap of Co_3O_4 and CoO peaks can be observed. In MnO_x/γ-Al_2O_3 sample, different phases of manganese oxide can be observed in the XRD spectra. The most intense peak of Mn_3O_4 is located at 36.2º, which is hardly recognizable due to the overlap of the peak with that of Co_3O_4.

Table 3.1. Chemical compositions and pore structures of the catalysts.

Catalyst	Mn and Co loading (wt %)		S_{BET} ($m^2 g^{-1}$)	Pore volume ($cm^3 g^{-1}$)
	Mn	Co		
γ-Al_2O_3	-	-	220	0.61
Mn/γ-Al_2O_3	10	-	200	0.56
Mn-Co/γ-Al_2O_3	10	2.5	186	0.54
Mn-Co/γ-Al_2O_3	10	5	178	0.53
Mn-Co/γ-Al_2O_3	10	10	180	0.49
Co/γ-Al_2O_3	-	10	210	0.59
Co-Mn/γ-Al_2O_3	2.5	10	194	0.55
Co-Mn/γ-Al_2O_3	5	10	183	0.52
Co-Mn/γ-Al_2O_3	10	10	174	0.47

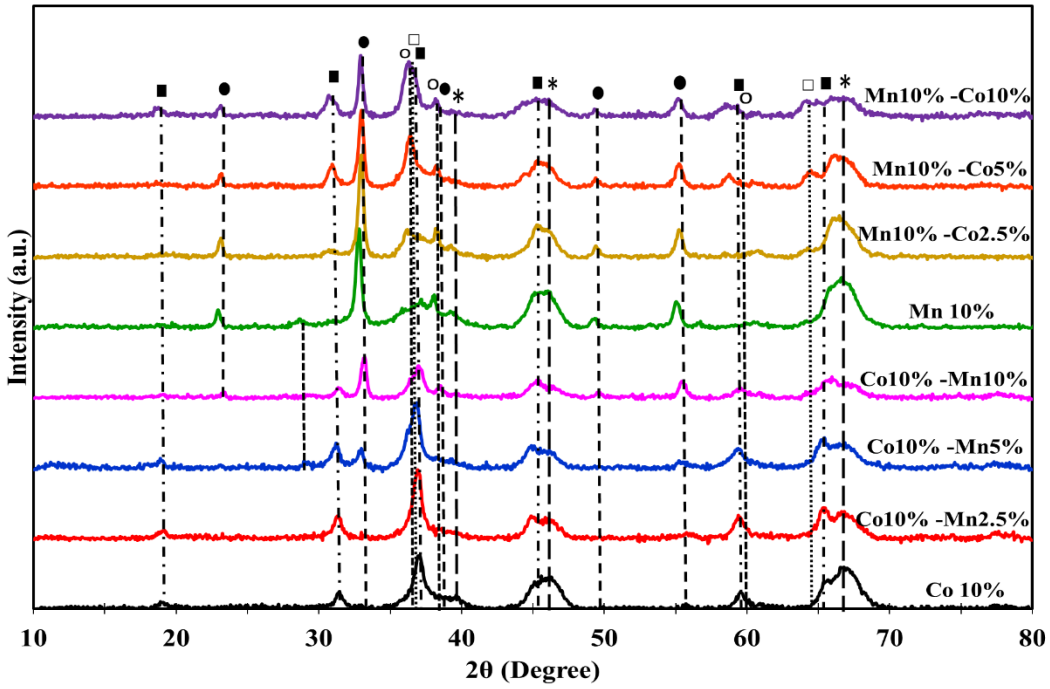

Figure 3.2. XRD patterns of the alumina supported catalysts (Al_2O_3 *, Mn_2O_3 ●, Mn_3O_4 ○, MnO_2 +, Co_3O_4 ■, CoO □).

Therefore, XRD spectra of the catalysts indicate that with change in the loading of the secondary metal, different phases of Mn and Co oxides are formed, while the oxidation state of the primary metal in the catalyst remains unchanged. From the XRD peaks, metal oxide crystallite sizes were estimated by using the Scherrer equation. Particle size of Mn_2O_3 is determined from XRD spectra using the most intense peak at 32.9° [21]. Co_3O_4 metal crystallite size was determined from XRD spectra using the Co_3O_4 peak at 2θ value of 31.4°. It was determined that Mn_2O_3 had crystallite size between 18 and 26 nm, whereas Co_3O_4 crystallites fall in the range of 9 and 21 nm size range. Catalyst dispersion values were estimated from the obtained particle sizes calculated from XRD peak broadening [26,124]. Table 3.2 presents Co_3O_4 and Mn_2O_3 crystallite size and dispersion values obtained from XRD spectra. The results indicate no specific correlation between the loading of the secondary metal and dispersion of the metals on the catalysts.

Table 3.2. Mn and Co oxides particle sizes and dispersions obtained from XRD spectra.

Catalyst	Mn_2O_3	Mn	Co_3O_4	Co
	Particle size (nm)	Dispersion (%)	Particle size (nm)	Dispersion (%)
Mn 10%/ γ-Al_2O_3	18	7	-	-
Mn10%-Co2.5%/ γ-Al_2O_3	26	5	N[a]	N[a]
Mn10%-Co5%/ γ-Al_2O_3	20	7	13	5
Mn10%-Co10%/ γ-Al_2O_3	23	6	9	7
Co10%/ γ-Al_2O_3	-	-	14	4
Co10%-Mn2.5%/ γ-Al_2O_3	N[a]	N[a]	21	3
Co10%-Mn5%/ γ-Al_2O_3	18	7	12	5
Co10%-Mn10%/ γ-Al_2O_3	18	7	12	5

[a] Not detected.

Figure 3.3 (a) shows the magnitude of the Fourier transform of Mn *K-edge* of the catalysts. The peak for Mn-O in the first coordination shell is similar for all the catalysts containing manganese oxide. However, the peak for Mn-Mn in the second coordination shell of Co10%-

Mn2.5% and Co10%-Mn5% is different from that of the other catalysts. In other words, local structure around manganese atom is similar for all the manganese-containing catalysts except for the catalysts with 2.5 and 5% manganese loading.

Figure 3.3 (b) shows the magnitude of the Fourier transform of Co *K-edge* EXAFS spectra of the catalysts. The first coordination shell (Co-O) is similar for all cobalt-containing catalysts. However, the peak for Co-Co in the second shell of Mn10%-Co2.5% and Mn10%-Co5% has shifted when compared to the Co-Co peak of the other catalysts. Therefore, the catalysts with 2.5 and 5% cobalt loading have different local structure around cobalt atom than the other cobalt-containing catalysts.

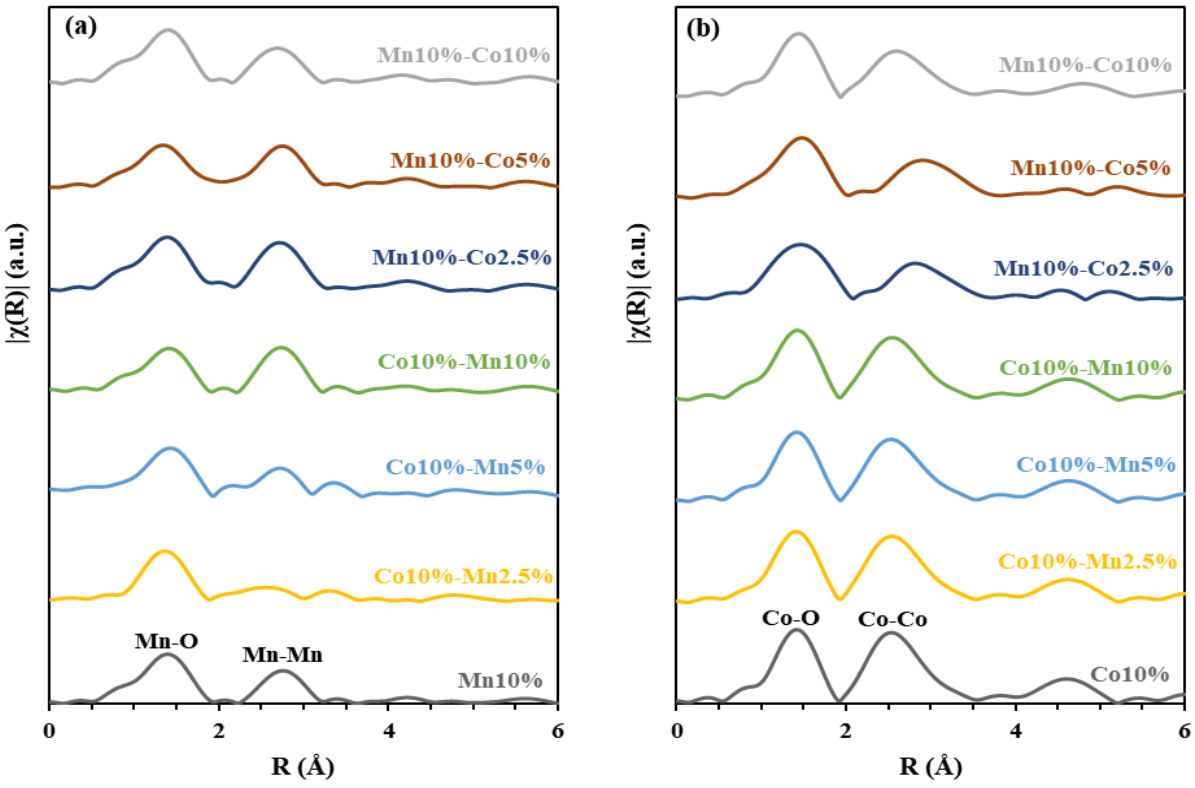

Figure 3.3. Magnitude of the Fourier transform of EXAFS spectra: (a) Mn K-edge; (b) Co K-edge.

Table 3.3 shows the presence of different phases of manganese oxide and cobalt oxide in the catalysts. These results were obtained from linear combination fitting of Mn *K-edge* and Co *K-*

edge XANES spectra. Mn_2O_3 is the dominant manganese phase in the catalysts that contain 10% manganese. Addition of cobalt to Mn10% catalyst did not change the formal oxidation state of manganese significantly. In contrast, Mn_3O_4 was the main manganese phase in the Co10%-Mn2.5% and Co10%-Mn5% catalysts. Increase in manganese loading decreased Mn_3O_4 and increased Mn_2O_3 content of the Co-Mn catalysts. Co_3O_4 is the dominant cobalt phase of the cobalt-containing catalysts except for Mn10%-Co2.5% and Mn10%-Co5% that contain significant amount of CoO phase as well. Addition of manganese to Co10% catalyst did not alter the formal oxidation state of cobalt.

Table 3.3. Result of linear combination fitting of Mn and Co K-edge XANES.

Catalyst	Mn_3O_4 (%)	Mn_2O_3 (%)	MnO_2 (%)	CoO (%)	Co_3O_4 (%)
Mn10 %/ γ-Al_2O_3	7	82	11	-	-
Mn10%-Co2.5%/ γ-Al_2O_3	20	80	0	45	55
Mn10%-Co5%/ γ-Al_2O_3	16	84	0	44	56
Mn10%-Co10%/ γ-Al_2O_3	7	85	8	16	84
Co10%/ γ-Al_2O_3	-	-	-	-	100
Co10%- Mn2.5%/ γ-Al_2O_3	69	29	2	-	100
Co10% -Mn5%/ γ-Al_2O_3	54	44	2	2	98
Co10%- Mn10%/ γ-Al_2O_3	27	73	0	3	97

Results obtained from XANES and XAFS analyses show that the local structure and oxidation state of transition metals (Mn or Co) formed during the first impregnation of the alumina remain unchanged even after addition of the secondary metal. In other words, Mn_2O_3 was the main manganese phase of Mn10%, and adding cobalt did not affect the manganese phase. Similarly, Co_3O_4 was the main cobalt phase of Co10%, and adding manganese did not influence the cobalt phase. On the other hand, as found by XANES, the oxidation states of the secondary metal changed, and by increasing the loading of the secondary metal, its oxidation state increased. This

agrees with the XRD results. The direct relationship between manganese loading and oxidation state has also been reported by Rezaei et al. [30].

3.4.2. Catalytic oxidation of acetone by ozone

Catalytic ozonation of acetone using single and mixed transition metal oxide catalysts was conducted at 25 °C. Figure 3.4 depicts acetone and ozone conversions using the eight catalysts at 150 min of the reaction. Acetone and ozone conversions increased by augmenting the Mn and Co-based catalysts with the secondary metal. However, the activity of the catalysts decreases as the loading of the secondary metal increases up to 10%. The order of adding metals in the catalyst preparation changed the catalytic properties. It can be observed that generally, Mn-based catalysts augmented by Co are more active than Co-based catalysts that are augmented by Mn. Mn oxides augmented with lower loading of Co showed the highest activity for the reaction. Both Mn10%-Co2.5% and Mn10%-Co5% catalysts achieved acetone conversion of approximately 84%. For Co-based catalyst, as Mn content increased, the catalyst activity kept decreasing. By adding appropriate content of Co to Mn-based catalyst, the acetone and ozone conversions increased by 26% and 54%, respectively. The results indicate about 53% and 52 % increase in acetone and ozone conversions by augmenting single Co catalyst with proper amount of Mn. Table 3.4 shows the reaction rates of acetone and ozone conversions on all studies catalysts. It can be observed that Mn10%-Co2.5% and Mn10%-Co5% had the highest acetone and ozone reaction rates.

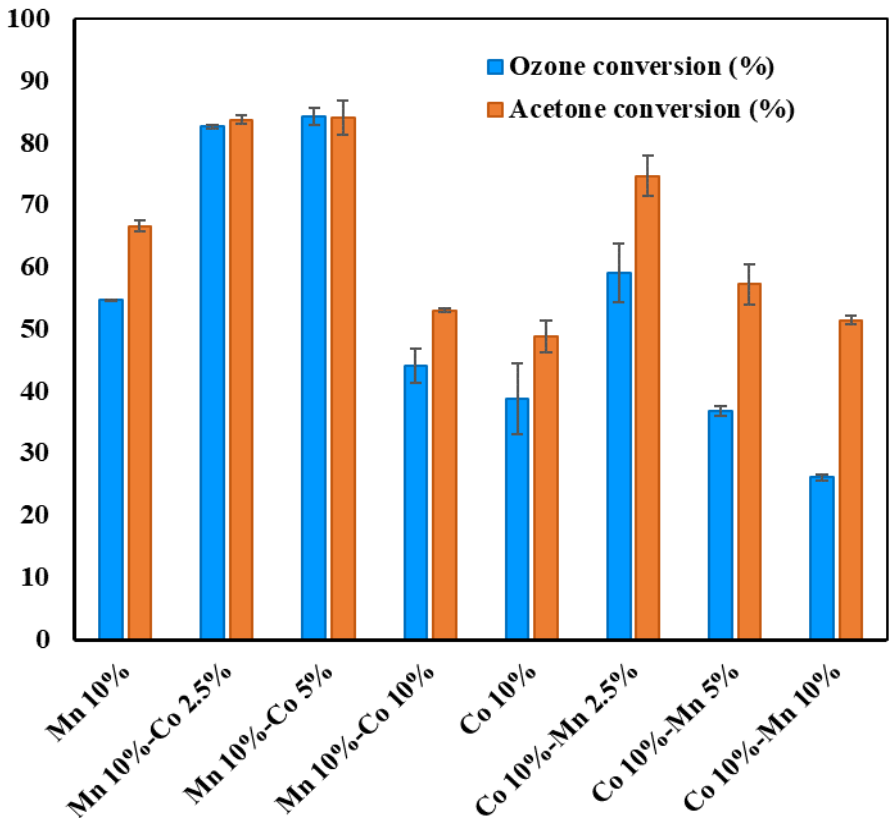

Figure 3.4. Acetone and ozone conversions (%) at 25 °C and 150 min of reaction, [acetone] = 150 ppm, and [O_3] = 1200 ppm, catalyst weight = 0.065 g, gas flow rate = 250 mL min^{-1}.

Table 3.4. Catalytic activity of single and mixed metal oxides catalysts for acetone ozonation at 150 min of reaction.

Catalyst	Acetone oxidation rate ($\times 10^5$ mol min^{-1} g^{-1})	Ozone decomposition rate ($\times 10^5$ mol min^{-1} g^{-1})	CO_x yield (%)
Mn10 %/ γ-Al_2O_3	1.57	11.26	91.31
Mn10%-Co2.5%/ γ-Al_2O_3	1.98	17.01	90.41
Mn10%-Co5%/ γ-Al_2O_3	1.98	17.34	90.53
Mn10%-Co10%/ γ-Al_2O_3	1.25	9.07	92.98
Co10%/ γ-Al_2O_3	1.15	8.00	95.71
Co10%- Mn2.5%/ γ-Al_2O_3	1.76	12.16	88.21
Co10% -Mn5%/ γ-Al_2O_3	1.35	7.60	91.48
Co10%- Mn10%/ γ-Al_2O_3	1.21	5.39	96.58

[a] [acetone] = 150 ppm, [O_3] = 1200 ppm, catalyst weight = 0.065 g, gas flow rate = 250 mL min^{-1}, 25 °C, Data were taken at 150 min of reaction.

The main reaction products of catalytic ozonation of acetone are CO and CO_2. The CO_x yields were determined for all catalysts and are shown in Table 3.4. CO_x yields for ozonation of acetone for all the catalysts were between 88% and 97%. The percentage of CO and CO_2 in the exhaust gas is presented in Figure 3.5. It should be mentioned that the results of CO_x yield and percentages of CO and CO_2 were comparable for all catalysts. The catalysts became gradually deactivated due to accumulation of carbonaceous species on their surface [21,29,79].

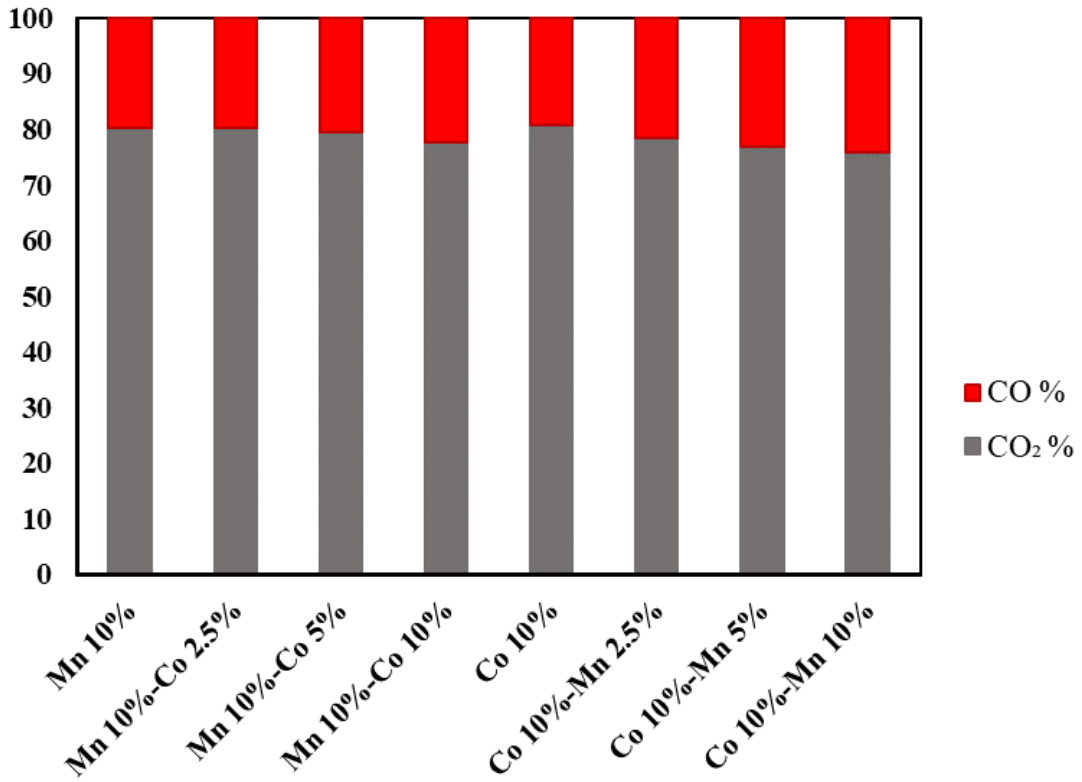

Figure 3.5. CO% and CO2% in the reaction product stream at 25 °C and 150 min of reaction, [acetone] = 150 ppm, and [O_3] = 1200 ppm, catalyst weight = 0.065 g, gas flow rate = 250 mL min^{-1}.

Long-term activity, as well as CO_x concentration, were determined for Mn10%-Co2.5% catalyst and the results are presented in Figure 3.6. The conversions of acetone and ozone after 24 h at 25°C reached 55 and 43%, respectively. CO_x concentrations and CO/CO_2 ratio remained almost unchanged within 24 h of reaction.

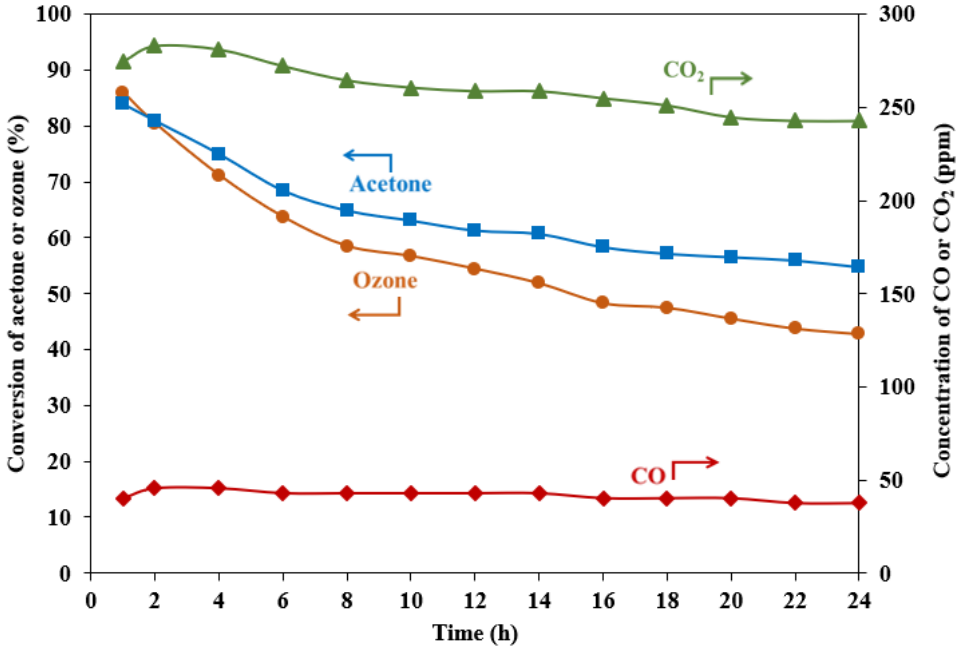

Figure 3.6. Long-term activity and product formation of Mn10%-Co2.5%/γ-alumina at 25°C, [acetone] = 150 ppm, and [O_3] = 1200 ppm, catalyst weight = 0.065 g, gas flow rate = 250 mL min^{-1}.

From the presented results, it can be understood that augmenting a single metal oxide catalyst improves its performance. However, the secondary metals at their lower loading of 2.5% or 5 % resulted in better decomposition of ozone and higher rate of acetone oxidation. In has been reported that in catalytic ozonation process, ozone decomposition occurs on the catalyst and active oxygen species are formed which are responsible for VOC oxidation [104,113]. Reed et al. have studied the effect of metal oxide loading from 3% to 20% on MnO_x/SiO_2 catalysts [113]. They have reported that lower oxidation states of higher loaded catalysts contribute to higher rate of acetone degradation. They suggested that when oxidation states of metal particles are lower, they could interact with ozone more easily to create active oxygen species. Einaga et al. [103] have investigated the structure of Mn oxides on alumina in different metal loadings in ozonation of benzene. They have concluded that catalysts with lower loadings (1-7.5%) have presented higher activities. Similar study by Rezaei et al. has found that catalysts with lower Mn oxidation states are more active in ozonation of toluene [30]. It has been reported that catalysts with lower

metal loadings have lower oxidation state and are more active in transferring electrons to ozone to induce ozone decomposition reaction [30].

3.4.3. In-situ DRIFTS studies and reaction pathway

The *in-situ* DRIFTS spectra of four selected catalysts during the reaction are depicted in Figure 3.7. According to Figure 3.7 (a-d), acetone is adsorbed on the catalysts. This can be confirmed by the characteristic acetone bands at 1371 and 1424-1427 cm^{-1}. The peak at around 1702 cm^{-1} (C=O stretching) and the broad band between 2400 and 3750 cm^{-1} (OH stretching) were other detected bands. Appearance of the peaks at 1590-1601 cm^{-1} (COO^- stretching of carboxylate species) confirmed adsorption of acetone which is partially oxidized to carboxylate groups [79,125,126]. A recent study has shown that in the presence of ozone, acetone is first oxidized to surface carboxylates; then, the surface carboxylates are further oxidized to alcohols, ketones, carboxylic acids, and eventually to carbon dioxide and carbon monoxide [79]. In a typical experimental run, after saturation of the catalyst with acetone, ozone was introduced into the system. New peaks appeared and the intensity of the characteristic peaks of acetone declined gradually as they are presented in the representative time spectra. As can be seen in Figure 3.7, the main bands are at around 1410-1427 (C–H asymmetric deformation vibration), 1462-1468 (methyl and methylene C–H bending), 1580-1600 (antisymmetric and symmetric COO^- stretching of carboxylates), 1700-1726 (C═O stretching of ketones and carboxylic acids), and 2700-3650 cm^{-1} (OH stretching of alcohols, carboxylic acids, and water). The intensity of the bands increased over the time of reaction.

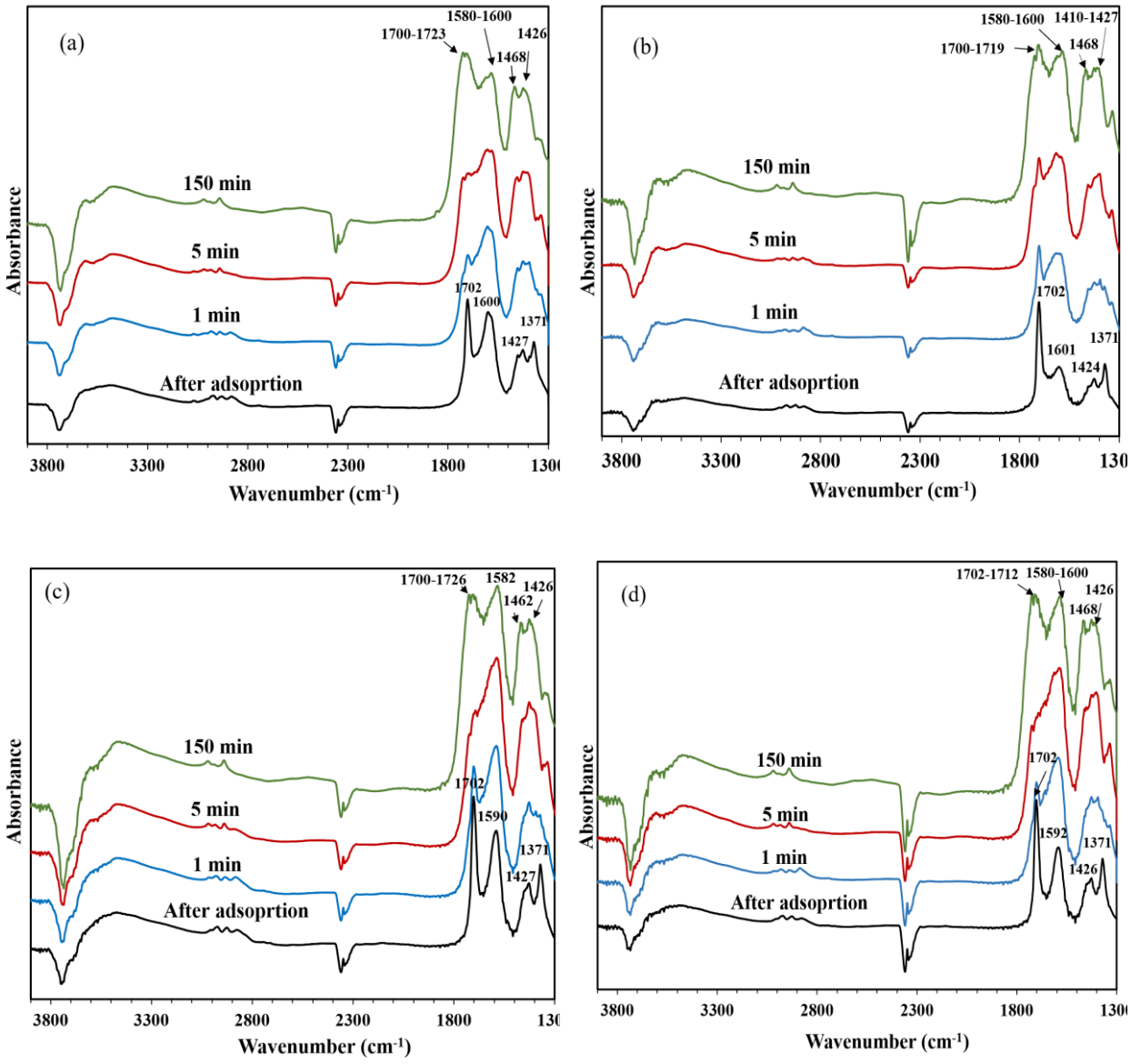

Figure 3.7. DRIFTS spectra of catalytic ozonation of acetone at 25 °C using alumina supported (a) Mn10%, (b) Co10% , (c) Mn10%-Co2.5%, and (d) Co10%-Mn2.5%; [acetone] = 150 ppm, [O^3] = 1200 ppm, catalyst weight = 0.065 g, gas flow rate = 250 mL min^{-1}.

By comparing the spectra of the four catalysts in Figure 3.7, it can be inferred that acetone degradation pathway is most probably the same for the alumina supported Mn10%, Co10%, Mn10%-Co2.5%, and Co10%-Mn2.5% catalysts. During adsorption of acetone, intensity of the peak at around 1600 cm^{-1} was relatively weaker in Co10% than other catalysts. This can suggest

that chemical adsorption was weaker in Co10%. However, the appeared peaks indicated that both chemical and physical adsorption occurred in all selected samples.

From the activity results discussed in Figure 3.4 and Table 3.4, addition of Mn2.5 % to Co-based catalyst and Co2.5 % to Mn-based catalyst enhances the activity of the single metal oxide catalysts. XANES and EXAFS studies indicate that the oxidation states and local structure of the primary metal does not change by addition of the secondary metal. Therefore, the secondary metal does not interact with the structure of the primary metal. As also can be observed in Figure 3.7, the single Mn 10% and Co 10% have similar spectra and it can be assumed that the reaction pathways on these two metals are the same.

It has been reported that ozone is decomposed on the surface of metal oxide catalysts to form atomic oxygen and peroxide species (Eqs. (3.3)-(3.5)). These studies have been carried out on supported manganese oxides [21,103,113] as well as cobalt oxides [75].

$$O_3 + \blacksquare \rightarrow O_2 + O\blacksquare \tag{3.3}$$

$$O_3 + O\blacksquare \rightarrow O_2 + O_2\blacksquare \tag{3.4}$$

$$O_2\blacksquare \rightarrow O_2 + \blacksquare \tag{3.5}$$

where ■ refers to surface of metal active sites.

Reed et al. studied catalytic ozonation of acetone over silica-supported Mn oxides with Mn loading from 3% to 20% [26]. They proposed that almost all the adsorbed acetone on the catalyst are located on silica sites. Therefore, silica acts as a reservoir for the acetone, which is physically adsorbed on the catalyst. Then, the adsorbed acetone molecules migrate to the Mn sites and react with active atomic oxygen. In another study on ozonation of acetone using alumina supported Mn oxides, it has been suggested by Aghbolaghy et al. that alumina is not an inert support. Alumina acts as reservoir for adsorbed acetone, and it also interacts with acetone to create surface carboxylate intermediates [79]. The role of alumina for catalytic ozonation of acetone

was studied by performing the reaction on pure alumina. Alumina alone was unable to oxidize the surface carboxylates that were formed, and Mn sites were essential for completing the oxidation process. According to *in-situ* DRIFTS results, the presence of similar bands for Mn 10 % and Co 10% catalyst suggest that both Mn and Co catalysts follow the same reaction pathway. In the case of Mn and Co mixed oxides, the intensity of the appeared peaks becomes stronger indicating the role of both metals in forming surface carboxylates in the reaction. It has been reported that lower oxidation states of Mn are preferable for ozonation of VOCs. This reason is attributed to the ability of Mn atoms in lower loaded sample in transferring electron to ozone [30,113]. In a similar research on supported Co oxide catalyst, enhanced activity of lower loading samples was related to increase in dispersion and decrease in oxidation state of cobalt which resulted in improved electron transferring ability and ozone utilization [75]. Therefore, lower oxidation states of Mn and Co in this work can enhance the ozone decomposition reaction and consequently the oxidation rate of VOCs.

In the presence of both Mn and Co sites, the surface carboxylates are oxidized to carboxylic acids, alcohols, and ketones, and eventually to CO and CO_2. According to the findings of this work and the results of the previous studies [79,100], it can be concluded that alumina, Mn, and Co are playing roles in ozone decomposition to create highly reactive atomically adsorbed oxygen species in the proposed mechanism. The incomplete oxidation of acetone and formation of undesired products accumulated on the catalysts cause gradual deactivation of the catalyst at 25 °C [79].

Based on the above discussion, the observed differences in the catalytic performance are due to structural differences between the catalysts. It has been reported by Einaga et al. that surface area plays an import role in increasing the catalyst activity in ozonation of benzene [29]. They found that irrespective of the type of the catalyst support, there is a linear relationship between specific surface area and reaction rate. In this work, it can be seen that by adding higher content of metal oxides on the support, the surface area decreases slightly. Although the activity of the catalyst increased considerably in Mn10%-Co2.5% and Co10%-Mn2.5% catalysts compared to single Mn10% and Co10%, the surface area decreased. Therefore, it can be deduced that surface area cannot justify the enhancement in catalyst activity.

On the other hand, researchers have reported the impact of metal loading on the oxidation state of metal and eventually catalyst activity [30,75,113]. The findings of this work also suggest the same conclusion about the effect of lower oxidation states on higher acetone conversion. In both alumina supported Mn and Co-based catalysts, by decreasing the loading of the secondary metal to 2.5%, its oxidation state decreased which led to higher conversions. It is suggested that Mn_3O_4 (mixed Mn oxidation state of +3 and +2) and CoO (oxidation state of +2) are the most active species among the observed Mn and Co phases. Mn_3O_4 and CoO constitute 20 and 45 % of the Mn and Co species in Mn10%-Co2.5% catalyst, respectively; while Mn10% catalyst contains only 7% Mn_3O_4 and Co10% catalyst contains no CoO. The catalysts containing higher amounts of CoO and Mn_3O_4 performed better than other catalysts.

3.5. Conclusions

Catalytic ozonation of acetone over a series of alumina supported single and mixed transition metal oxide catalysts was studied at room temperature. All catalysts lost their activity gradually at room temperature due to accumulation of intermediates on their surface. It was shown that addition of lower loading of the secondary metal to Co and Mn catalysts improved activity of the catalysts. By augmenting the catalyst with the second metal, the local structure and oxidation state of the primary metal remained the same. However, by changing the loading of the secondary metals, its oxidation state changed. It was suggested that activity of the catalysts is related to the metal's oxidation state and lower metal loadings (5 wt% or less) result in lower oxidation states. Catalysts having lower oxidation states are more active in transferring electrons to ozone, leading to higher ozone decomposition, and thus enhanced acetone oxidation.

Chapter 4:

Synthesis of MnO_x/Al_2O_3 Catalyst by Polyol Method and Its Application in Room Temperature Ozonation of Toluene in Air

The content of this chapter has been published in Journal of Catalysis Letters and presented in the following conferences:

Citation:

M. Ghavami, J. Soltan, N. Chen, Synthesis of MnO_x/Al_2O_3 catalyst by polyol method and its application in room temperature ozonation of toluene in air, Catalysis Letters (2021) 151:1418–1432.

Conference Proceedings:

M. Ghavami and J. Soltan, Comparison between polyol and impregnation method in preparation of alumina supported Mn oxides for oxidation of volatile organic compounds by ozone. 68th Canadian Chemical Engineering Conference, October 28-31, 2018, Toronto, Canada.

M. Ghavami and J. Soltan, Manganese oxide catalysts for ozonation of acetone and toluene: Effect of preparation method and calcination temperature. 69th Canadian Chemical Engineering Conference, October 20-23, 2019, Halifax, Canada.

Contribution of the Ph.D. candidate

Mehraneh Ghavami designed and performed all the experiments, generated, and analyzed the data, prepared all the figures and tables, and drafted and revised the manuscript. Dr. Jafar Soltan supervised, provided inspiration, scientific input, and guidance, commented on, and edited the manuscript. XANES and XAFS data were collected at the Canadian Light Source with the

assistance of Dr. Ning Chen. Dr. Ning Chen provided general guidance for analyses of the XAS data and revised the manuscript.

Contribution of this chapter to the overall Ph.D. Research

The second objective of the research is addressed in this section, which is "developing a novel method for catalyst preparation for ozonation of toluene in air at room temperature". Preparation procedure via polyol method and characterizations of catalysts are provided in this chapter. Experimental design using response surface methodology is used to estimate optimum conditions in polyol method. In addition, the impact of catalyst preparation on the activity of the catalyst is discussed.

4.1. Abstract

MnO_x/Al_2O_3-P catalyst was synthesized by polyol process and evaluated in catalytic ozonation of toluene in air at room temperature. The effects of polyol synthesis temperature and time were optimized using response surface methodology. The performance of the optimized polyol catalyst was compared with a catalyst prepared by the impregnation method (MnO_x/Al_2O_3-I). Polyol catalyst had higher toluene and ozone conversions with less carbon deposition and higher selectivity towards CO_2 in the product than the impregnated catalyst. Nearly 80 % of toluene was removed using MnO_x/Al_2O_3-P after 120 min of reaction, which is higher than MnO_x/Al_2O_3-I (70%). Characterization studies showed that MnO_x/Al_2O_3-P has smaller manganese particle size, higher dispersion, and higher surface area than MnO_x/Al_2O_3-I. Both catalysts were mostly composed of Mn^{3+} phase, while MnO_x/Al_2O_3-P had a higher amount of Mn^{2+}. The higher activity of the polyol catalyst is attributed to smaller manganese particle size, higher catalyst surface area, and lower oxidation state of manganese.

4.2. Introduction

Volatile organic compounds (VOCs) contribute significantly to air pollution in indoor environments and they can affect human health [127,128]. Some common sources of VOC emission in indoor air are personal care products, cleaning products, perfumes, glues, paints, solvents, building and construction materials, and tobacco smoke [129]. Toluene is a widely used solvent and one of the most common VOCs in indoor air [38,126,130]. Among VOCs, toluene appears to be one of the most resistant compounds to oxidize [88,131,132]. Catalytic ozonation is one of the promising techniques to eliminate VOCs in indoor air at low temperatures. Besides, inexpensive metals in the transition series can be used in catalytic ozonation instead of precious metals that are mostly used in catalytic combustion [75,133,134].

Catalytic ozonation of toluene has been studied using different catalysts such as MnO_x/Al_2O_3 [100,133,134], MnO_x/MCM-41[21], MgO/GAC [76], MnO_2/graphene [83], Mn and Ag/HZSM [126], and Zr/Ce_xO_2 [85]. Although many metal-based catalysts have been studied for the oxidation of various VOCs, among them, manganese is considered as one of the most active metals for ozonation of VOCs due to its activity in ozone decomposition, redox properties, and low cost compared to precious metals [135–137]. Among the possible supports for Mn, γ-Al_2O_3 is reported to exhibit the highest catalytic activity in ozonation of VOCs due to its large surface area and the ability to support Mn in its lower oxidation states [134].

Improving the catalytic activity and stability during the reaction is essential to enhance the performance of catalytic ozonation process. The catalyst's performance significantly depends on its preparation process and parameters such as the deposition methods of the active phase, and oxidative and reductive treatments [138]. Generally using metal particles with higher dispersion is essential to reduce coking issues that lead to catalyst deactivation [139]. It has been reported that the catalysts synthesized by polyol method have well-dispersed metal particles compared to the impregnation method [140,141]. In the polyol process, metal precursors go through dissolution and then reduction to metal ions and metal oxides form [142]. It has been noted in the literature that time and temperature of the synthesis reaction are the two important parameters that have a considerable impact on the nucleation rate as well as the growth rate of the metal particles [143,144]. In a typical polyol process, ethylene glycol (EG) acts as a reducing agent and

stabilizer. Besides, polyvinylpyrrolidone (PVP) can be used as a capping agent to prevent particle sintering and agglomeration [145,146]. By adjusting the preparation conditions in the polyol method, the morphology of the particles can be controlled [147].

A number of studies have been reported on the catalyst preparation by polyol process in the oxidation of VOCs. Lu et al. [141,147,148] prepared Cu, Co, Fe, and Ni catalysts supported on activated carbon (AC) using polyol method and used them in oxidation of xylene, toluene, and benzene in air. Bayrakdar et al. [139] used Al_2O_3 supported Ni catalysts synthesized by polyol method for partial catalytic oxidation of methane. The researchers in these investigations found that by using the polyol method, catalysts with higher dispersion of the active sites as well as higher thermal stability and catalytic activity were obtained. These studies were limited to catalytic oxidation of VOCs. However, catalytic ozonation using polyol catalyst has not been investigated so far. Moreover, the preparation and characteristics of alumina-supported manganese oxides produced with polyol methodology have not been reported. Room-temperature oxidation of toluene as a complicated compound has been a challenging reaction and only a few studies reported attempts to remove toluene at room temperature.

This study mainly focuses on the synthesis of alumina supported manganese oxides using polyol process by applying a statistical experimental design and response surface methodology (RSM) to optimize the synthesis parameters. The catalyst performance in the reaction was evaluated by RSM to obtain the conditions at which catalyst activity is maximum. The optimum polyol catalyst was prepared and evaluated in the removal of toluene at room temperature using catalytic ozonation reaction. The optimum catalyst properties and performance were compared with the catalyst prepared with impregnation method.

4.3. Experimental

4.3.1. Materials

γ-Al_2O_3 (S_{BET} = 220 m^2 g^{-1}) supplied by Alfa-Aesar was used as the catalyst support throughout this study. Manganese (II) acetate tetrahydrate (Sigma Aldrich, 99%) was used as the precursor for each catalyst. In the polyol technique, polyvynilpyrrolidone (PVP) (Sigma

Aldrich, K30, molecular weight = 40000) was used as a protective agent. Ethylene glycol (EG) (Sigma Aldrich, anhydrous, 99.8%) was used to reduce the metallic ions. No further purification treatment was done on the purchased materials prior to use.

4.3.2. Preparation of catalysts

4.3.2.1. Polyol MnO_x/Al_2O_3 catalyst

MnO_x/Al_2O_3 nanoparticles were synthesized using polyol method [140,141,149]. A schematic of the preparation method is given in Figure 4.1. The γ-Al_2O_3 support was ground and sieved into particle size less than 0.208 mm. Based on previous works, this catalyst size was chosen to eliminate transport resistance [64,102]. The experimental procedure was as follows: a given amount of the Al_2O_3 support was added to an ethylene glycol–PVP–Mn acetate precursor solution and the mixture was agitated with a magnetic stirrer overnight. Then, the suspension was heated to the target temperature (more details in section 4.4.1). The nominal ratio of the mass of manganese per mass of the catalyst was 5%. At the end of the reaction time, the mixture was rapidly cooled to room temperature using an ice bath. The catalyst thus obtained was separated using a centrifuge, and subsequently washed several times with ethanol and deionized water to remove the organic phase. Afterward, the catalyst was dried in an oven overnight and then was calcined in air at 475 °C for 4 h. Catalysts were denoted as MnO_x/Al_2O_3-P-X-Y (P denotes polyol, X and Y represent reaction temperature (°C) and reaction time (h), respectively).

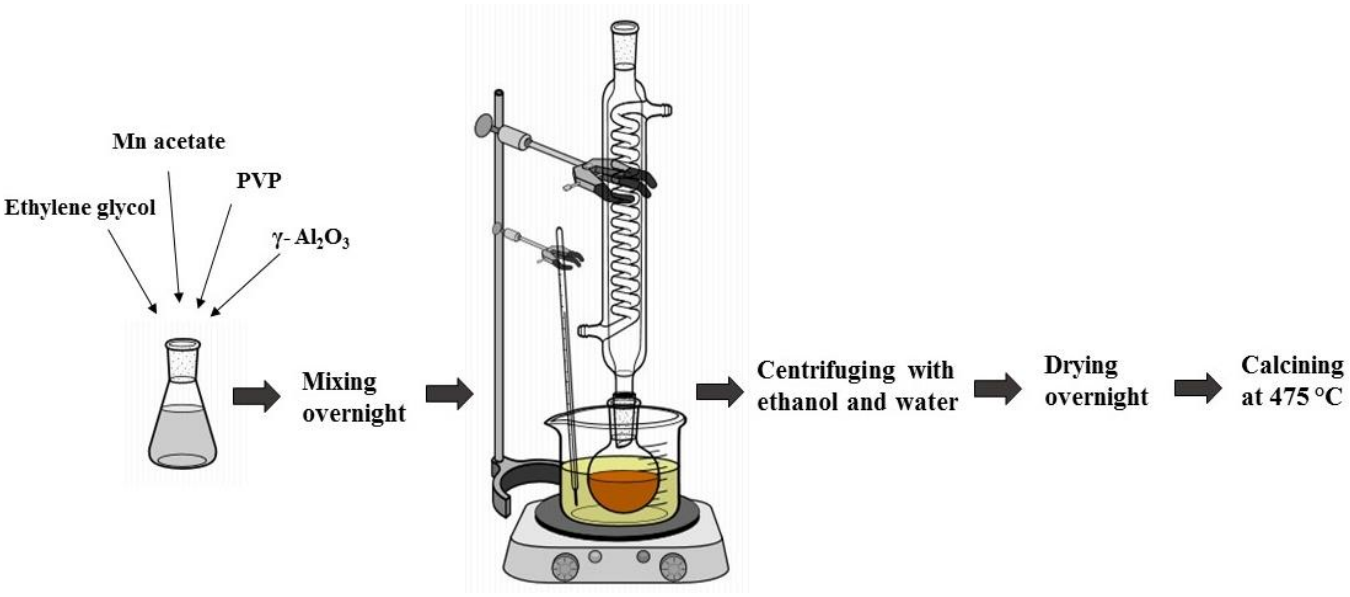

Figure 4.1.Schematic of the polyol preparation process

4.3.2.2. Impregnated MnO_x/Al_2O_3 catalyst

MnO_x/Al_2O_3 catalyst (catalyst designation: MnO_x/Al_2O_3-I, I denote impregnation) was prepared by dry impregnation method using powdered support with particle size less than 0.208 mm. Nominal mass of Mn per mass of the catalyst was used to eventually achieve the same actual loading as polyol sample (Based on the ICP-MS analysis on polyol sample explained in section 4.3.4). The synthesized catalyst was dried in oven overnight and then calcined for 4 h at 475 °C in air. Then, the catalyst was crushed and sieved to a final particle size of less than 0.208 mm.

4.3.3. Application of RSM for optimization of the catalyst

Design of experiments was conducted using optimal (custom) design as one of the classes of response surface methodology (RSM) to obtain optimum level of the catalyst activity in removal of toluene as a function of the catalyst synthesis parameters in polyol preparation process. The two selected operating parameters; reaction temperature (factor *A*,°C) and reaction time (factor *B*, h) were optimized using RSM based on D-optimal design method. In this method, the effects of factors influencing the process were investigated by performing 16 sets of experiments for a

replicated five points. These two factors play an important role in catalyst structure and morphology impacting catalyst activity [142,143,150,151]. The Design Expert® 11.0.5.0 (STAT-EASE Inc., Minneapolis, USA) software was used in the regression and graphical analyses of the data. The statistical analysis of the model was applied to evaluate the analysis of variance (ANOVA). In the modeling, two cubic models were developed to predict ozone and toluene conversions as model responses as a function of the two variables (synthesis reaction temperature and time). The models were eventually maximized to determine the catalyst synthesis temperature and time at which ozone and toluene conversions are highest. The optimized polyol catalyst was designated as MnO_x/Al_2O_3-P.

4.3.4. Catalyst characterization

The Brunauer–Emmett–Teller (BET) surface area and pore volume of catalysts were determined by nitrogen adsorption using an ASAP 2020 (Micromeritics) instrument. The catalysts were degassed for 2 h at 110°C and 0.5 mm Hg prior to the surface area and pore volume measurements. Transmission electron microscopy (TEM) was conducted with a Jeol 2010F field emission gun (FEG) operated at 200 keV to obtain particle size and dispersion of active site on the support surface. TEM instrument was equipped with high-angle annular dark-field (HAADF) and energy dispersive X-ray (EDX) spectroscopy attachments to determine the elemental composition and element mapping of the catalysts. For TEM, the samples were ultrasonically dispersed in ethanol and a drop of the solution was then placed on a porous carbon film supported on the Cu grid.

Dispersion (D) of the supported Mn catalyst was estimated from measured average manganese particle size obtained from TEM analysis, according to the following formula [152–154]:

$$D = \frac{6M}{a\rho Nd} \quad (4.1)$$

where M is molar mass of Mn; a is Mn atom surface area; ρ is density of Mn; d is mean metal particle size and N is the Avogadro number.

The actual manganese loading on the support was determined with an inductively coupled plasma mass spectrometer (ICP-MS) on an Agilent, 7700x instrument. Thermogravimetric analysis was used to analyze temperature-programmed weight loss of the polyol catalyst. A thermal analyzer (TGA Q500, TA Instruments) with standard furnace type was employed for this purpose. Samples were heated with the rate of 10 °C/min to 1000 °C under air and nitrogen flow.

X-ray diffraction (XRD) spectra were collected by a Rigaku Ultima IV X-Ray (Cu source, wavelength 1.54056Å) system in the 2θ range of 10–80° with a step size of 0.04°. X-ray Photoelectron Spectroscopy (XPS) measurements were performed using a Kratos (Manchester, UK) AXIS Supra system. The survey scan spectra were collected with a step size of 1 eV and a pass energy of 160 eV. High-resolution scans were conducted using 0.05 eV steps with a pass energy of 20 eV. Deconvolutions of the XPS spectra were performed using a CasaXPS® software.

Hydrogen temperature-programmed reduction (H_2-TPR) was carried out using 60 mg catalyst. The samples were preheated at 400 °C for 1 h in 100 ml/min of oxygen-nitrogen (50–50 v%) flow to remove excess moisture and then cooled to room temperature in a N_2 stream. The TPR experiments were conducted in 80 ml/min flow in a mixture of 3% H_2 balanced with N_2.

X-ray absorption near edge structure (XANES) of Mn K-edge was collected at the HXMA beamline of the Canadian Light Source. Catalysts were diluted with boron nitride (BN), ground, and pressed to thin disks. The prepared disks were protected by Kapton tape. All measurements were carried out in transmission mode using straight ion chamber detectors filled with helium gas. Data processing was performed by ATHENA® software.

4.3.5. Experimental setup of catalytic ozonation

Catalytic ozonation was conducted in a Pyrex glass reactor, installed horizontally in an oven (Binder, FP 115) with the experimental setup shown in Figure 4.2. Ozone was produced using an ozone generator (AZCO Industries LTD, HTU-500S) from oxygen stream (Praxair, 99.993%). The produced ozone was mixed with a stream of toluene/nitrogen (Praxair, 300 ppm toluene balanced with nitrogen) and nitrogen (Praxair, 99.999%) to establish respectively 120 and 1000

ppm of toluene and ozone at the inlet of the reactor. Flow rates of the streams were set using three Brooks, SLA 5850 mass flow controllers. 0.2 g of powdered catalysts were used for activity measurement. Catalysts were packed between two pieces of glass wool and the rest of the reactor was filled with glass beads. The total flow rate at the inlet of the reactor was 1000 ml/min (STP) resulting in a weight hour space velocity (WHSV) of 300 Lh^{-1} g^{-1}. Prior to introducing ozone to the system, toluene, nitrogen, and oxygen were passed over the catalyst bed until the catalyst became saturated and the outlet concentration of toluene reached the inlet level (120 ppm). Then, the ozone generator was turned on and ozonation of toluene was started at 25°C. The exhaust gas was passed through a long-path gas cell (PIKE, volume 0.1 L, 2.4 m optical length, KBr window) and analyzed using a coupled Nicolet iS50 FTIR spectrometer. FTIR spectra were collected at a resolution of 4 cm^{-1} by a deuterated L-alanine doped triglycine sulfate (DLaTGS) detector in the range of 4000-400 cm^{-1}. By using this detector and configuration, a high linearity for the gas phase analyses was obtained. A homogeneous reaction between ozone and toluene was negligible in this reaction.

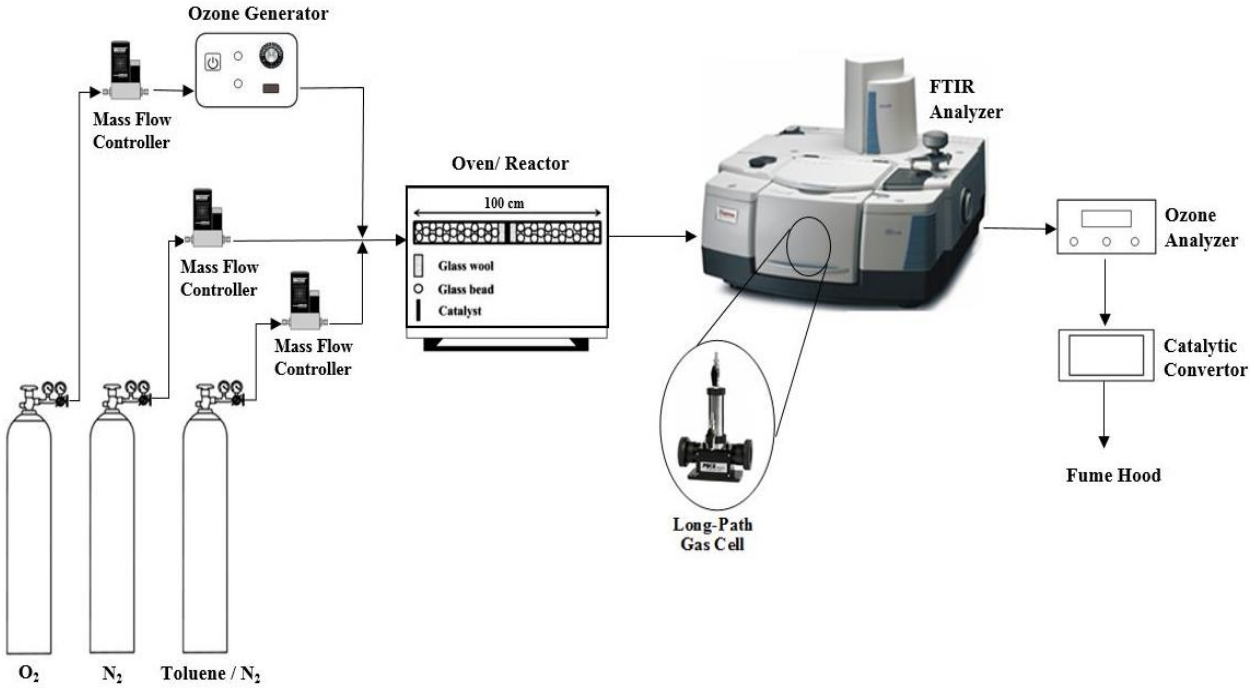

Figure 4.2.The experimental setup for catalytic ozonation of toluene in gas phase.

To perform DRIFTS (diffuse reflectance infrared Fourier transform spectroscopy) analyses, another configuration of the experimental set up was used, in which the long-path gas cell was replaced with a DRIFTS accessory (Harrick, Praying Mantis) on the FTIR spectrometer. Then, the reaction chamber, equipped with ZnSe windows, was coupled with the DRIFTS accessory and the FTIR spectrometer. To achieve higher sensitivity and faster scanning, a narrow band mercuric cadmium telluride (MCT-A) detector was used for DRIFTS operations. Spectra were collected at a resolution of 4 cm^{-1} in the range of 3900–1300 cm^{-1} to avoid saturation of the MCT-A detector.

4.3.6. Temperature-programmed (TPD, TPO) studies and byproducts identification

Temperature-programmed desorption (TPD) and temperature-programmed oxidation (TPO) studies were performed in a modified experimental setup described in detail elsewhere [75]. The reaction was performed in a reaction chamber (Harrick, HVC) equipped with a heater that allowed operation up to 900 °C. Catalyst weight and reaction gas flow rate were set to 50 mg and 250 ml/min to maintain WHSV of 300 Lh^{-1} g^{-1}. For TPD, the spent catalyst was immediately purged with nitrogen for 10 minutes after 120 min of reaction. Then, the catalyst was heated to 860 °C at a rate of 20 °C/min under N_2 flow. Similarly, for TPO, the spent catalyst was purged with N_2 for 10 minutes, and then followed by heating to 745 °C at 10 °C/min under the flow of 20 v% O_2 and 80 v% N_2.

A gas chromatograph (GC, Agilent, 7890A) coupled with a mass spectrometer (MS, Agilent, 5975C) was employed to identify the carbonaceous species accumulated on the catalyst. The extraction was conducted by washing the used catalysts with dichloromethane. The gas chromatograph was equipped with an Agilent standard HP-5MS column.

4.4. Results and discussion

4.4.1. Design of experiments for synthesis of optimized catalyst with polyol method

The synthesis reaction temperature and time are the two most important parameters in polyol method affecting the structure and morphology of the catalyst and subsequently catalyst activity in ozonation of toluene [143]. The ranges for these two independent variables were set between 140°C and 200°C for temperature and between 0.5 and 4 h for time, based on previous reports in the literature [139,140,146,155,156]. Response surface methodology (RSM) using Design Expert® software was used to design the required experiments to obtain the optimum condition in which the catalyst exhibits the highest activity. RSM is an appropriate method for obtaining a reliable correlation between independent variables and responses [157]. According to the design obtained from the software, 16 experiments, including 5 replicates were carried out to optimize catalyst synthesis variables (reaction time and temperature) for catalytic ozonation experiments. Each of the 16 catalysts was tested in the catalytic ozonation system. Table 4.1 shows ozone and toluene conversions in the 16 runs after 120 min of catalytic ozonation. It can be observed that with changing polyol synthesis time and temperature, ozone conversion varied between 32.1% and 56.1% and toluene conversion was within the range of 45.2% and 76.2 % observed for MnO_x/Al_2O_3-P-140-0.5 and MnO_x/Al_2O_3-P-166-2.05 samples, respectively.

Table 4.1.The experimental results of catalytic ozonation of toluene in gas phase using polyol catalysts synthesized at various temperatures and times in the 16 runs designed by Surface Response Methodology.

Run	Temperature (°C)	Time (h)	Ozone conversion (%)	Toluene conversion (%)
1	163	3.31	53.9	73.7
2	140	0.50	32.1	45.2
3	180	4.00	51.9	70.2
4	193	1.81	52.2	70.4
5	171	0.50	45.0	59.8
6	181	2.69	52.1	72.2
7	200	0.50	50.6	67.3
8	166	2.05	56.0	76.2
9	200	3.08	42.0	62.2
10	140	4.00	50.6	65.3
11	140	2.25	54.1	71.1
12	140	4.00	50.1	64.0
13	200	3.08	42.7	62.1
14	200	0.50	49.8	67.4
15	180	4.00	51.8	71.1
16	140	0.50	33.8	46.3

4.4.2. Optimization of the catalyst synthesis parameters and statistical analysis using RSM

The obtained results from 16 experiments were entered in the Design Expert, version 11 software, and two cubic models were developed to fit the results for toluene and ozone conversions as a function of the catalyst synthesis temperature and time:

(4.2)

$$Ozone\ conversion\ (\%) = -68.62067 + 0.342847\ \mathrm{A} + 62.81683\mathrm{B} + 0.018019\ \mathrm{AB} + 0.003614\ A^2 - 22.86784\ B^2 - 0.001268 A^2 B + 0.065727\ AB^2 - 0.000012\ A^3 + 1.42380\ B^3$$

(4.3)

$$Toluene\ conversion\ (\%) = -525.79992 + 8.68924\ \mathrm{A} + 50.33089\ \mathrm{B} + 0.263463\ \mathrm{AB} - 0.045811A^2 - 25.11159\ B^2 - 0.002113\ A^2B + 0.075079\ AB^2 + 0.000085\ A^3 + 1.38565\ B^3$$

Where *A* and *B* represent the temperature (°C) and time (h) of the synthesis with the polyol method, respectively.

The obtained experimental data for ozone and toluene conversions were analyzed using analysis of variance (ANOVA) and the results are presented in Tables 4.2 and 4.3. The ANOVA tables of the cubic models show that both models are significant based on the models' large F-value and small p-values. Furthermore, the ANOVA tables were used to determine the significance of the models' different terms. In general, terms with p values less than 0.05 show that model terms are significant. Values greater than 0.1 indicate model terms are not significant. Essentially, the smaller the P-value, the greater the contribution of the equivalent model terms toward the responses [157,158].

As demonstrated in Table 4.2 for prediction of ozone conversion, the catalyst preparation parameters; temperature (*A*) and time (*B*), all interaction between them, and the cubic term B^3 are significant as p-values for them are less than 0.05. In the case of toluene conversion (Table 4.3), variable *A* in a cubic model, all interaction between *A* and *B*, the quadratic terms of A^2 and B^2, and the cubic term of B^3 are significant. Overall, the statistical analysis for both models indicated that the lack of fit were insignificant and that is essential for a model to be accurately applied for prediction of the responses [157]. This indicates that there was only a 0.01% chance that the "Model F-value" could have occurred due to noise.

Table 4.2. ANOVA of the cubic model for prediction of ozone conversion

Source	Sum of Squares	df	Mean Square	F-value	p-value	
Model	746.64	9	82.96	230.43	< 0.0001	significant
A-Temperature	2.41	1	2.41	6.71	0.0412	
B-Time	2.16	1	2.16	6.01	0.0497	
AB	113.74	1	113.74	315.92	< 0.0001	
A^2	59.53	1	59.53	165.36	< 0.0001	
B^2	90.99	1	90.99	252.73	< 0.0001	
A^2B	4.35	1	4.35	12.08	0.0132	
AB^2	34.80	1	34.80	96.67	< 0.0001	
A^3	0.0209	1	0.0209	0.0581	0.8176	
B^3	11.60	1	11.60	32.23	0.0013	
Residual	2.16	6	0.3600			
Lack of Fit	0.0202	1	0.0202	0.0471	0.8368	not significant
Pure Error	2.14	5	0.4280			
Cor Total	748.80	15				
R^2	0.9971		Std. Dev.	0.6		
Adjusted R^2	0.9928		Mean	48.04		
Predicted R^2	0.9864		C.V. %	1.25		

Table 4.3. ANOVA of the cubic model for prediction of toluene conversion

Source	Sum of Squares	df	Mean Square	F-value	p-value	
Model	1176.98	9	130.78	313.91	< 0.0001	significant
A-Temperature	4.80	1	4.80	11.53	0.0146	
B-Time	0.1477	1	0.1477	0.3544	0.5734	
AB	113.12	1	113.12	271.52	< 0.0001	
A^2	97.20	1	97.20	233.31	< 0.0001	
B^2	188.00	1	188.00	451.26	< 0.0001	
A^2B	12.07	1	12.07	28.98	0.0017	
AB^2	45.41	1	45.41	109.01	< 0.0001	
A^3	0.9712	1	0.9712	2.33	0.1777	
B^3	10.99	1	10.99	26.38	0.0021	
Residual	2.50	6	0.4166			
Lack of Fit	0.6346	1	0.6346	1.70	0.2489	not significant
Pure Error	1.86	5	0.3730			
Cor Total	1179.48	15				
R^2	0.9979		Std. Dev.	0.6455		
Adjusted R^2	0.9947		Mean	65.28		
Predicted R^2	0.9488		C.V. %	0.9887		

The 3D plots of the cubic models help to understand the effect of independent variables on the responses and to determine the optimum condition. Figure 4.3 (a) and (b) show the effect of temperature and time of the polyol catalyst preparation on ozone and toluene conversions. According to Table 4.2 and Figure 4.3 (a), both terms of temperature (A) and time (B) are significant and have an impact on the response (ozone conversion). It can be observed that an increase in the level of catalyst preparation temperature and time, would result in improving ozone conversion. Although, with a further increase in the value of these two variables, no considerable improvement is noticed in ozone conversions. The impact of these variables on

toluene conversions is almost the same based on Table 4.3 and Figure 4.3 (b). According to the results, the most suitable catalyst preparation conditions for maximum ozone and toluene conversions occur when time is kept between 2 and 3 h and temperature is between 150 and 180°C. To compare the interaction of the two variables on ozone and toluene conversions, contour plots are shown in Figure 4.4. The measured suitable conditions are close to the conditions for the synthesis of supported metal catalysts reported in the literature [156].

By analyzing Figure 4.3 (a) and (b), it can be concluded that reduction temperature plays an important role in the activity of the catalysts prepared by polyol technique. It has been reported in the literature that metal particle size increases by increasing the reduction temperature during the polyol method preparation [151]. The effect of synthesis reduction time on MnO_x/Al_2O_3 indicated that adequate reaction time is essential for a complete reduction and a catalyst prepared with short reaction time does not show high activity. In this work, catalyst activity is maximum at the time of 1.5-3 h of the reduction, depending on the synthesis temperature. Lee et al. investigated the effect of reaction time in the polyol method from 10 min up to 4 h on CoNi particles at 180°C. They reported that until 2 h, metal particle sizes remained unchanged. Whereas if the reaction time increased to 4 h, particle sizes increased [150]. The influence of reduction time and temperature of polyol process over Cu-Zn/γ-Al_2O_3 catalyst in NO reduction with CO was investigated by Tseng et al. [143]. They observed that the catalytic activity in the samples prepared at an appropriate temperature is relatively higher than the samples synthesized at either lower or higher temperatures. However, their work investigated the impact of polyol synthesis parameters while the other parameter was kept constant, thus, the interaction of the parameters was not studied.

The optimum values of the selected variables were determined using a numerical optimization method in the Design Expert 11.0.5.0 software. The objective of this study was to determine the best conditions for the preparation of MnO_x/Al_2O_3 by the polyol method in which the activity of the catalyst in the reaction is maximum. It was predicted by the software that the highest ozone and toluene conversions would be 56 and 76 %, which would occur at the optimum conditions of 160 °C and 2.31 h of the polyol synthesis reaction. To confirm the validity of the developed model in the optimization, a catalyst with the optimized synthesis conditions using the polyol method was prepared and used in the catalytic ozonation of toluene. Duplicate verification

experiments were conducted and the average points for ozone and toluene conversions were found to be 58 and 80 %, respectively. The results are in good agreement with the predicted values obtained from the presented models.

To consider the validity of the model, the predicted ozone and toluene conversions were plotted versus the actual values at the 16 design points, as illustrated in Figure 4.5 (a) and (b). The actual values were determined from the experimental runs, and the predicted values were calculated from the presented models (Eqs. (4.2) and (4.3)). The R-squared and adjusted R-squared of the regression line for prediction of ozone conversion were found to be 0.9971 and 0.9928, respectively. These values for toluene conversions were 0.9979 and 0.9947, respectively. The reasonable agreement between R-squared and adjusted R-squared and their high value (close to 1) indicated that the models were describing a valid compromise between the experimental and predicted values at the design points.

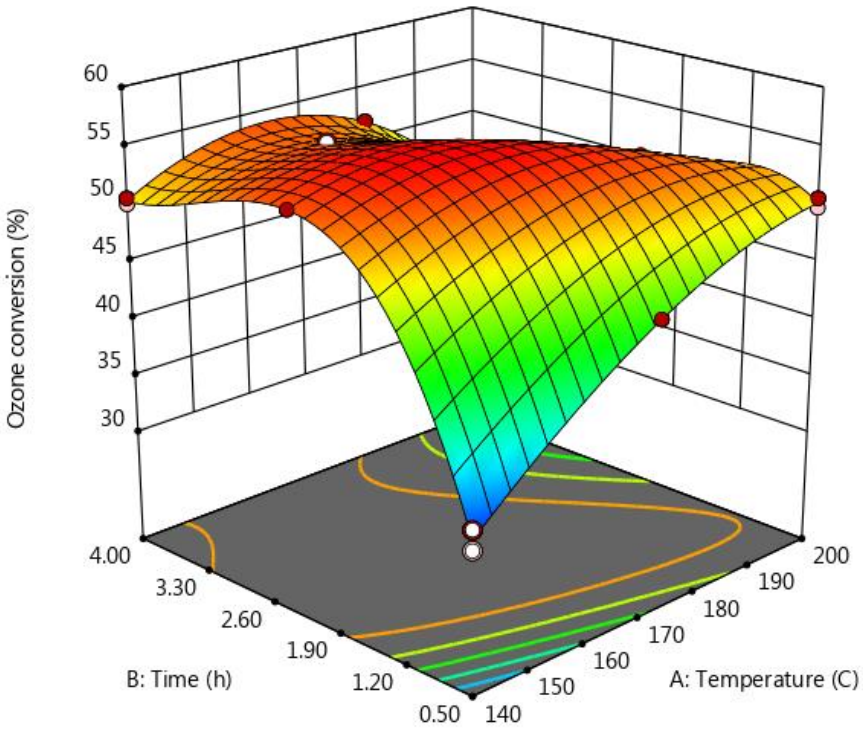

(a)

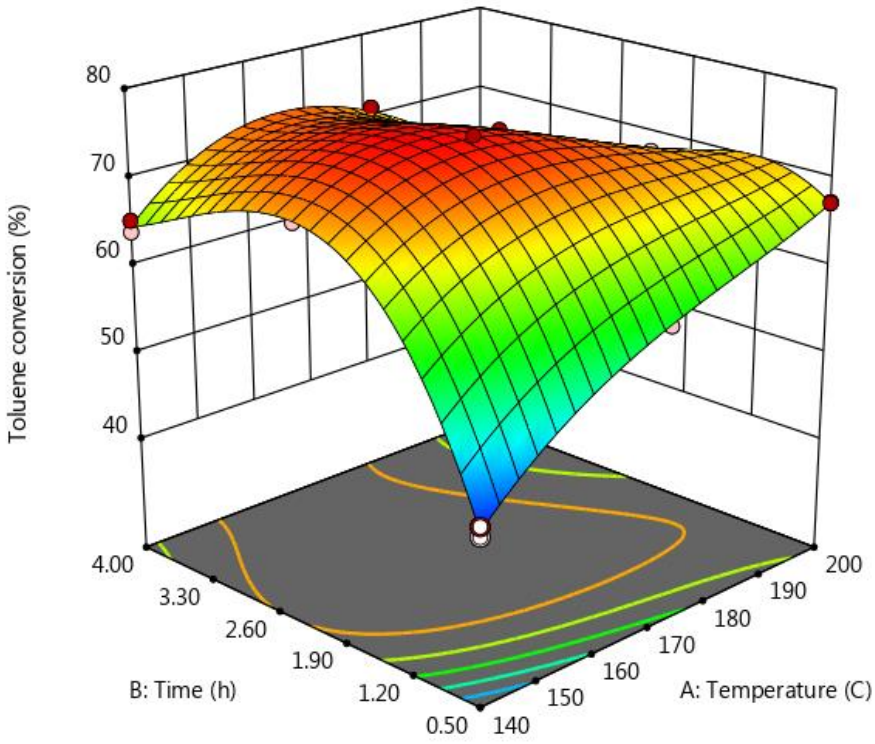

(b)

Figure 4.3. 3D response surface plot of the predicted (a) ozone conversion (%) and (b) toluene conversion (%) as a function of polyol synthesis temperature and time.

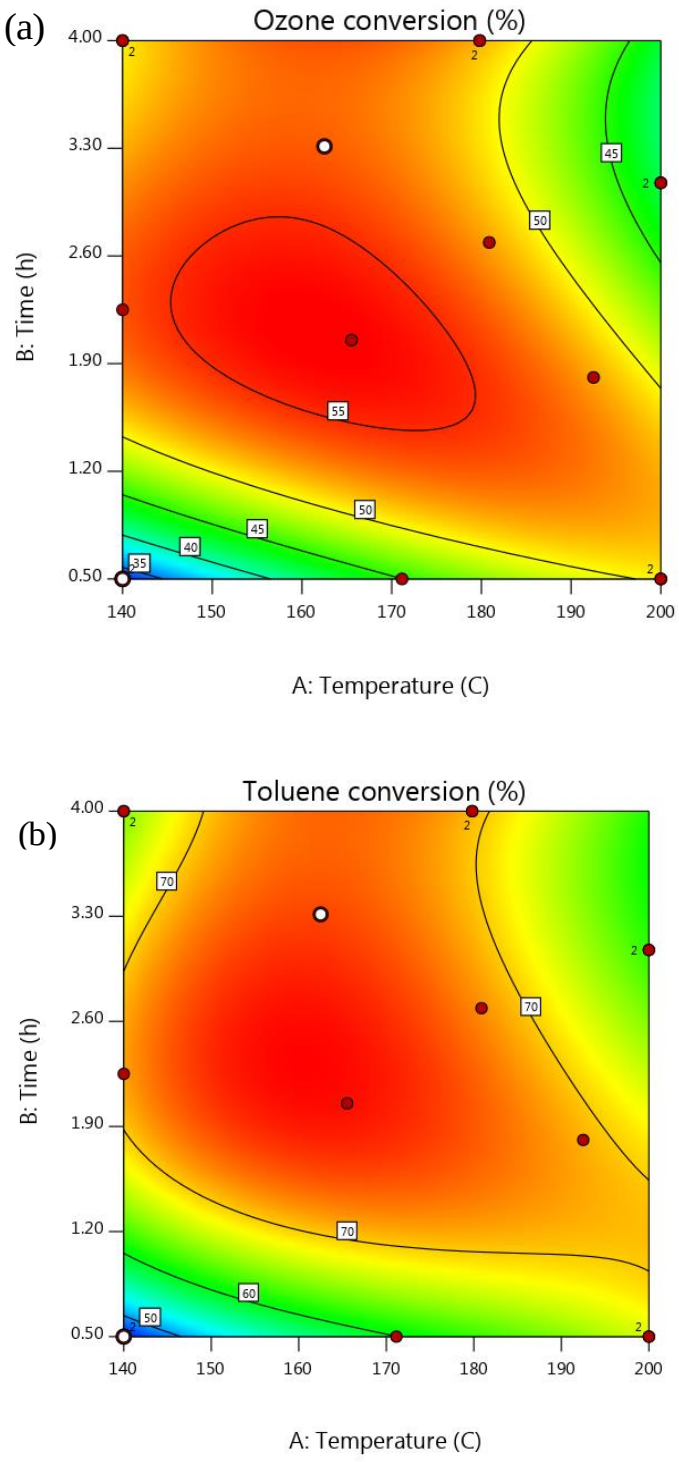

Figure 4.4.Contour plots of (a) ozone conversion (%) and (b) toluene conversion (%) as a function of polyol synthesis temperature and time.

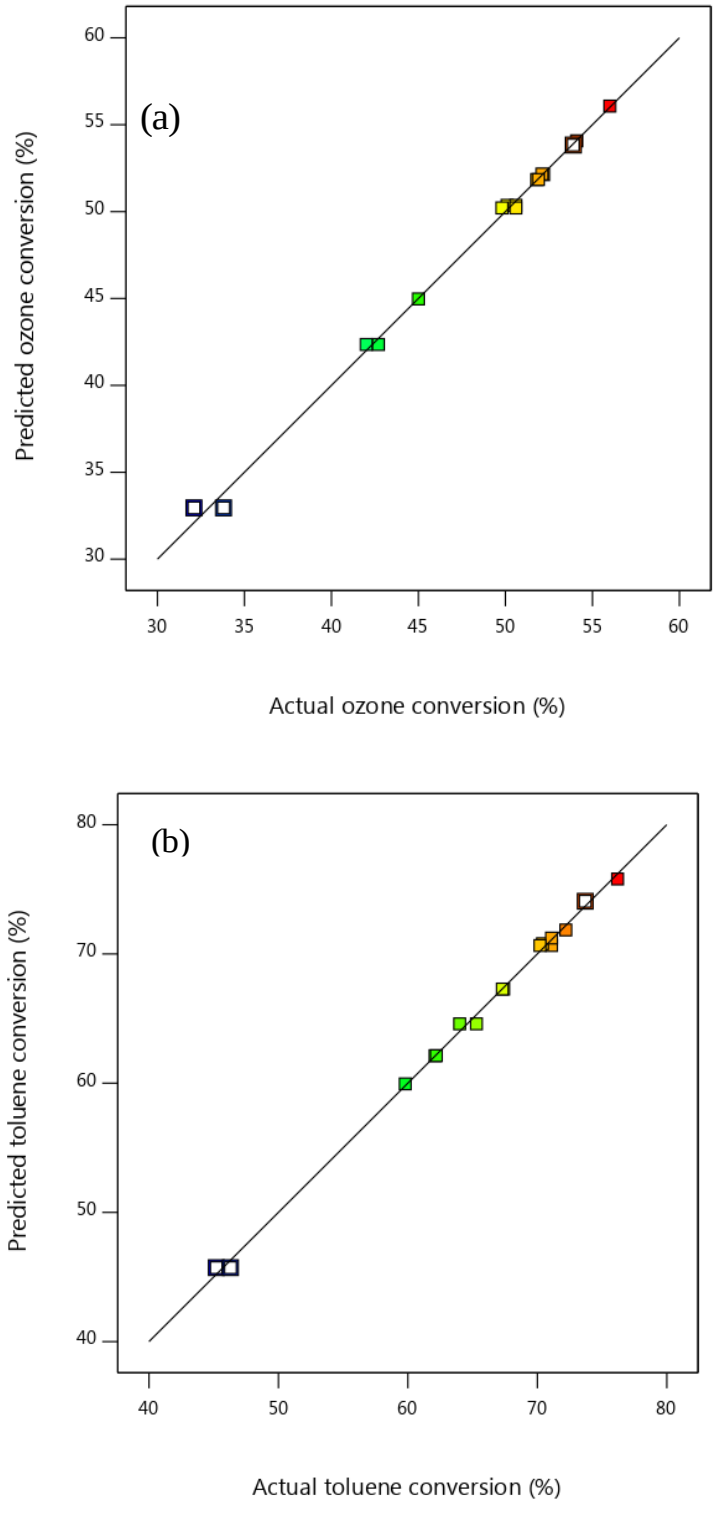

Figure 4.5.Plot of the actual and predicted values for (a) ozone conversion (%), (b) toluene conversions (%).

All the characterization studies were performed on the optimum polyol catalyst as well as the impregnated catalyst named MnO_x/Al_2O_3-P and MnO_x/Al_2O_3-I, respectively. The physical and chemical characteristics of the samples are given in Table 4.4. It can be observed from the BET surface area and pore volume results that the method of preparation affects the textural properties of the catalysts. The MnO_x/Al_2O_3-P showed higher specific surface area and pore volume than MnO_x/Al_2O_3-I. Similar results were reported by Soni et al. [145] and Naeem et al. [159] on supported metallic catalyst prepared by polyol and impregnation methods. The catalysts with high surface area have a large contact area for the reactants, resulting in high reaction activity.

Table 4.4.Physical and chemical parameters of the catalyst prepared by polyol and impregnation methods.

Catalyst	BET surface area (m^2/g)	Pore volume (cm^3/g)	Mn particle size [a] (nm)	Mn dispersion [b] (%)	Element contents (at. %) [c]		
					Mn	O	Al
MnO_x/Al_2O_3-P	198	0.57	3.9	27.8	1.64	63.22	35.14
MnO_x/Al_2O_3-I	177	0.52	5.3	20.4	1.43	64.72	33.85

[a] determined from TEM.
[b] calculated from eq. 4.1.
c determined by EDX analysis.

The manganese content of the MnO_x/Al_2O_3-P was measured by ICP-MS analysis to determine the actual loading of the catalyst. The results showed that the actual manganese content was 3.5 wt% and it is below the nominal value (5 wt%). Therefore, loading efficiency of the polyol prepared catalyst is 70% which is a common observation based on the similar studies using acetate precursor for polyol process [139,147]. The counterpart sample with impregnation method then was prepared by setting the nominal loading to finally obtain approximately 3.5 wt%; based on the fact that the actual loading of impregnation method in alumina supported Mn oxides catalyst is very close to the target loading [21,100,133].

Figure 4.6 shows the TEM images, metal particle size distribution, and HAADF-STEM image and EDX maps of MnO_x/Al_2O_3-P and MnO_x/Al_2O_3-I catalysts. It can be observed that the size of the manganese particles of Mn/Al_2O_3-P is smaller than that of Mn/Al_2O_3-I catalyst and consequently higher dispersion of manganese clusters can be expected. The average manganese

nanoparticle is nearly 3.9 and 5.3 nm in Mn/Al_2O_3-P and Mn/Al_2O_3-I catalysts, respectively. The HAADF-EDX analysis was used to identify the chemical composition of the samples. It confirmed the presence of manganese, aluminum, and oxygen in the structure of the catalyst and the uniform distribution of all elements throughout the samples. According to the EDX results, the manganese content of polyol and impregnated samples were 4.1 wt% and 3.9 wt%, respectively, which are in agreement with the experimental conditions and the results obtained from ICP-MS analysis.

(a)

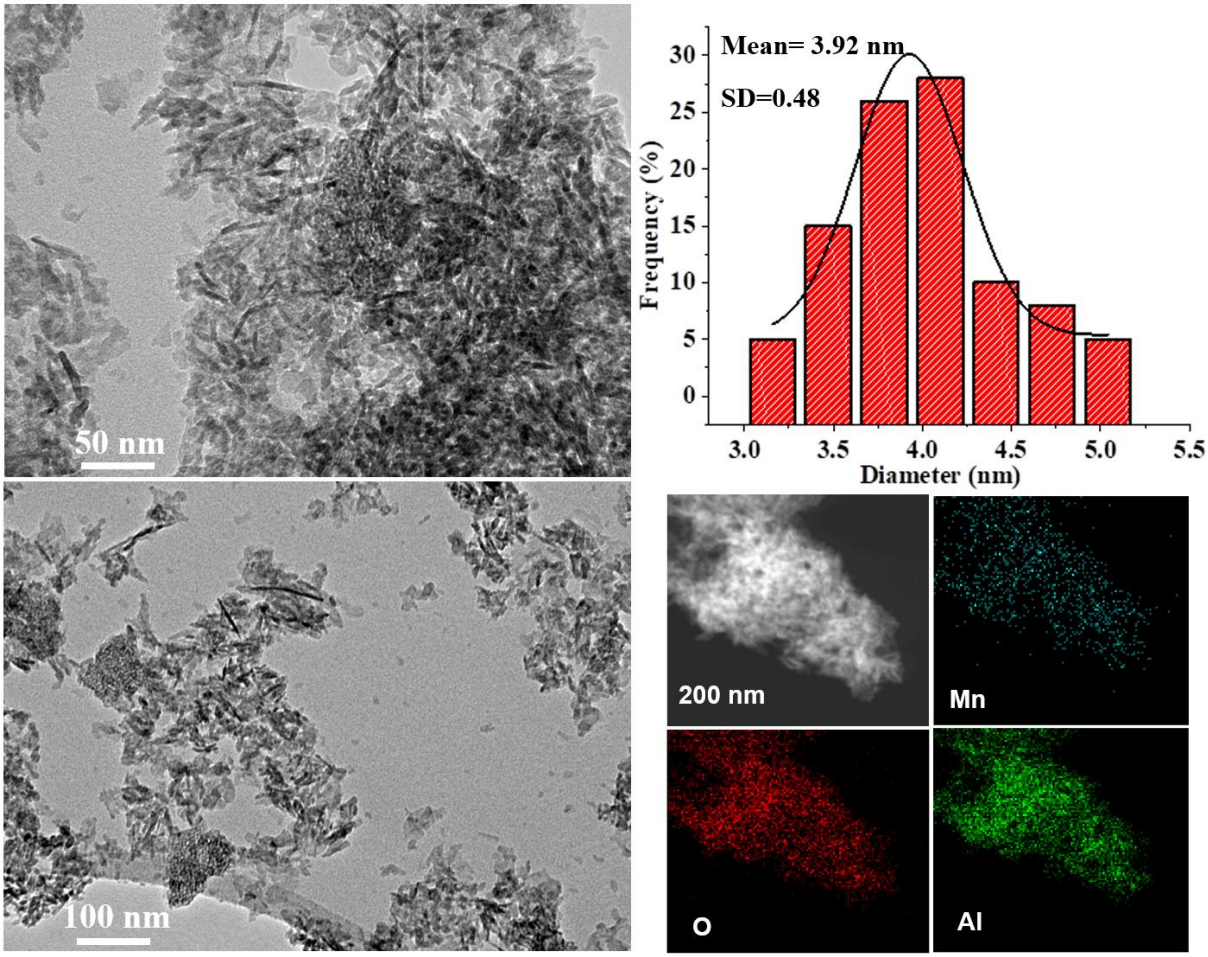

(b)

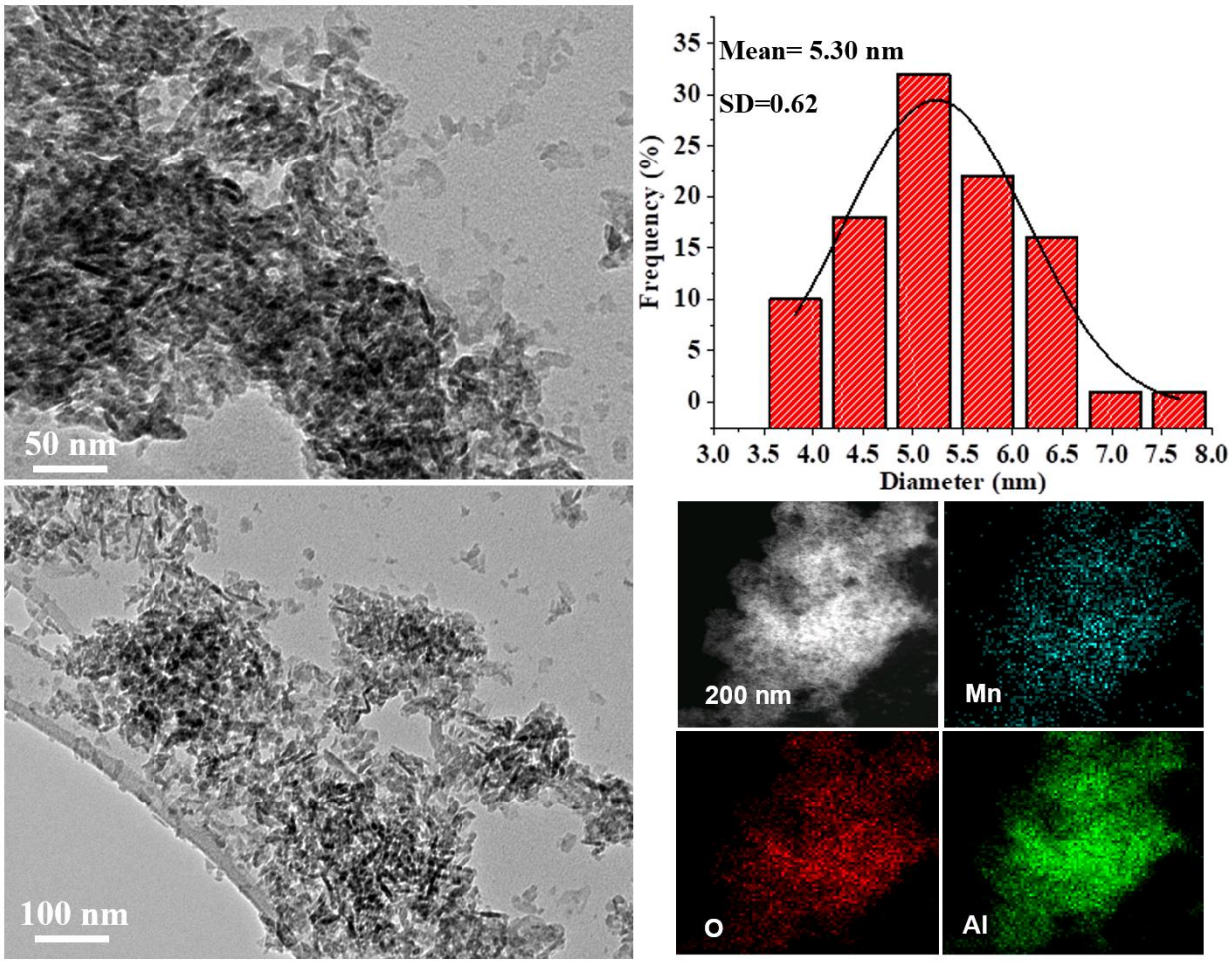

Figure 4.6.TEM images, particle size distribution, and HAADF-STEM image and EDX maps. (a) MnOx/Al_2O_3-P and (b) MnOx/Al_2O_3-I catalyst.

Thermogravimetric analysis of the MnO_x/Al_2O_3-P sample before calcination is presented in Figure 4.7. The sample was heated up to 1000 °C with a rate of 10°C/min and polyol catalyst weight loss was approximately 13%. Initially, the weight loss of almost 6 % occurred between 30 and 200 °C due to the release of physically adsorbed water. Afterward, the next 6 % of weight loss happened in the range of 200 to 500 °C that can be attributed to the elimination of the organic compounds in the sample. In the last part, from 500 to 1000 °C, there was only about 1% weight loss, which is most probably due to the change in oxidation states of the catalyst. As temperature rises, the manganese oxides phase will change, impacting the weight of the sample

[25,160]. In this work, the catalysts were calcined at 475 °C and based on the TGA results; this temperature is enough for removing all the contaminations and adsorbed water [141,149].

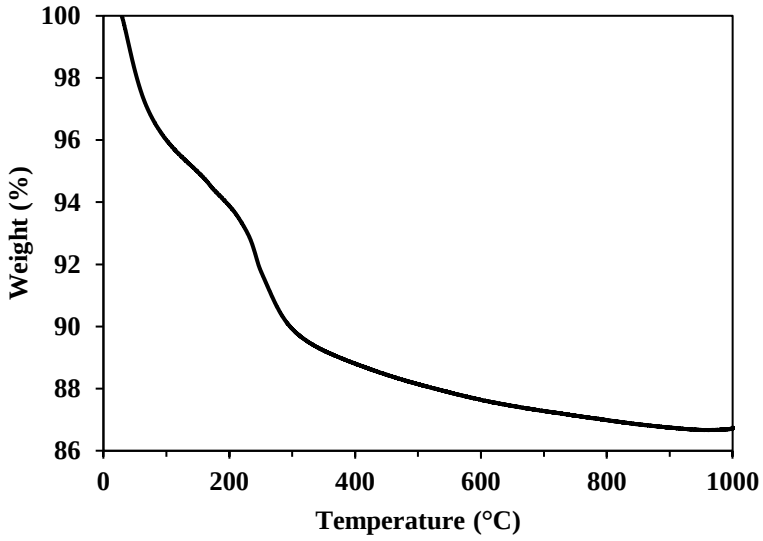

Figure 4.7..Weight loss during thermogravimetric analysis for MnOx/Al2O3-P catalyst.

The TPR results are shown in Figure 4.8. For MnO_x/Al_2O_3-I catalyst, a two-step reduction process was observed. The first peak that was attributed to reduction of MnO_2 to Mn_2O_3 and further to Mn_3O_4 occurred at 322 °C [64,126,161]. The second peak at 502 °C is related to reduction of Mn_3O_4 phase to MnO. The MnO_x/Al_2O_3-P catalyst showed only a single peak for reduction of Mn_3O_4 to MnO, which was shifted to a higher temperature compared to MnO_x/Al_2O_3-I catalyst. The TPR patterns are greatly influenced by the oxidation state of the catalyst [162]. Therefore, the results indicated that the primary manganese species in MnO_x/Al_2O_3-P consists of Mn_3O_4, whereas in MnO_x/Al_2O_3-I a combination of MnO_2, Mn_2O_3, and Mn_3O_4 was observed. The XRD patterns of MnO_x/Al_2O_3-I, MnO_x/Al_2O_3-P, and Al_2O_3 are shown in Figure 4.9. XRD can only detect the characteristic peaks of Al_2O_3 without any peaks corresponding to Mn oxides. This indicates that supported catalysts were highly dispersed. Rezaei et al. investigated the effect of different manganese precursors in ozonation of toluene [21]. They found that Mn acetate precursor shows no manganese oxides peaks in XRD, however, both precursors exhibited almost the same activity.

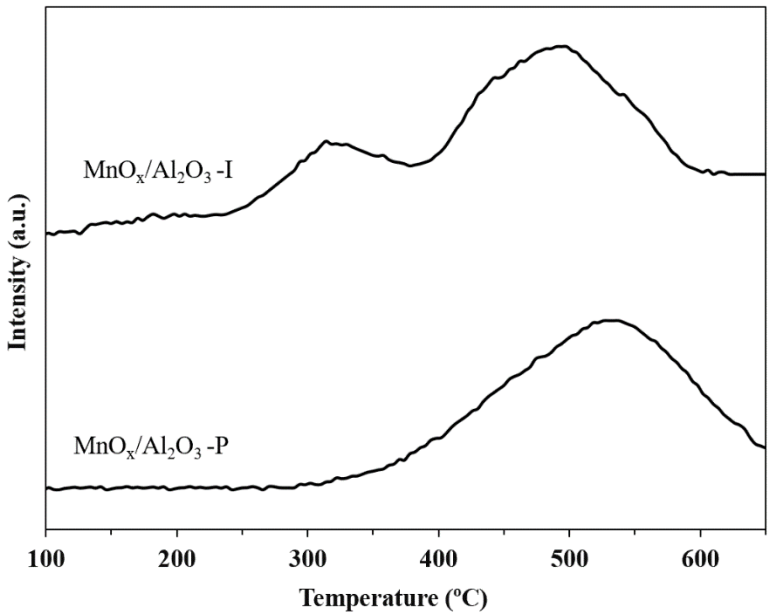

Figure 4.8.TPR profile of the MnOx/Al_2O_3-P and MnOx/Al_2O_3-I.

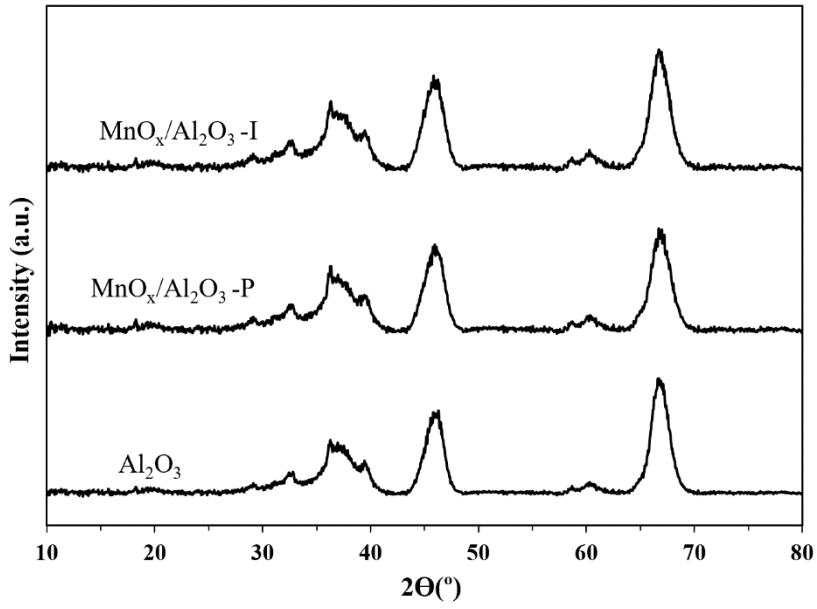

Figure 4.9.XRD patterns of Al_2O_3, MnOx/Al_2O_3-P, and MnO_x/Al_2O_3-I.

XPS analyses were carried out to determine the surface elemental composition and oxidation states of manganese in the catalysts. Figure 4.10 shows the Mn 2p XPS spectra of MnO_x/Al_2O_3-I and MnO_x/Al_2O_3-P catalysts which consist of two main peaks of spin-orbit couplet with Mn $2p_{1/2}$ having a higher binding energy peak and Mn $2p_{3/2}$ with a lower binding energy peak. By deconvolution of Mn 2p spectra, the Mn $2p_{1/2}$ and Mn $2p_{3/2}$ can be separated into three characteristic peaks for both catalysts. The Mn $2p_{3/2}$ spectra give three peaks whose binding energies are located at 640.2–640.8 eV, 641.6–641.8 eV, and 643.2–643.6 eV, assigned to Mn^{2+}, Mn^{3+}, and Mn^{4+}, respectively [163–166].

The results demonstrate that surface of both MnO_x/Al_2O_3-I and MnO_x/Al_2O_3-P catalysts contain mixed manganese phases. The surface compositions of manganese phases are shown in Figure 4.10 and the quantitative analysis results are comparable for both catalysts. It is important to note that, Mn^{3+} was the dominant species on the surfaces of both catalysts, while MnO_x/Al_2O_3-P contains a higher amount of Mn^{2+} and a smaller amount of Mn^{4+} than MnO_x/Al_2O_3-I.

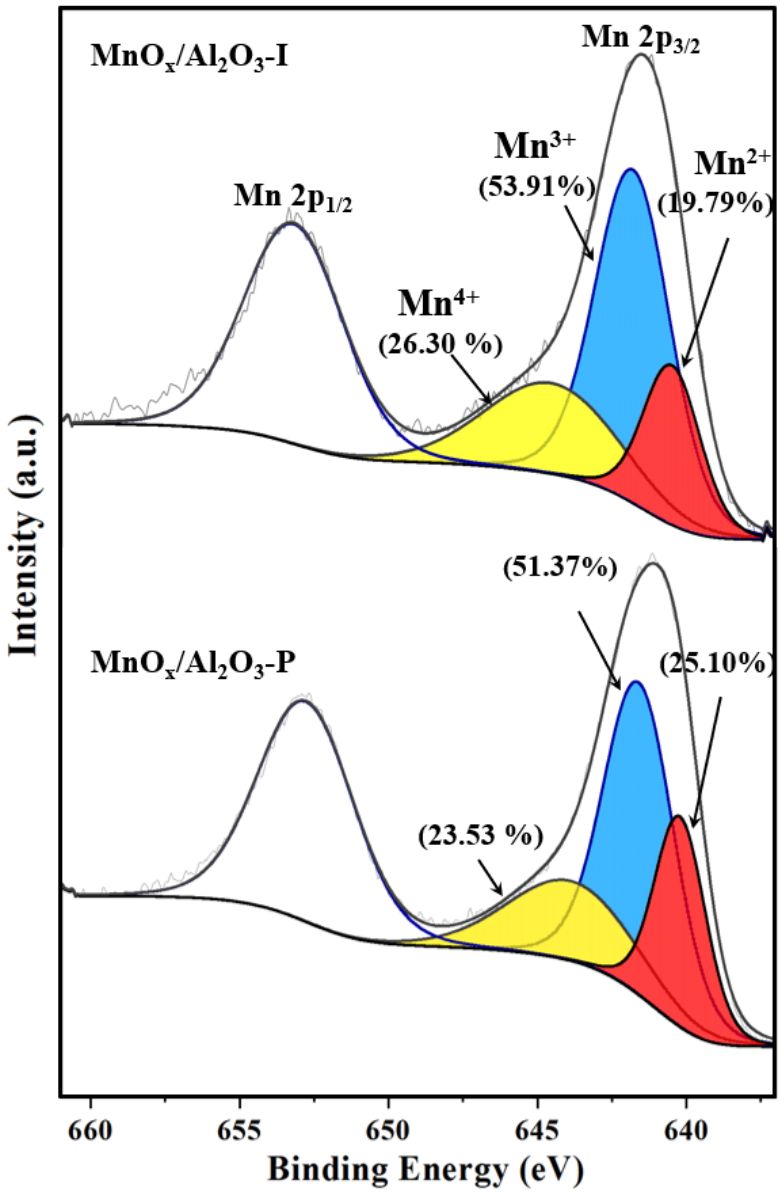

Figure 4.10.Mn 2p region XPS spectra of MnO_x/Al_2O_3-P and MnO_x/Al_2O_3-I catalysts.

Mn *K-edge* normalized XANES spectra of the MnO_x/Al_2O_3-I and MnO_x/Al_2O_3-P catalysts as well as the pure reference materials (MnO, Mn_3O_4, Mn_2O_3, and MnO_2) are shown in Figure 4.11. Overall, the spectra of both MnO_x/Al_2O_3-I and MnO_x/Al_2O_3-P were mixed spectra of the reference materials. However, both catalysts' spectra are mainly similar to Mn_3O_4. At energies below 6550 eV, MnO_x/Al_2O_3-I and MnO_x/Al_2O_3-P catalysts spectra were mixed spectra of Mn_3O_4 and Mn_2O_3. It can be observed that before the edge, the spectra of MnO_x/Al_2O_3-P is

located at the left side of the MnO_x/Al_2O_3-I suggesting that polyol catalyst is composed of more Mn_3O_4 and has lower oxidation states than the impregnated catalyst. Linear combination fitting of Mn *K-edge* XANES data was used to quantify the presence of different reference materials. Mn *K-edge* absorption energy (E_0) of Mn_3O_4 and Mn_2O_3 reference materials were obtained as 6546.88 and 6553.73 eV, respectively. In addition, absorption energy of Mn *K-edge* of the MnO_x/Al_2O_3-I and MnO_x/Al_2O_3-P were determined to be 6547.66 and 6547.42 eV, respectively, which are very close to Mn *K-edge* absorption energy of Mn_3O_4. It was found that for the MnO_x/Al_2O_3-P sample, Mn_3O_4 was the dominant phase with 69 % abundance, followed by 32% Mn_2O_3. MnO_x/Al_2O_3-I catalyst was in the form of 51 % Mn_3O_4, 47% Mn_2O_3, and 2 % MnO_2. It should be noted that Mn_3O_4 is a mixture of Mn^{3+} and Mn^{2+} oxidation states with Mn^{3+}/Mn^{2+} abundance ratio of 2. Therefore, by comparing the results of XPS and XANES analyses, it can be concluded that Mn^{3+} is the dominant phase of manganese in both MnO_x/Al_2O_3-I and MnO_x/Al_2O_3-P catalysts. However, MnO_x/Al_2O_3-P had more Mn^{+2} than MnO_x/Al_2O_3-I, indicating that manganese in polyol catalyst has a lower oxidation state than that in the impregnated catalyst. It has been reported by Rezaei et al. that lower oxidation states of manganese are more desirable in ozone decomposition and toluene oxidation [30]. Similar results have been found by other researchers that catalysts with a lower oxidation state of manganese are more active in catalytic ozonation of VOCs [103,113]. Due to the preparation procedure of polyol method, higher dispersion of catalysts can be obtained. As dispersion of manganese atoms increases, the oxidation state of manganese decreases [30]. Ozone decomposition is an essential step for catalytic ozonation reaction. It produced the atomic oxygen that reacts with VOCs. When the oxidation state of manganese decreases, the mobility of manganese atoms increases, facilitating their electron transfer to ozone. Therefore, better ozone decomposition rate and higher atomic oxidation increased the rate of toluene ozonation.

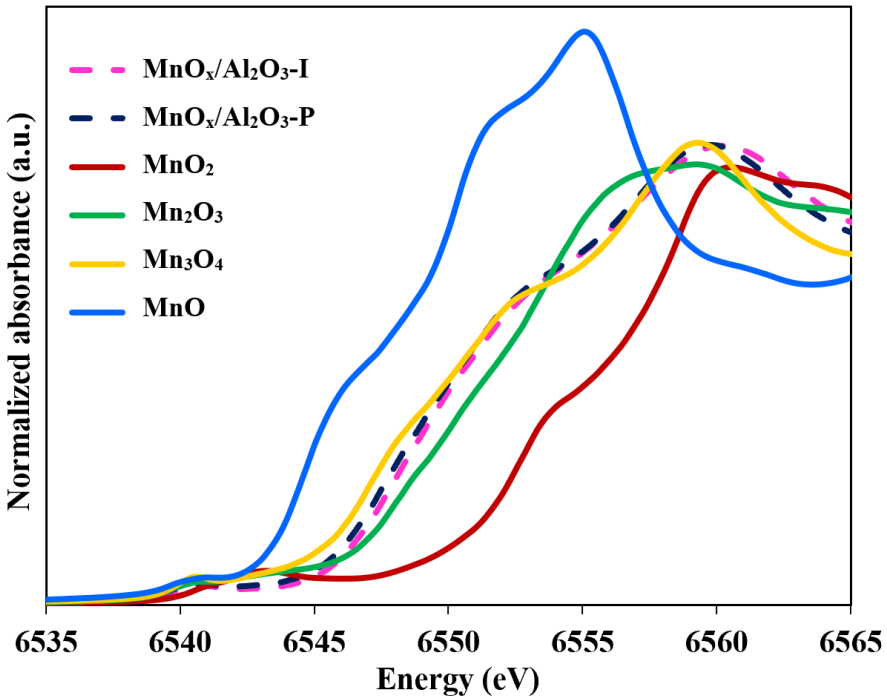

Figure 4.11. XANES spectra of Mn K-edge of catalysts and reference materials.

4.4.3. Catalytic ozonation of toluene

Performance of the MnO_x/Al_2O_3-P and MnO_x/Al_2O_3-I catalysts were evaluated in the catalytic ozonation of toluene in air. The results of the toluene and ozone conversion with reaction time for the two catalysts are presented in Figure 4.12 (a) and (b). Experiments were repeated and standard errors for toluene and ozone conversion profiles were within ±5%. The Standard errors for CO_2 and CO concentrations were within ±4 and ±5.5 ppm, respectively.

After 120 min of reaction, ozone and toluene conversions for MnO_x/Al_2O_3-P were approximately 58 and 80 %, respectively. MnO_x/Al_2O_3-P exhibited higher toluene and ozone conversions than MnO_x/Al_2O_3-I catalyst. It should be noted that MnO_x/Al_2O_3-P effectively removed almost all of the toluene and ozone during the initial 30 min of the reaction and then started to be deactivated similar to the impregnated catalyst.

Carbon dioxide and carbon monoxide were the main reaction products detected in the product stream. Figure 4.12 (c) shows the concentration of CO_2 and CO in the exhaust stream during

catalytic ozonation of toluene using MnO_x/Al_2O_3-P and MnO_x/Al_2O_3-I catalysts. CO concentration using both catalysts were almost constant during the reaction. In the case of CO_2, the concentration increased at the beginning of the reaction for both catalysts and after reaching a maximum at around 40 to 60 min of reaction, started to gradually drop due to accumulation of reaction byproducts that lead to catalyst deactivation. Higher selectivity towards CO_2 in the polyol catalyst and the higher amount for total CO_x production can be attributed to its higher conversion compared to the impregnated catalyst. The trend for CO_x concentrations and the activity decline have been also reported by other researchers for oxidation of toluene and other VOCs [29,79,100,126,167].

Catalytic ozonation over pure γ-Al_2O_3 and Mn_3O_4 were conducted and the results are presented in Figure 4.12 (d). The toluene and ozone conversions were remarkably lower than MnO_x/Al_2O_3 catalysts. These observations confirm the importance of Mn sites on the alumina for catalytic ozonation of toluene. It also suggests that alumina is not inert in the reaction with toluene. Table 4.5 summarizes conversions, reaction rates of toluene and ozone, CO_x yields, and carbon balance on MnO_x/Al_2O_3-P and MnO_x/Al_2O_3-I catalysts after 120 min of reaction at 25 °C.

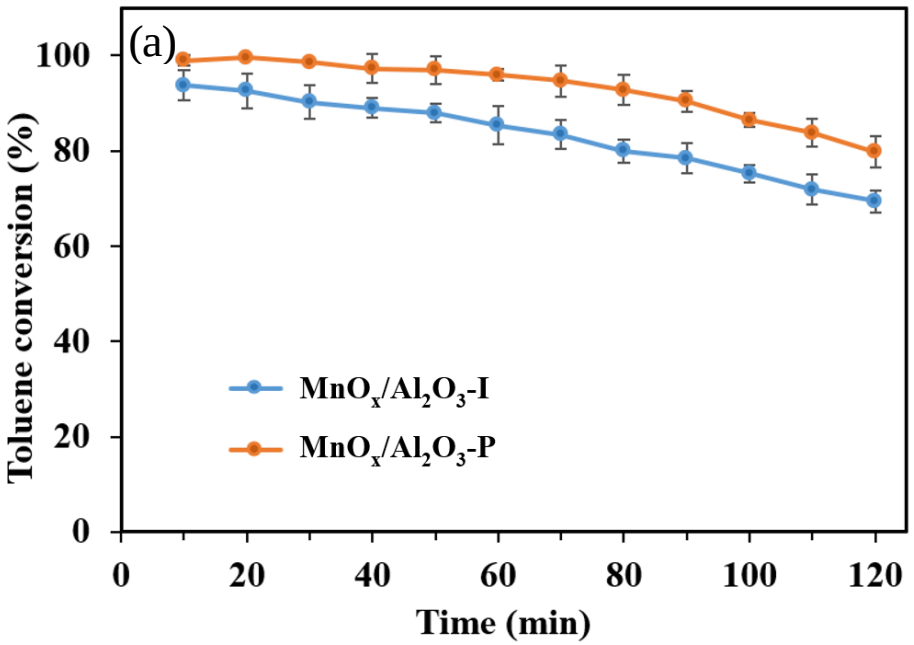

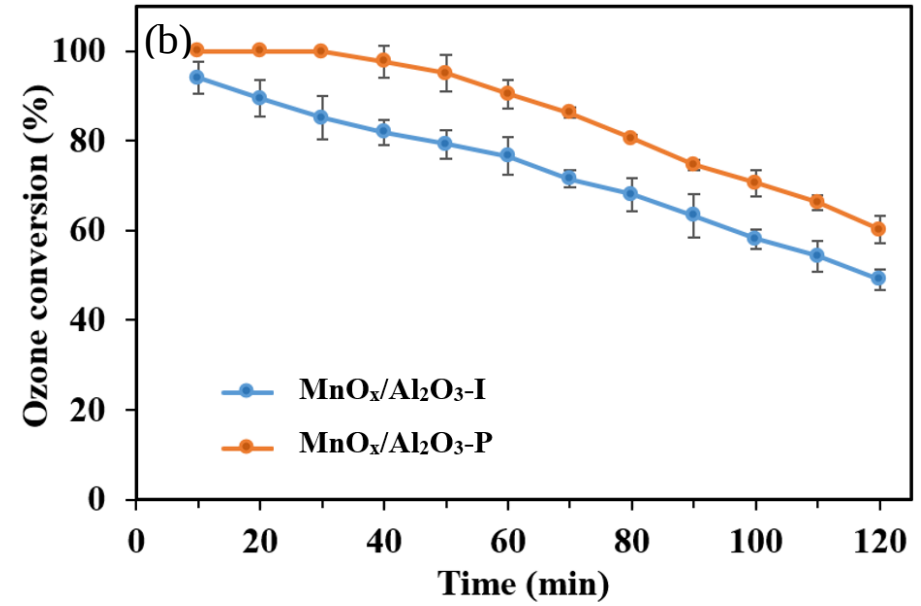
(b)
Ozone conversion (%)
Time (min)
MnOx/Al2O3-I
MnOx/Al2O3-P

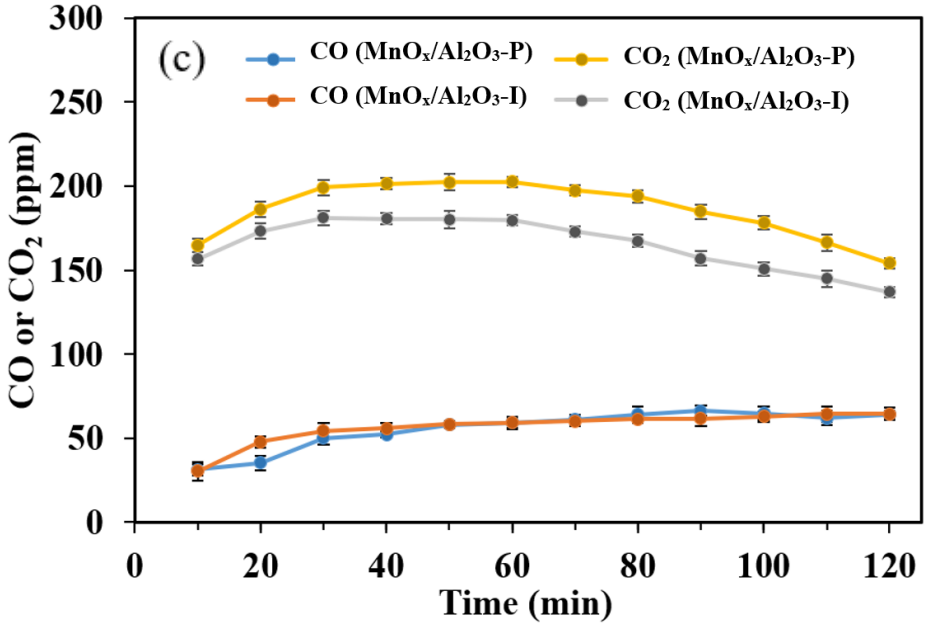
(c)
CO or CO2 (ppm)
Time (min)
CO (MnOx/Al2O3-P)
CO (MnOx/Al2O3-I)
CO2 (MnOx/Al2O3-P)
CO2 (MnOx/Al2O3-I)

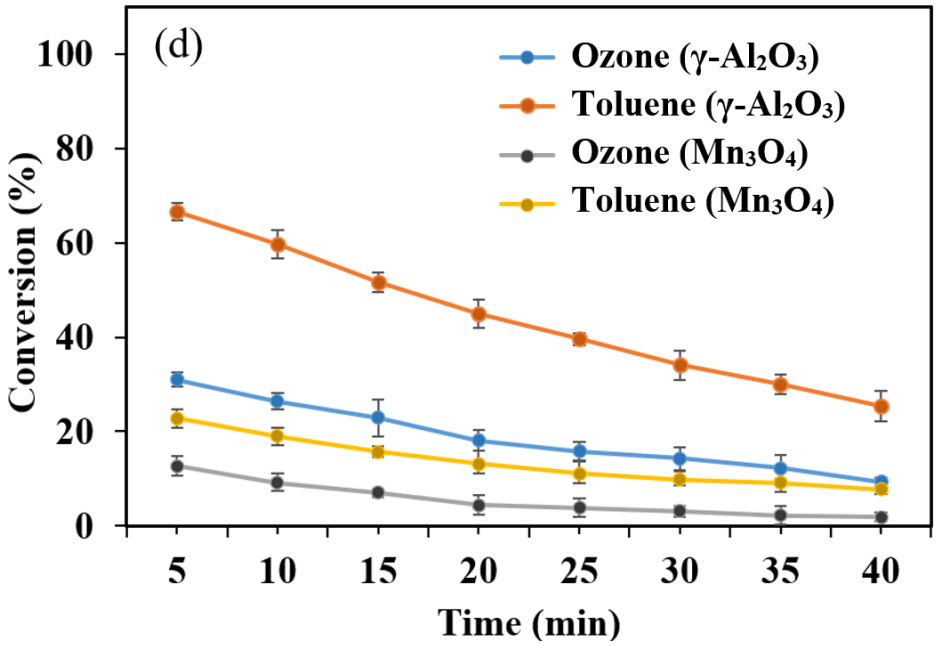

Figure 4.12.Catalytic ozonation of toluene at 25 °C, (a) toluene conversion ,(b) ozone conversion, and (c) CO and CO_2 concentrations using MnO_x/Al_2O_3-P and MnO_x/Al_2O_3-I catalysts ; (d) toluene and ozone conversions using γ-Al_2O_3 and Mn_3O_4, [O_3] = 1000 ppm, [toluene

Table 4.5.Conversion, reaction rate, CO_x yield, and carbon balance of toluene removal in gas phase reaction with ozone using MnO_x/Al_2O_3-P and MnO_x/Al_2O_3-I catalysts at 25 °C and 120 min of reaction.

Catalyst	Toluene conversion (%)	Ozone conversion (%)	Toluene oxidation rate ($\times 10^5$ mol min^{-1} g^{-1})	Ozone decomposition rate ($\times 10^4$ mol min^{-1} g^{-1})	Co_x yield (%)[a]	Carbon balance (%)
MnO_x/Al_2O_3-P	79.8	60.2	1.96	1.34	34.3	95.6
MnO_x/Al_2O_3-I	69.3	49.1	1.70	1.10	32.1	88.1

[a] Calculated based on 100 × ([CO] + [CO_2])/(7× [$Toluene_{, reacted}$]).

In-situ DRIFTS spectroscopy was conducted to investigate the formation of reaction byproducts on the surface of the catalysts during the reaction. Figure 4.13 shows *in-situ* DRIFTS spectra of MnO_x/Al_2O_3-P and MnO_x/Al_2O_3-I catalysts during catalytic ozonation of toluene. In the process, first toluene is adsorbed on the catalyst, which can be confirmed by formation of characteristic band assigned to aromatic ring stretching at 1,496 cm^{-1} and another peak at around

1,580-1,604 cm^{-1} attributed to the overlap of aromatic ring stretching and COO^- stretching of carboxylates [126,168,169]. By introducing ozone to the system after catalyst saturation, several new peaks appear. The peaks assignable to C–H asymmetric deformation vibration (1,426-1,427 cm^{-1}), COO^- asymmetric stretching vibration (1,436-1,438 cm^{-1}), and C=O stretching (1,728-1,780 cm^{-1}) were noticed instantly. The intensities of these bands gradually increase as the reaction proceeds. The broad band from 2,400 to 3,650 cm^{-1} is attributed to the overlap of OH stretching of alcohols, carboxylic acids, and water. Similar observations have been reported for ozonation of several VOCs over MnO_x/Al_2O_3 [79,100,103,170]. Although some differences in the intensity of the peaks are observed for the MnO_x/Al_2O_3-P and MnO_x/Al_2O_3-I catalysts, the characteristics band and wavenumbers for both samples were similar, indicating that both catalysts followed the same reaction pathway.

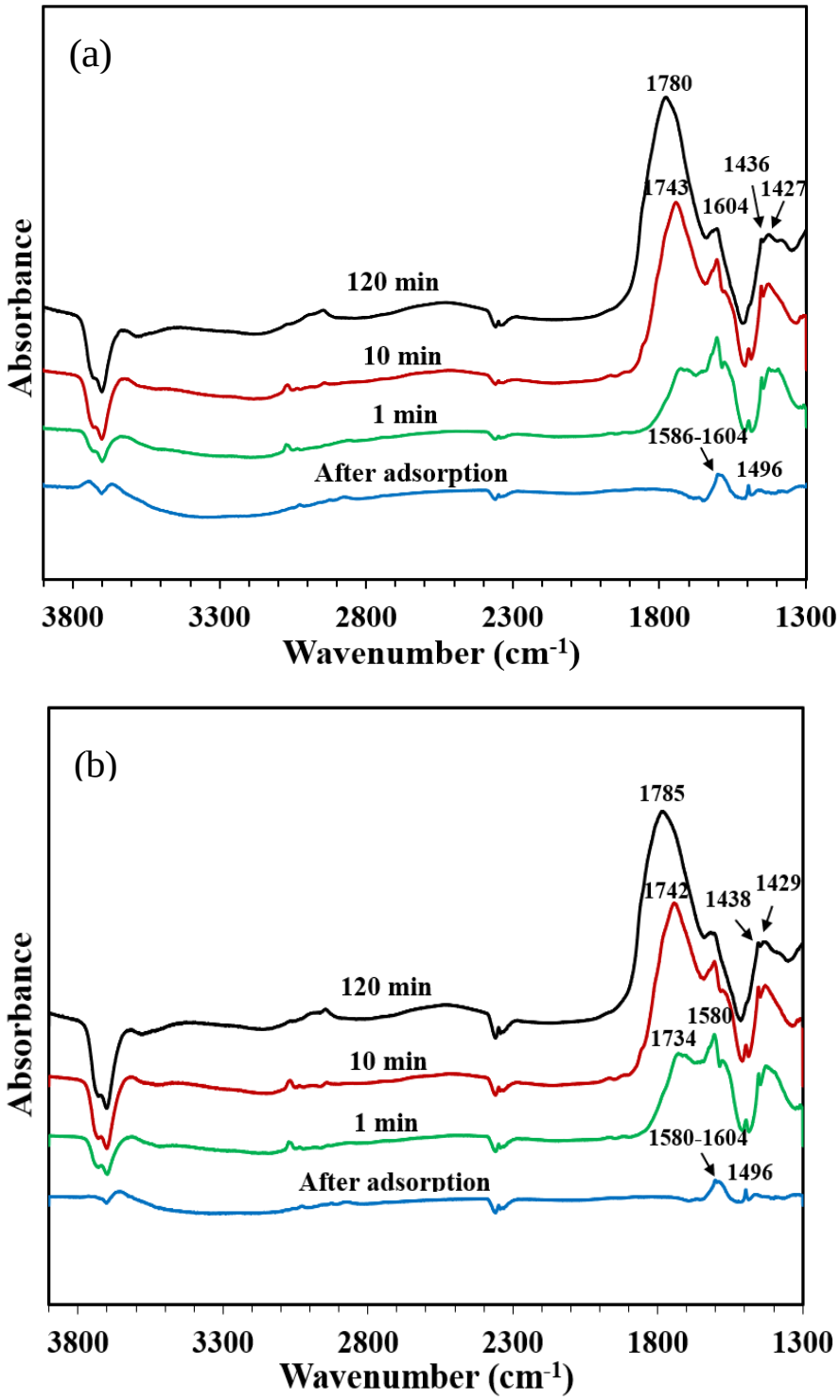

Figure 4.13.*In-situ* DRIFTS spectra of the catalytic ozonation of toluene at 25 °C (a) MnO_x/Al_2O_3-P and (b) MnO_x/Al_2O_3-I ,[O_3] = 1000 ppm, [toluene] = 120 ppm.

4.4.4. Temperature-programmed analyses of spent catalysts and byproduct identification

The main reaction products for this reaction are CO_2 and CO. Temperature-programmed analyses, as well as byproduct identification using GC-MS, were carried out to identify the accumulated byproducts that lead to catalyst deactivation in catalytic ozonation of toluene using MnO_x/Al_2O_3-P and MnO_x/Al_2O_3-I catalysts. (Details of this section have been presented in Supplementary Material)

TPD and TPO experiments were conducted on the catalysts that had been used for ozonation of toluene for 120 min. TPD of the spent catalysts was conducted under flow of nitrogen and heating rate of 20 °C/min. The profiles of concentration for CO_2 and CO in the exhaust stream during TPD of the spent catalysts are shown in Figure 4.14. At the low temperature range (25-350 ºC) in addition to CO and CO_2, acetic acid, formic acid, and toluene were detected. At higher temperature region (550-850 °C), toluene along with benzene and methane were detected. CO_x formation at all temperatures in TPD can be ascribed to desorption of adsorbed CO_x and oxidation of adsorbed carbon deposits by lattice oxygen on the surface of the catalyst [171]. Two peaks were observed for the evolution of CO_2 and CO. The peaks at low temperatures corresponded to desorption of CO_2 and CO which were formed during the reaction and the peaks at higher temperatures were assigned to oxidation of adsorbed intermediate products such as carboxylates. Detection of toluene at lower temperature can be attributed to its desorption. However, at higher temperature region (550-850 °C), the presence of toluene along with benzene and methane implies that they evolved from decomposition of larger surface carboxylate compounds and both samples released comparable amounts of these products.

It can be observed that polyol catalyst released less CO and more CO_2 than the impregnated catalyst during TPD analysis (Figure 4.14). For comparison, the lower intensity peak of CO at lower temperatures could be related to less CO that was produced using polyol catalyst in the reaction. The peak of CO_2 formation by the polyol and impregnated samples occurred at 350 and 400 °C, respectively. Since TPD tests were performed in the absence of oxygen, the formation of CO_2 can be ascribed to oxidation of carbon deposits by lattice oxygen on the surface of the catalyst. This can suggest that oxidation activity of polyol catalyst was higher than impregnated catalyst. The surface oxygen species in the catalysts were responsible for surface oxidation of adsorbed toluene during TPD patterns. The profile of desorbed acetic acid and formic acid

during TPD are presented in Figure 4.15 for both used catalysts. It was observed that the signal related to formic acid and acetic acid were lower in the spent polyol catalyst than impregnated one, indicating that a higher amount of carbonaceous materials accumulated on the impregnated catalyst.

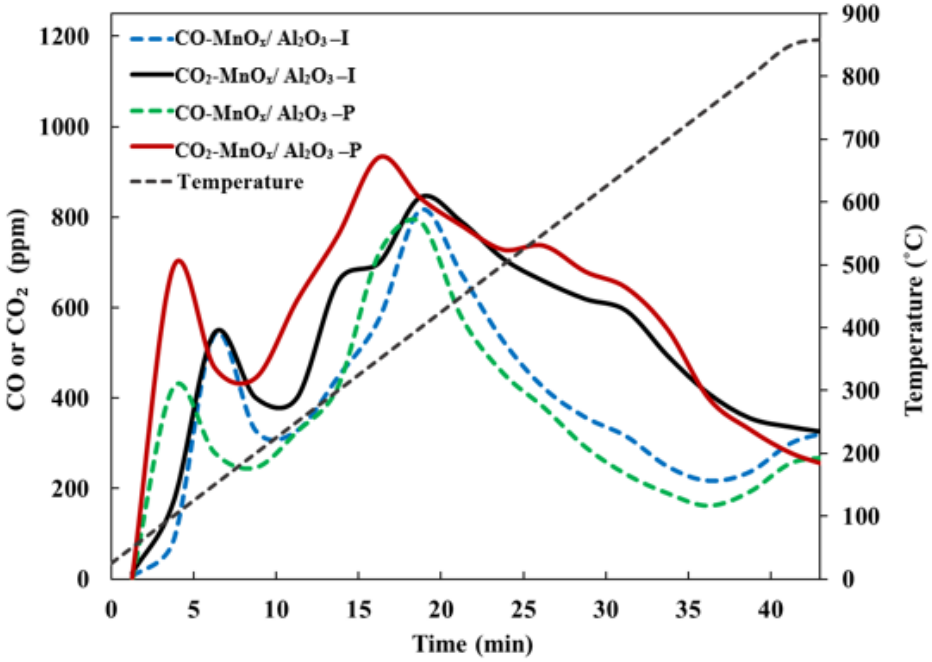

Figure 4.14.Variation of CO and CO_2 concentrations during TPD analysis of the spent MnO_x/Al_2O_3-P and MnO_x/ Al_2O_3-I catalysts.

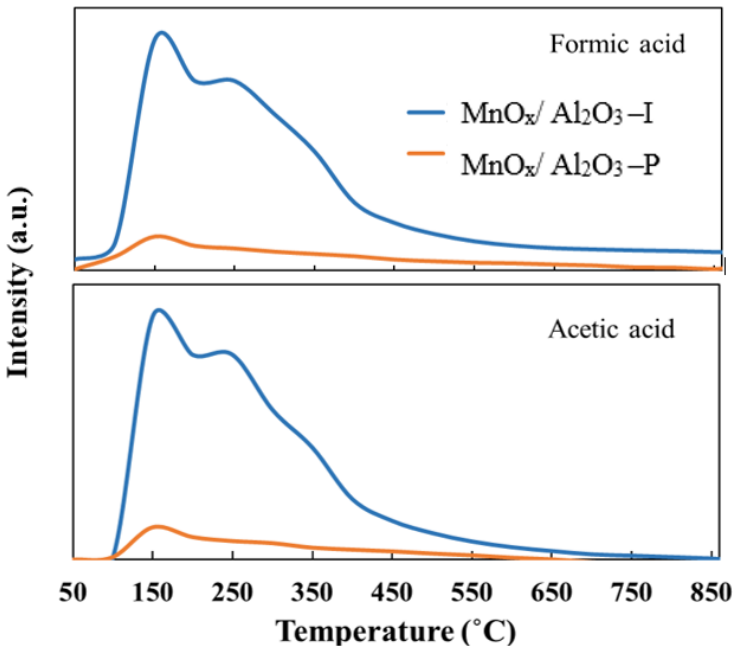

Figure 4.15.TPD profiles of desorption of intermediate from the spent MnO_x/Al_2O_3-P and MnO_x/Al_2O_3-I catalysts.

TPO of the spent catalysts was carried out under flow of oxygen-nitrogen mixture (20-80 v%) and heating rate of 10 °C/min. Figure 4.16 depicts the variations of CO and CO_2 concentration during TPO analysis. Two peaks were detected for CO_x elution during TPO analysis. The low temperature (below 180 °C) peak corresponded to the oxidation of weakly bound surface byproducts on the catalyst which are identified as acetic acid, formic acid, and toluene (based on TPD analysis). The other peak at higher temperature (280-420 °C) was attributed to the oxidation of strongly bound byproducts such as benzene and toluene. These species require higher temperatures for complete decomposition. The ratio of CO to CO_2 decreases with increasing temperature due to the nature of different adsorbed species and oxidation of CO to CO_2 at high temperatures [172]. Most of CO_2 is produced in the range of 280-420 °C, with maximum of approximately 3,300 ppm in both polyol and impregnated catalysts. In addition, the peak of CO reached a maximum concentration of 613 ppm in polyol catalyst at 100 °C, whereas in impregnated catalyst it reached to 554 ppm at 340 °C. This implies that strongly bound byproducts at higher temperatures were oxidized more completely on polyol catalyst.

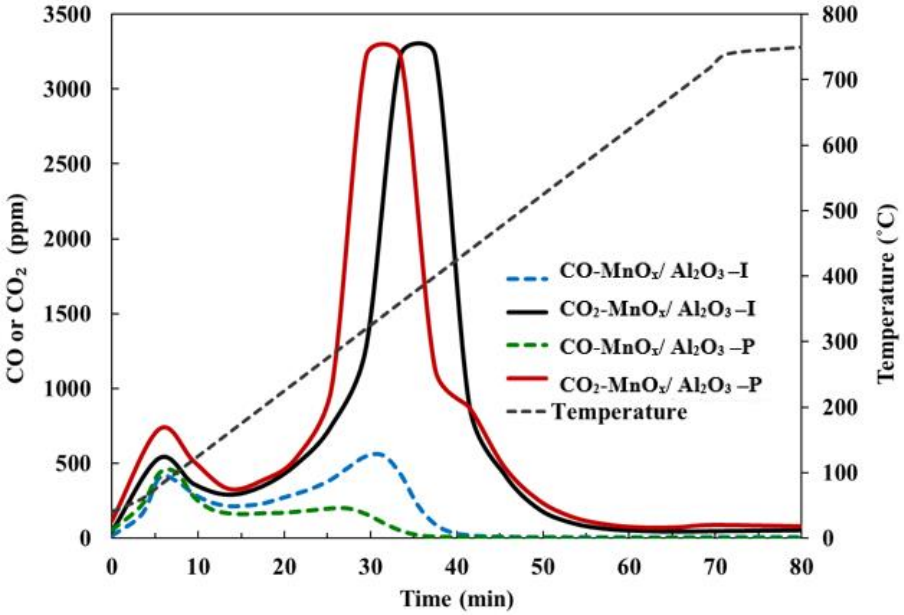

Figure 4.16.Variation of CO and CO_2 concentrations during TPO analysis of the spent MnO_x/Al_2O_3-P and MnO_x/Al_2O_3-I catalysts.

In TPO analysis, acetic acid, formic acid, toluene, and benzene were detected. Similar to TPD analysis, the intensities of designated peaks for acetic acid and formic acid were much lower in polyol catalyst than impregnated catalysts (Figure 4.17). Therefore, TPO and TPD analyses identified the byproducts that were deposited on the surface of catalysts during the ozonation of toluene. These byproducts are qualitatively the same for the main components (CO and CO_2), whereas the quantitative values of intermediate species are different for the two catalysts.

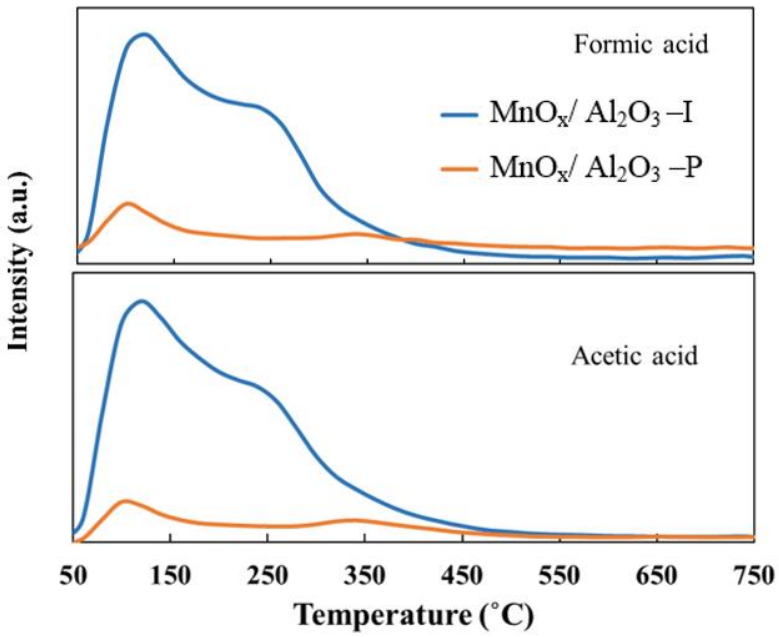

Figure 4.17.TPO profiles of desorption of intermediates from the spent MnO_x/Al_2O_3-P and MnO_x/Al_2O_3-I catalysts.

The intermediate compounds on the spent MnO_x/Al_2O_3-P and MnO_x/Al_2O_3-I catalysts were extracted with dichloromethane and were analyzed with GC-MS. Several organic compounds such as oxalic acid, formic acid, acetic acid, ethanol, benzaldehyde, benzyle alcohol, and benzoic acid were found in both samples. However, by comparing the detected spectrum from the two catalysts; some intermediates such as benzaldehyde and benzoic acid appeared in higher intensity in MnO_x/Al_2O_3-I catalyst than MnO_x/Al_2O_3-P catalyst. These are more complex and heavy intermediates. The intermediates are the consequence of incomplete reactions of free radicals and toluene. During the room temperature operation, these components gradually block the active sites of the catalyst, leading to catalyst deactivation [21,76].

According to the presented results, polyol and impregnation methods lead to production of different structures in the catalyst. The impregnation method is relatively simple for the preparation of supported catalysts but there is no control over the structure and morphology of the particles. Whereas the polyol process involves a redox reaction that makes it easier to control metal particle size and morphology. The catalyst prepared by polyol process has smaller manganese particle size, higher surface area, and lower oxidation states than the catalyst

prepared by impregnation method. These parameters impact the activity of catalyst in ozonation of VOCs. Reed et al. stated that in the first step of ozone decomposition on the Mn sites, two electrons are transferred from Mn to ozone. Mn oxides with lower oxidation states facilitate the oxygen species delivery in the reaction [113]. During the catalytic ozonation, the VOCs and intermediate compounds migrate from support to metal sites. As crystallite size decreased and dispersion of manganese increased, the manganese atoms became more accessible for the transfer of VOCs from support to manganese [75,113].

4.4.5. Possible reaction mechanism of toluene ozonation

In the catalytic ozonation process, ozone is decomposed on the surface of the catalysts to produce atomic oxygen and peroxide species (Eqs. (4.4)-(4.6)) [21,100,113,173].

$$O_3 + {}^* \rightarrow O_2 + O^* \quad (4.4)$$

$$O_3 + O^* \rightarrow O_2 + O_2^* \quad (4.5)$$

$$O_2^* \rightarrow O_2 + {}^* \quad (4.6)$$

where * refers to the active sites. According to breakthrough curves of toluene adsorption over pure Mn_3O_4, Mn_2O_3, γ-Al_2O_3, and MnO_x/γ-Al_2O_3 catalysts, the breakthrough time for Mn_3O_4 and Mn_2O_3 were shorter (less than 5 min) compared to γ-Al_2O_3 (40 min) and MnO_x/γ-Al_2O_3 catalyst (30 min). It can be deducted that toluene is mainly adsorbed on γ-Al_2O_3 sites of the MnO_x/γ-Al_2O_3 catalyst. It has been reported that alumina not only participates in the process of adsorption of toluene but also it plays a role in the interaction between toluene and atomic oxygen species to produce surface carboxylate intermediates [100]. Meanwhile, the interaction of toluene with metal oxides has been stated to occur via abstraction of H atoms from the methyl group and reaction with oxygen species. Several intermediate species such as benzyl alcohol, benzaldehyde, and benzoic acid can be produced that are further oxidized to carbon oxides [12,126,174]. To further oxidize surface carboxylates, Mn sites are essential for continuing the oxidation of generated intermediate species [100].

It has been suggested that alumina is not an inert support in ozonation of VOCs [79,100]. It was proposed that alumina acts as a reservoir for adsorbed toluene, and it also interacts with toluene to create surface carboxylate intermediates [79]. As explained in section 4.4.4, polyol catalyst produces less heavy reaction intermediates than the impregnated catalyst. Byproducts such as acetic acid and formic acid are generated more in the reaction on the impregnated catalyst leading to lower activity of the catalyst.

4.5. Conclusions

MnO_x/Al_2O_3 catalyst was prepared using polyol process and the synthesis temperature and time were optimized for oxidation of toluene using ozone. Removal of toluene was studied in the catalytic ozonation reaction using 16 designed catalysts prepared with varying temperature and time during catalyst preparation in polyol process. Application of the optimum polyol catalyst in room temperature catalytic ozonation resulted in toluene conversion as high as 80 %. The polyol catalyst was compared with the impregnated catalyst in terms of their performance and properties. MnO_x/Al_2O_3-P exhibited superior toluene conversion and ozone decomposition than the impregnated catalyst. The higher activity of the catalyst can be attributed to its properties. It was observed that manganese cluster size in polyol catalyst is smaller than that of impregnated catalyst resulting in higher dispersion of manganese particles. Moreover, polyol process led to enhanced surface area and pore volume of the catalyst. XPS and XANES analyses showed that Mn^{3+} is the dominant phase of manganese in both polyol and impregnation catalysts. However, manganese in polyol catalyst has lower oxidation state than impregnated catalyst. Byproducts intermediates in the reaction are generated more in impregnated catalyst that reduce the catalyst activity.

Chapter 5:

Enhancing catalytic ozonation of acetone and toluene in air using MnO_x/Al_2O_3 catalysts at room temperature

The content of this chapter has been published in Industrial & Engineering Chemistry Research and presented in the following conferences:

Citation:

M. Ghavami, J. Soltan, N. Chen, Enhancing catalytic ozonation of acetone and toluene in air using MnO_x/Al_2O_3 catalysts at room temperature, Industrial & Engineering Chemistry Research (2021). https://doi.org/10.1021/acs.iecr.1c02288.

Conference Proceedings:

M. Ghavami and J. Soltan, Manganese oxide catalysts for ozonation of acetone and toluene: Effect of preparation method and calcination temperature. 69th Canadian Chemical Engineering Conference, October 20-23, 2019, Halifax, Canada.

M. Ghavami and J. Soltan, Insights into the effect of calcination temperature on catalytic properties and activity in catalytic ozonation of VOCs over MnO_x/γ-Al_2O_3. Prairie Environmental Chemistry Colloquium, June 2-3, 2020, University of Saskatchewan, Saskatoon, Canada.

M. Ghavami, J. Soltan and N. Chen, The effect of calcination temperature on catalytic ozonation of VOCs over MnO_x/Al_2O_3. AUM & CLS 2.0 Event, October 7-8, 2020, Canadian Light Source, Saskatoon, Canada.

Contribution of the Ph.D. candidate

Mehraneh Ghavami designed and performed all the experiments, generated, and analyzed the data, prepared all the figures and tables, and drafted and revised the manuscript. Dr. Jafar Soltan supervised, provided inspiration, scientific input, and guidance, commented on, and edited the manuscript. XANES and XAFS data were collected at the Canadian Light Source with the assistance of Dr. Ning Chen. Dr. Ning Chen provided general guidance for analyses of the XAS data and revised the manuscript. Suggestions from the advisory committee members (alphabetic order: Dr. Ning Chen, Dr. Catherine Niu, Dr. Hui Wang, and Dr. Lifeng Zhang) were used to improve the quality of this work.

Contribution of this chapter to the overall Ph.D. Research

This chapter covers the third phase of the research, which is "determining the effect of calcination temperature on the structural properties and - activity of the catalysts". In this section, acetone and toluene in single component and binary mixtures were oxidized using catalysts prepared by two different methods and calcined at various temperatures. The impact of different ratios of acetone and toluene in the mixture was investigated using the best catalysts. In addition, XANES and EXAFS analysis provided on fresh and spent catalyst to determine the difference in the behavior of acetone and toluene in the reaction.

5.1. Abstract

Series of MnO_x/Al_2O_3 catalysts were synthesized by polyol and dry impregnation methods and calcined in the range of 400-800 ºC. The impacts of preparation procedure and calcination temperature were investigated to enhance the catalytic degradation of a single component and binary mixtures of acetone and toluene at room temperature. Polyol method produces catalysts with higher surface area, smaller cluster size, and lower oxidation state than the impregnation method. The results indicated that the oxidation state of manganese shifted to lower values by increasing the calcination temperature which had a beneficial influence on the catalytic performance. As calcination temperature rises to 800 ºC, the catalyst exhibited excellent

catalytic activity in acetone degradation while no significant change was observed in degradation of toluene. In the binary mixture, the oxidation behaviors were different from the single component system. The toluene conversion was promoted whereas the acetone conversion was inhibited. The XANES and EXAFS results of the spent catalysts showed that, unlike acetone, toluene altered the local structure of manganese oxides during the reaction. The catalyst was susceptible for the reduction process with toluene due to accumulation of carbonaceous species resulting from incomplete oxidation of toluene.

5.2. Introduction

VOCs are common chemical pollutants in indoor air released predominantly from human activities and household items such as adhesives, paints, printers, and building materials. VOCs in the environment are considered serious health concerns [175,176]. Catalytic ozonation is an effective technique for removal of VOCs in indoor air. Compared to the catalytic oxidation process, in catalytic ozonation, apparent activation energy decreases considerably and catalytic reaction proceeds at low temperatures [14]. Manganese based catalysts have shown superior activity for ozonation of VOCs and are among the most active metals in transition metal series [14,17,77,86]. Increased attention towards manganese-based catalysts is due to their activity in ozone decomposition, their redox properties, and being cheaper than the precious metals [30,177]. Alumina supported manganese oxides have been reported to exhibit the highest activity in the oxidation of VOCs [14,178,179].

One of the challenges in the catalytic ozonation process is performing the reaction at room temperature. Catalyst deactivation and accumulation of byproducts on the surface of the catalyst are inevitable in this process [30,180]. Therefore, it is important to enhance the catalyst's activity and stability to reduce catalyst deactivation at room temperature. The catalytic activity can be improved by altering properties such as metal oxidation state, cluster size, surface area, and dispersion [81,181,182]. The preparation method and calcination temperature have been reported to be significant parameters affecting the structural properties of the catalysts [93,95,182,183]. Einaga et al. [27] investigated the impact of the preparation procedure of unsupported manganese oxides catalysts on their properties. They further calcined the obtained catalysts at different temperatures and used them for ozonation of benzene. They found that benzene oxidation rate was dependent on the catalyst’s surface area and relatively independent of preparation method or

calcination temperature. In another research, a strong influence of calcination temperature of Mn/SiO_2 on benzene oxidation has been reported [25]. They indicated that manganese oxides phase in Mn/SiO_2 catalyst is a mixture of Mn_2O_3 and MnO_2 at lower calcination temperature. The MnO_2 at higher calcination temperature transformed to Mn_2O_3. The formation of Mn_2O_3 was responsible for its higher activity in benzene oxidation. Lu et al. [140] synthesized CuO/CeO_2 catalysts by polyol process and impregnation methods, calcined them at 300, 500, and 700 °C, and used them in oxidation of CO. Polyol catalysts showed greater CO removal activity in their study. They found that catalyst calcined at 500 °C had greater removal efficiency compared to those calcined at 300 °C and 700 °C. They also reported that crystalline size increased when the calcination temperature exceeded 600 °C which also affected the crystal phase and eventually impacted the catalyst activity.

In this paper, MnO_x/Al_2O_3 catalysts were synthesized using polyol and dry impregnation methods and calcined at different temperatures for catalytic ozonation of acetone and toluene. Among VOCs, toluene and acetone were chosen as model compounds due to their abundance in the indoor environment and their different chemical structures [184–186] Acetone and toluene are common solvents in the pharmaceutical industry [187]. The catalytic ozonation of acetone and toluene as a single compound over various catalysts has been widely studied in the literature [12,79,113,126]. However, few reports are available on catalytic ozonation of mixture systems over a range of concentrations. The objective of this study is to investigate the ozonation of single acetone and toluene and their mixture with different acetone/toluene concentrations at room temperature. The catalysts were analyzed by Brunauer–Emmett–Teller (BET) surface area measurement, transmission electron microscopy (TEM), high-angle annular dark-field and scanning transmission electron microscope (HAADF-STEM) mapping, X-ray photoelectron spectroscopy (XPS), X-ray absorption near-edge structure (XANES), extended X-ray absorption fine structure (EXAFS) and *In-situ* diffuse reflectance infrared Fourier transform spectroscopy (DRIFTS) analysis. To better understand the comparison of these two VOCs in the reaction, the spent catalysts were characterized by XANES, EXAFS, and temperature programmed oxidation (TPO) techniques.

5.3. Experimental

5.3.1. Catalytic activity tests

The catalytic ozonation reactions at room temperature were conducted in a Pyrex tubular glass reactor, installed in an oven (Binder, FP 115) (Figure 5.1). An ozone generator (AZCO Industries LTD, HTU-500S) was utilized to produce ozone from pure oxygen stream (Praxair, 99.993%). The generated ozone was mixed with a stream of VOC(s)-nitrogen and nitrogen to produce 120 and 1000 ppm of VOC(s) and ozone at the inlet of the reactor. Flow rates of VOC(s)-nitrogen and oxygen streams were set at 600 and 400 mL min^{-1} (STP), respectively. It should be mentioned that the total VOC(s) concentration in the inlet stream was 120 ppm for all catalytic ozonation experiments. Flow rates of the streams were set using three Brooks, SLA 5850 mass flow controllers. 0.2 g of powdered catalyst was used for each activity measurement. Catalysts were put between two pieces of glass wool and the rest of the reactor was filled with glass beads. The total flow rate at the inlet of the reactor was 1000 mL min^{-1} (STP) resulting in the weight hour space velocity (WHSV) of 300 L h^{-1} g^{-1}. Before introducing ozone to the system, gas streams of VOC(s), nitrogen, and oxygen were passed over the catalyst bed until the catalyst became saturated and the outlet concentration of VOC(s) reached the inlet level (120 ppm). Then, the ozone generator was turned on and the ozonation reaction was started at 25°C. The exhaust stream was analyzed by a long-path gas cell (PIKE, volume 0.1 L, 2.4 m optical length, KBr window), coupled with a Nicolet iS50 FTIR spectrometer.

The VOC and ozone conversions were calculated using Eqs. (5.1) and (5.2), where C_{in} and C_{out} represent their concentrations in the inlet and outlet of the reactor, respectively.

$$X_{VOC} = \frac{C_{VOC,in} - C_{VOC,out}}{C_{VOC,in}} \times 100\% \quad (5.1)$$

$$X_{Ozone} = \frac{C_{Ozone,in} - C_{Ozone,out}}{C_{Ozone,in}} \times 100\% \quad (5.2)$$

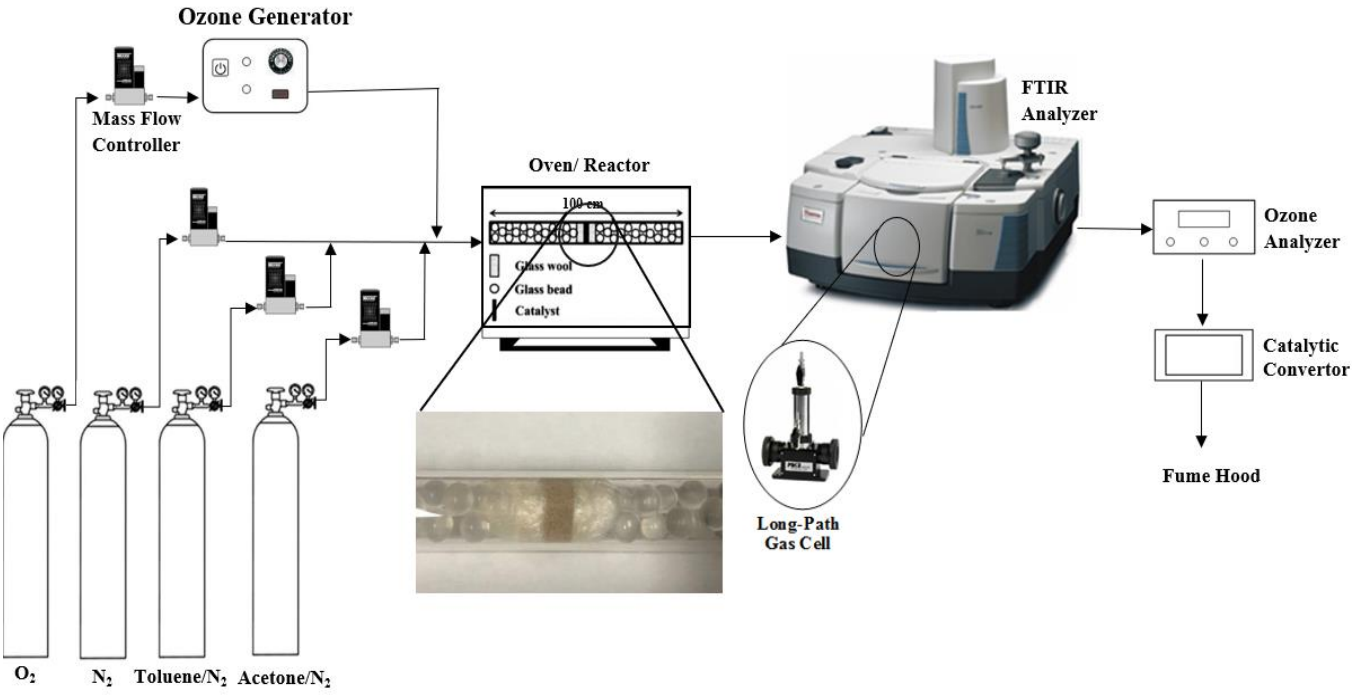

Figure 5.1. Schematic of the experimental setup for catalytic ozonation of toluene and acetone

5.3.2. Preparation of MnO_x/Al_2O_3-P

MnOx/Al_2O_3-P catalysts were synthesized using the polyol method. γ-Al_2O_3 (Alfa-Aesar) was used as support with particle sizes less than 0.208 mm. Based on our previous research, this catalyst size was chosen to eliminate transport resistances [98,102]. For the 5% nominal metal loading on the support, 0.45 g manganese (II) acetate tetrahydrate (Sigma Aldrich, 99%) was mixed with 0.10 g polyvynilpyrrolidone (PVP) (Sigma Aldrich, K30, molecular weight = 40,000) and 36.4 mL ethylene glycol (EG) (Sigma Aldrich, anhydrous, 99.8%). 1.86 g γ-Al_2O_3 was added, and the mixture was agitated with a magnetic stirrer overnight. Then, the mixture was heated under reflux to 160 ºC for almost 140 min using silicone oil bath. Details of the synthesis procedure can be found in our previous work [188]. At the end of reduction time, the mixture was rapidly cooled to room temperature using an ice bath. The catalyst thus obtained was separated using a centrifuge, and subsequently washed several times with ethanol and deionized water to remove the organic phase [149,189]. ICP-MS analysis showed that the actual loading was 3.5 %. The catalyst was dried in an oven overnight and calcined at different temperatures of

400, 500, 600, 700, or 800 °C. The catalysts were denoted as MnO_x/Al_2O_3-P-A (A refers to the calcination temperature (°C)).

5.3.3. Preparation of MnO_x/Al_2O_3-I

MnO_x/Al_2O_3-I with 3.5% manganese content was prepared by dry impregnation method with particle size less than 0.208 mm. γ-Al_2O_3 and manganese (II) acetate tetrahydrate were used as support and precursor, respectively. The synthesized catalysts were dried and calcined at the same conditions as MnO_x/Al_2O_3-P catalysts. Then, the catalyst was crushed and sieved to a final particle size of less than 0.208 mm. The catalysts were referred to as MnO_x/Al_2O_3-I-A (A refers to the calcination temperature (°C)).

5.3.4. Catalyst characterization

The BET surface area and pore volume of the catalysts were measured by nitrogen adsorption using an ASAP 2020 instrument (Micromeritics). The catalysts were degassed for 2 h at 110 °C and 0.5 mm Hg before the surface area and pore volume measurements. TEM images were obtained using Jeol 2010F field emission gun (FEG) operated at 200 keV to estimate particle size and dispersion of active metal on the support. TEM instrument was coupled with HAADF and energy dispersive X-ray (EDX) spectroscopy attachments to provide the catalyst's elemental composition and elemental mapping. Dispersion (D) of the supported catalyst was estimated from metal particle size based on the following formula:

$$D = \frac{6M}{a\rho Nd} \tag{5.3}$$

where M is molar mass of Mn (g mol^{-1}); a is Mn atom surface area (m^2); ρ is the density of Mn (g m^{-3}); d is mean metal particle size (m); N is the Avogadro's number.

XPS analysis was performed using a Kratos (Manchester, UK) AXIS Supra system. The survey scan spectra were collected with a step size of 1 eV and a pass energy of 160 eV. High

resolution scans were conducted using 0.05 eV steps with a pass energy of 20 eV. The XPS analysis was performed using the CasaXPS program.

XANES and EXAFS studies were carried out to obtain information about the oxidation states and local structure of the catalysts. XANES and EXAFS data were collected at the Mn *K-edge* in transmission mode at Hard X-ray Micro Analysis (HXMA) beamline at the Canadian Light Source. Catalysts were diluted with boron nitride (BN), ground, and pressed into thin disks. The prepared disks were protected by Kapton tape. During the XAFS analyses, the HXMA beamline was configured in its focus operation mode with Si(1 1 1) monochromator crystals and Rh mirrors as collimating and focusing mirrors in the X-ray beam path, respectively. Samples of the reference materials, including MnO (99% manganosite, Alfa Aesar), Mn_3O_4 (97% hausmannite, Sigma-Aldrich), Mn_2O_3(99% bixibyite, Sigma-Aldrich), and MnO_2 (99.9% pyrolusite, Alfa Aesar), were also measured in transmission mode. Data processing was performed by ATHENA and ARTEMIS software [122,190].

Fourier transforms were performed in k space from 3 $Å^{-1}$ to accordingly terminated at 12 $Å^{-1}$. EXAFS fittings were conducted in R space from 1 to 3.5 Å. Coordination numbers (CNs) were fixed based on the crystallography data for the two reference materials of Mn_3O_4 and Mn_2O_3 to determine amplitude reduction factor ($S_o{}^2$). The obtained $S_o{}^2$ value was used as a fixed parameter in EXAFS analysis of the catalysts to estimate the coordination numbers.

TPO analysis was performed on the selected catalysts in a modified experimental setup presented in detail elsewhere [79]. Briefly, the reaction was performed in a reaction chamber (Harrick, HVC-DRM-5) equipped with a temperature controller that allows operation up to 900 ºC. Inlet gas flow rate and catalyst weight were set to 250 mL min^{-1} and 50 mg to reach WHSV at 300 L h^{-1} g^{-1}. The spent catalyst was purged with nitrogen flow after the reaction for 10 min and then heated to 745 °C at 10 ºC min^{-1} under a 250 mL min^{-1} atmospheric flow of oxygen-nitrogen (20–80 v%).

In-situ DRIFTS experiments were performed in a reaction chamber (Harrick, HVC-DRM-5) equipped with ZnSe windows. The reaction chamber was coupled with the DRIFTS accessory which was placed in the FTIR spectrometer. To avoid the saturation of the MCT-A detector, data were collected at a resolution of 4 cm^{-1} in the range of 3900–1300 cm^{-1}.

5.4. Results and discussion

5.4.1. Catalyst characterization

The physical characteristics of the selected samples are given in Table 5.1. It shows that the method of synthesis and calcination temperature affect the catalysts' structural properties. The MnO_x/Al_2O_3-P catalysts had higher specific surface area and pore volume and smaller Mn cluster sizes than MnO_x/Al_2O_3-I. With an increase in calcination temperature, surface area decreases due to metal particle size growth that can lead to pore blockage. The average Mn cluster sizes of the samples obtained from TEM images are given in Table 5.1. An increase in Mn cluster size was observed in the catalysts calcined at 800 °C compared to 500 °C samples. The results were consistent with the literature that the increase of calcination temperature corresponds to a decrease in BET specific surface area and an increase in metal cluster size [140,191,192].

Table 5.1.Physical and chemical parameters of the catalysts.

Catalyst	BET surface area ($m^2\ g^{-1}$)	Pore volume ($cm^3\ g^{-1}$)	Mn particle size [a] (nm)	Mn dispersion [b] (%)
MnO_x/Al_2O_3-P-500	203	0.58	4.1	26.4
MnO_x/Al_2O_3-I-500	184	0.54	5.4	20.1
MnO_x/Al_2O_3-P-800	187	0.57	6.2	17.5
MnO_x/Al_2O_3-I-800	176	0.51	7.0	15.5

[a] average value determined from TEM.
[b] calculated from Eq. 5.3.

Figure 5.2 shows the TEM images, metal particle size distribution, and HAADF-EDX analysis of the four selected catalysts. The size of the Mn particles of Mn/Al_2O_3-P is smaller than that of Mn/Al_2O_3-I catalysts and consequently higher dispersion of Mn particles can be expected. The trend shows an increase in Mn particle size with an increase in calcination temperature. The dispersion of Mn clusters was calculated from the particle size of the TEM analysis using Eq. (5.3) and presented in Table 5.1. The HAADF-EDX analysis was used to identify the chemical composition of the samples. It confirmed the presence of Mn, Al, and O and the uniform

distribution of all elements throughout all samples. TEM images show that Mn nanoparticles in samples calcined at 800 ºC are uniform and slightly agglomerated.

MnO_x/Al_2O_3-I-500

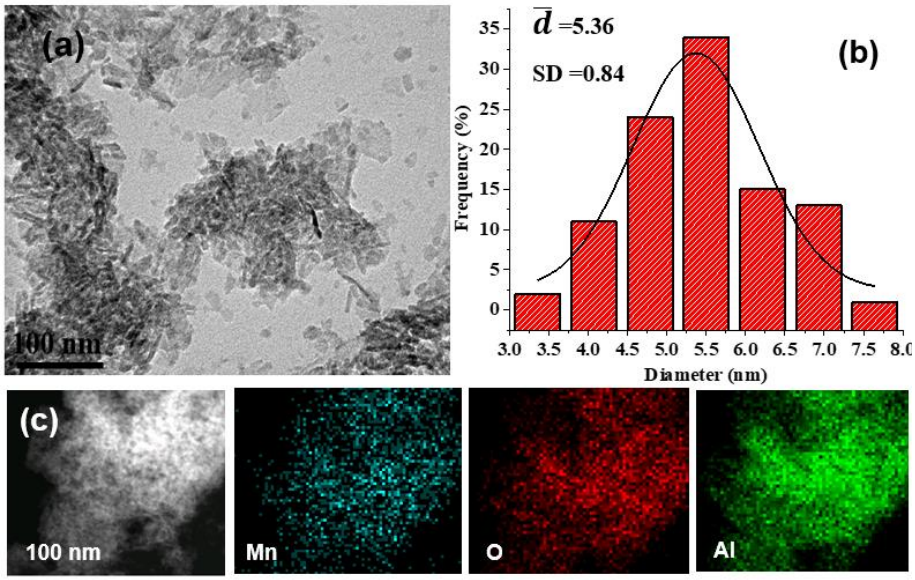

MnO_x/Al_2O_3-P-500

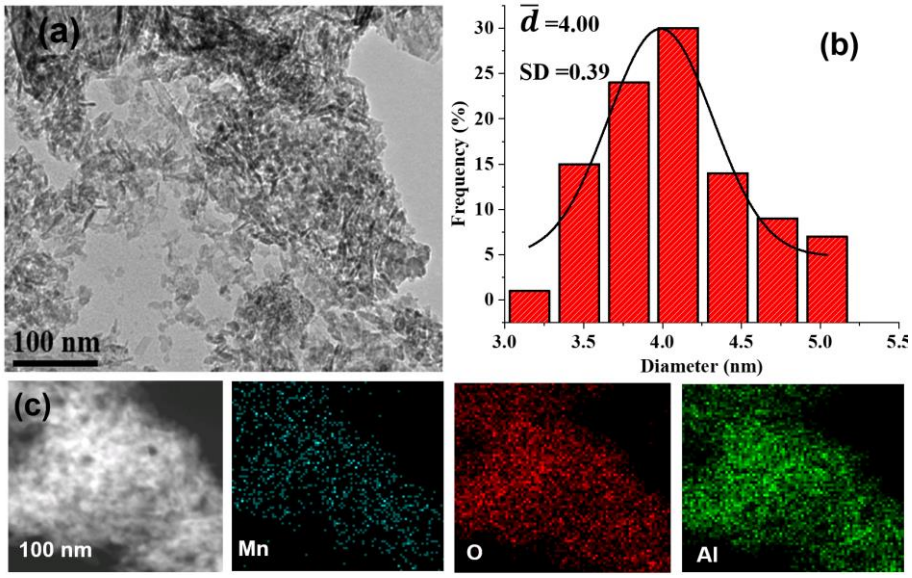

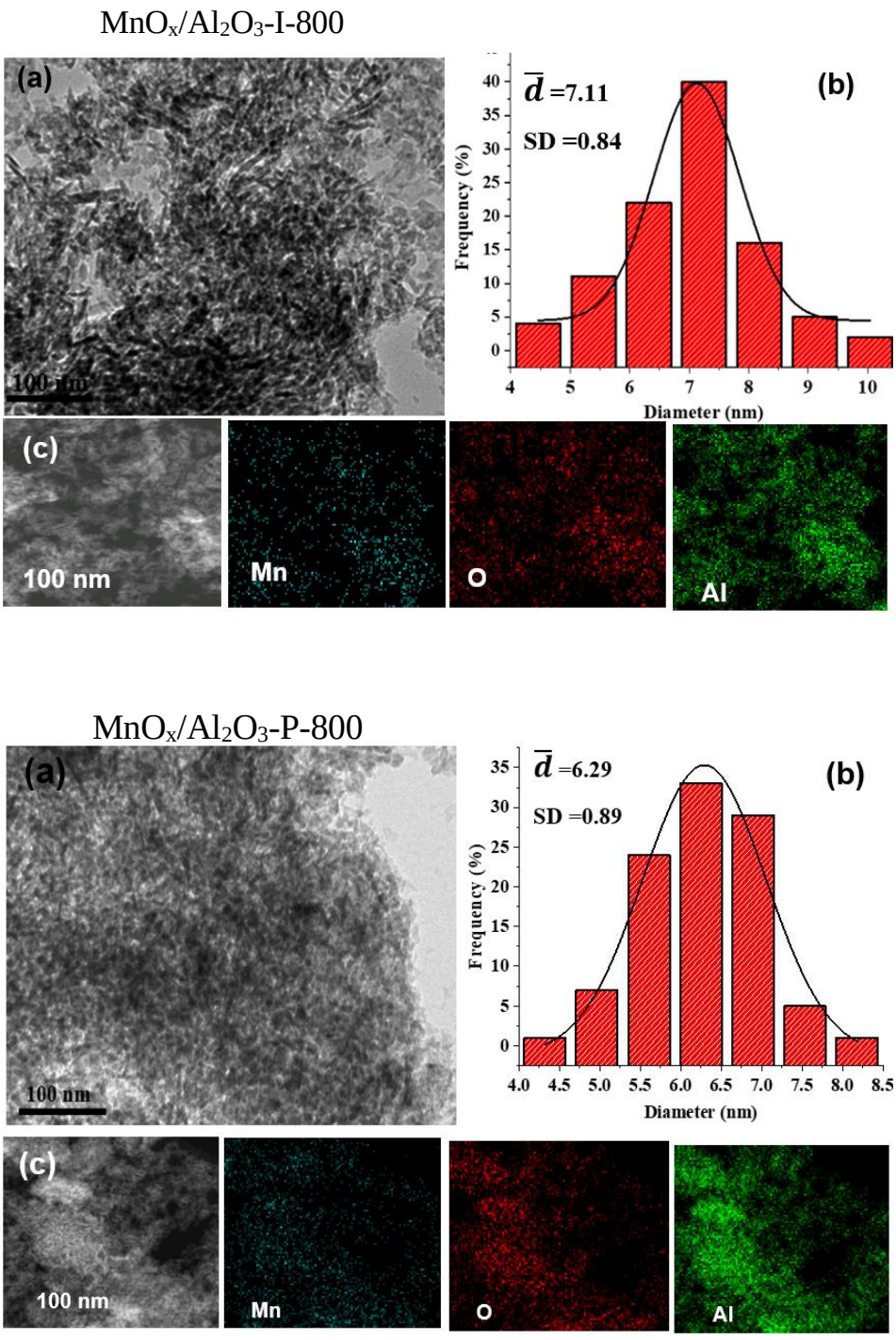

Figure 5.2. TEM images, (b) Mn particle size distribution, and (c) HAADF-EDX elemental mapping of the catalysts.

XPS analysis was conducted to investigate the state of Mn on the surface of the catalyst. Figure 5.3 shows the high-resolution Mn 2p spectra of the catalysts. The Mn $2p_{3/2}$ spectra of the samples decomposed into three characteristic peaks corresponding to Mn^{2+}, Mn^{3+}, and Mn^{4+} species at binding energies of 640.2-640.5 eV, 641.6-641.9 eV, and 643.3-644.0 eV, respectively [163,165,193,194]. In the MnO_x/Al_2O_3-P-800 and MnO_x/Al_2O_3-I-800 samples, the Mn $2p_{3/2}$ peak shows the presence of a shake-up satellite peak. This shoulder around binding energy of 646.3 eV was attributed to the satellite peak of MnO [163,165,194,195]. The results indicated that Mn^{3+} is the dominant state of Mn in all catalysts. The amount of Mn^{2+} species on the surface of polyol catalysts was higher than the impregnated ones. As calcination temperature increases, the metal oxide phase on the surface of the catalyst was reduced and the satellite peak of MnO appeared. These observations may suggest that the lower oxidation state of manganese on the surface of the catalyst can be correlated with the presence of oxygen vacancies which is essential for oxidation of organic components.

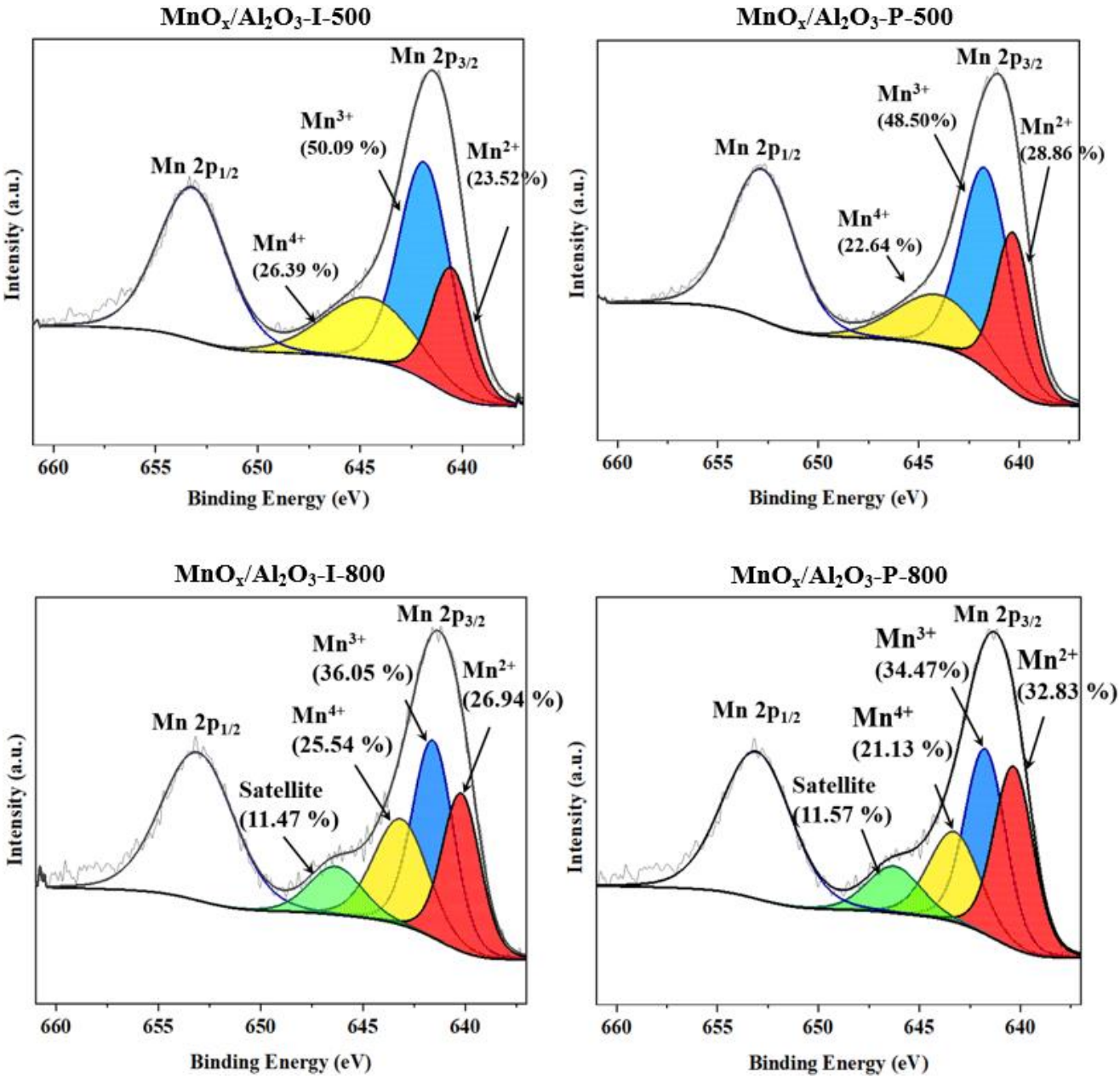

Figure 5.3. XPS spectra of Mn 2p of the catalysts.

Mn *K-edge* XANES spectra of the pure reference materials and all the catalysts were collected to investigate the manganese oxide phases of the catalysts (Figure 5.4 (a) and (b)). Mn *K-edge* XANES spectra of the samples with different preparation methods and calcination temperature were compared to the spectra of the reference materials. The samples show similar spectra to those of Mn_3O_4 and Mn_2O_3. Figure 5.4(b) illustrates that the edge jump of the XANES

spectra of the catalyst becomes more similar to that in Mn_3O_4 as the calcination temperature increases. Mn *K-edge* absorption energy (E_0) of the samples was between 6547.50 and 6548.38 eV, which were very close to Mn *K-edge* absorption energy of Mn_3O_4 (6547.00 eV). A gradual shift in absorption energy towards lower energy was observed as calcination temperature increased in both impregnated and polyol catalysts. Figure 5.4 (c) displays the progressive changing of edge jump and its dependency on calcination temperature, revealing change in the relative weight of Mn phases. Linear combination fitting was used to quantify the presence of each reference material. The results are presented in Table 5.2.

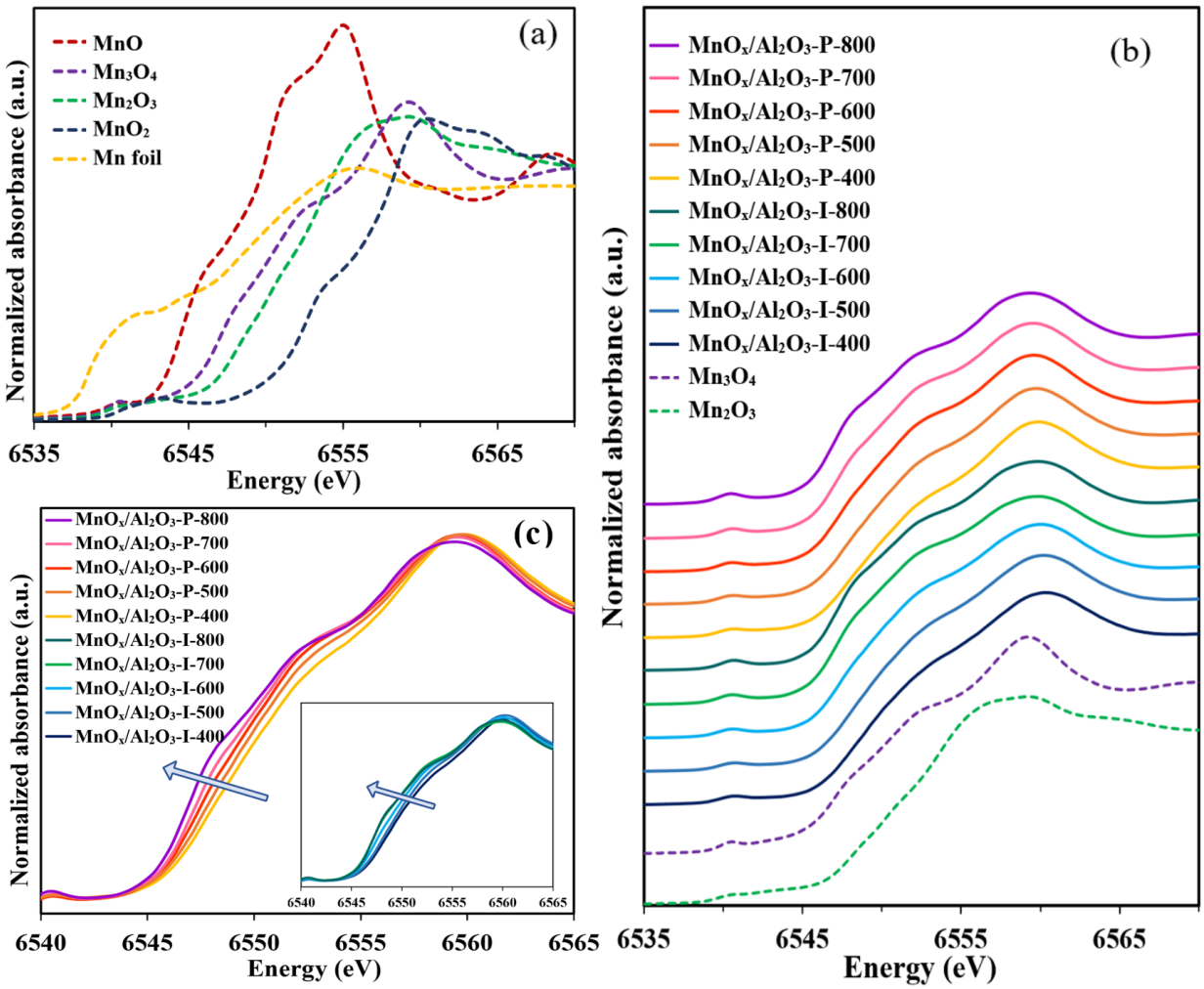

Figure 5.4. Mn K-edge XANES spectra of (a) the reference materials and (b,c) the catalysts.

Table 5.2. Composition of catalysts based on linear combination fitting of Mn K-edge XANES.

Catalyst	Mn_3O_4 (%)	Mn_2O_3 (%)	MnO_2 (%)
MnO_x/Al_2O_3-P-400	57	36	7
MnO_x/Al_2O_3-P-500	67	33	-
MnO_x/Al_2O_3-P-600	83	17	-
MnO_x/Al_2O_3-P-700	94	6	-
MnO_x/Al_2O_3-P-800	100	-	-
MnO_x/Al_2O_3-I-400	47	41	12
MnO_x/Al_2O_3-I-500	49	48	3
MnO_x/Al_2O_3-I-600	73	27	-
MnO_x/Al_2O_3-I-700	97	3	-
MnO_x/Al_2O_3-I-800	96	4	-

The results in Table 5.2 indicated that Mn_3O_4 is the dominant form of manganese oxides in all catalysts and with an increase in the calcination temperature, the content of Mn_3O_4 species increased. Overall, the polyol catalysts are composed of more Mn_3O_4 and have lower averaged Mn oxidation states than impregnated catalysts. The polyol catalyst calcined at 800 °C consists of 100% Mn_3O_4. It should be pointed out that the catalysts with calcination temperatures of 700 and 800 °C are mainly composed of Mn_3O_4 with a negligible amount of Mn_2O_3.

It has been reported by Rezaei et al. that the lower oxidation states of manganese are more desirable in ozone decomposition and toluene oxidation [30]. Similar results have been reported by other researchers indicating that lower oxidation states of manganese are more active in degradation of VOCs [103,113]. Kim et al. [162] have reported that the catalytic activity was in the order of Mn_3O_4 >Mn_2O_3 >MnO_2 for oxidation of VOCs, this was attributed to the oxygen mobility on the catalyst [162]. In ozone decomposition, which is a critical step in catalytic ozonation reaction, atomic oxygens are produced and react with VOCs. As oxidation state of manganese decreases, the mobility of manganese atoms increases, and electron transfer to ozone is enhanced.

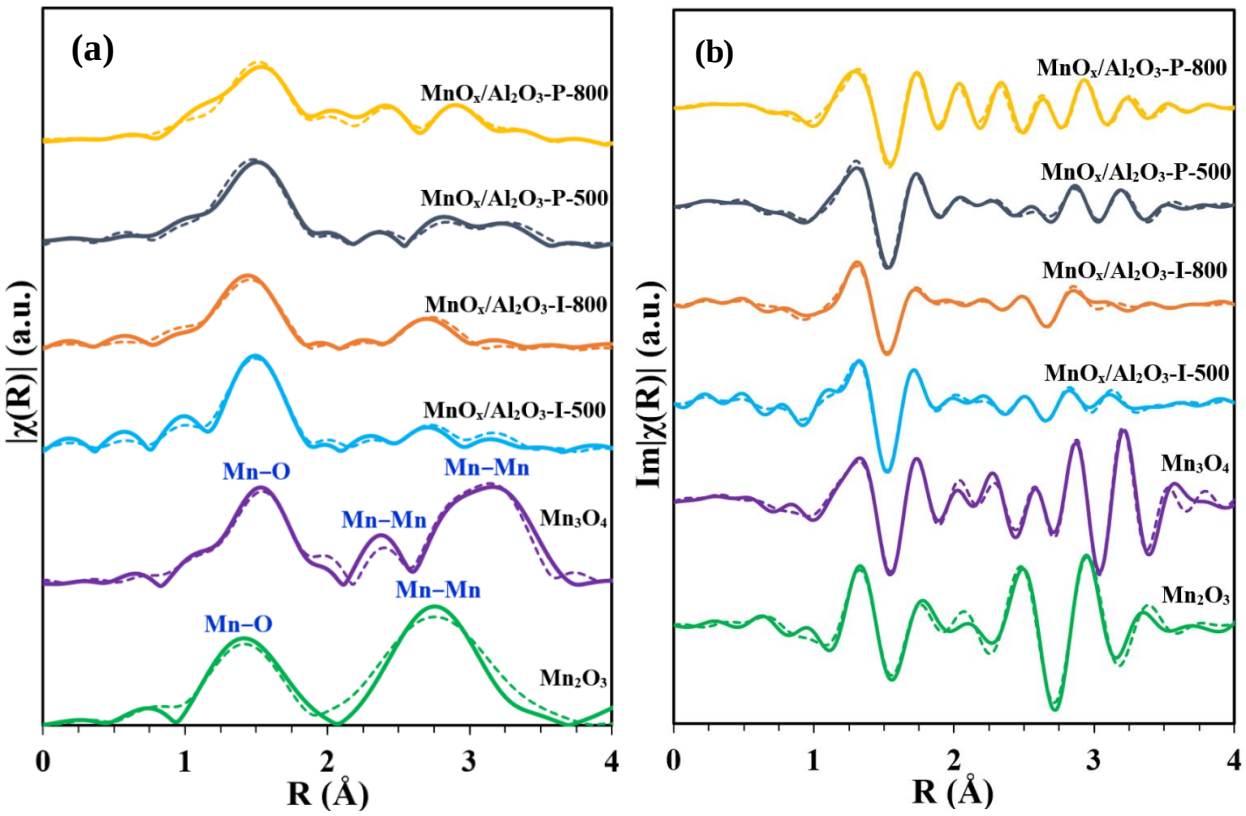

Figure 5.5. (a) Magnitude and (b) imaginary part of the Fourier transform of Mn K-edge EXAFS spectra, Experimental curves (solid lines), and fitting curves (dash lines).

According to XANES results, the catalysts were mainly combinations of Mn_3O_4 and Mn_2O_3. Figure 5.5 shows the magnitude and imaginary part of the Fourier transform of Mn *K-edge* EXAFS spectra and the fitted models of the selected samples as well as Mn_3O_4 and Mn_2O_3. For the reference Mn_2O_3, two peaks appeared at 1.41 and 2.76 Å, assigned to the Mn–O and Mn–Mn bonds. For Mn_3O_4, the peak at 1.53 Å is ascribed to Mn–O, while the peaks at 2.38 and 3.16 Å are related to Mn–Mn bonds. The structures of Mn_3O_4 and Mn_2O_3 consist of two sites of Mn atoms of different Mn–O coordination. The first site of the standard structure of Mn_3O_4 has octahedral and the second site has tetrahedral coordination of oxygen with Mn atoms with occupancy of 2:1, respectively. The first site has 4 oxygen bonds at 1.93 Å and 2 bonds at 2.28 Å, while the second site has 4 oxygen bonds at 2.04 Å. The crystal structure of Mn_2O_3 has a site with occupancy of 75% which has 6 oxygen neighboring atoms: two oxygen bonds at 1.90 Å, two oxygen bonds at 1.98 Å, and another set of two oxygen bonds at 2.25 Å. The other site with 25% occupancy has six oxygen atoms at 1.99 Å. The presence of two Mn sites in the structure of

reference samples and close atomic coordinates make the EXAFS fitting complicated. The averaging method was applied using the aggregate FEFF calculation to simplify the EXAFS analysis. Table 5.3 reports the EXAFS fitting results for Mn_3O_4 and Mn_2O_3 samples.

Table 5.3. EXAFS fitting results for the Mn oxides reference materials.

Catalyst	Path/bond	CN[a]	R (Å)[b]	σ^2($\times10^{-3}$ Å^2)[c]	ΔE_o (eV)[d]	S_o^2	R_f (%)[e]
Mn_2O_3 (Averaging	Mn–O	1.5	1.90 ± 0.03	3.8 ± 3.4	- 4.9 ± 2.3	0.710 ±	2.2
method)	Mn–O	3	1.99 ± 0.03			0.188	
	Mn–O	1.5	2.25 ± 0.03				
	Mn–Mn	6	3.11 ± 0.03	8.2 ± 3.3			
	Mn–Mn	6	3.57 ± 0.02				
Mn_3O_4 (Averaging	Mn–O	2.7	1.93 ± 0.01	3.3 ± 0.7	4.3 ± 0.9	0.713 ±	1.9
method)	Mn–O	1.3	2.04 ± 0.01			0.062	
	Mn–O	1.3	2.28 ± 0.01				
	Mn–Mn	1.3	2.89 ± 0.02	5.2 ± 0.8			
	Mn–Mn	2.7	3.12 ±0.02				
	Mn–Mn	5.3	3.44 ±0.02				
	Mn–O	8	3.79 ±0.09	9.9 ± 4.3			

[a] CN: coordination number.
[b] R: bond distance.
[c] σ^2: Debye–Waller factor.
[d] ΔE_o: change in energy scale.
e The absolute percentage misfit between theory and data.

Coordination numbers in the EXAFS analysis of reference materials were fixed based on the standard structures. Therefore, the S_o^2 value was determined to be approximately 0.71 for both Mn_2O_3 and Mn_3O_4. The obtained S_o^2 value was used for fitting of the catalysts and the results for EXAFS analysis of the polyol and impregnated catalysts are summarized in Tables 5.4 and 5.5, respectively. All values for *R* factors (R_f) were low (around 2% or less) for all EXAFS fittings, suggesting that the models have been fitted closely to the EXAFS data.

Table 5.4. EXAFS fitting results of the polyol catalysts.

Catalyst	Path/bond	CN	R (Å)	σ^2($\times10^{-3}$ Å^2)	ΔE_o (eV)	R_f (%)
MnO_x/Al_2O_3-P-400	Mn–O	4.3 ± 0.9	1.93 ± 0.02	7.7 ± 2.2	1.9 ± 2.1	2.4
	Mn–O	1.4 ± 1.1	2.28 ± 0.02			
	Mn–Mn	2.1 ± 0.9	2.89 ± 0.04			
	Mn–Mn	0.8 ± 0.7	3.12 ± 0.04	9.2 ± 1.0		
	Mn–Mn	1.0 ± 1.0	3.44 ± 0.04			
MnO_x/Al_2O_3-P-500	Mn–O	4.4 ± 0.9	1.93 ± 0.01	7.9 ± 2.6	4.1 ± 2.3	1.5
	Mn–O	1.2 ± 0.98	2.25 ± 0.01			
	Mn–O	0.7 ± 1.1	2.28 ± 0.01			
	Mn–Mn	0.5 ± 0.3	2.89 ± 0.03	2.5 ± 0.8		
	Mn–Mn	0.4 ± 0.5	3.44 ±0.03			
	Mn–O	1.5 ± 1.3	3.79 ±0.03			
MnO_x/Al_2O_3-P-600	Mn–O	1.3 ± 1.2	1.93 ± 0.01	0.7 ± 0.2	-1.5 ± 2.8	1.9
	Mn–O	1.5 ±1.3	2.04 ± 0.01			
	Mn–Mn	1.1 ± 0.6	2.89 ± 0.01			
	Mn–Mn	2.5 ± 1.0	3.12 ± 0.02	8.3 ± 0.6		
	Mn–Mn	0.9 ± 1.1	3.44 ±0.02			
MnO_x/Al_2O_3-P-700	Mn–O	2.8 ± 1.4	1.93 ± 0.03	6.1 ± 3.6	-0.5 ± 3.0	1.7
	Mn–O	0.9 ±1.5	2.04 ± 0.03			
	Mn–O	0.8 ± 0.8	2.28 ± 0.03			
	Mn–Mn	0.9 ± 0.9	2.89 ± 0.05	9.6 ± 2.8		
	Mn–Mn	2.3 ± 1.3	3.12 ±0.05			
	Mn–Mn	0.5 ± 0.9	3.44 ±0.05			
MnO_x/Al_2O_3-P-800	Mn–O	1.4 ± 0.6	1.93 ± 0.06	1.6 ± 2.4	2.8 ± 1.4	2.1
	Mn–O	1.9 ± 0.6	2.04 ± 0.06			
	Mn–O	1.1 ± 0.3	2.28 ± 0.06			
	Mn–Mn	2.4 ± 0.6	2.89 ± 0.07	7.4 ± 3.6		
	Mn–Mn	3.8 ± 1.1	3.12 ±0.06			
	Mn–Mn	1.5 ± 0.8	3.44 ±0.01			

Table 5.5. EXAFS fitting results of the impregnated catalysts.

Catalyst	Path/bond	CN	R (Å)	σ^2($\times10^{-3}$ Å^2)	ΔE_o (eV)	R_f (%)
MnO_x/Al_2O_3-I-400	Mn–O	3.1 ± 0.4	1.93 ± 0.01	3.9 ± 1.8	- 1.14 ± 1.7	2.2
	Mn–Mn	0.5 ± 0.4	2.89 ± 0.08	5.0 ± 0.7		
	Mn–Mn	0.8 ± 0.7	3.11 ± 0.08	5.0 ± 0.7		
MnO_x/Al_2O_3-I-500	Mn–O	2.8 ± 0.2	1.93 ± 0.01	3.6 ± 0.7	3.0 ± 1.2	1.2
	Mn–O	0.2 ± 0.4	2.25 ± 0.01			
	Mn–O	0.1 ± 0.3	2.28 ± 0.01			
	Mn–Mn	0.7 ± 0.3	2.89 ± 0.08	5.8 ± 2.8		
	Mn–Mn	1.3 ± 0.3	3.12 ±0.08			
	Mn–O	3.7 ± 0.9	3.79 ±0.09	9.4 ± 4.1		
MnO_x/Al_2O_3-I-600	Mn–O	2.4 ± 0.8	1.93 ± 0.05	3.9 ± 2.9	1.0 ± 1.5	1.4
	Mn–O	1.1 ± 0.7	2.04 ± 0.05			
	Mn–O	0.9 ± 0.4	2.28 ± 0.05			
	Mn–Mn	1.4 ± 0.5	2.89 ± 0.07	8.4 ± 3.2		
	Mn–Mn	1.5 ± 0.6	3.12 ±0.07			
MnO_x/Al_2O_3-I-700	Mn–O	2.3 ± 0.5	1.93 ± 0.04	4.4 ± 1.9	1.3 ± 1.7	1.9
	Mn–O	1.0 ± 0.3	2.04 ± 0.04			
	Mn–O	0.8 ± 0.4	2.28 ± 0.04			
	Mn–Mn	1.6 ± 0.5	2.88 ± 0.06	10.0 ± 0.8		
	Mn–Mn	2.2 ± 0.7	3.12 ± 0.06			
	Mn–Mn	0.4 ± 0.6	3.44 ± 0.06			
MnO_x/Al_2O_3-I-800	Mn–O	2.8 ± 0.8	1.93 ± 0.03	6.3 ± 2.3	-2.4 ± 1.3	1.5
	Mn–O	0.2 ± 0.9	2.04 ± 0.03			
	Mn–Mn	1.1 ± 0.5	2.89 ± 0.07	9.8 ± 3.2		
	Mn–Mn	2.6 ± 0.8	3.12 ± 0.07			

As presented in Table 5.4, starting with MnO_x/Al_2O_3-P-400 sample, the first coordination shell was fitted with 4.3 and 1.4 oxygen atoms at 1.93 and 2.28 Å corresponding to the molecular structure of Mn_2O_3. In the second shell, 2.1, 0.8, and 1.0 Mn atoms were found at 2.89, 3.12, and 3.44 Å, which is a mixture of the second shell structure of Mn_2O_3 and Mn_3O_4. As calcination temperature rises, the average local environment of Mn changed, and based on the presented models, the structures became more similar to Mn_3O_4. The configurations of MnO_x/Al_2O_3-P-700 and MnO_x/Al_2O_3-P-800 catalysts are very similar to the local structure of Mn_3O_4. The same trend

can be observed in the impregnated catalysts reported in Table 5.5. In some samples, a very broad and weak peak at the second shell demonstrated the reason for the low coordination numbers of Mn in the EXAFS fitting.

The results acquired from EXAFS analyses support the XANES findings that the local structure and oxidation states of Mn change with calcination temperature. Higher calcination temperature leads to lower oxidation states of Mn which is an essential factor in the activity of the catalyst in the ozonation of VOCs.

5.4.2. Catalyst activity

The activities of the catalysts in catalytic ozonation of single acetone and toluene are shown in Figure 5.6. Toluene conversion was not seriously affected by variation in calcination temperature. However, acetone conversion increased when the calcination temperature was raised to 800 °C. An acetone conversion of 95% was achieved using MnO_x-Al_2O_3-P-800 catalyst. The acetone conversion was enhanced by about 33% when calcining the catalyst at 800 °C compared to 400 °C. Polyol catalysts generally exhibited higher VOC and ozone conversion compared to the impregnated catalysts. In the case of toluene removal, the polyol catalyst performed approximately 17% better than the impregnated ones.

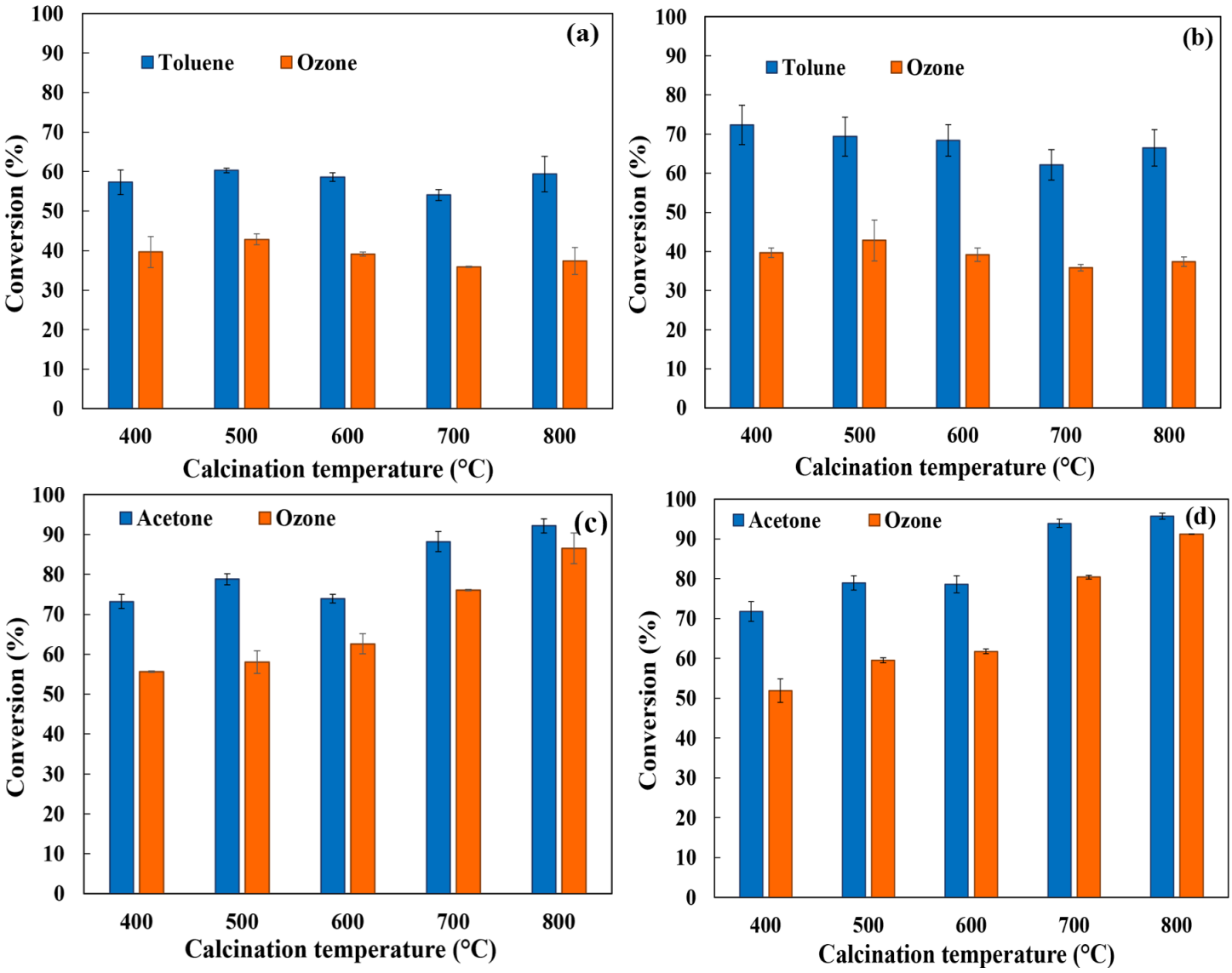

Figure 5.6. Effect of calcination temperature on toluene, acetone and ozone conversions (%): (a,c) Impregnation, (b,d) polyol catalysts, Catalytic ozonation at 25 °C and 150 min of reaction, 0.2 g catalyst, [O_3] = 1000 ppm, [VOC] = 120 ppm.

Catalytic ozonation of mixtures of toluene and acetone were performed on selected catalysts. Figure 5.7 shows the VOCs and ozone conversions in the binary mixture reactions. The results indicated that in the binary mixture experiments, toluene conversion was remarkably higher than acetone conversion, while in single component reaction, conversion of toluene was less than acetone. It should be pointed out that MnO_x-Al_2O_3-P-800 catalyst removed 100% of toluene during 150 min of reaction in a mixture of acetone/toluene 1:1 (Figure 5.7 (b)). Investigation on

the behavior of VOCs in a binary mixture with different concentrations of acetone and toluene was also conducted. Table 5.6 shows acetone, toluene, and ozone conversions in catalytic ozonation reaction at different acetone/toluene ratios. Regardless of the composition ratio of these two VOCs, toluene was removed better than acetone in a binary mixture. As the concentration of toluene was increased in the mixture, the conversions of VOCs and ozone dropped, although the conversion of toluene was consistently higher than acetone. The results suggest that toluene is more resistant to oxidation than acetone. The reason for better toluene removal in the mixture can be attributed to the inhibiting and promoting behaviors commonly observed in the catalytic oxidation reaction [102,187].

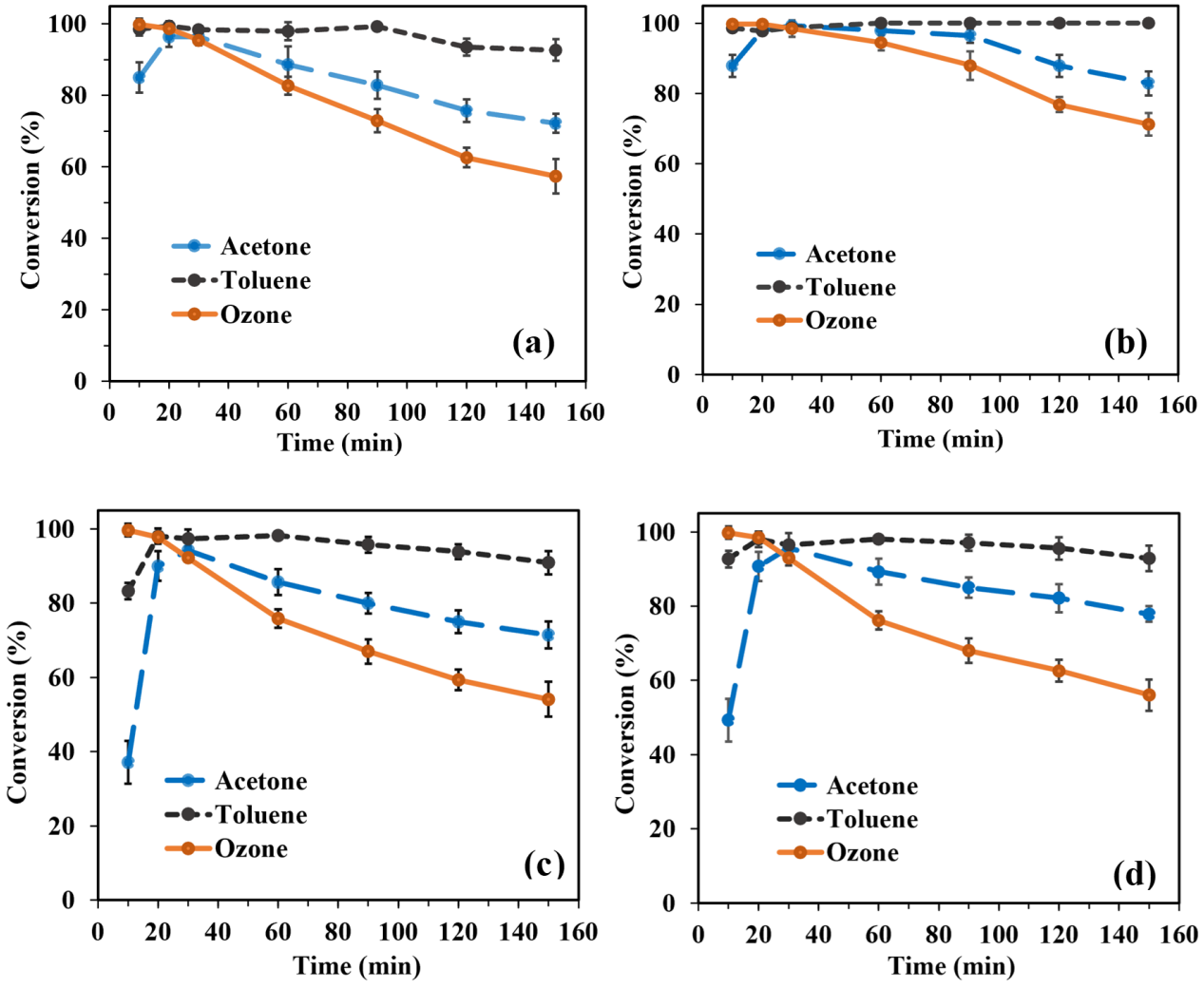

Figure 5.7. Conversions of acetone, toluene, and ozone in binary mixture, (a) MnO_x-Al_2O_3-I-800, (b) MnO_x-Al_2O_3-P-800, (c) MnO_x-Al_2O_3-I-500, (d) MnO_x-Al_2O_3-P-500, catalytic ozonation at 25 °C, [O_3] = 1000 ppm, [acetone] = 60 ppm, [toluene] = 60 ppm, 0.2 g catalyst.

Table 5.6. Conversions of acetone, toluene, and ozone in binary mixtures with different concentrations after 150 min of ozonation.

	Acetone	Toluene	Acetone	Toluene	Acetone	Toluene
	30 ppm	90 ppm	60 ppm	60 ppm	90 ppm	30 ppm
MnO_x-Al_2O_3-P-800						
Toluene conversion (%)	92.6		100.0		99.8	
Acetone conversion (%)	77.1		82.9		93.6	
Ozone conversion (%)	46.8		71.2		76.5	
MnO_x-Al_2O_3-I-800						
Toluene conversion (%)	90.3		92.7		97.8	
Acetone conversion (%)	72.5		74.1		89.1	
Ozone conversion (%)	40.4		58.4		75.9	

Using breakthrough curves of adsorption of VOCs in the mixture over the catalyst (Figure 5.8), it was observed that acetone is adsorbed strongly on the catalyst in the absence of ozone. This means that acetone competes with toluene for the adsorption on the catalyst and compels the toluene molecules to be desorbed gradually. The competitive adsorption between acetone and toluene may justify the significant difference in the catalytic ozonation of their binary system [196]. Sabatier principle states “the interaction of catalyst and the substrate should be not too week that can not activate the reactant and not too strong to be able to dissociate the products” [197]. Aghbolaghy et al. attributed the higher conversion of toluene in the mixture to the lower apparent activation energy of toluene [102]. The other reason is the inhibitory effect on acetone removal due to the accumulation of carbonaceous materials that are created from incomplete oxidation of toluene. Bianchi et al. [185] noted that toluene degradation is more complicated than acetone. This was attributed to the presence of an aromatic ring in its structure that resulted in the generation of more byproducts. The byproducts are also considered pollutants and are oxidized in turn.

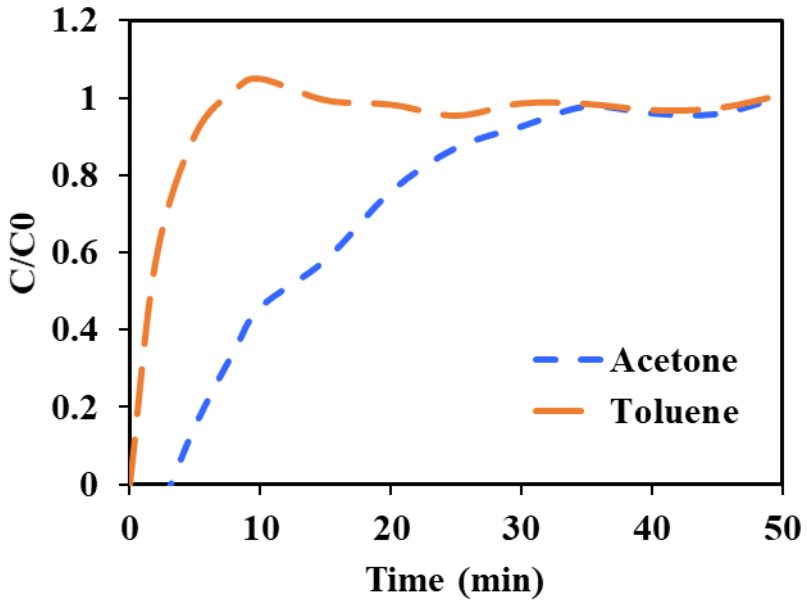

Figure 5.8. Breakthrough curves of adsorption of toluene and acetone (1:1 mixture) on MnO_x/Al_2O_3-I-800.

The main reaction products in the exhaust stream were CO and CO_2. The CO/CO_2 ratio decreased as calcination temperature increased and the values for polyol samples were slightly lower. In other words, polyol catalysts exhibited slightly higher selectivity towards CO_2. A similar pattern was observed for both acetone and toluene reactions. Figure 5.9 shows CO_x composition using MnO_x-Al_2O_3-I-800 and MnO_x-Al_2O_3-P-800 catalysts for a single component and binary mixture reactions. The results demonstrated that toluene produces a higher amount of CO than acetone. As toluene concentration increased in the binary mixture, the CO concentration also increased. This can suggest that the oxidation of toluene is incomplete. TPO experiments on the spent catalyst indicated that the severe catalyst deactivation during the ozonation of toluene is mainly due to the accumulation of carbonaceous species. The formation of components such as acetic acid and formic acid on the surface was because of incomplete oxidation of toluene.

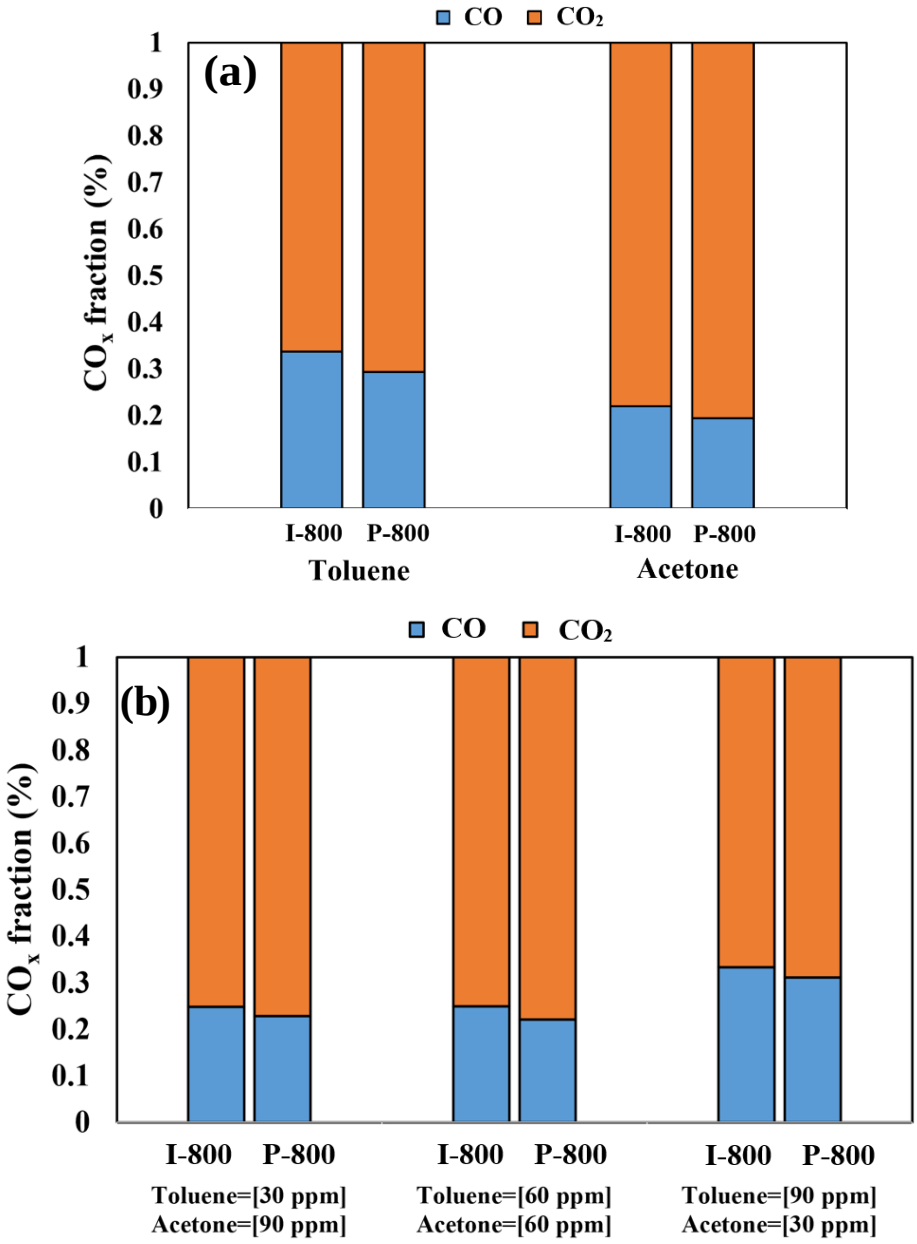

Figure 5.9.CO_x fraction in the exhaust stream for (a) single component and (b) binary mixture after 150 min of reaction using MnO_x-Al_2O_3-I-800 and MnO_x-$Al2O_3$-P-800, catalytic ozonation at 25 °C, [O_3] = 1000 ppm, [VOC] = 120 ppm, 0.2 g catalyst.

TPO runs were performed on the selected catalysts after acetone and toluene reaction with ozone. During TPO analysis of toluene, other than CO_2 and CO, acetic and formic acids were also produced, however, these peaks did not appear for acetone. The amount of acetic acid and formic acid released from polyol catalysts were significantly lower than the impregnated catalysts (Figure 5.10). According to the presented results, the catalyst calcinated at 800 ºC

generated less of these intermediate species. Accumulation of these carbonaceous species on the surface reduces the activity of the catalyst and eventually causes its deactivation.

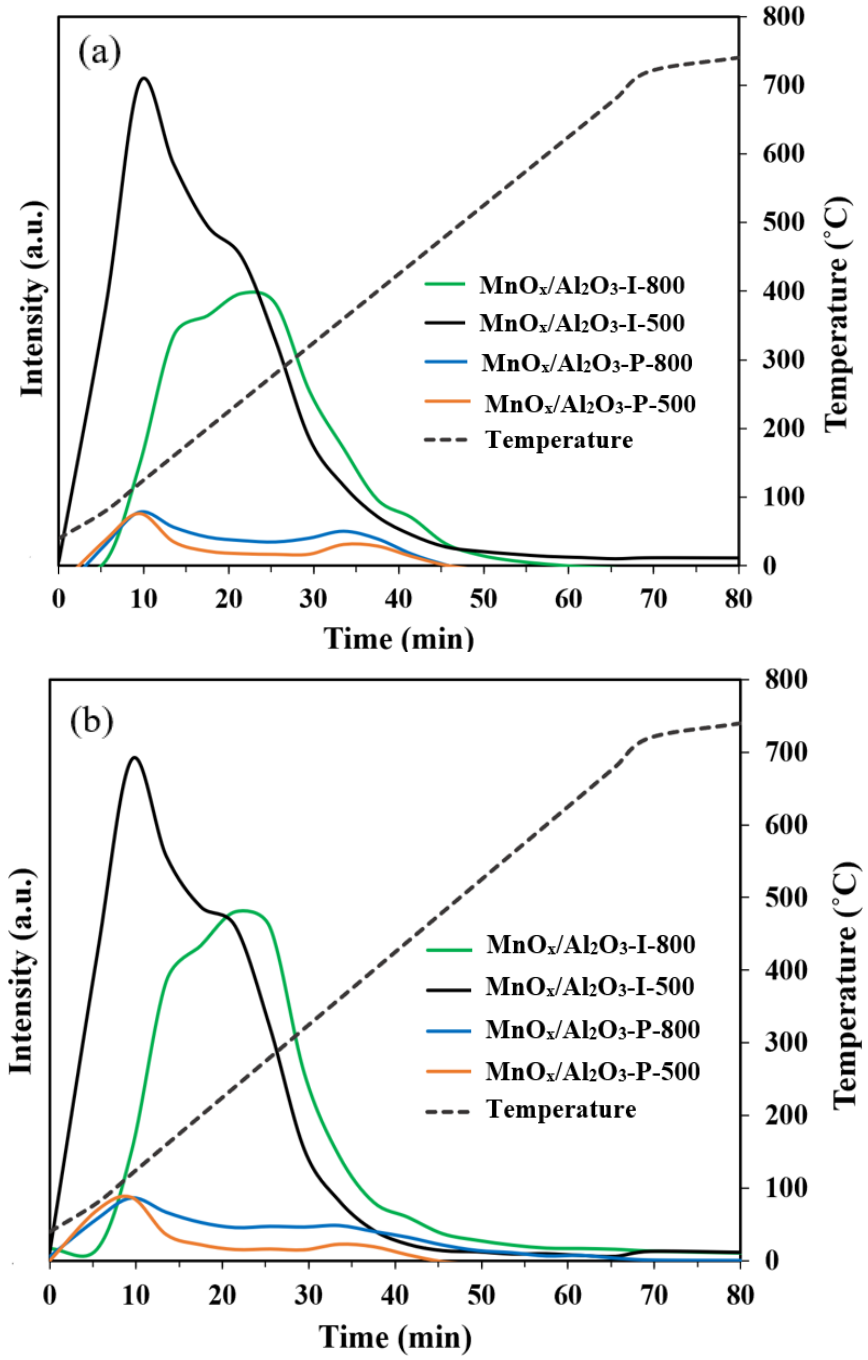

Figure 5.10.TPO profiles of desorption of (a) acetic acid and (b) formic acid from the spent catalysts in catalytic ozonation of toluene.

The greater number of intermediate products in the toluene ozonation reaction can be attributed to the structure of toluene that consists of seven carbon atoms compared to acetone with three carbon atoms. The more carbon atoms need more oxidation processes to convert toluene to CO_x and meanwhile, other carbonaceous compounds are produced.

Long-term activity test was performed on catalytic ozonation of acetone using MnO_x-Al_2O_3-p-800 catalyst. The results of the conversions and CO_x concentrations are presented in Figure 5.11. The regeneration characteristics of the catalysts were studied on the selected samples. The spent catalysts were heated to 400 ºC for 1 h in air to remove the intermediate products on the surface of the catalyst. The regenerated catalysts were used for a second catalytic ozonation test of toluene and acetone. The activity of the regenerated catalysts was more than 90% of the fresh catalysts. The results are shown in Figure 5.12.

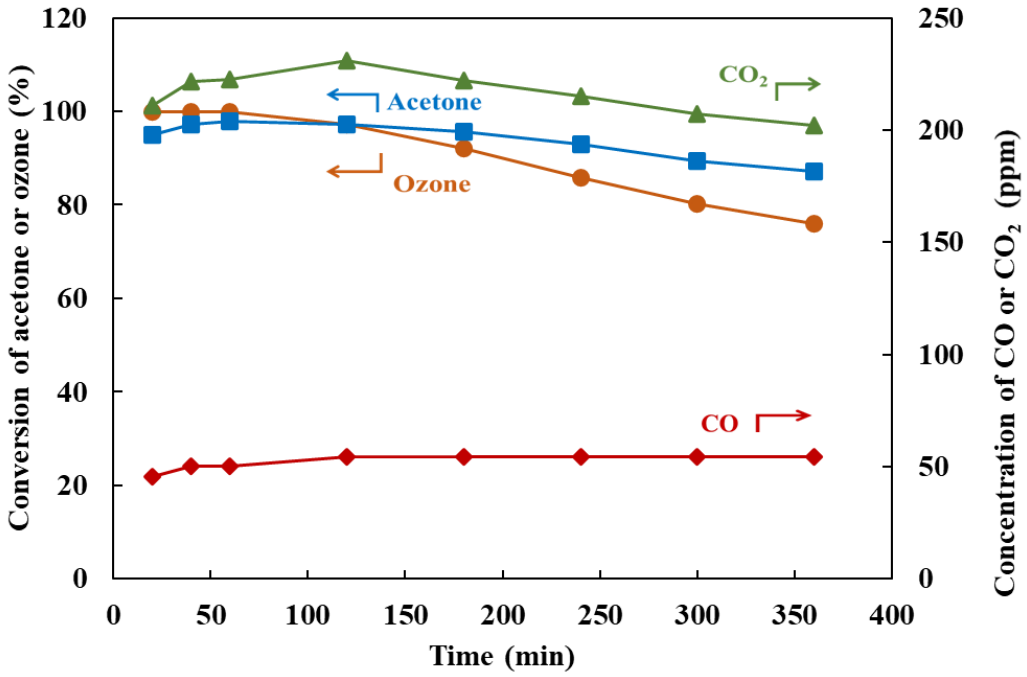

Figure 5.11.Long-term activity and CO_x concentration of MnO_x-Al_2O_3-p-800, [O_3] = 1000 ppm, [acetone] = 120 ppm, 0.2 g catalyst.

MnO_x/Al_2O_3-I-800

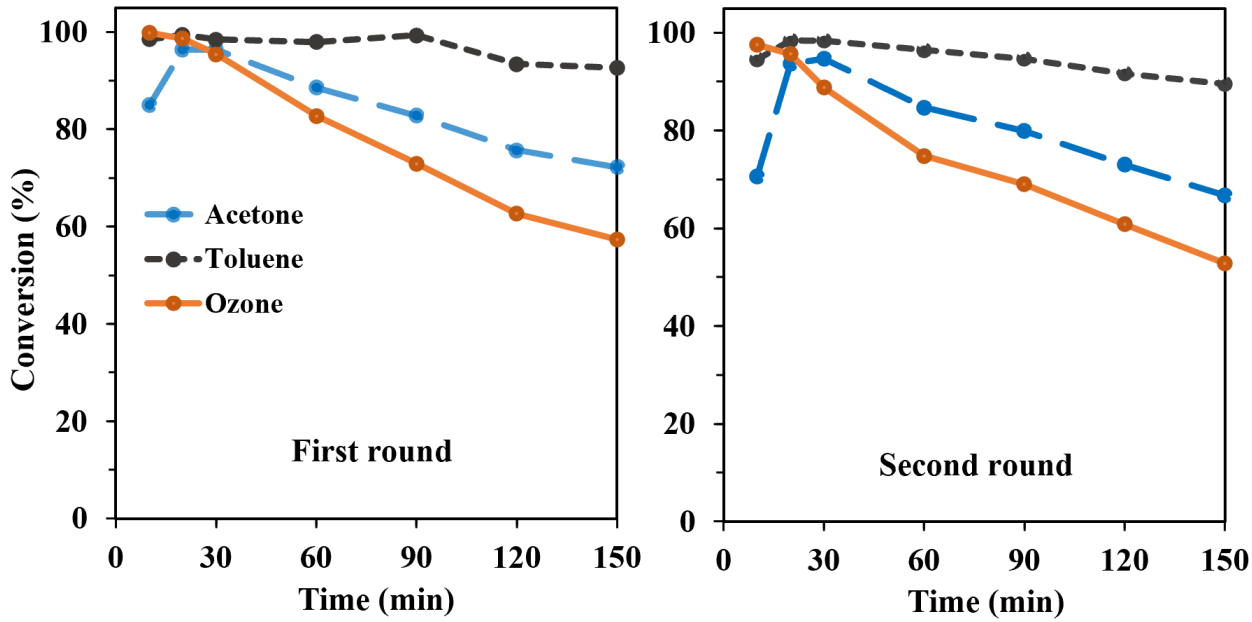

MnO_x/Al_2O_3-P-800

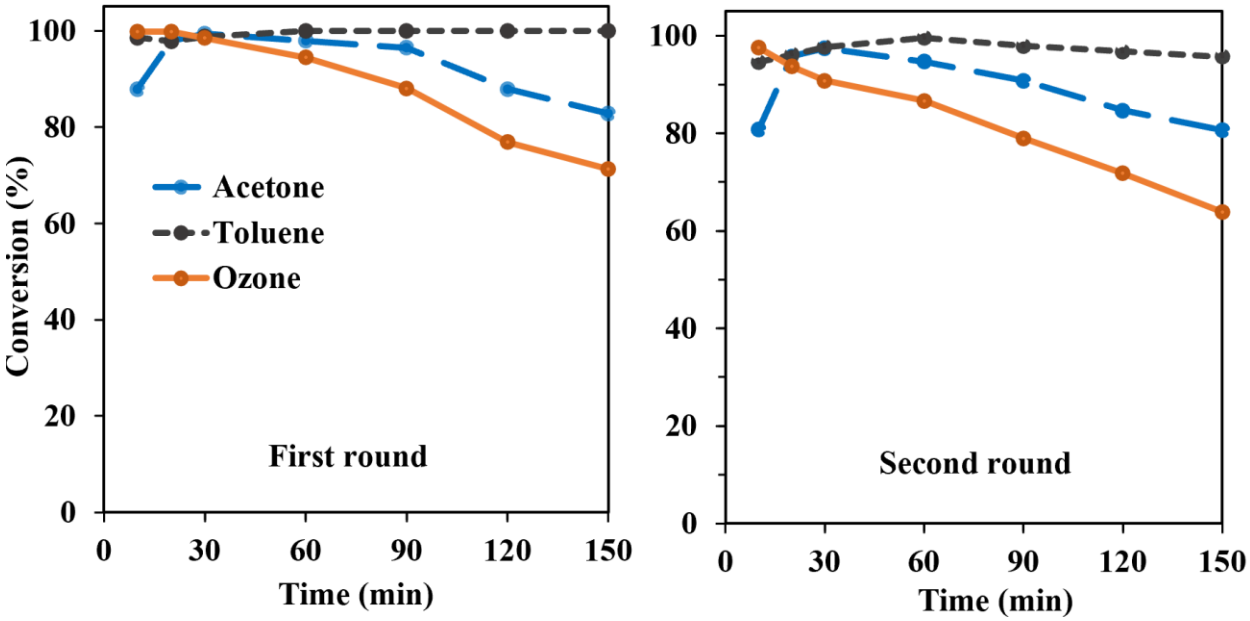

Figure 5.12.Catalytic ozonation of acetone and toluene using fresh (first round) and regenerated (second round) catalysts. [O_3] = 1000 ppm, [acetone] = 60 ppm, [toluene] = 60 ppm, 0.2 g catalyst.

5.4.3. XANES and EXAFS study on the spent catalysts

The spent catalysts were characterized by XANES and EXAFS to investigate the structural change that occurred on the catalysts after the reaction with acetone and toluene. For the sake of simplicity and consistency, "MnO_x/Al_2O_3" will be substituted with the "Fresh" or "Spent" in the name of the samples in presented results of this section. The XANES and the Fourier transform of EXAFS spectra of Mn for the fresh and spent catalysts are shown in Figure 5.13 (a-c). The EXAFS results are in agreement with the XANES spectra suggesting that the structure of the catalysts is altered after reaction with toluene. Compared with the fresh catalysts, the XANES pattern of the spent catalysts in the toluene reaction is quite different, showing shifted white line and edge jump positions to lower energy indicating a reduction of Mn oxides. In contrast, the XANES spectra of the fresh and spent catalysts after reaction with acetone are similar. EXAFS spectra of the fresh and used catalysts over acetone ozonation are also very similar indicating that the manganese local structure of the catalysts remained unchanged.

The Fourier transform of EXAFS spectra of the reference pure manganese oxides and Mn foil is shown in Figure 5.13 (c). The positions of the first and second coordination shells in the fresh catalysts are very close to Mn_3O_4. However, the spectra of the spent catalysts used in the reaction of toluene exhibited similarities to MnO and Mn^0 (Mn foil). As calcination temperature increased, less distortion can be seen in the spent catalysts' EXAFS spectra, and the first coordination shell of the samples calcined at 800 ºC is close to the fresh catalyst.

As the XANES and EXAFS analysis on the fresh and spent catalysts indicated, the reduction of Mn oxides can be clearly observed in the spent catalysts that were used in ozonation of toluene. The spectra for toluene spent catalysts shifted to lower energy indicating a decrease in the average oxidation states of catalysts.

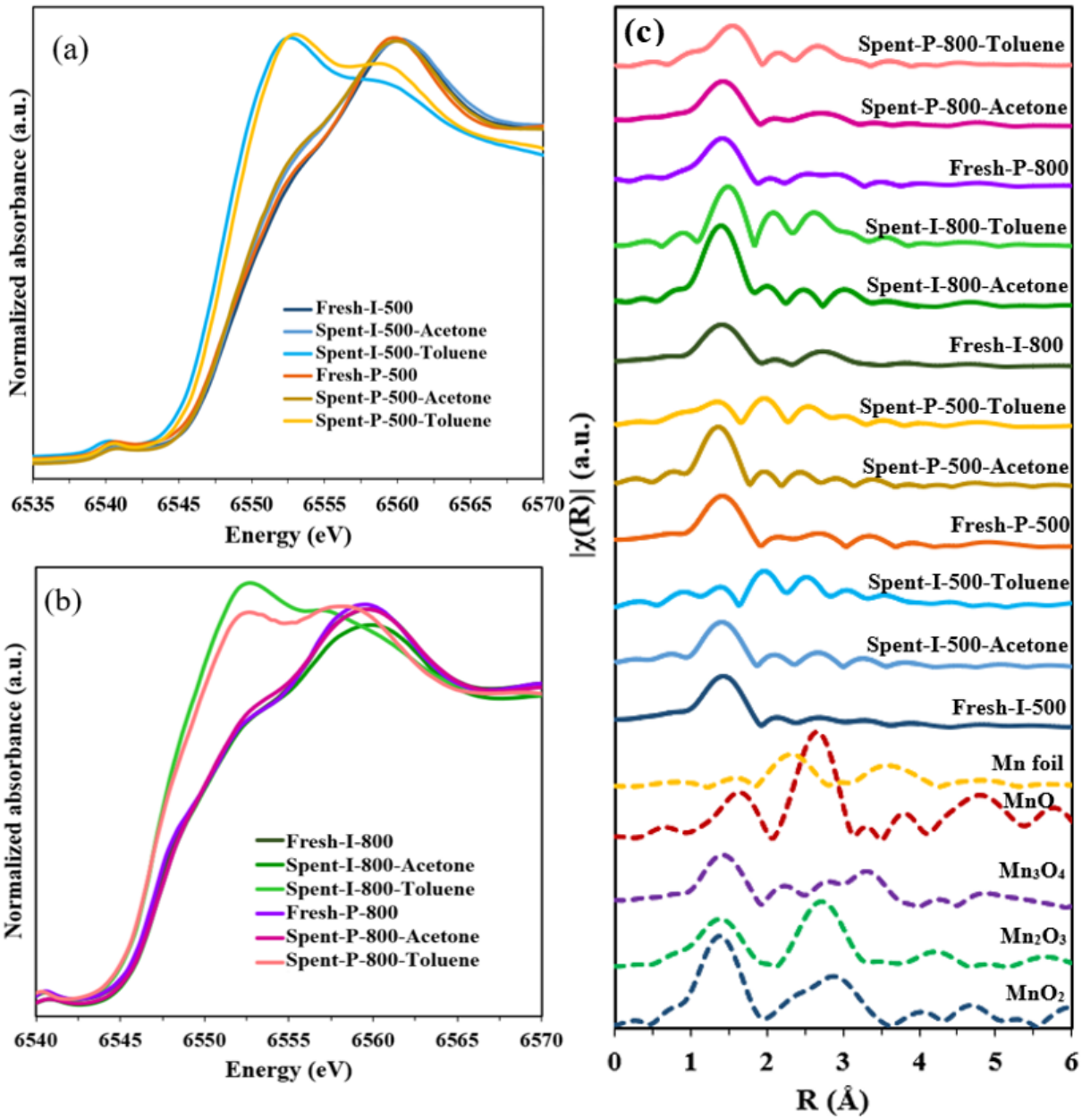

Figure 5.13.(a,b) XANES spectra of Mn K-edge; (c) Fourier transformed Mn K-edge EXAFS spectra for reference materials, fresh, and spent catalysts in ozonation of acetone and toluene.

The difference in the behavior of the catalyst after reaction with these two types of VOCs can be attributed to more intermediate generation and byproduct accumulation that occurred in the reaction with toluene as discussed in the above sections. The spent catalysts after ozonation of toluene experience more byproduct accumulation that can be ascribed to the change in the structure of the catalysts.

5.4.4. Catalytic ozonation of toluene and acetone over MnO_x/Al_2O_3 Catalysts

The *in-situ* DRIFTS spectra were used to study the formation of byproducts during the reaction. The DRIFTS spectra during the adsorption (in the absence of ozone) and immediately after adding ozone in toluene and acetone reactions (1 min, 10 min, and 120 min) are shown in Figure 5.14 and Figure 5.15, respectively. The bands observed in the adsorption of acetone and toluene suggest that there is lower adsorption of toluene in the absence of ozone compared to acetone. A peak during the adsorption of toluene was observed at 1496 cm^{-1} that is related to the aromatic ring vibration [79,169]. Another weak peak appeared at 1602 cm^{-1} that can be attributed to COO^- stretching of carboxylates. On the contrary, several bands at 1371, 1426, 1592, and 1702 cm^{-1} were observed during adsorption of acetone. Among them, the band at 1586-1604 cm^{-1} (COO^- stretching of carboxylates) indicated that acetone was partially oxidized by the lattice oxygen and generated surface carboxylates.

In the presence of ozone in the system, the intensity of the band at around 1586-1604 cm^{-1} increased considerably, indicating partial oxidation of acetone and toluene to surface carboxylates. The other detected peaks at around 1420-1426, 1454, 1464, 1702-1780 were related to C–H asymmetric deformation vibration, aromatic ring stretching, C–H bending, and C=O stretching of ketones and carboxylic acids, respectively. The broad peak from 2400 to 3750 cm^{-1} was related to the overlap of OH stretching of alcohols, carboxylic acids, and water.

By comparing the DRIFTS spectra of the polyol and impregnated catalysts, it can be inferred that catalytic ozonation of these VOCs follows a similar mechanism. However, the relative intensity of the bands at 1702-1780 cm^{-1} was different among the catalysts. These peaks were stronger for impregnated catalysts that justify the result of TPO analysis regarding the higher number of intermediates produced in the reaction. The accumulation of these carboxylic acids caused the deactivation patterns of the catalysts [18,198].

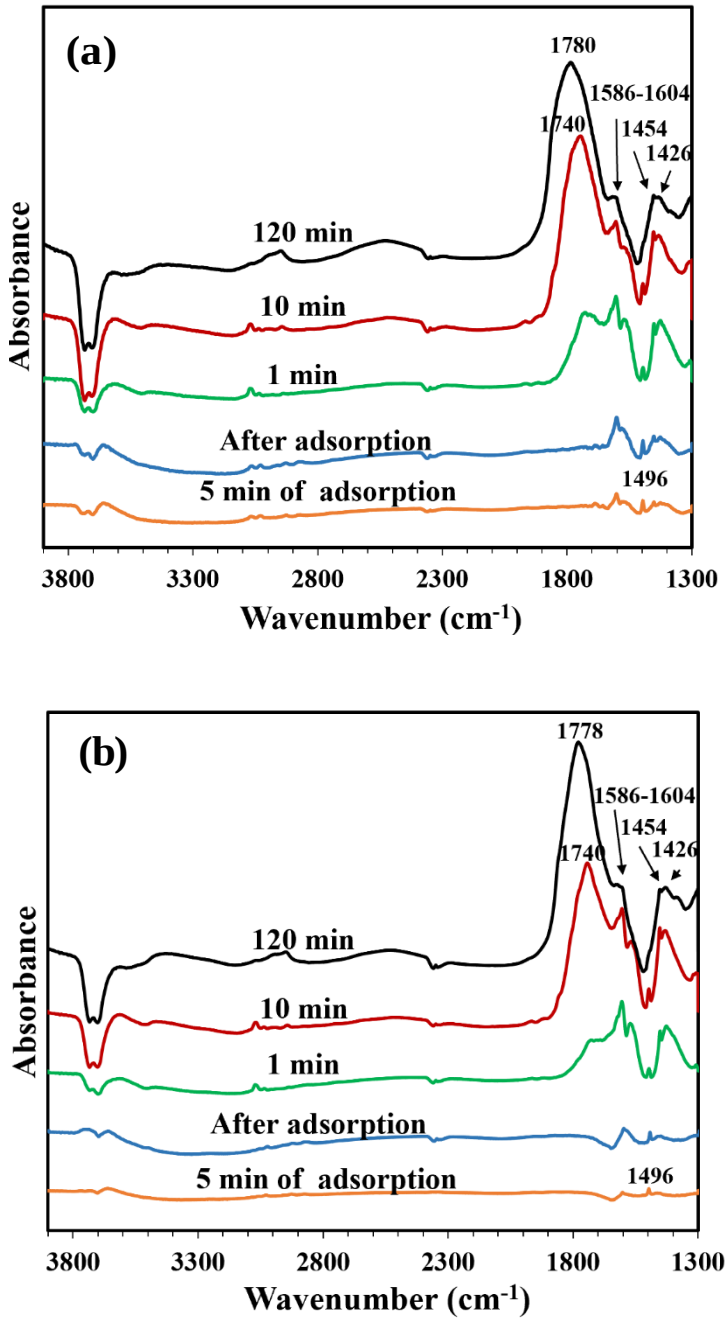

Figure 5.14.In-situ DRIFTS spectra of catalysts during catalytic ozonation of toluene (a) MnO_x-Al_2O_3-I-800, (b) MnO_x-Al_2O_3-P-800; 0.065 g catalyst; 25 ºC; [O_3] = 1000 ppm, and [toluene] = 120 ppm.

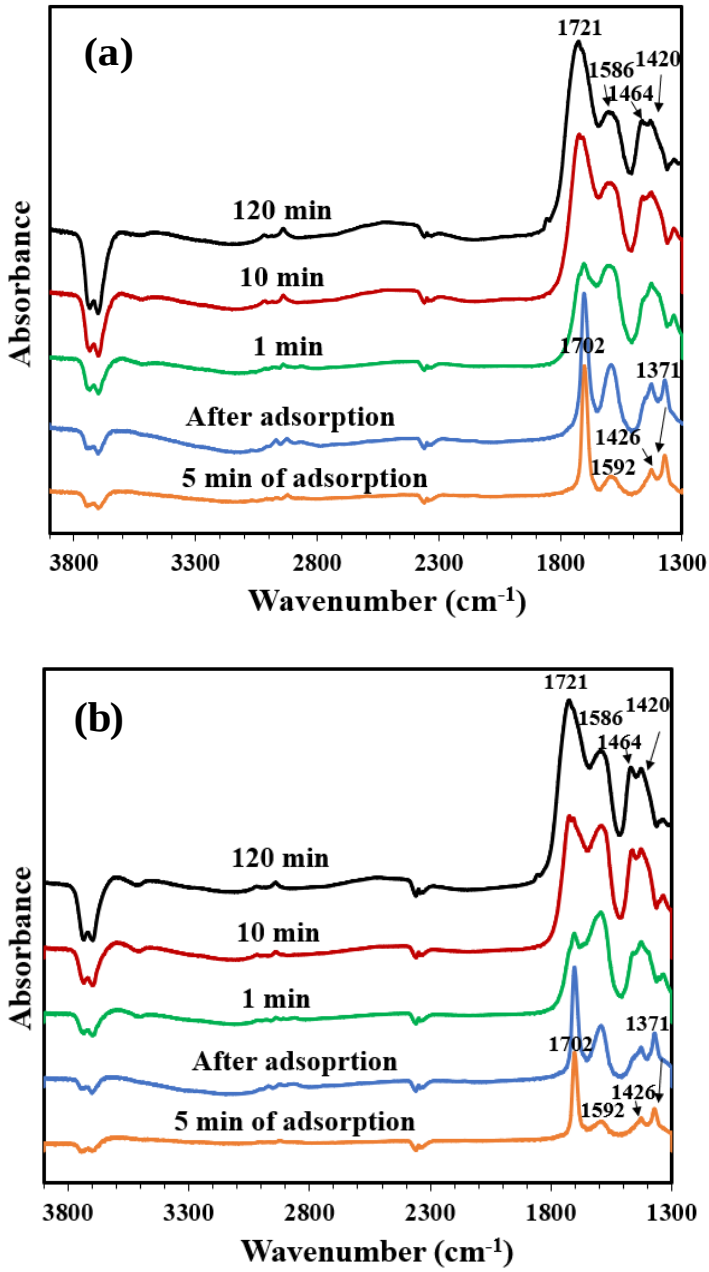

Figure 5.15.In-situ DRIFTS spectra of catalysts during catalytic ozonation of acetone (a) MnO_x-Al_2O_3-I-800, (b) MnO_x-Al_2O_3-P-800; 0.065 g catalyst; 25 ^oC; [O_3] = 1000 ppm, and [acetone] = 120 ppm.

Although the intensity of the DRIFTS spectra among the studied catalyst is not the same, the identified functional groups suggest that the catalytic ozonation of acetone or toluene follow similar reaction pathways over the impregnated and polyol catalysts. The obtained results inculcate a proposed reaction pathway of acetone and toluene ozonation which is in agreement with the literature [26,102,112,126]. Figure 5.16 shows the proposed reaction pathway for

acetone and toluene ozonation over alumina supported Mn oxides. Oxygen species (O^{2-}, O_2^{2-}, O^-) were produced from ozone decomposition [77,126]. However, it has been suggested that atomic oxygen (O^{2-}) is involved in the oxidation of VOCs and the molecular oxygen species do not contribute to the reaction [199]. The VOC adsorbs on the surface. Alumina plays a role in the adsorption of VOCs and also partially oxidizes them to generate surface carboxylate intermediates [79]. As demonstrated in the *in-situ* DRIFTS results, the surface carboxylates can be produced during the adsorption of the VOCs. However, their intensities increase substantially after introducing ozone to the reaction mixture. The generated atomic oxygens from ozone decomposition interacted with the surface carboxylates and formed the reaction intermediates, which further oxidized to generate the final products of the reaction. The synergy between MnO_x and alumina is essential in this reaction. The adsorbed VOCs on the active sites and the atomic oxygen species resulting from ozone decomposition react on the surface of the catalyst. A promoted catalyst with higher oxygen mobility seems to facilitate the migration of adsorbed species between the metal oxide and support and eventually enhance the catalytic activity.

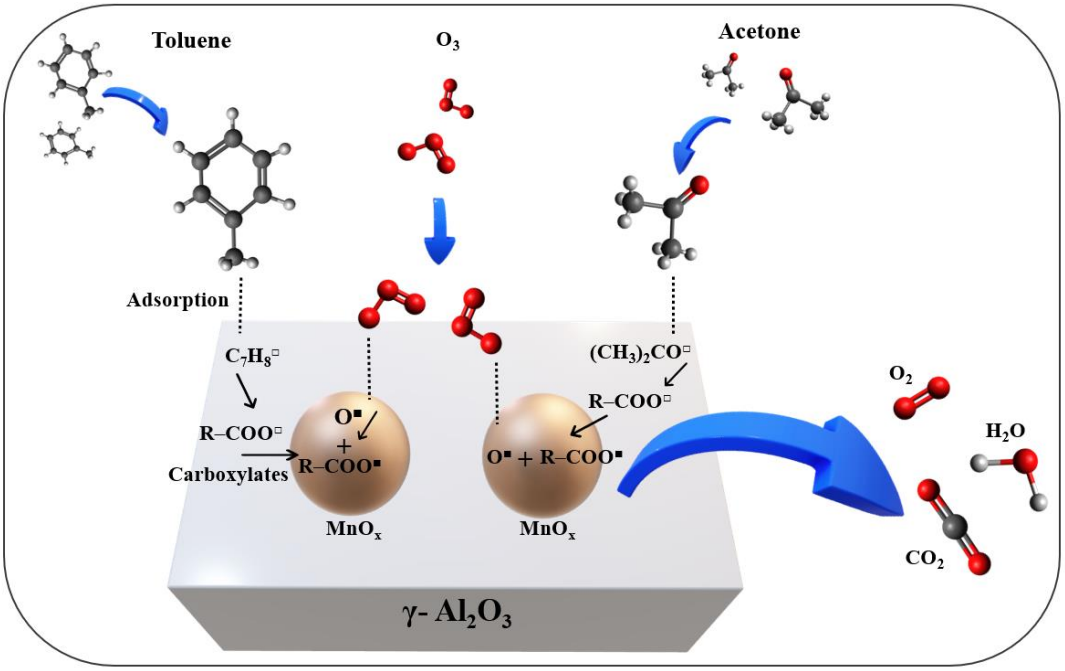

Figure 5.16.The possible pathway of oxidation of acetone and toluene during catalytic reaction with ozone at room temperature.

As discussed above, the oxidation behavior of single acetone and toluene in the reaction with their binary mixture is quite different. The promotional and inhibitory oxidation behaviors of the components in binary VOC mixtures have been reported in the literature [102,131,200]. The main reason for this observation is ascribed to the competitive adsorption between the components [201]. This effect is related to the affinity of these VOCs for the surface sites of the catalyst. In the mixture, the competition is for occupying the active sites during the reaction. Toluene has more affinity to interact with radical oxygen species. As illustrated above, intermediate species were generated from the toluene reaction. These carbonaceous components occupy the active sites as well. causing the acetone conversion to drop.

5.5. Conclusion

In this work, a series of MnO_x/Al_2O_3 catalysts were prepared with polyol and impregnation methods and calcinated at different temperatures for use in catalytic ozonation of acetone and toluene. The calcination temperature and preparation method affect the properties of the catalysts such as cluster size, surface area, dispersion, and oxidation states of manganese species. When calcined at a higher temperature, manganese cluster size increased while the oxidation states of Mn oxides, surface area, and dispersion of the catalyst decreased. The catalysts calcined at higher temperatures showed better activity in the oxidation of acetone achieving about 95% conversion. Toluene conversion was not significantly influenced by calcination temperature. Compared with the catalysts obtained by impregnation method, polyol catalysts exhibited higher activity for both VOCs oxidation. In the binary mixtures, toluene and acetone exhibited promotional and inhibitory behaviors, respectively. A similar observation was obtained at different concentrations of acetone and toluene in the binary mixtures. It should be noted that when the ratio of toluene to acetone increased in the binary systems, the conversions dropped. Analysis of the spent catalysts showed that reaction with toluene alters the local structure of the catalysts, and the Mn oxides were reduced in the spent catalyst.

Chapter 6:

Kinetics and mechanism of catalytic ozonation of acetone in air over MnO_x/Al_2O_3 catalyst

The content of this chapter has been published in Reaction Kinetics, Mechanisms and Catalysis as an original research article.

Citation:

M. Ghavami, J. Soltan, Kinetics and mechanism of catalytic ozonation of acetone in air over MnO_x/Al_2O_3 catalyst, Reaction Kinetics, Mechanisms and Catalysis (2021). https://doi.org/10.1007/s11144-021-02024-6.

Contribution of the Ph.D. candidate

All the experiments were conducted by Mehraneh Ghavami in consultation with Dr. Jafar Soltan. All the written text and data analyses were prepared by Mehraneh Ghavami. Dr. Jafar Soltan supervised and provided consultation during the experimental period and manuscript preparation.

Contribution of this chapter to the overall Ph.D. Research

This section provides the kinetics and mechanistic studies of catalytic ozonation reaction of acetone over the best catalysts obtained in chapter 5. In this chapter, the aim is to present the most appropriate kinetic model for catalytic ozonation of acetone. The potential kinetic models were applied to estimate the rate constants and thermodynamic parameters of catalyst ozonation in the presence of MnO_x/Al_2O_3 catalysts.

6.1. Abstract

The catalytic ozonation of acetone using MnO_x/Al_2O_3 catalysts prepared by polyol and impregnation methods was investigated. The synthesized catalysts exhibited excellent catalytic activity at room temperature with conversions of around 95 %. Although many studies focus on catalytic processes to oxidize VOCs more efficiently, the mechanism behind this reaction is still unknown. The *In-situ* DRIFTS and activity results show that alumina not only acts as a support for MnO_x, but it also involves in the reaction with acetone and creates surface carboxylate intermediates. MnO_x sites are required for further oxidation of the generated intermediates to the final products. Therefore, Langmuir-Hinshelwood dual-site (LHd) mechanism was evaluated to demonstrate the reaction pathway. The kinetic data were expressed well by LHd model, indicating that both MnO_x and Al_2O_3 sites are essential and involved in the reaction. The cooperation of these sites on the surface of the catalyst provides the adjacent attack and migration of intermediates and enables the dual-site mechanism. The reaction order, activation energy, and kinetic parameters were determined for both catalysts and confirmed that the model is physically meaningful. Other than LHd, common Langmuir-Hinshelwood single-site (LHs) and power law (PL) kinetic models were tested to describe the acetone ozonation process and kinetic mechanism. Although the models can describe the reaction kinetic adequately, the LHs did not properly fit the experimental data suggesting that more than a single site is involved in the reaction and PL model is unable to provide the mechanistic view for the reaction.

6.2. Introduction

Catalytic ozonation can be effectively applied to oxidize volatile organic compounds (VOCs) in air at ambient temperature. This technique has been developed to significantly lower the required temperature to destroy VOCs compared to the catalytic oxidation process [202]. Hence, catalytic ozonation has gained increasing research interest in recent years, and researchers dedicated great efforts to develop efficient catalysts for VOC degradation [25,77].

Supported manganese oxides are one of the most promising catalysts for the oxidation of different types of VOCs using catalytic ozonation technology [12,77,96,203]. In addition to the

metal in the structure of the catalyst, the type of support impacts the catalyst's performance in this reaction. Among the metal oxide supports, alumina has been reported to exhibit the best performance in VOC degradation. Comparable studies of manganese oxide using various supports have been conducted by Chen et al. [14] for ozonation of chlorobenzene and by Rezaei et al. [21] for ozonation of toluene. Alumina-supported manganese oxides offer desirable properties such a redox ability, high surface area, and high surface adsorbed oxygen species [14]. Moreover, oxidation states of Mn is an important factor in improving the oxygen mobility and subsequently the catalytic activity [162,204]. Alumina promotes Mn to decompose to its lower oxidation state which is more favorable in catalytic oxidation of VOCs [21,29].

Even though many studies have been performed on improving the catalytic ozonation technique, the mechanism behind this process still needs further investigation. Langmuir-Hinshelwood single-site (LHs) mechanism was proposed by Reed et al. for catalytic ozonation of acetone using silica-supported manganese oxide catalysts [26]. Rezaie et al. investigated LHs mechanism on catalytic ozonation of toluene over alumina-supported manganese oxides [98]. In both studies, only manganese oxides were considered as the active sites which were involved in the final LH expression, and the role of the catalyst support was not considered in the mechanism. Reed et al. reported that TPD and Raman spectroscopy results revealed that the adsorbed acetones are all on the silica support sites due to the affinity of silica for acetone at low temperatures [100]. Therefore, in the proposed LH mechanism the role of support was considered as a reservoir for the adsorbed VOC intermediates, and it was assumed that the adsorbed species migrated to Mn sites for reaction.

In a recent study by Aghbolaghy et al., It has been shown that the support in this reaction can contribute to the adsorption of VOCs on the surface of the catalyst, generation of the reaction intermediates, and migration of the adsorbed species on the catalyst surface, and the reaction between them [14]. The *In-situ* diffuse reflectance Fourier transform spectroscopy (DRIFTS) and breakthrough curves of VOC adsorption over MnO_x/Al_2O_3 and γ-Al_2O_3 results show that alumina not only acts as a reservoir for VOC and a support for higher dispersion of manganese oxide, but also it reacts with the VOCs in the presence of ozone and creates surface carboxylate intermediates. Manganese oxide sites are essential for further oxidation of the generated

intermediates. Therefore, the importance of support in the reaction pathway and determining the kinetic model has been overlooked in most of the kinetic studies so far.

In this study, the main goal is to clarify the roles of the catalyst support and metal in the reaction pathway and determine the most suitable kinetic model for catalytic ozonation of acetone over MnO_x/Al_2O_3 catalyst. Hu et al. proposed Langmuir-Hinshelwood dual-site (LHd) mechanism for catalytic ozonation of toluene using graphene-supported manganese oxides. They reported that the synergy between MnO_2 and graphene sites which was proved by XPS analyses enabled the adjacent attack and eventually dual-site mechanism. Since the synthesized MnO_x/Al_2O_3 catalysts render promising activity results in ozonation of acetone at room temperature, and the interaction of MnO_x and Al_2O_3 match the dual-site mechanism model, the proposed LHd was used to express the kinetic data. Langmuir-Hinshelwood single-site (LHs) and power law (PL) models were also studied using the experimental data for comparison. Thermodynamic and kinetic parameters were determined as they provide more detail regarding the reaction pathway.

6.3. Experimental and data analysis

6.3.1. Catalyst synthesis and characterization

The MnO_x/Al_2O_3 catalyst was prepared by impregnation and polyol methods. Manganese (II) acetate tetrahydrate (Sigma Aldrich, 99%) and γ-Al_2O_3 (Alfa-Aesar) were used as the precursor and support. The particle size of γ-Al_2O_3 was less than 0.208 mmm to eliminate transport resistances [64,102]. For preparation of catalyst using polyol method, manganese (II) acetate tetrahydrate was mixed with polyvynilpyrrolidone (PVP) (Sigma Aldrich, K30, molecular weight = 40,000) and ethylene glycol (EG) (Sigma Aldrich, anhydrous, 99.8%). γ-Al_2O_3 was added, and the mixture was agitated with a magnetic stirrer overnight. Then, the mixture was heated under reflux to 160 ºC for almost 140 min. Afterward, the mixture was rapidly cooled to room temperature using an ice bath. The catalyst was separated using a centrifuge and washed several times with ethanol and deionized water to remove the organic phase [149,189]. The catalyst was dried in an oven overnight and calcined in air at 800 ºC for 4 h. The catalyst was denoted as

MnO_x/Al_2O_3-P (P denotes polyol). For the catalyst prepared by impregnation method (MnO_x/Al_2O_3-I), γ-Al_2O_3 and the solution of manganese (II) acetate tetrahydrate were mixed. The synthesized catalyst was dried in the oven overnight and then calcined for 4 h at 800 °C. ICP-MS analysis confirmed the actual manganese loading of approximately 3.5 wt% in catalysts.

The catalysts were examined using various characterization techniques as reported in our previous work. In this study, we reported the Brunauer–Emmett–Teller (BET) surface area and pore volume and X-ray absorption near edge structure (XANES) findings. BET measurements were conducted by nitrogen adsorption using an ASAP 2020 instrument (Micromeritics). XANES of Mn K-edge was collected at the HXMA beamline of the Canadian Light Source. Catalysts were diluted with boron nitride (BN), ground, and pressed to thin disks. The prepared disks were protected by Kapton tape. All measurements were carried out in transmission mode using straight ion chamber detectors filled with helium gas. X-ray Photoelectron Spectroscopy (XPS) data were recorded using a Kratos (Manchester, UK) AXIS Supra system. The survey scan spectra were collected with a step size of 1 eV and a pass energy of 160 eV. Deconvolutions of the XPS spectra were performed using a CasaXPS® software.

In-situ DRIFTS experiments were performed in a modified experimental setup explained in detail elsewhere [188]. The reaction was carried out in a reaction chamber (Harrick, HVC) equipped with ZnSe windows. The reaction chamber was coupled with the DRIFTS accessory which was placed in the FTIR spectrometer. To avoid the saturation of the MCT-A detector, data were collected at a resolution of 4 cm^{-1} in the range of 3,900–1,300 cm^{-1}.

6.3.2. Steady-state kinetic study

The kinetic experimental data was collected in a Pyrex tubular glass reactor at atmospheric pressure which was installed in an oven (Binder, FP 115). An ozone generator (AZCO Industries LTD, HTU-500S) was used to generate ozone from oxygen (Praxair, 99.993%). The flow rates of the oxygen, acetone-nitrogen, and nitrogen (for dilution purposes) streams were set using three Brooks, SLA 5850 mass flow controllers. The inlet gas was fed into a tubular reactor loaded with approximately 40 mg of catalyst. The catalyst was diluted with silica carbide to

prevent gas phase channeling and temperature gradients along the catalyst bed. Silica carbide is inert in this reaction [98]. Catalysts were put between two pieces of glass wool and the reactor was filled with glass beads. The final catalysts' particle size of 0.208 mm or less was selected, which did not exhibit mass transfer limitations for catalytic ozonation of acetone [98,102].

Kinetic data were obtained at three different temperatures (40, 50, and 60 °C) since catalyst activity is not stable at temperatures below 40 °C. The total flow rate was set at 2,000 STP mL/min for all experiments with different acetone concentrations (100–300 ppm, i.e., 4.09–12.27 $\times 10^{-3}$ mol m^{-3}) and fixed ozone concentration (1,150 ppm, i.e., 51.30 $\times 10^{-3}$ mol m^{-3}). The acetone conversion (X_{ace}) was calculated using Eq. (6.1), where $C_{ace,in}$ and $C_{ace,out}$ represent the concentrations of acetone in the inlet and outlet of the reactor, respectively. The steady-state reaction rate was calculated using Eq. (6.2), where r_{ace}, $C_{ace,in}$, v, X_{ace}, and W are the steady-state reaction rates of acetone, acetone feed concentration, total gas flow rate, steady-state acetone conversion, and catalyst weight, respectively.

$$X_{ace.} = \frac{C_{ace,in} - C_{ace,out}}{C_{ace,in}} \times 100\% \quad (6.1)$$

$$r_{ace.} = \frac{C_{ace,in} v X_{ace}}{W} \quad (6.2)$$

6.3.3. Kinetic models

Three kinetic models and equations were developed to describe the kinetic data obtained from experiments of ozonation of acetone. The kinetics parameters for each model were initially calculated using Excel Solver and the final values were obtained using MATLAB R2010 by minimizing the sum of square of errors in the experimental and predicted reaction rate.

6.1.1.1. Langmuir-Hinshelwood dual-site model

The Langmuir-Hinshelwood dual-site model (LHd) was proposed by Hu et al. [101] on catalytic ozonation of toluene using MnO_2/graphene. The first steps of ozone decomposition are

similar to the traditional LHs mechanism proposed by Reed et al. [26] . However, it was assumed that there are two active sites of MnO_2 and graphene present in the reaction which should be considered in the kinetic model. Therefore, the final step of LHs model which is the reaction between adsorbed toluene and oxygen species on MnO_x sites was eliminated, and instead, the reaction between the adsorbed toluene in graphene site with adjacent atomic oxygen species in MnO_2 site was considered. The model expression was derived based on assumption that the last step in the mechanism can be considered the rate determining step for catalytic ozonation of VOCs. Step (4) is supposed to occur under equilibrium adsorption state and finally the pseudo steady-state hypothesis was considered to derive the final rate law equation. The proposed steps for ozonation of acetone over MnO_x/Al_2O_3 are shown below [101]:

Step (1): $O_3 + * \rightarrow O_2 + O$ (6.3)

Step (2): $O_3 + O* \rightarrow O_2 + O_2*$ (6.4)

Step (3): $O_2* \rightarrow O_2 + *$ (6.5)

Step (4): $C_3H_6O + \blacksquare \rightleftarrows C_3H_6O\blacksquare$ (6.6)

Step (5): $C_3H_6O\blacksquare + O* \rightarrow products$ (6.7)

The final equation model as derived by Hu et al. [101] for the LHd mechanism can be expressed as Eq. (6.8).

$$r_{ace.} = \frac{k_1 K_{ace.} k_5 [C_3H_6O][O_3]}{(1+K_{ace.}[C_3H_6O])(k_2[O_3]+\frac{K_{ace.}k_5[C_3H_6O]}{1+K_{ace.}[C_3H_6O]}+k_1[O_3]+\frac{k_1k_2[O_3]^2}{k_3})} \quad (6.8)$$

6.1.1.2. Langmuir-Hinshelwood single-site model

The Langmuir-Hinshelwood single-site (LHs) mechanism was proposed by Reed et al. [26] for ozonation of acetone over MnO_x/SiO_2. The LHs consists of several steps of ozone decomposition (steps1-3) which include generation of atomic oxygen and peroxide species, followed by acetone adsorption (step 4), migration of the adsorbed acetone (step 5), and finally

reaction with atomic oxygen (step 6). The steps of LHs mechanism for ozonation of acetone using MnO_x/Al_2O_3 catalysts describes as follow [26]:

Step (1): $O_3 + * \rightarrow O_2 + O*$ (6.9)

Step (2): $O_3 + O* \rightarrow O_2 + O_2*$ (6.10)

Step (3): $O_2* \rightarrow O_2 + *$ (6.11)

Step (4): $C_3H_6O + \blacksquare \rightleftarrows C_3H_6O\blacksquare$ (6.12)

Step (5): $C_3H_6O\blacksquare + * \rightarrow C_3H_6O* + \blacksquare$ (6.13)

Step (6): $C_3H_6O* + nO* \rightarrow products$ (6.14)

where $*$ represents a surface manganese site and ■ represents a surface alumina site. The possible steps after step (6) are assumed to be insignificant for the kinetic study. The detailed derivation to obtain the equation to calculate the rate law is given by Reed et al. [26]. It was considered that the final step which is the reaction between the adsorbed intermediates is the slowest step for the catalytic ozonation of acetone. The final equation for LHs model is shown is Eq. (6.15) as if there is *n* oxygen atoms in step (5):

$$r_{ace.} = K_{ace.} \frac{k_1' [C_3H_6O][O_3]^n}{(1+k_2' [O_3]+K_{ace.}[C_3H_6O])^{n+1}} \quad (6.15)$$

where r_{ace} is acetone reaction rate, K_a is equilibrium adsorption constant, k_1' and k_2' are reaction rate constants. Equilibrium adsorption constants and reaction rate constants were calculated using Van't Hoff and Arrhenius equations, respectively.

$$\ln K_{ace.} = \left(\frac{-\Delta H_{ace.}}{R}\right)\frac{1}{T} + \frac{\Delta S_{ace.}}{R} \quad (6.16)$$

$$k_1' = \frac{k_1}{k_3} k_5 \quad (6.17)$$

$$k_2' = \frac{k_1}{k_3} \quad (6.18)$$

6.1.1.3. Power law model

The power law (PL) model included three unknown parameters (k, α, and β), as stated in Eq. (6.19):

$$r_{ace.} = k C_{ace.}^{\alpha} C_{ozo.}^{\beta} \quad (6.19)$$

where $r_{ace.}$ is acetone reaction rate, $C_{ace.}$ and $C_{azo.}$are the concentration of acetone and ozone. α and β are orders of reaction with respect to acetone and ozone, respectively. k is the reaction rate constant. Reaction rate data were fit to Eq. (6.19) by using nonlinear least-squares regression analysis. After the kinetic parameters were calculated for each temperature, Arrhenius equations were employed to determine the pre-exponential factor A and apparent activation energy E_a. R is the universal gas constant and T is the reaction temperature in Kelvin.

$$\ln k = \ln A + \left(\frac{-E_a}{R}\right)\frac{1}{T} \quad (6.20)$$

6.3.4. Model assessment

The goodnesses of fit of the models are evaluated based on the coefficient of determination (R^2), multiple correlation coefficients (ρ^2) and F value in Fisher's F-test (F_C) [98,205]. DF (degrees of freedom) is determined as the difference between the number of experimental data points and the number of fitting parameters.

$$\rho^2 = 1 - \frac{\sum_i (r_{experiment,i} - r_{fitted,i})^2}{\sum_i (r_{experiment,i})^2} \quad (6.21)$$

$$F_C = \frac{\sum_i (r_{fitted,i})^2}{\sum_i (r_{experimnet,i} - r_{fitted,i})^2 / DF} \quad (6.22)$$

The Sum of squared differences (SSQ) between experimental and calculated data was minimized to obtain the model parameters:

$$SSQ = \sum_i (r_{experiment,i} - r_{fitted,i})^2 \quad (6.23)$$

Besides the statistical significance of the model, the physico-chemical tests as shown in Eqs. (6.24) and (6.25) are also conducted to ascertain the physical meaning of adsorption entropy and enthalpy [101,206,207]. Eq. (6.24) suggests that adsorption of a molecule on the surface results in loss of entropy and the amount of the entropy loss $-\Delta S^0_{ads}$ during adsorption cannot exceed the gas phase entropy S^0_g and should also be higher than 41.9 J $mol^{-1}K^{-1}$. Loss of entropy and adsorption enthalpy ΔH^0_{ads} should be restrained as displayed in Eq. (6.25) which is an empirical rule. It states that when molecules are tightly bounded to the surface of the catalyst, it corresponds to a high negative value for $-\Delta H^0_{ads}$, the surface motion becomes limited, and the value for negative loss of entropy will be larger.

$$41.9 < -\Delta S^0_{ads} < S^0_g \quad (6.24)$$

$$-\Delta S^0_{ads} \leq 51.1 - 1.4\Delta H^0_{ads} \quad (6.25)$$

6.4. Results and discussion

6.4.1. Characterization of MnO_x/Al_2O_3

BET analysis determined the surface area of MnO_x/Al_2O_3-I and MnO_x/Al_2O_3-P catalysts to be 176 and 187 $m^2\ g^{-1}$, respectively. XANES analysis indicated that Mn *K-edge* absorption energy (E_0) of both MnO_x/Al_2O_3-I and MnO_x/Al_2O_3-P catalysts was 6547.5 eV, which was close to that of Mn_3O_4 (6547.00 eV). Linear combination fitting of the XANES spectra revealed that Mn_3O_4 is

the dominant manganese phase in both catalysts. Mn_2O_3 makes only 4% of total manganese phases in MnO_x/Al_2O_3-I, and it is not present in MnO_x/Al_2O_3-P.

The XPS spectra of the catalysts are shown in Figure 6.1. The O 1s spectra can be deconvolved into three peaks, the peaks at 530.3-530.4 and 531.3-531.4 eV are assigned to lattice oxygen of manganese oxides and alumina, respectively. The peak in the range of 532.2 - 532.4 eV is attributed to chemisorbed oxygen [208–211]. The ratio of chemisorbed oxygen to total oxygen species on the catalyst surface is strongly correlated with the catalyst activity according to the literature. The chemisorbed oxygen is reported to be the most active form of oxygen and essential for oxidation reactions [126,212]. The percentages of chemisorbed oxygen to total oxygen over MnO_x/Al_2O_3-P and MnO_x/Al_2O_3-I catalysts are depicted in Figure 6.1. It was observed that MnO_x/Al_2O_3-P and MnO_x/Al_2O_3-I catalysts have comparable values of oxygen vacancy.

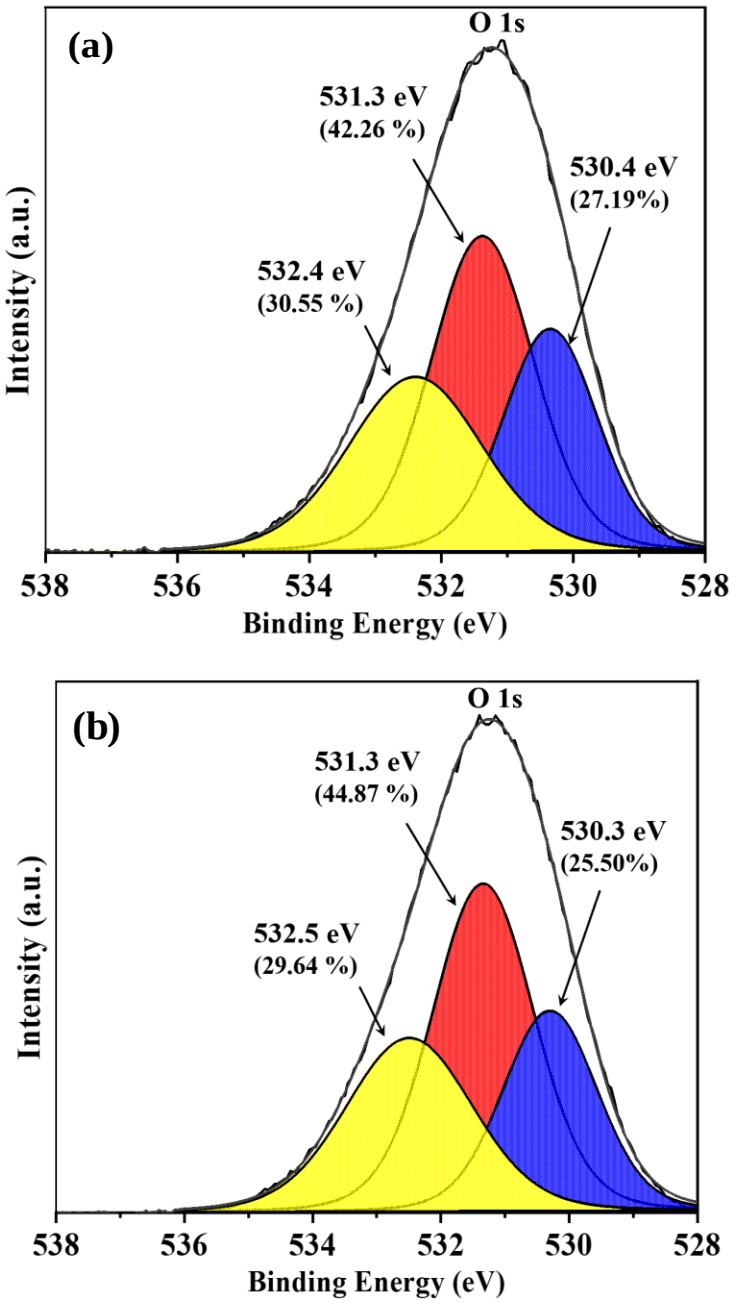

Figure 6.1. O 1s XPS spectrum of (a) MnO_x/Al_2O_3-P and (b) MnO_x/Al_2O_3-I catalysts.

6.4.2. Kinetics of catalytic ozonation of acetone

The two synthesized catalysts exhibited superior performance in the reaction of degradation of acetone. To find the temperature at which the reaction is stable, continuous experiments was performed in a wider temperature range (Figure 6.2). The catalytic ozonation reaction was

started at room temperature and continuously monitored for 150 min at 25 °C. Then, the operating temperature was increased to 40, 55, and 70 °C and the reaction was monitored for 80 min at each temperature without changing the catalyst or flow. The concentrations of acetone and ozone were kept at 120 and 1150 ppm, respectively and the reaction occurred over 0.2 g of catalyst.

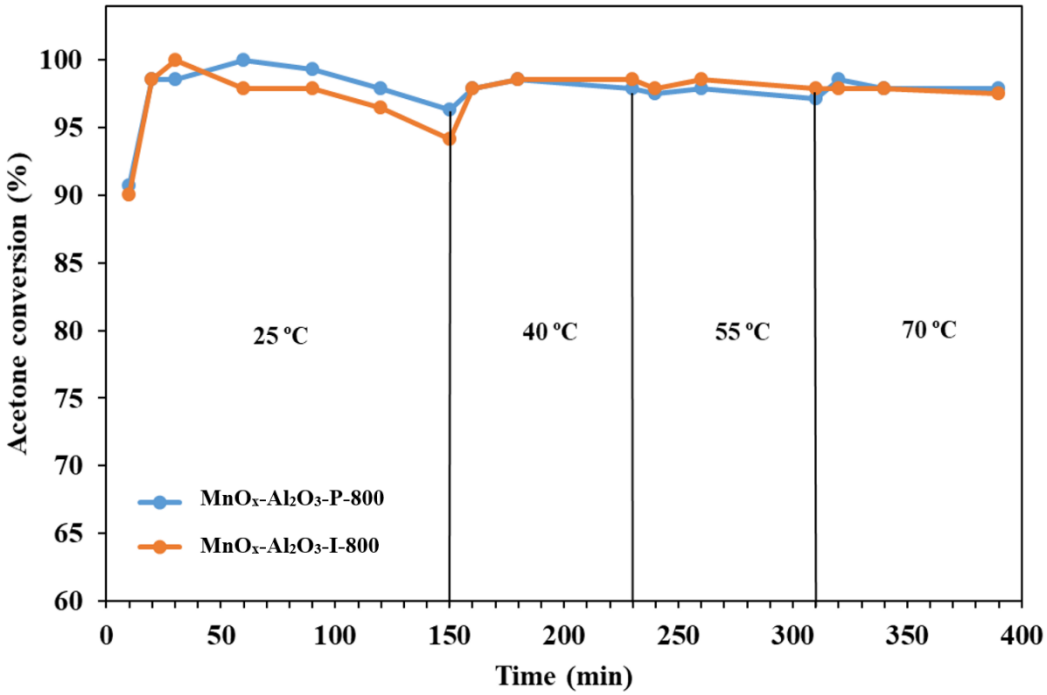

Figure 6.2. Acetone conversion as a function of reaction temperature over MnO_x/Al_2O_3-P-800 and MnO_x/Al_2O_3-P-800 catalysts. [O_3] = 1150 ppm, [acetone] = 120 ppm, 0.2 g catalyst.

To establish a low-conversion operation for kinetic study measurements, the lowest temperatures that the reaction is stable (40, 50, and 60 °C), and the highest possible gas flow rate for the existing experimental setup and relatively low catalyst weight were selected. In these reactions, the conversions of acetone changes from 5.1% to 26.2% and that of ozone from 2.3% to 23.7% as reaction temperature and the concentration of acetone changed accordingly. The results of reaction rates with the change in acetone concentration are presented in Figure 6.3.

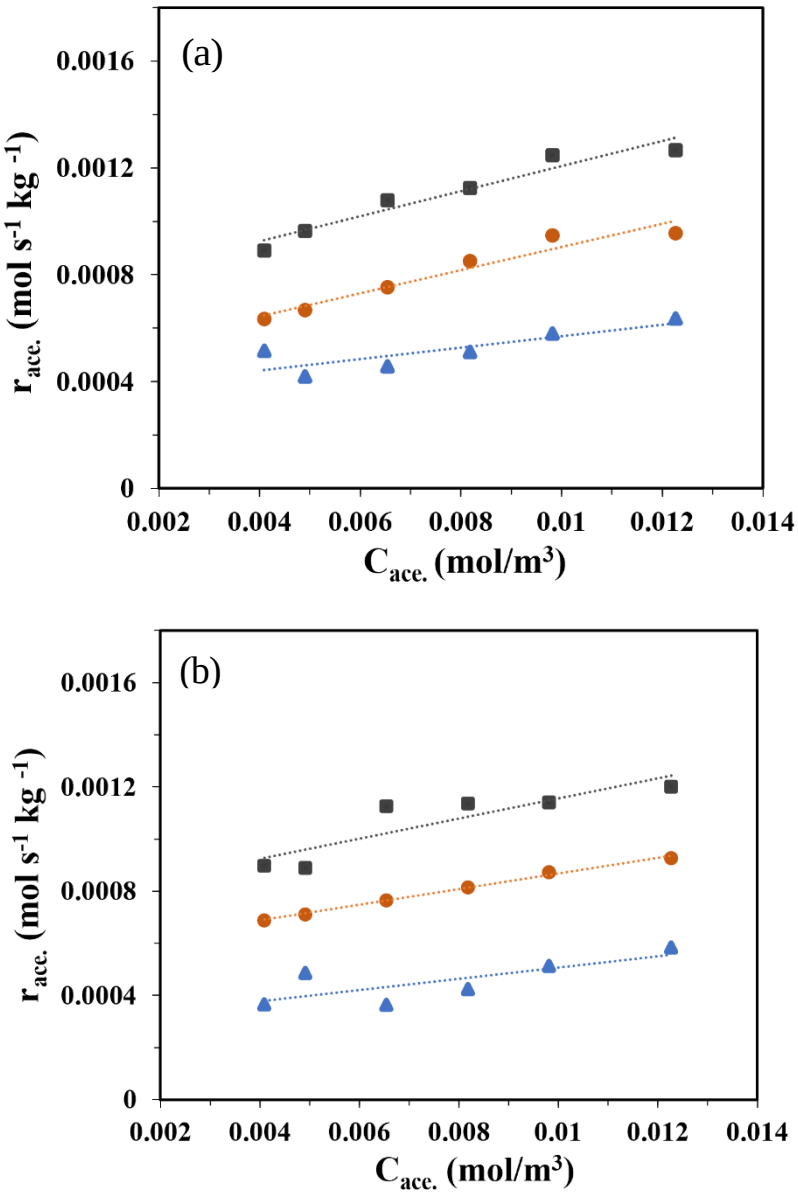

Figure 6.3. Changes of reaction rates as the inlet concertation of acetone over (a) MnO_x/Al_2O_3-P and (b) MnO_x/Al_2O_3-I

6.1.1.4. Langmuir-Hinshelwood dual-site model

In the case of LHd mechanism, it is assumed that two active sites of manganese oxides and alumina exist that both play role in the reaction. As demonstrated in Eqs. (6.3) to (6.7), the first site (MnO_x) is used for ozone decomposition and generation of atomic oxygen. Acetone molecule is adsorbed on the second site (alumina). The adsorbed intermediate species which are

atomic oxygen and adsorbed acetone on the MnO_x and alumina sites react on the surface of the catalyst. By performing *in-situ* DRIFTS experiments over pure γ-Al_2O_3 and MnO_x/Al_2O_3, it can be observed that alumina is not an inert support in this reaction, and it reacts with acetone and generate surface carboxylate intermediates. As Figure. 6.4 demonstrates, catalytic ozonation over pure γ-Al_2O_3 and MnO_x/Al_2O_3 generated peaks around 1586 cm^{-1} which are attributed to COO^- stretching of carboxylates. The strong C=O stretching peak at 1700-1725 cm^{-1} appeared in MnO_x/Al_2O_3, while a weak peak was detected for γ-Al_2O_3. This suggests that Mn sites are essential in this reaction for decomposing ozone molecules and oxidizing surface carboxylates. The catalytic activity test using 120 ppm acetone and 1150 ppm ozone at room temperature over 0.2 g pure γ-Al_2O_3 resulted in acetone conversion of around 60 % in the first 5 minutes and it reached to 20% after 40 min of ozonation. The same amount of pure Mn_3O_4 lost its activity in the first 5 minutes of the reaction with the conversion of less than 10% after 40 min of reaction (Figure. 6.5). While using the MnO_x/Al_2O_3 catalysts, the conversions were higher than 90%. The selection of the metal and support and their synergetic cooperation is very critical. Interaction of metal and support can facilitate the migration of the intermediate species among active sites and enable the reaction between them.

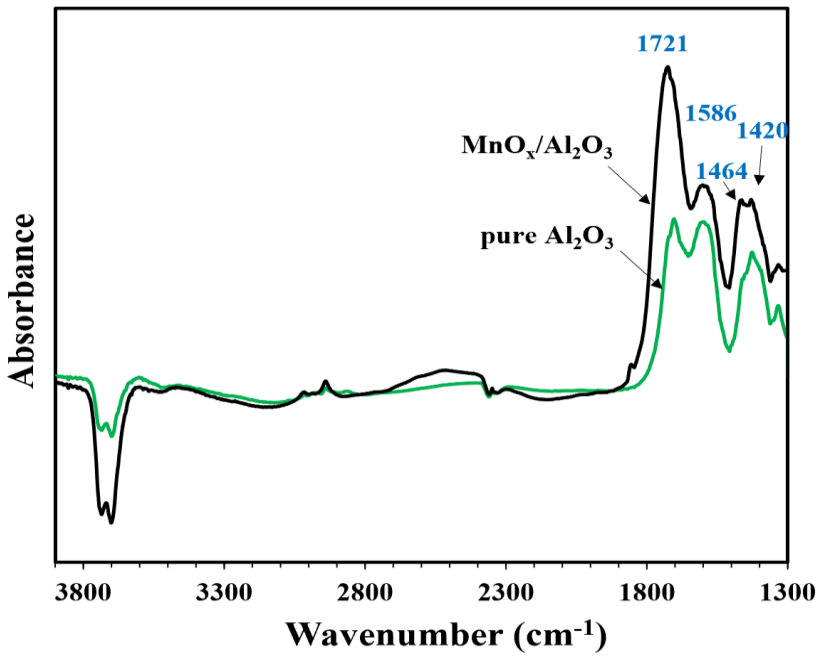

Figure 6.4. In-situ DRIFTS spectra of catalytic ozonation of acetone at 60 min of reaction with MnO_x/Al_2O_3 and pure Al_2O_3.

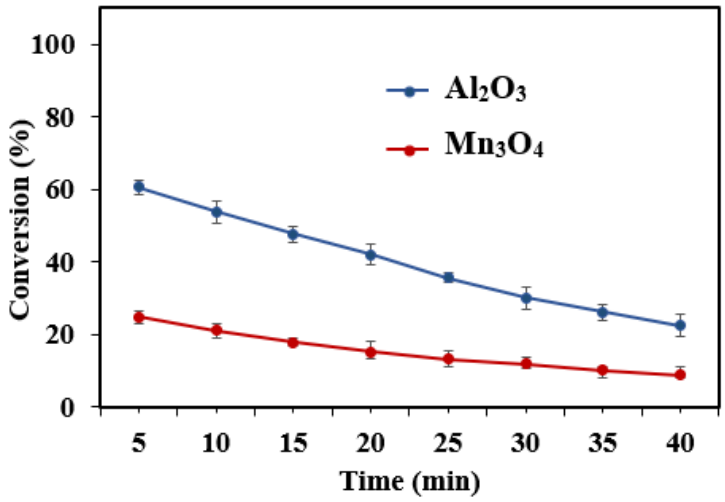

Figure 6.5. Catalytic ozonation of acetone at 25 on γ-alumina, [O_3] = 1150 ppm, [acetone] = 120 ppm, 0.2 g catalyst.

The reaction rate and equilibrium constants at each temperature as well as pre-exponential factors, activation energy, entropy, and enthalpy of acetone adsorption are listed in Table 6.1 for LHd model. Arrhenius and Van't Hoff plots are depicted in Figure B.1 and Figure B.2. The pre-exponential factor for step (1) is much larger than steps (2) and (3) related to ozone decompositions suggesting that this step is much faster. Similar results were obtained from the steps (1) and (2) of LHs mechanism of this work and the literature [98,101]. The low value of *A* for step (2) indicates that the amount of peroxide species on the surface are low and they are negligible compared to the fraction of active sites occupied by acetone. The rate constants of step (5) were lower than other steps in this mechanism indicating that this step is a slow step and rate-determining. The activation energy for step (5) was calculated as 43.6 and 48.6 kJ mol^{-1} for MnO_x/Al_2O_3-P and MnO_x/Al_2O_3-I catalysts, respectively. The pre-exponential parameter of this step was found to be relatively high and it has been reported by Hu et al. that high activation energy of this step influences the impact of pre-exponential parameter and thus the rate constants for this step were very low [101]. The values of entropy and enthalpy of acetone adsorption for both catalysts are negative, indicating an exothermic process. The values of the adsorption enthalpy of acetone in this work are close to the reported value of (30.8-31.3 kJ mol^{-1}) over CuCe based catalyst [213]. Therefore, the calculated physical parameters of the LHd model indicate that the model is physically meaningful.

Table 6.1. Estimated kinetic parameters based on the Langmuir–Hinshelwood dual-site (LHd) model.

Rate constant	Temperature (°C)			*A* (mol kg $^{-1}$s^{-1})	*E* (kJ mol^{-1})	Δ*H* (kJ mol^{-1})	Δ*S* (J mol^{-1} K^{-1})
	40	50	60				
MnO_x-Al_2O_3-P-800							
k_1	(7.68 ± 0.48) ×10^5	(13.80 ± 0.91) ×10^5	(32.74 ± 2.4) ×10^5	(2.11± 0.18) ×10^{16}	62.68 ± 2.71	-	-
k_2	2.46 ± 0.02	2.57 ± 0.01	2.85 ± 0.01	27.43 ± 3.04	6.30 ± 0.30	-	-
k_3	1.10 ± 0.01	1.48 ± 0.01	1.73 ± 0.01	(2.07 ± 0.38) ×10^3	19.58 ± 0.54	-	-
k_5	(7.28 ± 0.40) ×10^{-4}	(12.02 ± 0.82) ×10^{-4}	(19.9 0± 0.67) ×10^{-4}	(1.37 ± 0.19) ×10^4	43.61 ± 0.30	-	-
$K_{ace.}$	604.4 ± 9.2	416.6 ± 8.3	226.8 ± 6.1	-	-	-42.4 ± 0.5	-81.6 ± 1.8
MnO_x-Al_2O_3-I-800							
k_1	(8.30 ± 0.61) ×10^5	(28.84 ± 4.85) ×10^5	(41.61 ± 5.32) ×10^5	(4.97 ± 2.36)×10^{17}	70.22 ± 2.68	-	-
k_2	2.96 ± 0.02	3.24 ± 0.02	3.43 ± 0.02	34.76 ± 21.12	6.40 ± 2.08	-	-
k_3	1.23 ± 0.01	1.44 ± 0.01	2.01 ± 0.02	(41.07± 2.08)×10^2	21.19 ± 0.16	-	-
k_5	(6.30 ± 0.37) ×10^{-4}	(12.00 ± 0.78) ×10^{-4}	(19.31± 0.81) ×10^{-4}	(8.30± 1.7)×10^4	48.60 ± 0.71	-	-
$K_{ace.}$	698.2 ± 11.8	462.08 ± 9.4	229.42 ± 7.1	-	-	-48.1 ± 0.6	-98.7 ± 2.1

6.1.2. Langmuir-Hinshelwood single-site model

In LHs model, the mechanism consists of ozone decomposition, toluene adsorption, and the reaction with atomic oxygen as described in Eqs. (6.9) to (6.14). It has been assumed that further steps after step (6) are fast and are not controlling the kinetics of the process. As can be observed in the derived expression in Eq. (6.15), the active site of alumina is not considered in the final LHs model. The results of model fitting and estimated parameter values for the LHs model are summarized in Table 6.2. Arrhenius and Van't Hoff plots are shown in Figures B.3 and B.4. The value of *n* in the LHs model was calculated to be 2. The first pre-exponential factor is significantly larger than the second one indicating that the first step is much faster. This is in agreement with the findings of Oyama et al. [26] and Rezaei et al. [98] that the first step in the mechanism is the fastest in the ozone decomposition cycle. The final step of the LHs mechanism which consists of the reaction between intermediates is believed to be a slow step in the reaction. The values for the entropy and enthalpy of acetone adsorption were calculated to be negative, inferring exothermic adsorption.

Table 6.2. Estimated kinetic parameters based on the Langmuir–Hinshelwood single-site (LHs) model.

Rate constant	Temperature (°C)			A (mol kg $^{-1}s^{-1}$)	E (kJ mol^{-1})	ΔH (kJ mol^{-1})	ΔS (J mol^{-1} K^{-1})
	40	50	60				
MnO_x-Al_2O_3-P-800							
k_1	1.57 ± 0.01	2.83 ± 0.02	4.28 ± 0.04	(2.94 ± 0.16) ×10^7	43.52 ± 1.20	-	-
k_2	(8.61 ± 0.58)×10^{-3}	(9.83 ± 0.62) ×10^{-3}	(12.28 ± 0.77) ×10^{-3}	3.07 ± 0.5	15.31 ± 0.43	-	-
$K_{ace.}$	38.78 ± 5.3	32.43 ± 3.8	28.98 ± 3.3	-	-	-12.61 ± 1.1	-10.10 ± 2.46
MnO_x-Al_2O_3-I-800							
k_1	1.45 ± 0.01	2.89 ± 0.03	4.43 ± 0.04	(1.86 ± 0.08) ×10^8	48.49 ± 4.84		
k_2	(9.82 ± 0.67)×10^{-3}	(10.91 ± 0.83)×10^{-3}	(14.27 ± 1.02)×10^{-3}	4.67 ± 0.61	16.12 ± 0.17		
K_{ace}	32.77 ± 4.10	27.17 ± 2.83	24.38 ± 2.92	-	-	-12.82 ± 0.52	-12.12 ± 0.44

6.1.2.1. Power law model

The results of the PL fitting are presented in Table 6.3. The high values of R^2 (above 0.9) indicate that PL model is able to represent the reaction rate. The reaction orders (α and β) display the dependency of reaction rate on the concentration of acetone and ozone. The positive values for α and β demonstrate that an increase in the concentration of acetone or ozone enhances the reaction rate. The concentration of ozone has a greater impact on the reaction kinetics compared to acetone, corresponding well with previous studies [26,98,102]. Aghbolaghy et al. have reported reaction orders of 0.109 and 0.506 for acetone and ozone in catalytic ozonation of acetone on MnO_x/Al_2O_3 [102]. The obtained values for α and β over MnO_x/SiO_2 catalyst were reported to be 0.194 and 0.634 by Reed et al. [26].

The apparent activation energy (E_a) was elevated from the slope of the linear relationship of ln k and $1/T$ as per Eq. (6.20). The Arrhenius plots based on PL model are shown in Figure B.5. The obtained values of apparent activation energy for MnO_x/Al_2O_3-P-800 and MnO_x/Al_2O_3-I-800 are 34.1 and 38.7 kJ/mol, respectively. The lower apparent activation energy for MnO_x/Al_2O_3-P-800 confirms the higher activity of the polyol catalyst, which is in agreement with the activity results. The calculated value of apparent activation energy for the impregnated catalyst is close to the value (40 kJ/mol) obtained by Aghbolaghy et al. [102] for catalytic ozonation of acetone over MnO_x/Al_2O_3. The values of apparent activation energy for catalytic ozonation of acetone in this study were remarkably lower than that for catalytic oxidation of acetone [16,101,214].

Table 6.3. Fitting results of the power-law model.

Catalyst	A (mol kg $^{-1}$s^{-1})	E (kJ mol^{-1})	α	β	R^2
MnO_x-Al_2O_3-P-800	2074 ± 105	34.1 ± 1.2	0.133 ± 0.024	0.481 ± 0.018	0.932
MnO_x-Al_2O_3-I-800	11384 ± 2816	38.7 ± 2.6	0.140 ± 0.019	0.485 ± 0.022	0.950

The estimated and experimental results of the models are shown in the parity plots in Figure 6.4. Among the three models, the PL and LHd models exhibited a better agreement between estimated and experimental rates. It can be suggested that catalytic ozonation of acetone using

MnO_x/Al_2O_3 catalyst is following dual-site mechanism and Langmuir-Hinshelwood single-site expression can not express the reaction mechanism well. Similar results were reported by Hu et al. for ozonation of toluene using MnO_2/graphene catalyst [101].

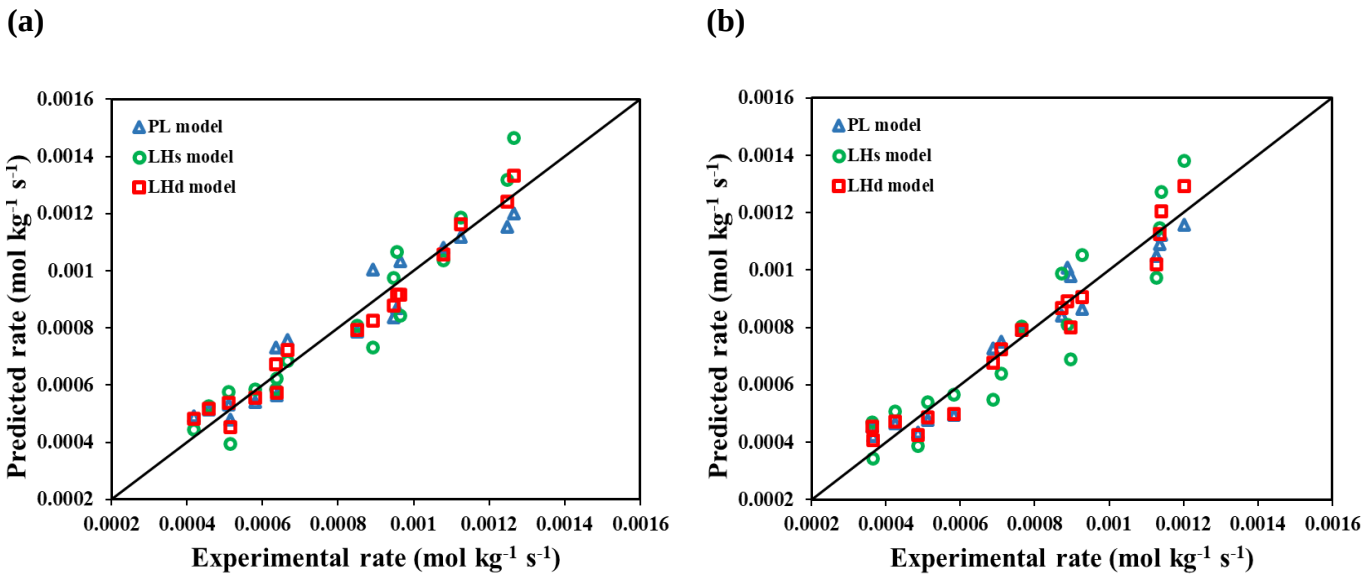

Figure 6.6. Parity plot of the experimental and predicted reaction rates for (a) MnO_x/Al_2O_3-P and (b) MnO_x/Al_2O_3-I.

6.4.3. Model verification

The statistical results related to the model verification are shown in Table 6.4. The results indicated that LHd model (R^2>0.95) estimated the experimental data significantly better than LHs model (R^2>0.8). The experimental data that are excluded from developing the model parameters were used to find the deviation as the errors (%) in Table 6.4. The deviations were calculated to be less than 5% in PL and LHd models, whereas for LHs model the errors were much higher (up to 11.9%).

The values of ρ^2 and F_C are determined to compare the experimental and fitted data and to validate each model. Models with higher value of Fc have higher regression significance which is more desirable. The F_C values of the PL model are greater than the LHs and LHd models due

to the high number of parameters of LH models. As mentioned above, PL model is a simple kinetic model that is useful for finding the reaction orders of reactants, and it is not able to describe the reaction pathway. The LHs and LHd models have comparable F_C values, while the LHd model has a significantly higher number of parameters. ρ^2 values of all models being greater than 0.9 and high values of F_C suggest that the models can adequately predict the reaction rates. However, overall better statistical validation results of LHd model suggest that this model can more accurately predict the experimental data. Other than the statistical discrimination of the model, the obtained values for enthalpy and entropy meet the constraints in Eqs. (6.24) and (6.25). The results of kinetic study over the two catalysts suggest that regardless of the catalyst preparation method, the reaction over the catalysts follows the same pathway. In addition, the results of the kinetic models over the two different catalysts were used to validate the rate data.

Table 6.4. Statistical results of the fitted models.

Models	Catalyst	Model verification /error (%)	SSQ	F_C	ρ^2	R^2
PL	MnO_x-Al_2O_3-P-800	4.30	8.67×10^{-8}	1675	0.993	0.930
	MnO_x-Al_2O_3-I-800	3.42	6.56×10^{-8}	2068	0.994	0.949
LHs	MnO_x-Al_2O_3-P-800	6.35	1.34×10^{-7}	766	0.989	0.891
	MnO_x-Al_2O_3-I-800	11.90	2.07×10^{-7}	451	0.982	0.839
LHd	MnO_x-Al_2O_3-P-800	0.98	4.21×10^{-8}	579	0.997	0.961
	MnO_x-Al_2O_3-I-800	2.66	5.85×10^{-8}	397	0.995	0.955

6.5. Conclusions

Kinetic modeling of catalytic ozonation of acetone over MnO_x/Al_2O_3 catalyst was investigated using three models. The catalysts were prepared by polyol and impregnation methods and displayed excellent catalytic performance in the ozonation of acetone at room temperature. The LHd model represented kinetic data very well inferring that the reaction pathway of ozonation of acetone over MnO_x/Al_2O_3 catalyst proceeds through LH dual-site mechanism. It means that both MnO_x and alumina sites are essential and play a role in creating the intermediates from ozone decomposition and acetone adsorption. The synergy between MnO_x and alumina enabled the reaction between these intermediate species and the LHd

mechanism. The PL model correlated with the experimental data well and the reaction orders and activation energies were estimated accordingly. The reaction orders indicated that both acetone and ozone had a positive influence on the reaction and the impact of ozone was greater than acetone. The LHs mechanism did not properly fit the experimental data indicating that more than a single site is involved in the reaction.

Chapter 7:

Conclusions and Recommendations for Future Work

7.1. Overall discussions and conclusions

The overall research focussed on development of alumina supported Mn based catalyst for catalytic ozonation of VOCs at room temperature.

Chapter 2 of the thesis helped to understand VOC removal techniques, catalytic ozonation of VOCs, and potential catalysts for catalytic oxidation of VOCs with ozone. Catalytic ozonation using supported and unsupported catalysts has been applied for oxidation of a variety of VOCs at low temperatures.

In the first objective in chapter 3, catalytic ozonation of acetone over a series of alumina supported single and mixed transition metal oxide catalysts was studied at room temperature. It was shown that addition of lower loading of the secondary metal to Co and Mn catalysts improved activity of the catalysts. By augmenting the catalyst with the second metal, the local structure and oxidation state of the primary metal remained the same. However, by changing the loading of the secondary metals, its oxidation state changed. It was suggested that the activity of the catalysts is related to the metal's oxidation state and lower metal loadings (5 wt-% or less) result in lower oxidation states.

The second objective was discussed in chapter 4, and it focused on synthesis of MnO_x/Al_2O_3 catalyst using polyol process. The synthesis temperature and time were optimized for oxidation of toluene using ozone. Application of the optimum polyol catalyst in room temperature catalytic ozonation resulted in toluene conversion as high as 80%. Polyol catalyst exhibited superior toluene conversion and ozone decomposition over the impregnated catalyst. It was observed that manganese cluster size in polyol catalyst is smaller than that of the impregnated catalyst resulting in higher dispersion of manganese particles. Moreover, polyol process led to enhanced surface area and pore volume of the catalyst. XPS and XANES analyses showed that Mn^{3+} is the

dominant phase of manganese in both polyol and impregnation catalysts. However, manganese in polyol catalyst has lower oxidation state than impregnated catalyst. Byproducts and intermediates in the reaction are generated more in impregnated catalyst that reduce the catalyst activity.

In chapter 5 and the third objective, MnO_x/Al_2O_3 catalysts were calcinated at different temperatures for catalytic ozonation of acetone and toluene. When calcined at a higher temperature, Mn cluster size increased while the oxidation state of Mn, surface area, and dispersion of the catalyst decreased. The catalysts calcined at higher temperatures showed better activity in the oxidation of acetone achieving about 95% conversion. Toluene conversion was not significantly influenced by calcination temperature. In the binary mixtures, toluene and acetone exhibited promotional and inhibitory behaviors, respectively. The characteristic analysis of the spent catalysts showed that reaction with toluene alters the local structure of the catalysts, and the Mn oxides were reduced in the spent catalyst.

In the final study in chapter 6, the kinetic and mechanism of catalytic ozonation of acetone over the best MnO_x/Al_2O_3 catalysts were investigated. Power law and Langmuir-Hinshelwood dual site models correlated well with the experimental data. The LHd mechanism suggests that the reaction is governed by both metal and support sites. The MnO_x site is essential for the ozone decomposition and alumina site is playing role in acetone adsorption. The connection between these sites facilitates the migration of the intermediates and enables the reaction.

Overall, it was concluded that Mn-based catalysts by addition of Co, change in preparation procedure, and increase in calcination temperature result in higher removal efficiency of VOCs due to change in catalyst's properties especially metal oxidation states.

7.2. Recommendation for future work

Some thoughts and recommendations for future research:

- Mn-Co mixed oxides catalyst could be further modified and enhanced for catalytic ozonation of VOCs at room temperature. Synthesizing alumina supported mix oxides catalyst using polyol method could be beneficial and by addition of both metal precursors in the preparation process simultaneously, the impact of more interaction of Mn and Co can be investigated.
- Attempts could be made to investigate the effect of potential supports such as CeO_2, SiO_2, USY in catalytic ozonation of VOCs using polyol method for catalyst preparation.
- The performance of the synthesized catalysts could be tested under air with different levels of relative humidity. The effect of relative humidity on the activity of the catalysts and characterization of the spent catalysts could be beneficial for better understanding of ozonation of VOCs in air.
- Pilot-scale performance testing can be used to investigate the possibility of removal of some biological air contaminants using catalytic ozonation. As an example, COVID-19 airborne particles or other viruses or bacteria using the the best catalyst in ozonation of various VOCs can be used as starting point for this research.

List of References

[1] V. Van Tran, D. Park, Y.C. Lee, Indoor air pollution, related human diseases, and recent trends in the control and improvement of indoor air quality, Int. J. Environ. Res. Public Health. 17 (2020) 2927. doi:10.3390/ijerph17082927.

[2] WHO, 7 million premature deaths annually linked to air pollution. Accessed at: http://www.who.int/mediacentre/news/releases/2014/air-pollution/en/, Cent. Eur. J. Public Health. 22 (2014) 53–59.

[3] P.M. Mannucci, M. Franchini, Health effects of ambient air pollution in developing countries, Int. J. Environ. Res. Public Health. 14 (2017) 1048. doi:10.3390/ijerph14091048.

[4] J.C. Uzoigwe, T. Prum, E. Bresnahan, M. Garelnabi, The emerging role of outdoor and indoor air pollution in cardiovascular disease, N. Am. J. Med. Sci. 5 (2013) 445. doi:10.4103/1947-2714.117290.

[5] J. Bennett, P. Davy, B. Trompetter, Y. Wang, N. Pierse, M. Boulic, R. Phipps, P. Howden-Chapman, Sources of indoor air pollution at a New Zealand urban primary school; a case study, Atmos. Pollut. Res. 10 (2019) 435–444. doi:10.1016/j.apr.2018.09.006.

[6] P. Amoatey, H. Omidvarborna, M.S. Baawain, A. Al-Mamun, Indoor air pollution and exposure assessment of the gulf cooperation council countries: A critical review, Environ. Int. 121 (2018) 491–506. doi:10.1016/j.envint.2018.09.043.

[7] J. Xu, M. Szyszkowicz, B. Jovic, S. Cakmak, C.C. Austin, J. Zhu, Estimation of indoor and outdoor ratios of selected volatile organic compounds in Canada, Atmos. Environ. 14 (2016) 523–531. doi:10.1016/j.atmosenv.2016.07.031.

[8] J.P.D. Abbatt, C. Wang, The atmospheric chemistry of indoor environments, Environ. Sci. Process. Impacts. 22 (2020) 25–48. doi:10.1039/c9em00386j.

[9] Environmental Protection Agency, Volatile Organic Compounds' Impact on Indoor Air

Quality, Epa. (2018). https://www.epa.gov/indoor-air-quality-iaq/volatile-organic-compounds-impact-indoor-air-quality.

[10] N.B. Goodman, A. Steinemann, A.J. Wheeler, P.J. Paevere, M. Cheng, S.K. Brown, Volatile organic compounds within indoor environments in Australia, Build. Environ. 122 (2017) 116–125. doi:10.1016/j.buildenv.2017.05.033.

[11] S. Malakar, P. Das Saha, D. Baskaran, R. Rajamanickam, Comparative study of biofiltration process for treatment of VOCs emission from petroleum refinery wastewater—A review, Environ. Technol. Innov. 8 (2017) 441–461. doi:10.1016/j.eti.2017.09.007.

[12] R. Yang, P. Han, Y. Fan, Z. Guo, Q. Zhao, Y. Wang, S. Che, S. Lin, R. Zhu, The performance and reaction pathway of δ-MnO2/USY for catalytic oxidation of toluene in the presence of ozone at room temperature, Chemosphere. 247 (2020) 125864. doi:10.1016/j.chemosphere.2020.125864.

[13] P. Liu, G. Wei, H. He, X. Liang, H. Chen, Y. Xi, J. Zhu, The catalytic oxidation of formaldehyde over palygorskite-supported copper and manganese oxides: Catalytic deactivation and regeneration, Appl. Surf. Sci. 464 (2019) 287–293. doi:10.1016/j.apsusc.2018.09.070.

[14] G. Chen, Z. Wang, F. Lin, Z. Zhang, H. Yu, B. Yan, Z. Wang, Comparative investigation on catalytic ozonation of VOCs in different types over supported MnOx catalysts, J. Hazard. Mater. 391 (2020) 122218. doi:10.1016/j.jhazmat.2020.122218.

[15] Y. Liu, J. Deng, S. Xie, Z. Wang, H. Dai, Catalytic removal of volatile organic compounds using ordered porous transition metal oxide and supported noble metal catalysts, Cuihua Xuebao/Chinese J. Catal. 37 (2016) 1193–1205. doi:10.1016/S1872-2067(16)62457-9.

[16] A. Dong, S. Gao, X. Wan, L. Wang, T. Zhang, L. Wang, X. Lang, W. Wang, Labile oxygen promotion of the catalytic oxidation of acetone over a robust ternary Mn-based mullite GdMn2O5, Appl. Catal. B Environ. 271 (2020) 118932. doi:10.1016/j.apcatb.2020.118932.

[17] H. Huang, H. Lu, Y. Zhan, G. Liu, Q. Feng, H. Huang, M. Wu, X. Ye, VUV photo-oxidation of gaseous benzene combined with ozone-assisted catalytic oxidation: Effect on transition metal catalyst, Appl. Surf. Sci. 391 (2017) 662–667. doi:10.1016/j.apsusc.2016.07.040.

[18] J. Shao, F. Lin, Z. Wang, P. Liu, H. Tang, Y. He, K. Cen, Low temperature catalytic ozonation of toluene in flue gas over Mn-based catalysts: Effect of support property and SO2/water vapor addition, Appl. Catal. B Environ. 266 (2020) 118662. doi:10.1016/j.apcatb.2020.118662.

[19] R. Fang, W. Huang, H. Huang, Q. Feng, M. He, J. Ji, B. Liu, D.Y.C. Leung, Efficient MnO x /SiO 2 @AC catalyst for ozone-catalytic oxidation of gaseous benzene at ambient temperature, Appl. Surf. Sci. 470 (2019) 439–447. doi:10.1016/j.apsusc.2018.11.146.

[20] Y. Shu, M. He, J. Ji, H. Huang, S. Liu, D.Y.C. Leung, Synergetic degradation of VOCs by vacuum ultraviolet photolysis and catalytic ozonation over Mn-xCe/ZSM-5, J. Hazard. Mater. 364 (2019) 770–779. doi:10.1016/j.jhazmat.2018.10.057.

[21] E. Rezaei, J. Soltan, Low temperature oxidation of toluene by ozone over MnOx/γ-alumina and MnOx/MCM-41 catalysts, Chem. Eng. J. 198 (2012) 482–490. doi:10.1016/j.cej.2012.06.016.

[22] M. Jin, J.H. Kim, J.M. Kim, J.K. Jeon, J. Jurng, G.N. Bae, Y.K. Park, Benzene oxidation with ozone over MnOx/SBA-15 catalysts, Catal. Today. 204 (2013) 108–113. doi:10.1016/j.cattod.2012.09.026.

[23] M. Wang, P. Zhang, J. Li, C. Jiang, The effects of Mn loading on the structure and ozone decomposition activity of MnOx supported on activated carbon, Cuihua Xuebao/Chinese J. Catal. 35 (2014) 335–341. doi:10.1016/s1872-2067(12)60756-6.

[24] M. Kim, E. Park, J. Jurng, Oxidation of gaseous formaldehyde with ozone over MnOx/TiO2 catalysts at room temperature (25 °C), Powder Technol. 325 (2018) 368–372. doi:10.1016/j.powtec.2017.10.031.

[25] H. Einaga, N. Maeda, S. Yamamoto, Y. Teraoka, Catalytic properties of copper-manganese mixed oxides supported on SiO2 for benzene oxidation with ozone, Catal.

Today. 245 (2015) 22–27. doi:10.1016/j.cattod.2014.09.018.

[26] C. Reed, Y. Xi, S.T. Oyama, Distinguishing between reaction intermediates and spectators: A kinetic study of acetone oxidation using ozone on a silica-supported manganese oxide catalyst, J. Catal. 235 (2005) 378–392. doi:10.1016/j.jcat.2005.08.014.

[27] H. Einaga, N. Maeda, Y. Teraoka, Effect of catalyst composition and preparation conditions on catalytic properties of unsupported manganese oxides for benzene oxidation with ozone, Appl. Catal. B Environ. 142 (2013) 406–413. doi:10.1016/j.apcatb.2013.05.041.

[28] B. Zhu, X.S. Li, P. Sun, J.L. Liu, X.Y. Ma, X. Zhu, A.M. Zhu, A novel process of ozone catalytic oxidation for low concentration formaldehyde removal, Cuihua Xuebao/Chinese J. Catal. 142 (2017) 406–413. doi:10.1016/S1872-2067(17)62890-0.

[29] H. Einaga, A. Ogata, Benzene oxidation with ozone over supported manganese oxide catalysts: Effect of catalyst support and reaction conditions, J. Hazard. Mater. 164 (2009) 1236–1241. doi:10.1016/j.jhazmat.2008.09.032.

[30] E. Rezaei, J. Soltan, N. Chen, Catalytic oxidation of toluene by ozone over alumina supported manganese oxides: Effect of catalyst loading, Appl. Catal. B Environ. 136–137 (2013) 239–247. doi:10.1016/j.apcatb.2013.01.061.

[31] H. Huang, X. Ye, W. Huang, J. Chen, Y. Xu, M. Wu, Q. Shao, Z. Peng, G. Ou, J. Shi, X. Feng, Q. Feng, H. Huang, P. Hu, D.Y.C. Leung, Ozone-catalytic oxidation of gaseous benzene over MnO2/ZSM-5 at ambient temperature: Catalytic deactivation and its suppression, Chem. Eng. J. 264 (2015) 24–31. doi:10.1016/j.cej.2014.11.072.

[32] H. Pluschke, P., & Schleibinger, Indoor air pollution, Springer, 2018.

[33] World Health Organization, Indoor air quality: organic pollutants,Copenhagen, Denmark, 1989.

[34] J.A. Hoskins, Health Effects due to Indoor Air Pollution, Indoor Built Environ. 12 (2003) 427–433. doi:10.1177/1420326X03037109.

[35] J. Zhang, K.R. Smith, Household air pollution from coal and biomass fuels in China:

Measurements, health impacts, and interventions, Environ. Health Perspect. 115 (2007) 848–855. doi:10.1289/ehp.9479.

[36] M.A. Bari, W.B. Kindzierski, A.J. Wheeler, M.È. Héroux, L.A. Wallace, Source apportionment of indoor and outdoor volatile organic compounds at homes in Edmonton, Canada, Build. Environ. 90 (2015) 114–124. doi:10.1016/j.buildenv.2015.03.023.

[37] S.A. Hosseini, Catalytic Oxidation of Volatile Organic Compounds by Using Spinel Mixed Oxide Catalyst- A Review, Adv. Ceram. Sci. Eng. 5 (2016) 1–10. doi:10.14355/acse.2016.05.001.

[38] D.A. Sarigiannis, S.P. Karakitsios, A. Gotti, I.L. Liakos, A. Katsoyiannis, Exposure to major volatile organic compounds and carbonyls in European indoor environments and associated health risk, Environ. Int. (2011) 743–765. doi:10.1016/j.envint.2011.01.005.

[39] C. Walgraeve, K. Demeestere, J. Dewulf, K. Van Huffel, H. Van Langenhove, Diffusive sampling of 25 volatile organic compounds in indoor air: Uptake rate determination and application in Flemish homes for the elderly, Atmos. Environ. 45 (2011) 5828–5836. doi:10.1016/j.atmosenv.2011.07.007.

[40] H. Huang, Y. Xu, Q. Feng, D.Y.C. Leung, Low temperature catalytic oxidation of volatile organic compounds: A review, Catal. Sci. Technol. 5 (2015) 2649–2669. doi:10.1039/c4cy01733a.

[41] M. Bahri, F. Haghighat, Plasma-based indoor air cleaning technologies: The state of the art-review, Clean - Soil, Air, Water. 42 (2014) 1667–1680. doi:10.1002/clen.201300296.

[42] Y. Huang, S.S.H. Ho, R. Niu, L. Xu, Y. Lu, J. Cao, S. Lee, Removal of indoor volatile organic compounds via photocatalytic oxidation: A short review and prospect, Molecules. 21 (2016) 56. doi:10.3390/molecules21010056.

[43] C. Yang, G. Miao, Y. Pi, Q. Xia, J. Wu, Z. Li, J. Xiao, Abatement of various types of VOCs by adsorption/catalytic oxidation: A review, Chem. Eng. J. 370 (2019) 1128–1153. doi:10.1016/j.cej.2019.03.232.

[44] M.S. Kamal, S.A. Razzak, M.M. Hossain, Catalytic oxidation of volatile organic compounds (VOCs) - A review, Atmos. Environ. 140 (2016) 117–134.

doi:10.1016/j.atmosenv.2016.05.031.

[45] L. Zhu, D. Shen, K.H. Luo, A critical review on VOCs adsorption by different porous materials: Species, mechanisms and modification methods, J. Hazard. Mater. 389 (2020) 122102. doi:10.1016/j.jhazmat.2020.122102.

[46] J. Cao, S. Wang, J. Li, Y. Xing, X. Zhao, D. Li, Porous nanosheets assembled Co3O4 hierarchical architectures for enhanced BTX (Benzene, Toluene and Xylene) gas detection, Sensors Actuators, B Chem. 315 (2020) 128120. doi:10.1016/j.snb.2020.128120.

[47] Z. Du, J. Mo, Y. Zhang, Q. Xu, Benzene, toluene and xylenes in newly renovated homes and associated health risk in Guangzhou, China, Build. Environ. 72 (2014) 75–81. doi:10.1016/j.buildenv.2013.10.013.

[48] M. Sleiman, P. Conchon, C. Ferronato, J.M. Chovelon, Photocatalytic oxidation of toluene at indoor air levels (ppbv): Towards a better assessment of conversion, reaction intermediates and mineralization, Appl. Catal. B Environ. 86 (2009) 159–165. doi:10.1016/j.apcatb.2008.08.003.

[49] L. Zhong, S. Batterman, C.W. Milando, VOC sources and exposures in nail salons: a pilot study in Michigan, USA, Int. Arch. Occup. Environ. Health. 92 (2019) 141–153. doi:10.1007/s00420-018-1353-0.

[50] A. Berenjian, N. Chan, H.J. Malmiri, Volatile Organic Compounds removal methods: A review, Am. J. Biochem. Biotechnol. 8 (2012) 220–229. doi:10.3844/ajbbsp.2012.220.229.

[51] G.R. Parmar, N.N. Rao, Emerging control technologies for volatile organic compounds, Crit. Rev. Environ. Sci. Technol. 39 (2009) 41–78. doi:10.1080/10643380701413658.

[52] T. Dobre, O.C. Pârvulescu, G. Iavorschi, M. Stroescu, A. Stoica, Volatile Organic Compounds Removal from Gas Streams by Adsorption onto Activated Carbon, Ind. Eng. Chem. Res. 53 (2014) 3622–3628. doi:10.1021/ie402504u.

[53] S. Detchanamurthy, P.A. Gostomski, Biofiltration for treating VOCs: An overview, Rev. Environ. Sci. Biotechnol. 11 (2012) 231–241. doi:10.1007/s11157-012-9288-5.

[54] L. Malhautier, G. Quijano, M. Avezac, J. Rocher, J.L. Fanlo, Kinetic characterization of toluene biodegradation by Rhodococcus erythropolis: Towards a rationale for microflora enhancement in bioreactors devoted to air treatment, Chem. Eng. J. (2014) 199–204. doi:10.1016/j.cej.2014.02.099.

[55] Z. Shayegan, F. Haghighat, C.S. Lee, Photocatalytic oxidation of volatile organic compounds for indoor environment applications: Three different scaled setups, Chem. Eng. J. 357 (2019) 533–546. doi:10.1016/j.cej.2018.09.167.

[56] A.H. Mamaghani, F. Haghighat, C.S. Lee, Photocatalytic oxidation technology for indoor environment air purification: The state-of-the-art, Appl. Catal. B Environ. 203 (2017) 247–269. doi:10.1016/j.apcatb.2016.10.037.

[57] H. Destaillats, M. Sleiman, D.P. Sullivan, C. Jacquiod, J. Sablayrolles, L. Molins, Key parameters influencing the performance of photocatalytic oxidation (PCO) air purification under realistic indoor conditions, Appl. Catal. B Environ. 128 (2012) 159–170. doi:10.1016/j.apcatb.2012.03.014.

[58] M.F. Mustafa, X. Fu, Y. Liu, Y. Abbas, H. Wang, W. Lu, Volatile organic compounds (VOCs) removal in non-thermal plasma double dielectric barrier discharge reactor, J. Hazard. Mater. 347 (2018) 317–324. doi:10.1016/j.jhazmat.2018.01.021.

[59] X. Fan, T.L. Zhu, M.Y. Wang, X.M. Li, Removal of low-concentration BTX in air using a combined plasma catalysis system, Chemosphere. 75 (2009) 1301–1306. doi:10.1016/j.chemosphere.2009.03.029.

[60] F. Thevenet, L. Sivachandiran, O. Guaitella, C. Barakat, A. Rousseau, Plasma-catalyst coupling for volatile organic compound removal and indoor air treatment: A review, J. Phys. D. Appl. Phys. 47 (2014) 224011. doi:10.1088/0022-3727/47/22/224011.

[61] F.I. Khan, A. Kr. Ghoshal, Removal of Volatile Organic Compounds from polluted air, J. Loss Prev. Process Ind. 13 (2000) 527–545. doi:10.1016/S0950-4230(00)00007-3.

[62] M. Konsolakis, S.A.C. Carabineiro, P.B. Tavares, J.L. Figueiredo, Redox properties and VOC oxidation activity of Cu catalysts supported on Ce1-xSmxOδ mixed oxides, J. Hazard. Mater. 261 (2013) 512–521. doi:10.1016/j.jhazmat.2013.08.016.

[63] S.A.C. Carabineiro, X. Chen, O. Martynyuk, N. Bogdanchikova, M. Avalos-Borja, A. Pestryakov, P.B. Tavares, J.J.M. Órfão, M.F.R. Pereira, J.L. Figueiredo, Gold supported on metal oxides for volatile organic compounds total oxidation, Catal. Today. 244 (2015) 103–114. doi:10.1016/j.cattod.2014.06.034.

[64] E. Rezaei Geshnizgani, Low temperature oxidation of VOCs in air by catalytic ozonation, University of Saskatchewan, 2014.

[65] H. Claus, Ozone Generation by Ultraviolet Lamps†, Photochem. Photobiol. 97 (2021) 471–476. doi:10.1111/php.13391.

[66] T. Batakliev, V. Georgiev, M. Anachkov, S. Rakovsky, G.E. Zaikov, Ozone decomposition, Interdiscip. Toxicol. 7 (2014) 47–59. doi:10.2478/intox-2014-0008.

[67] S.T. Oyama, Chemical and Catalytic Properties of Ozone, Catal. Rev. - Sci. Eng. 42 (2000) 279–322. doi:10.1081/CR-100100263.

[68] R. Atkinson, W.P.L. Carter, Kinetics and Mechanisms of the Gas-Phase Reactions of Ozone with Organic Compounds under Atmospheric Conditions, Chem. Rev. 84 (1984) 437–470. doi:10.1021/cr00063a002.

[69] J.M. Tatibouët, S. Valange, H. Touati, Near-ambient temperature ozone decomposition kinetics on manganese oxide-based catalysts, Appl. Catal. A Gen. 569 (2019) 126–133. doi:10.1016/j.apcata.2018.10.026.

[70] J. Jia, P. Zhang, L. Chen, Catalytic decomposition of gaseous ozone over manganese dioxides with different crystal structures, Appl. Catal. B Environ. 15 (2016) 210–218. doi:10.1016/j.apcatb.2016.02.055.

[71] R. Radhakrishnan, S.T. Oyama, Ozone decomposition over manganese oxide supported on ZrO2 and TiO2: A kinetic study using in situ laser raman spectroscopy, J. Catal. 199 (2001) 282–290. doi:10.1006/jcat.2001.3167.

[72] R. Radhakrishnan, S.T. Oyama, J.G. Chen, K. Asakura, Electron transfer effects in ozone decomposition on supported manganese oxide, J. Phys. Chem. B. 105 (2001) 4245–4253. doi:10.1021/jp003246z.

[73] J. Kim, J.E. Lee, H.W. Lee, J.K. Jeon, J.H. Song, S.C. Jung, Y.F. Tsang, Y.K. Park, Catalytic ozonation of toluene using Mn–M bimetallic HZSM-5 (M: Fe, Cu, Ru, Ag) catalysts at room temperature, J. Hazard. Mater. 397 (2020) 122577. doi:10.1016/j.jhazmat.2020.122577.

[74] H.C. Wang, H.S. Liang, M.B. Chang, Chlorobenzene oxidation using ozone over iron oxide and manganese oxide catalysts, J. Hazard. Mater. 186 (2011) 1781–1787. doi:10.1016/j.jhazmat.2010.12.070.

[75] M. Aghbolaghy, M. Ghavami, J. Soltan, N. Chen, Effect of active metal loading on catalyst structure and performance in room temperature oxidation of acetone by ozone, J. Ind. Eng. Chem. 77 (2019) 118–127. doi:10.1016/j.jiec.2019.04.026.

[76] F. Rezaei, G. Moussavi, A.R. Bakhtiari, Y. Yamini, Toluene removal from waste air stream by the catalytic ozonation process with MgO/GAC composite as catalyst, J. Hazard. Mater. 306 (2016) 348–358. doi:10.1016/j.jhazmat.2015.11.026.

[77] H. Huang, W. Huang, Y. Xu, X. Ye, M. Wu, Q. Shao, G. Ou, Z. Peng, J. Shi, J. Chen, Q. Feng, Y. Zan, H. Huang, P. Hu, Catalytic oxidation of gaseous benzene with ozone over zeolite-supported metal oxide nanoparticles at room temperature, Catal. Today. 258 (2015) 627–633. doi:10.1016/j.cattod.2015.01.006.

[78] M. Tian, S. Liu, L. Wang, H. Ding, D. Zhao, Y. Wang, J. Cui, J. Fu, J. Shang, G.K. Li, Complete Degradation of Gaseous Methanol over Pt/FeOx Catalysts by Normal Temperature Catalytic Ozonation, Environ. Sci. Technol. 54 (2020) 1938–1945. doi:10.1021/acs.est.9b06342.

[79] M. Aghbolaghy, J. Soltan, R. Sutarto, The role of surface carboxylates in catalytic ozonation of acetone on alumina-supported manganese oxide, Chem. Eng. Res. Des. 128 (2017) 73–84. doi:10.1016/j.cherd.2017.10.002.

[80] X. Huang, J. Yuan, J. Shi, W. Shangguan, Ozone-assisted photocatalytic oxidation of gaseous acetaldehyde on TiO2/H-ZSM-5 catalysts, J. Hazard. Mater. 171 (2009) 827–832. doi:10.1016/j.jhazmat.2009.06.070.

[81] M. Jin, J.W. Kim, J.M. Kim, J. Jurng, G.N. Bae, J.K. Jeon, Y.K. Park, Effect of

calcination temperature on the oxidation of benzene with ozone at low temperature over mesoporous α-Mn2O3, Powder Technol. 214 (2011) 458–462. doi:10.1016/j.powtec.2011.08.046.

[82] M. Li, K.N. Hui, K.S. Hui, S.K. Lee, Y.R. Cho, H. Lee, W. Zhou, S. Cho, C.Y.H. Chao, Y. Li, Influence of modification method and transition metal type on the physicochemical properties of MCM-41 catalysts and their performances in the catalytic ozonation of toluene, Appl. Catal. B Environ. 107 (2011) 245–252. doi:10.1016/j.apcatb.2011.07.018.

[83] M. Hu, K.S. Hui, K.N. Hui, Role of graphene in MnO2/graphene composite for catalytic ozonation of gaseous toluene, Chem. Eng. J. 254 (2014) 237–244. doi:10.1016/j.cej.2014.05.099.

[84] J.H. Park, J.M. Kim, M. Jin, J.K. Jeon, S.S. Kim, S.H. Park, S.C. Kim, Y.K. Park, Catalytic ozone oxidation of benzene at low temperature over MnOx/AL-SBA-16 catalyst, Nanoscale Res. Lett. 4 (2012) 1–5. doi:10.1186/1556-276X-7-14.

[85] Y. Teramoto, K. Kosuge, M. Sugasawa, H.H. Kim, A. Ogata, N. Negishi, Zirconium/cerium oxide solid solutions with addition of SiO2as ozone-assisted catalysts for toluene oxidation, Catal. Commun. 61 (2015) 112–116. doi:10.1016/j.catcom.2014.12.022.

[86] H. Einaga, S. Futamura, Comparative study on the catalytic activities of alumina-supported metal oxides for oxidation of benzene and cyclohexane with ozone, React. Kinet. Catal. Lett. 81 (2004) 121–128. doi:10.1023/B:REAC.0000016525.91158.c5.

[87] Y. Liu, H. Zhou, R. Cao, X. Liu, P. Zhang, J. Zhan, L. Liu, Facile and green synthetic strategy of birnessite-type MnO2 with high efficiency for airborne benzene removal at low temperatures, Appl. Catal. B Environ. 245 (2019) 569–582. doi:10.1016/j.apcatb.2019.01.023.

[88] V.P. Santos, M.F.R. Pereira, J.J.M. Órfão, J.L. Figueiredo, The role of lattice oxygen on the activity of manganese oxides towards the oxidation of volatile organic compounds, Appl. Catal. B Environ. 99 (2010) 353–363. doi:10.1016/j.apcatb.2010.07.007.

[89] M. Sugasawa, A. Ogata, Effect of different combinations of metal and zeolite on ozone-

assisted catalysis for toluene removal, Ozone Sci. Eng. 33 (2011) 158–163. doi:10.1080/01919512.2010.547431.

[90] M.A. Peña, J.L.G. Fierro, Chemical structures and performance of perovskite oxides, Chem. Rev. 101 (2001) 1981–2017. doi:10.1021/cr980129f.

[91] M.B. Gawande, R.K. Pandey, R. V. Jayaram, Role of mixed metal oxides in catalysis science - Versatile applications in organic synthesis, Catal. Sci. Technol. 2 (2012) 1113–1125. doi:10.1039/c2cy00490a.

[92] L.Y. Lin, C.Y. Wang, H. Bai, A comparative investigation on the low-temperature catalytic oxidation of acetone over porous aluminosilicate-supported cerium oxides, Chem. Eng. J. 264 (2015) 835–844. doi:10.1016/j.cej.2014.12.042.

[93] W. Tang, X. Wu, D. Li, Z. Wang, G. Liu, H. Liu, Y. Chen, Oxalate route for promoting activity of manganese oxide catalysts in total VOCs' oxidation: Effect of calcination temperature and preparation method, J. Mater. Chem. A. 2 (2014) 2544–2554. doi:10.1039/c3ta13847j.

[94] V.P. Santos, S.A.C. Carabineiro, P.B. Tavares, M.F.R. Pereira, J.J.M. Órfão, J.L. Figueiredo, Oxidation of CO, ethanol and toluene over TiO2 supported noble metal catalysts, Appl. Catal. B Environ. 99 (2010) 198–205. doi:10.1016/j.apcatb.2010.06.020.

[95] X. Tang, Y. Li, X. Huang, Y. Xu, H. Zhu, J. Wang, W. Shen, MnOx-CeO2 mixed oxide catalysts for complete oxidation of formaldehyde: Effect of preparation method and calcination temperature, Appl. Catal. B Environ. 62 (2006) 265–273. doi:10.1016/j.apcatb.2005.08.004.

[96] Y. Yuan, Z. Qin, Z. Xu, SBA_15 Templated Mesoporous MnOx for Catalytic Ozonation of Toluene, Catal. Letters. 150 (2020) 365–374.

[97] H. Einaga, S. Yamamoto, N. Maeda, Y. Teraoka, Structural analysis of manganese oxides supported on SiO2 for benzene oxidation with ozone, Catal. Today. 242 (2015) 287–293. doi:10.1016/j.cattod.2014.05.018.

[98] E. Rezaei, J. Soltan, EXAFS and kinetic study of MnOx/γ-alumina in gas phase catalytic oxidation of toluene by ozone, Appl. Catal. B Environ. 148 (2014) 70–79.

doi:10.1016/j.apcatb.2013.10.041.

[99] H. Einaga, S. Futamura, Oxidation behavior of cyclohexane on alumina-supported manganese oxides with ozone, Appl. Catal. B Environ. 60 (2005) 49–55. doi:10.1016/j.apcatb.2005.02.017.

[100] M. Aghbolaghy, J. Soltan, N. Chen, Role of surface carboxylates in the gas phase ozone-assisted catalytic oxidation of toluene, Catal. Letters. 147 (2017) 2421–2433. doi:10.1007/s10562-017-2143-0.

[101] M. Hu, Z. Yao, K.N. Hui, K.S. Hui, Novel mechanistic view of catalytic ozonation of gaseous toluene by dual-site kinetic modelling, Chem. Eng. J. 308 (2017) 710–718. doi:10.1016/j.cej.2016.09.086.

[102] M. Aghbolaghy, J. Soltan, N. Chen, Low temperature catalytic oxidation of binary mixture of toluene and acetone in the presence of ozone, Catal. Letters. 148 (2018) 3431–3444. doi:10.1007/s10562-018-2536-8.

[103] H. Einaga, M. Harada, A. Ogata, Relationship between the structure of manganese oxides on alumina and catalytic activities for benzene oxidation with ozone, Catal. Letters. 129 (2009) 422–427. doi:10.1007/s10562-008-9814-9.

[104] H. Einaga, Y. Teraoka, A. Ogata, Catalytic oxidation of benzene by ozone over manganese oxides supported on USY zeolite, J. Catal. 305 (2013) 227–237. doi:10.1016/j.jcat.2013.05.016.

[105] R.A. Wood, M.D. Burchett, R. Alquezar, R.L. Orwell, J. Tarran, F. Torpy, The potted-plant microcosm substantially reduces indoor air VOC pollution: I. Office field-study, Water. Air. Soil Pollut. 177 (2006) 59–80. doi:10.1007/s11270-006-9124-z.

[106] S.S.T. Bastos, S.A.C. Carabineiro, J.J.M. Órfão, M.F.R. Pereira, J.J. Delgado, J.L. Figueiredo, Total oxidation of ethyl acetate, ethanol and toluene catalyzed by exotemplated manganese and cerium oxides loaded with gold, Catal. Today. 180 (2012) 148–154. doi:10.1016/j.cattod.2011.01.049.

[107] L. Bo, S. Sun, Microwave-assisted catalytic oxidation of gaseous toluene with a Cu-Mn-Ce/cordierite honeycomb catalyst, Front. Chem. Sci. Eng. 13 (2018) 385–392.

doi:10.1007/s11705-018-1738-3.

[108] Z. Wang, J. Zhou, Y. Zhu, Z. Wen, J. Liu, K. Cen, Simultaneous removal of NOx, SO2 and Hg in nitrogen flow in a narrow reactor by ozone injection: Experimental results, Fuel Process. Technol. 88 (2007) 817–823. doi:10.1016/j.fuproc.2007.04.001.

[109] Q. Ma, Z. Wang, F. Lin, M. Kuang, R. Whiddon, Y. He, J. Liu, Characteristics of O3 Oxidation for Simultaneous Desulfurization and Denitration with Limestone-Gypsum Wet Scrubbing: Application in a Carbon Black Drying Kiln Furnace, Energy and Fuels. 30 (2016) 2302–2308. doi:10.1021/acs.energyfuels.5b02717.

[110] Q. Wang, M. Tang, Y. Peng, C. Du, S. Lu, Ozone assisted oxidation of gaseous PCDD/Fs over CNTs-containing composite catalysts at low temperature, Chemosphere. 199 (2018) 502–509. doi:10.1016/j.chemosphere.2018.01.169.

[111] F. Lin, Z. Wang, Q. Ma, Y. Yang, R. Whiddon, Y. Zhu, K. Cen, Catalytic deep oxidation of NO by ozone over MnOx loaded spherical alumina catalyst, Appl. Catal. B Environ. 198 (2016) 100–111. doi:10.1016/j.apcatb.2016.05.058.

[112] Y. Xi, C. Reed, Y.-K. Lee, S.T. Oyama, Acetone Oxidation Using Ozone on Manganese Oxide Catalysts, J. Phys. Chem. B. 109 (2005) 17587–17596. doi:10.1021/jp052930g.

[113] C. Reed, Y.K. Lee, S. Ted Oyama, Structure and oxidation state of silica-supported manganese oxide catalysts and reactivity for acetone oxidation with ozone, J. Phys. Chem. B. 110 (2006) 4207–4216. doi:10.1021/jp054288w.

[114] X. Liu, J. Zeng, W. Shi, J. Wang, T. Zhu, Y. Chen, Catalytic oxidation of benzene over ruthenium-cobalt bimetallic catalysts and study of its mechanism, Catal. Sci. Technol. 7 (2017) 213–221. doi:10.1039/c6cy02141g.

[115] R. Fiorenza, C. Crisafulli, G.G. Condorelli, F. Lupo, S. Scirè, Au-Ag/CeO2 and Au-Cu/CeO2 Catalysts for Volatile Organic Compounds Oxidation and CO Preferential Oxidation, Catal. Letters. 145 (2015) 1691–1702. doi:10.1007/s10562-015-1585-5.

[116] T. Barakat, V. Idakiev, R. Cousin, G.S. Shao, Z.Y. Yuan, T. Tabakova, S. Siffert, Total oxidation of toluene over noble metal based Ce, Fe and Ni doped titanium oxides, Appl. Catal. B Environ. 146 (2014) 138–146. doi:10.1016/j.apcatb.2013.05.064.

[117] P. Konova, M. Stoyanova, A. Naydenov, S. Christoskova, D. Mehandjiev, Catalytic oxidation of VOCs and CO by ozone over alumina supported cobalt oxide, Appl. Catal. A Gen. 298 (2006) 109–114. doi:10.1016/j.apcata.2005.09.027.

[118] L.F. Liotta, M. Ousmane, G. Di Carlo, G. Pantaleo, G. Deganello, G. Marcì, L. Retailleau, A. Giroir-Fendler, Total oxidation of propene at low temperature over Co3O4-CeO2 mixed oxides: Role of surface oxygen vacancies and bulk oxygen mobility in the catalytic activity, Appl. Catal. A Gen. 347 (2008) 81–88. doi:10.1016/j.apcata.2008.05.038.

[119] Q. Zhao, Q. Liu, C. Song, N. Ji, D. Ma, X. Lu, Enhanced catalytic performance for VOCs oxidation on the CoAlO oxides by KMnO 4 doped on facile synthesis, Chemosphere. 218 (2019) 895–906. doi:10.1016/j.chemosphere.2018.11.131.

[120] G. Deganello, F. Giannici, A. Martorana, G. Pantaleo, A. Prestianni, A. Balerna, L.F. Liotta, A. Longo, Metal-support interaction and redox behavior of Pt(1 wt %)/Ce0.6Zr0.4O2, J. Phys. Chem. B. 110 (2006) 8731–8739. doi:10.1021/jp057427i.

[121] X. Yao, Y. Li, Z. Fan, Z. Zhang, M. Chen, W. Shangguan, Plasma Catalytic Removal of Hexanal over Co-Mn Solid Solution: Effect of Preparation Method and Synergistic Reaction of Ozone, Ind. Eng. Chem. Res. 57 (2018) 4214–4224. doi:10.1021/acs.iecr.8b00191.

[122] B. Ravel, M. Newville, ATHENA, ARTEMIS, HEPHAESTUS: Data analysis for X-ray absorption spectroscopy using IFEFFIT, in: J. Synchrotron Radiat., 2005: pp. 537–541. doi:10.1107/S0909049505012719.

[123] B. Solsona, T.E. Davies, T. Garcia, I. Vázquez, A. Dejoz, S.H. Taylor, Total oxidation of propane using nanocrystalline cobalt oxide and supported cobalt oxide catalysts, Appl. Catal. B Environ. 84 (2008) 176–184. doi:10.1016/j.apcatb.2008.03.021.

[124] A. Borodziński, M. Bonarowska, Relation between Crystallite Size and Dispersion on Supported Metal Catalysts, Langmuir. 13 (1997) 5613–5620. doi:10.1021/la962103u.

[125] M.D. Hernández-Alonso, I. Tejedor-Tejedor, J.M. Coronado, M.A. Anderson, J. Soria, Operando FTIR study of the photocatalytic oxidation of acetone in air over TiO2-ZrO2 thin films, Catal. Today. 143 (2009) 364–373. doi:10.1016/j.cattod.2009.02.033.

[126] J. Li, H. Na, X. Zeng, T. Zhu, Z. Liu, In situ DRIFTS investigation for the oxidation of toluene by ozone over Mn/HZSM-5, Ag/HZSM-5 and Mn-Ag/HZSM-5 catalysts, Appl. Surf. Sci. 311 (2014) 690–696. doi:10.1016/j.apsusc.2014.05.138.

[127] F. Thevenet, O. Debono, M. Rizk, F. Caron, M. Verriele, N. Locoge, VOC uptakes on gypsum boards: Sorption performances and impact on indoor air quality, Build. Environ. 137 (2018) 138–146. doi:10.1016/j.buildenv.2018.04.011.

[128] S. Ren, W. Liang, Q. Li, Y. Zhu, Effect of Pd/Ce loading on the performance of Pd–Ce/γ-Al2O3 catalysts for toluene abatement, Chemosphere. 251 (2020) 126382. doi:10.1016/j.chemosphere.2020.126382.

[129] G. Demirel, O. Ozden, T. Dogeroglu, E.O. Gaga, Personal exposure of primary school children to BTEX, NO2 and ozone in Eskisehir, Turkey: Relationship with indoor/outdoor concentrations and risk assessment, Sci. Total Environ. 473 (2014) 537–548. doi:10.1016/j.scitotenv.2013.12.034.

[130] Y. Zeng, Y. Zhan, R. Xie, K. Hu, J. Cao, D. Lei, B. Liu, M. He, H. Huang, Toluene oxidation over mesoporous TiO2 in a combined process of wet-scrubbing and UV-catalysis, Chemosphere. 244 (2020) 125567. doi:10.1016/j.chemosphere.2019.125567.

[131] C. He, P. Li, J. Cheng, Z.P. Hao, Z.P. Xu, A comprehensive study of deep catalytic oxidation of benzene, toluene, ethyl acetate, and their mixtures over Pd/ZSM-5 catalyst: Mutual effects and kinetics, Water. Air. Soil Pollut. 209 (2010) 365–376. doi:10.1007/s11270-009-0205-7.

[132] A. Ginestet, D. Pugnet, J. Rowley, K. Bull, H. Yeomans, Development of a new photocatalytic oxidation air filter for aircraft cabin, Indoor Air. 15 (2005) 326–334. doi:10.1111/j.1600-0668.2005.00369.x.

[133] E. Rezaei, J. Soltan, N. Chen, J. Lin, Effect of noble metals on activity of MnOx/γ-alumina catalyst in catalytic ozonation of toluene, Chem. Eng. J. 214 (2013) 219–228. doi:10.1016/j.cej.2012.10.044.

[134] H.W. Ryu, M.Y. Song, J.S. Park, J.M. Kim, S.-C. Jung, J. Song, B.-J. Kim, Y.-K. Park, Removal of toluene using ozone at room temperature over mesoporous Mn/Al2O3

catalysts, Environ. Res. 172 (2019) 649–657.

[135] M.H. Castaño, R. Molina, S. Moreno, Mn-Co-Al-Mg mixed oxides by auto-combustion method and their use as catalysts in the total oxidation of toluene, J. Mol. Catal. A Chem. 370 (2013) 167–174. doi:10.1016/j.molcata.2013.01.008.

[136] B. Li, Q. Huang, X.K. Yan, X.L. Xu, Y. Qiu, B. Yang, Y.W. Chen, S.M. Zhu, S.B. Shen, Low-temperature catalytic combustion of benzene over Ni-Mn/CeO2/cordierite catalysts, J. Ind. Eng. Chem. 20 (2014) 2359–2363. doi:10.1016/j.jiec.2013.10.013.

[137] Q. Zhao, Q. Liu, C. Song, N. Ji, D. Ma, X. Lu, Enhanced catalytic performance for VOCs oxidation on the CoAlO oxides by KMnO4 doped on facile synthesis, Chemosphere. 218 (2019) 895–906. doi:10.1016/j.chemosphere.2018.11.131.

[138] D.W. Lee, B.R. Yoo, Advanced metal oxide (supported) catalysts: Synthesis and applications, J. Ind. Eng. Chem. (2014) 3947–3959. doi:10.1016/j.jiec.2014.08.004.

[139] E. Bayrakdar, T. Gürkaynak Altinçekiç, M.A.F. Öksüzömer, Effects of PVP on the preparation of nanosized Al2O3 supported Ni catalysts by polyol method for catalytic partial oxidation of methane, Fuel Process. Technol. 283 (2013) 1–9. doi:10.1016/j.fuproc.2012.12.009.

[140] C.Y. Lu, W.C. Chang, M.Y. Wey, CuO/CeO2 catalysts prepared with different cerium supports for CO oxidation at low temperature, Mater. Chem. Phys. 141 (2013) 512–518. doi:10.1016/j.matchemphys.2013.05.052.

[141] C.Y. Lu, M.Y. Wey, L.I. Chen, Application of polyol process to prepare AC-supported nanocatalyst for VOC oxidation, Appl. Catal. A Gen. 325 (2007) 163–174. doi:10.1016/j.apcata.2007.03.030.

[142] T.G. Altinçekiç, I. Boz, Influence of synthesis conditions on particle morphology of nanosized Cu/ZnO powder by polyol method, Bull. Mater. Sci. 31 (2008) 619–624. doi:10.1007/s12034-008-0098-x.

[143] H.H. Tseng, H.Y. Lin, Y.F. Kuo, Y.T. Su, Synthesis, characterization, and promoter effect of Cu-Zn/γ-Al2O3catalysts on NO reduction with CO, Chem. Eng. J. 160 (2010) 13–19. doi:10.1016/j.cej.2010.02.039.

[144] N. Hikmah, N. Faeqah, A. Hadi, Synthesis of Silver-Copper Nanoparticles via Polyol Method: Effect of Reaction Time and Temperature, Adv. Mater. Res. 1113 (2015) 605–610. doi:10.4028/www.scientific.net/AMR.1113.605.

[145] K.C. Soni, R. Krishna, S. Chandra Shekar, B. Singh, Catalytic oxidation of carbon monoxide over supported palladium nanoparticles, Appl. Nanosci. 6 (2016) 7–17. doi:10.1007/s13204-015-0419-5.

[146] Y. Jeong, J.Y. Kang, I. Kim, H. Jeong, J.K. Park, J.H. Park, J.C. Jung, Preparation of Cu/ZnO catalyst using a polyol method for alcohol-assisted low temperature methanol synthesis from syngas, Korean J. Chem. Eng. 33 (2016) 114–119. doi:10.1007/s11814-015-0118-7.

[147] C.Y. Lu, M.Y. Wey, Y.H. Fu, The size, shape, and dispersion of active sites on AC-supported copper nanocatalysts with polyol process: The effect of precursors, Appl. Catal. A Gen. 344 (2008) 36–44. doi:10.1016/j.apcata.2008.03.036.

[148] C.Y. Lu, H.H. Tseng, M.Y. Wey, T.W. Hsueh, The comparison between the polyol process and the impregnation method for the preparation of CNT-supported nanoscale Cu catalyst, Chem. Eng. J. 145 (2009) 461–467. doi:10.1016/j.cej.2008.04.033.

[149] C.Y. Lu, H.H. Tseng, M.Y. Wey, L.Y. Liu, J.H. Kuo, K.H. Chuang, Al2O3-supported Cu-Co bimetallic catalysts prepared with polyol process for removal of BTEX and PAH in the incineration flue gas, Fuel. 88 (2009) 340–347. doi:10.1016/j.fuel.2008.09.012.

[150] Y.M. Lee, G.W. Qin, C.G. Lee, B.H. Koo, K.Y. Moon, Y. Shimada, O. Kitakami, Effect of reaction time on formation of CoNi particles prepared via the polyol method, Met. Mater. Int. 13 (2007) 207–210. doi:10.1007/BF03027806.

[151] R. Carrera-Cerritos, C. Salazar-Hernandez, I.R. Galindo-Esquivel, R. Fuentes-Ramirez, Effect of the Reduction Temperature of PdAg Nanoparticles during the Polyol Process in the Ethanol Electrooxidation Reaction, J. Nanomater. 2018 (2018) 1–9. doi:10.1155/2018/9451421.

[152] J.C. Medina, M. Figueroa, R. Manrique, J. Rodríguez Pereira, P.D. Srinivasan, J.J. Bravo-Suárez, V.G. Baldovino Medrano, R. Jiménez, A. Karelovic, Catalytic consequences of

Ga promotion on Cu for CO2 hydrogenation to methanol, Catal. Sci. Technol. 7 (2017) 3375–3387. doi:10.1039/c7cy01021d.

[153] S. Hanukovich, A. Dang, P. Christopher, Influence of Metal Oxide Support Acid Sites on Cu-Catalyzed Nonoxidative Dehydrogenation of Ethanol to Acetaldehyde, ACS Catal. 9 (2019) 3537–3550. doi:10.1021/acscatal.8b05075.

[154] M. Li, H. Amari, A.C. van Veen, Metal-oxide interaction enhanced CO2 activation in methanation over ceria supported nickel nanocrystallites, Appl. Catal. B Environ. 239 (2018) 27–35. doi:10.1016/j.apcatb.2018.07.074.

[155] H.A.E. Dole, R.J. Isaifan, F.M. Sapountzi, L. Lizarraga, D. Aubert, A. Princivalle, P. Vernoux, E.A. Baranova, Low temperature toluene oxidation over Pt nanoparticles supported on yttria stabilized-zirconia, Catal. Letters. 143 (2013) 996–1002. doi:10.1007/s10562-013-1071-x.

[156] R. Isaifan, E.O. Holly Dole, L. Lizarraga, E.A. Baranova, P. Vernoux, Catalytic CO oxidation over Pt nanoparticles prepared from the polyol reduction method supported on Yttria-Stabilized Zirconia, ECS Trans. 35 (2011) 43–57.

[157] M. Feilizadeh, G. Mul, M. Vossoughi, E. coli inactivation by visible light irradiation using a Fe–Cd/TiO2 photocatalyst: Statistical analysis and optimization of operating parameters, Appl. Catal. B Environ. 168 (2015) 441–447. doi:10.1016/J.APCATB.2014.12.034.

[158] J. Li, Q. Liu, Q. qing Ji, B. Lai, Degradation of p-nitrophenol (PNP) in aqueous solution by Fe0-PM-PS system through response surface methodology (RSM), Appl. Catal. B Environ. 200 (2017) 633–646. doi:10.1016/j.apcatb.2016.07.026.

[159] M.A. Naeem, A.S. Al-Fatesh, A.E. Abasaeed, A.H. Fakeeha, Activities of Ni-based nano catalysts for CO2-CH4reforming prepared by polyol process, Fuel Process. Technol. 122 (2014) 141–152. doi:10.1016/j.fuproc.2014.01.035.

[160] N. Saadatkhah, A. Carillo Garcia, S. Ackermann, P. Leclerc, M. Latifi, S. Samih, G.S. Patience, J. Chaouki, Experimental methods in chemical engineering: Thermogravimetric analysis—TGA, Can. J. Chem. Eng. (2020) 34–43. doi:10.1002/cjce.23673.

[161] M.C. Álvarez-Galván, B. Pawelec, V.A. De La Peña O'Shea, J.L.G. Fierro, P.L. Arias,

Formaldehyde/methanol combustion on alumina-supported manganese-palladium oxide catalyst, Appl. Catal. B Environ. 51 (2004) 83–91. doi:10.1016/j.apcatb.2004.01.024.

[162] S.C. Kim, W.G. Shim, Catalytic combustion of VOCs over a series of manganese oxide catalysts, Appl. Catal. B Environ. 98 (2010) 180–185. doi:10.1016/j.apcatb.2010.05.027.

[163] K. Prabu, M. Prabu, A.K. Venugopal, A.T. Venugopalan, W.V.Y.S. Sandilya, C.S. Gopinath, T. Raja, Effective and selective oxidation of 2-butanol over Mn supported catalyst systems, Appl. Catal. A Gen. 525 (2016) 237–246. doi:10.1016/j.apcata.2016.08.005.

[164] G. Long, M. Chen, Y. Li, J. Ding, R. Sun, Y. Zhou, X. Huang, G. Han, W. Zhao, One-pot synthesis of monolithic Mn-Ce-Zr ternary mixed oxides catalyst for the catalytic combustion of chlorobenzene, Chem. Eng. J. (2018) 964–973. doi:10.1016/j.cej.2018.07.091.

[165] H.R. Barai, A.N. Banerjee, S.W. Joo, Improved electrochemical properties of highly porous amorphous manganese oxide nanoparticles with crystalline edges for superior supercapacitors, J. Ind. Eng. Chem. 56 (2017) 212–224. doi:10.1016/j.jiec.2017.07.014.

[166] W. Tang, W. Li, D. Li, G. Liu, X. Wu, Y. Chen, Synergistic effects in porous Mn-Co mixed oxide nanorods enhance catalytic deep oxidation of benzene, Catal. Letters. 144 (2014) 1900–1910. doi:10.1007/s10562-014-1340-3.

[167] H. Einaga, S. Futamura, Effect of water vapor on catalytic oxidation of benzene with ozone on alumina-supported manganese oxides, J. Catal. 243 (2006) 446–450. doi:10.1016/j.jcat.2006.07.021.

[168] F. Zhang, B. Hong, W. Zhao, Y. Yang, J. Bao, C. Gao, S. Sun, Ozone modification as an efficient strategy for promoting the photocatalytic effect of TiO2 for air purification, Chem. Commun. 55 (2019) 3757–3760. doi:10.1039/c9cc00814d.

[169] H. Sun, Z. Liu, S. Chen, X. Quan, The role of lattice oxygen on the activity and selectivity of the OMS-2 catalyst for the total oxidation of toluene, Chem. Eng. J. 270 (2015) 58–65. doi:10.1016/j.cej.2015.02.017.

[170] L. Long, J. Zhao, L. Yang, M. Fu, J. Wu, B. Huang, D. Ye, Room temperature catalytic

ozonation of toluene over MnO2/Al2O3, Cuihua Xuebao/Chinese J. Catal. 32 (2011) 904–916. doi:10.1016/S1872-2067(10)60216-1.

[171] L. Sivachandiran, F. Thevenet, A. Rousseau, Regeneration of isopropyl alcohol saturated MnXOY surface: COMPARISON of thermal, ozonolysis and non-thermal plasma treatments, Chem. Eng. J. 246 (2014) 184–195. doi:10.1016/j.cej.2014.02.058.

[172] H. Einaga, S. Futamura, Catalytic oxidation of benzene with ozone over alumina-supported manganese oxides, J. Catal. 227 (2004) 304–312. doi:10.1016/j.jcat.2004.07.029.

[173] R. Fang, W. Huang, H. Huang, Q. Feng, M. He, J. Ji, B. Liu, D.Y.C. Leung, Efficient MnOx/SiO2 @AC catalyst for ozone-catalytic oxidation of gaseous benzene at ambient temperature, Appl. Surf. Sci. 470 (2019) 439–447. doi:10.1016/j.apsusc.2018.11.146.

[174] U. Menon, V. V. Galvita, G.B. Marin, Reaction network for the total oxidation of toluene over CuO-CeO2/Al2O3, J. Catal. 283 (2011) 1–9. doi:10.1016/j.jcat.2011.05.024.

[175] N. Sakai, S. Yamamoto, Y. Matsui, M.F. Khan, M.T. Latif, M. Ali Mohd, M. Yoneda, Characterization and source profiling of volatile organic compounds in indoor air of private residences in Selangor State, Malaysia, Sci. Total Environ. 586 (2017) 1279–1286. doi:10.1016/j.scitotenv.2017.02.139.

[176] L. Yu, L. Wang, W. Xu, L. Chen, M. Fu, J. Wu, D. Ye, Adsorption of VOCs on reduced graphene oxide, J. Environ. Sci. (China). 67 (2018) 171–178. doi:10.1016/j.jes.2017.08.022.

[177] T. Gopi, G. Swetha, S.C. Shekar, R. Krishna, C. Ramakrishna, B. Saini, P.V.L. Rao, Ozone catalytic oxidation of toluene over 13X zeolite supported metal oxides and the effect of moisture on the catalytic process, Arab. J. Chem. (2016) 4502–4513. doi:10.1016/j.arabjc.2016.07.018.

[178] S.C. Jung, Y.K. Park, H.Y. Jung, U. Il Kang, J.W. Nah, S.C. Kim, Effects of calcination and support on supported manganese catalysts for the catalytic oxidation of toluene as a model of VOCs, Res. Chem. Intermed. 42 (2016) 185–199. doi:10.1007/s11164-015-2333-6.

[179] K. Kruanak, C. Jarusutthirak, Degradation of 2,4,6-trichlorophenol in synthetic wastewater by catalytic ozonation using alumina supported nickel oxides, J. Environ. Chem. Eng. 7 (2019) 102825. doi:10.1016/j.jece.2018.102825.

[180] H. Einaga, Y. Teraoka, A. Ogat, Benzene oxidation with ozone over manganese oxide supported on zeolite catalysts, in: Catal. Today, 2011: pp. 571–574. doi:10.1016/j.cattod.2010.10.067.

[181] J. Jo, S. Baek Lee, S.Y. Mok, Effect of calcination temperature of Mnxoy/Γ-Al2O3 catalyst on ozone decomposition, in: Res. World Int. Conf., Poland, 2017: pp. 5–8.

[182] G. Aguila, S. Guerrero, P. Araya, Effect of the preparation method and calcination temperature on the oxidation activity of CO at low temperature on CuO–CeO2/SiO2 catalysts., Appl. Catal. A Gen. 462 (2013) 56–63.

[183] W.X. Tang, H. Di Liu, X.F. Wu, Y.F. Chen, Higher Oxidation State Responsible for Ozone Decomposition at Room Temperature over Manganese and Cobalt Oxides: Effect of Calcination Temperature, Ozone Sci. Eng. 36 (2014) 502–512. doi:10.1080/01919512.2014.894454.

[184] A. Jonoidi Jafari, M. Kermani, A. Hosseini-Bandegharaei, A. Rastegar, M. Gholami, A. Alahabadi, G. Farzi, Synthesis and characterization of Ag/TiO2/composite aerogel for enhanced adsorption and photo-catalytic degradation of toluene from the gas phase, Chem. Eng. Res. Des. 150 (2019) 1–13. doi:10.1016/j.cherd.2019.07.017.

[185] C.L. Bianchi, S. Gatto, C. Pirola, A. Naldoni, A. Di Michele, G. Cerrato, V. Crocellà, V. Capucci, Photocatalytic degradation of acetone, acetaldehyde and toluene in gas-phase: Comparison between nano and micro-sized TiO2, Appl. Catal. B Environ. 146 (2014) 123–130. doi:10.1016/j.apcatb.2013.02.047.

[186] E. Gallego, F.J. Roca, J.F. Perales, G. Sánchez, P. Esplugas, Characterization and determination of the odorous charge in the indoor air of a waste treatment facility through the evaluation of volatile organic compounds (VOCs) using TD-GC/MS, Waste Manag. 32 (2012) 2469–2481. doi:10.1016/j.wasman.2012.07.010.

[187] Z. Wang, P. Ma, K. Zheng, C. Wang, Y. Liu, H. Dai, C. Wang, H.C. Hsi, J. Deng, Size

effect, mutual inhibition and oxidation mechanism of the catalytic removal of a toluene and acetone mixture over TiO2 nanosheet-supported Pt nanocatalysts, Appl. Catal. B Environ. 274 (2020) 11893. doi:10.1016/j.apcatb.2020.118963.

[188] M. Ghavami, J. Soltan, N. Chen, Synthesis of MnOx/Al2O3 Catalyst by Polyol Method and Its Application in Room Temperature Ozonation of Toluene in Air, Catal. Letters. (2020) 1–15.

[189] F. Fievet, S. Ammar-Merah, R. Brayner, F. Chau, M. Giraud, F. Mammeri, J. Peron, J.Y. Piquemal, L. Sicard, G. Viau, The polyol process: a unique method for easy access to metal nanoparticles with tailored sizes, shapes and compositions, Chem. Soc. Rev. 47 (2018) 5187–5233. doi:10.1039/c7cs00777a.

[190] J.J. Rehr, R.C. Albers, Theoretical approaches to x-ray absorption fine structure, Rev. Mod. Phys. 72 (2000) 621. doi:10.1103/RevModPhys.72.621.

[191] O. Amadine, Y. Essamlali, A. Fihri, M. Larzek, M. Zahouily, Effect of calcination temperature on the structure and catalytic performance of copper-ceria mixed oxide catalysts in phenol hydroxylation, RSC Adv. 7 (2017) 12586–12597. doi:10.1039/c7ra00734e.

[192] S.M. Lee, K.H. Park, S.S. Kim, D.W. Kwon, S.C. Hong, Effect of the Mn oxidation state and lattice oxygen in Mn-based TiO2 catalysts on the low-temperature selective catalytic reduction of NO by NH3, J. Air Waste Manag. Assoc. 62 (2012) 1085–1092. doi:10.1080/10962247.2012.696532.

[193] X. Liu, S. Jiang, H. Li, J. Yang, Z. Yang, J. Zhao, H. Peng, K. Shih, Elemental mercury oxidation over manganese oxide octahedral molecular sieve catalyst at low flue gas temperature, Chem. Eng. J. 356 (2019) 142–150. doi:10.1016/j.cej.2018.08.225.

[194] W. Gac, M. Greluk, G. Słowik, S. Turczyniak-Surdacka, Structural and surface changes of cobalt modified manganese oxide during activation and ethanol steam reforming reaction, Appl. Surf. Sci. 440 (2018) 1047–1062. doi:10.1016/j.apsusc.2018.01.242.

[195] M.C. Biesinger, B.P. Payne, A.P. Grosvenor, L.W.M. Lau, A.R. Gerson, R.S.C. Smart, Resolving surface chemical states in XPS analysis of first row transition metals, oxides

and hydroxides: Cr, Mn, Fe, Co and Ni, Appl. Surf. Sci. 257 (2011) 2717–2730. doi:10.1016/j.apsusc.2010.10.051.

[196] V. Chevalier, J. Martin, D. Peralta, A. Roussey, F. Tardif, Performance of HKUST-1 Metal-Organic Framework for a VOCs mixture adsorption at realistic concentrations ranging from 0.5 to 2.5 ppmv under different humidity conditions, J. Environ. Chem. Eng. 7 (2019) 103131. doi:10.1016/j.jece.2019.103131.

[197] M. Che, Nobel Prize in chemistry 1912 to Sabatier: Organic chemistry or catalysis?, Catal. Today. (2013) 162–171. doi:10.1016/j.cattod.2013.07.006.

[198] M. Ghavami, M. Aghbolaghy, J. Soltan, N. Chen, Room temperature oxidation of acetone by ozone over alumina-supported manganese and cobalt mixed oxides, Front. Chem. Sci. Eng. (2020) 1–11. doi:10.1007/s11705-019-1900-6.

[199] H. Zhao, Y. Dong, P. Jiang, G. Wang, J. Zhang, K. Li, C. Feng, An α-MnO2 nanotube used as a novel catalyst in ozonation: Performance and the mechanism, New J. Chem. 38 (2014) 1743–1750. doi:10.1039/c3nj01523h.

[200] H. Chen, H. Zhang, Y. Yan, Catalytic combustion of volatile organic compounds over a structured zeolite membrane reactor, Ind. Eng. Chem. Res. 52 (2013) 12819–12826. doi:10.1021/ie401882w.

[201] A. Zuhairi Abdullah, M.Z.A. Bakar, S. Bhatia, A Kinetic Study of Catalytic Combustion of Ethyl Acetate and Benzene in Air Stream over Cr-ZSM-5 Catalyst, Ind. Eng. Chem. Res. 42 (2003) 6059–6067. doi:10.1021/ie020989t.

[202] D. Xia, W. Xu, Y. Wang, J. Yang, Y. Huang, L. Hu, C. He, D. Shu, D.Y.C. Leung, Z. Pang, Enhanced Performance and Conversion Pathway for Catalytic Ozonation of Methyl Mercaptan on Single-Atom Ag Deposited Three-Dimensional Ordered Mesoporous MnO2, Environ. Sci. Technol. 52 (2018) 13399–13409. doi:10.1021/acs.est.8b03696.

[203] H. Einaga, N. Maeda, Y. Nagai, Comparison of catalytic properties of supported metal oxides for benzene oxidation using ozone, Catal. Sci. Technol. 5 (2015) 3147–3158. doi:10.1039/c5cy00315f.

[204] L. Wang, C. Zhang, H. Huang, X. Li, W. Zhang, M. Lu, M. Li, Catalytic oxidation of

toluene over active MnOx catalyst prepared via an alkali-promoted redox precipitation method, React. Kinet. Mech. Catal. 118 (2016) 605–619. doi:10.1007/s11144-016-1011-z.

[205] W. Yang, X. Zhang, J. Su, Y. Wang, Q. Zhao, J. Zhou, Kinetics of n-butanol oxidation over Pt/ZSM-5 catalyst, Fuel Process. Technol. 179 (2018) 108–113. doi:10.1016/j.fuproc.2018.06.020.

[206] M.P. Heynderickx, J.W. Thybaut, H. Poelman, D. Poelman, G.B. Marin, Kinetic modeling of the total oxidation of propane over CuO-CeO2/γ-Al2O3, Appl. Catal. B Environ. 95 (2010) 26–38. doi:10.1016/j.apcatb.2009.11.018.

[207] G.F. Froment, On fundamental kinetic equations for chemical reactions and processes, Curr. Opin. Chem. Eng. (2014) 1–6. doi:10.1016/j.coche.2014.02.002.

[208] W. Xie, F. Zhou, X. Bi, D. Chen, Z. Huang, Y. Li, S. Sun, J. Liu, Decomposition of Nickel(II)−Ethylenediaminetetraacetic acid by Fenton−Like reaction over oxygen vacancies-based Cu−Doped Fe3O4@Γ−Al2O3 catalyst: A synergy of oxidation and adsorption, Chemosphere. 221 (2019) 563–572. doi:10.1016/j.chemosphere.2019.01.083.

[209] S. Yang, Y. Feng, J. Wan, W. Zhu, Z. Jiang, Effect of CeO 2 addition on the structure and activity of RuO 2 /γ-Al 2 O 3 catalyst, Appl. Surf. Sci. 246 (2005) 222–228. doi:10.1016/j.apsusc.2004.11.013.

[210] Z. Lei, L. Min, K. Tingting, Z. Lei, H. Huibin, J. Yang, Y. Chao, W. Yan, L. Mengting, Preparation of MnOx Supported LiOH Activated Soybean Oil Sludge Catalyst and Its Analysis in Denitration Mechanism of Selective Catalytic Oxidation (SCO), Sci. Rep. 9 (2019) 1–10. doi:10.1038/s41598-019-47947-2.

[211] P. Wang, S. Su, J. Xiang, F. Cao, L. Sun, S. Hu, S. Lei, Catalytic oxidation of Hg0 by CuO-MnO2-Fe2O3/γ-Al2O3 catalyst, Chem. Eng. J. 225 (2013) 68–75. doi:10.1016/j.cej.2013.03.060.

[212] C. Shi, Y. Wang, A. Zhu, B. Chen, C. Au, Mn xCo 3 - XO 4 solid solution as high-efficient catalysts for low-temperature oxidation of formaldehyde, Catal. Commun. 28 (2012) 18–22. doi:10.1016/j.catcom.2012.08.003.

[213] C. Hu, Catalytic combustion kinetics of acetone and toluene over Cu0.13Ce0.87Oy

catalyst, Chem. Eng. J. 168 (2011) 1185–1192. doi:10.1016/j.cej.2011.02.006.

[214] L.M. Gandía, A. Gil, S.A. Korili, Effects of various alkali-acid additives on the activity of a manganese oxide in the catalytic combustion of ketones, Appl. Catal. B Environ. 33 (2001) 1–8. doi:10.1016/S0926-3373(01)00155-2.

Appendix A: Calibration curves of FTIR setup

The experimental setup attached to Nicolet iS50 FTIR spectrometer was calibrated for gas streams of acetone, toluene, carbon dioxide, and carbon monoxide passing through a long-path gas cell (PIKE, KBr window). Calibration curves were obtained based on the intensity of the peaks at 1738, 729, 2361 and 2174 cm^{-1} for acetone, toluene, carbon dioxide, and carbon monoxide, respectively.

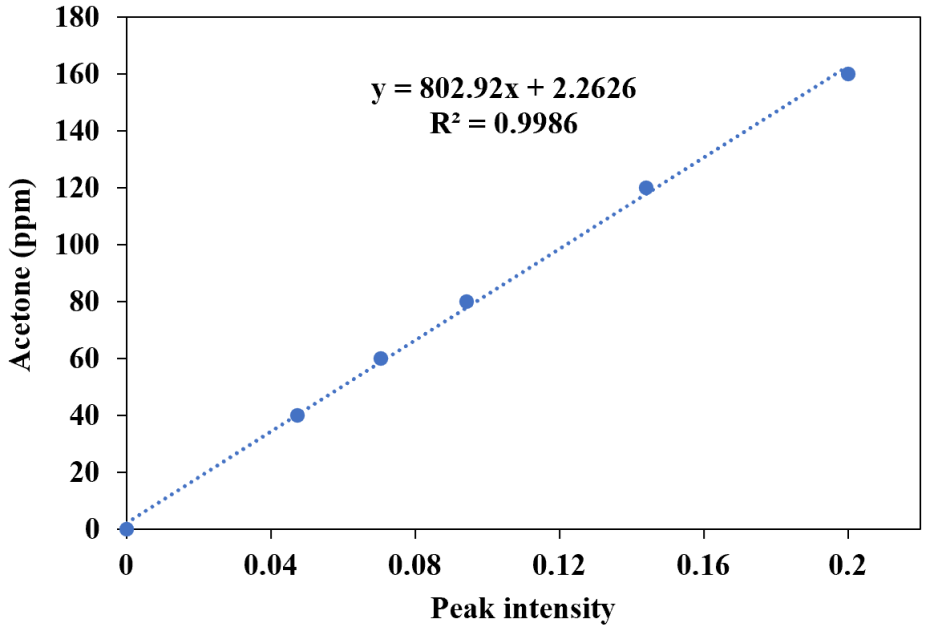

Figure A.1. Acetone calibration based on peak height at 1738 cm^{-1}.

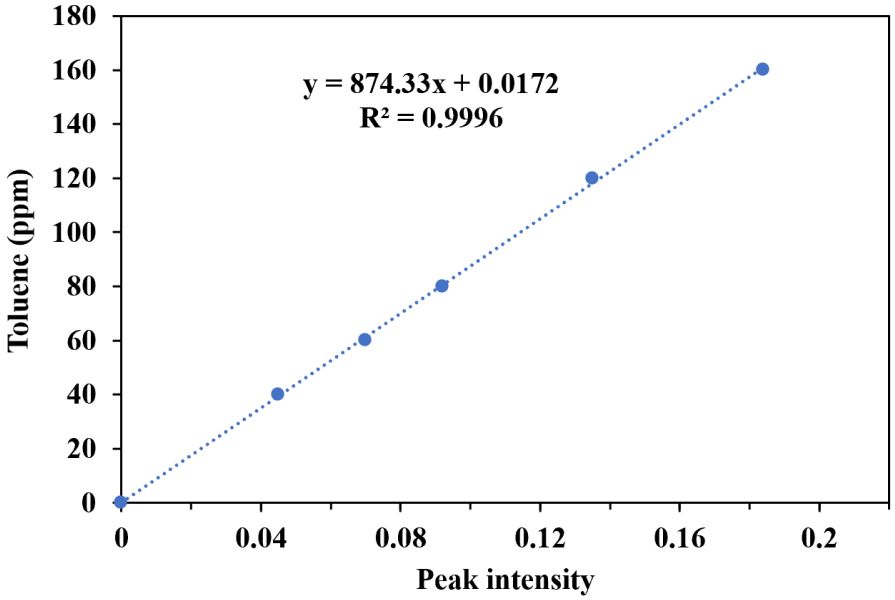

Figure A.2. Toluene calibration based on peak height at 729 cm^{-1}.

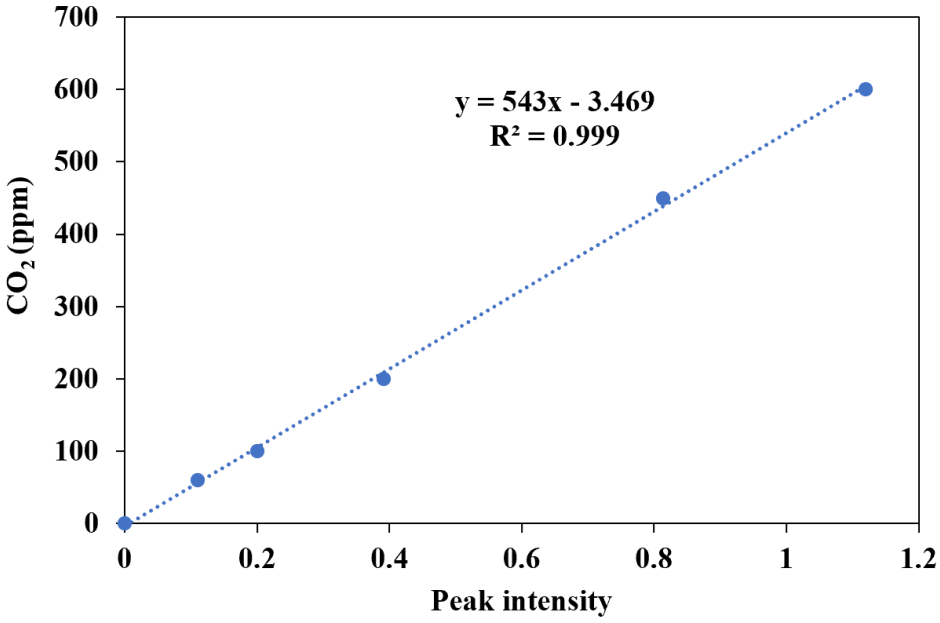

Figure A.3. CO_2 calibration based on peak height at 2361 cm^{-1}.

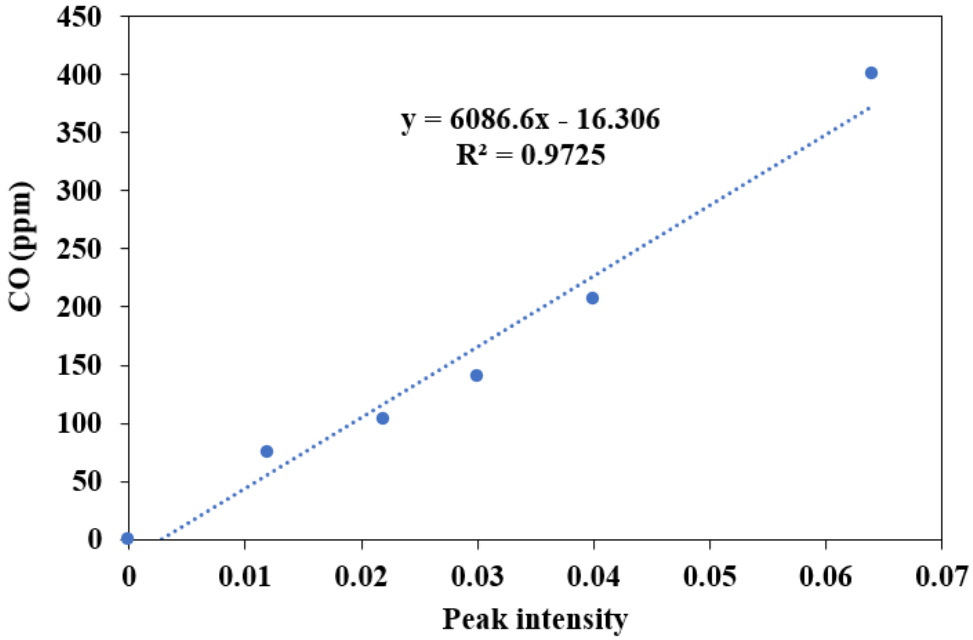

Figure A.4. CO calibration based on peak height at 2174 cm^{-1}.

Appendix B: Arrhenius plots and Van't Hoff plots for kinetic study measurements

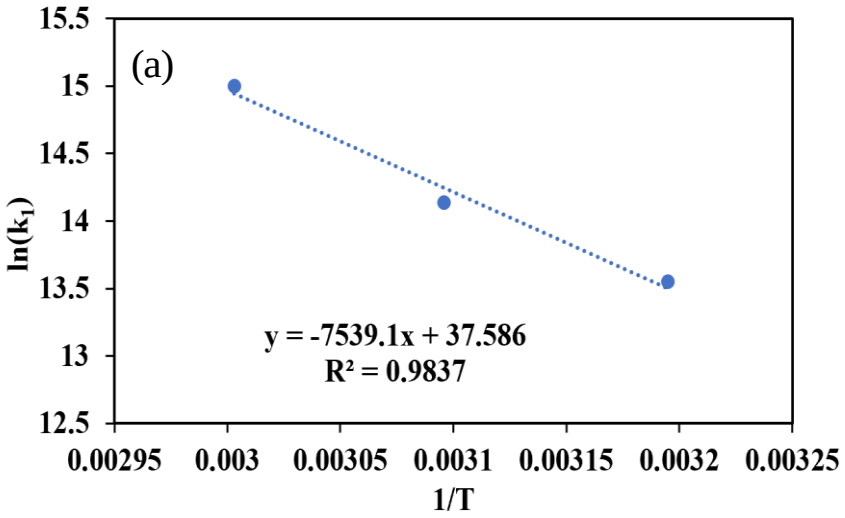

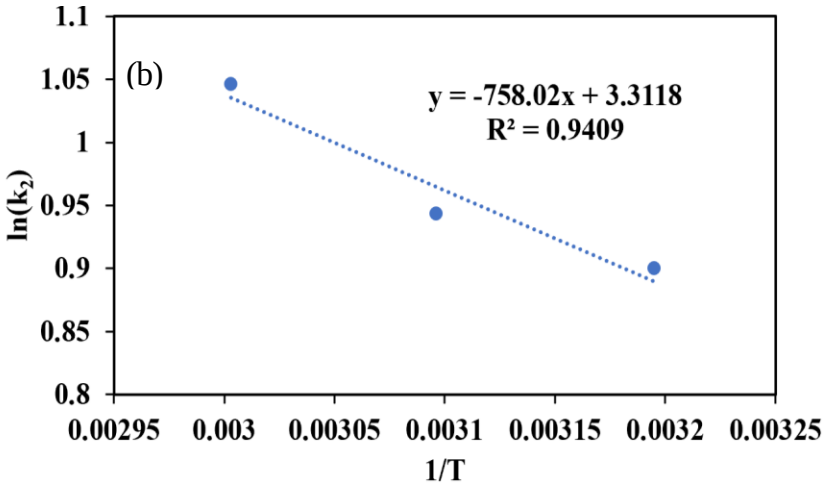

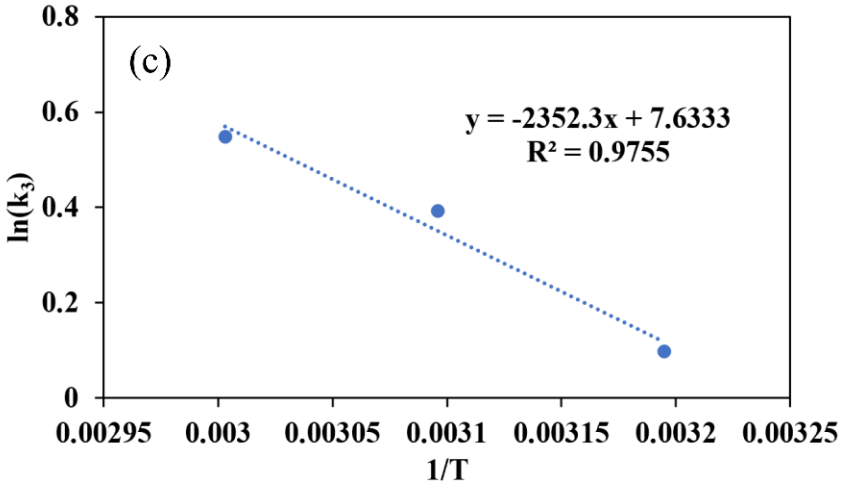

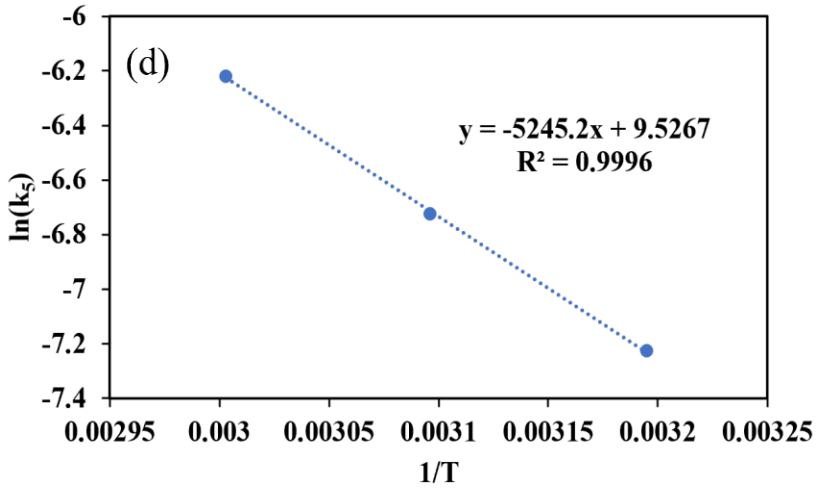

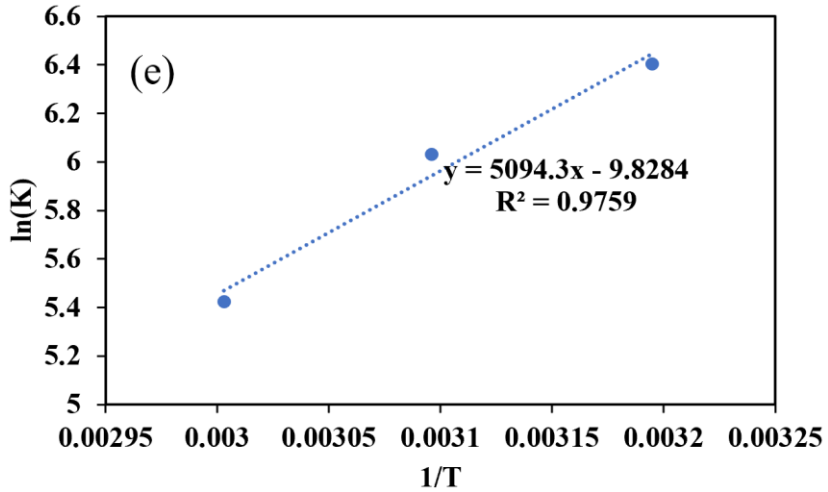

Figure B.1. Arrhenius plots (a) step 1, (b) step 2, (c) step 3, (d) step 5 and (e) Van't Hoff plot for the LHd model for MnO_x/Al_2O_3-P.

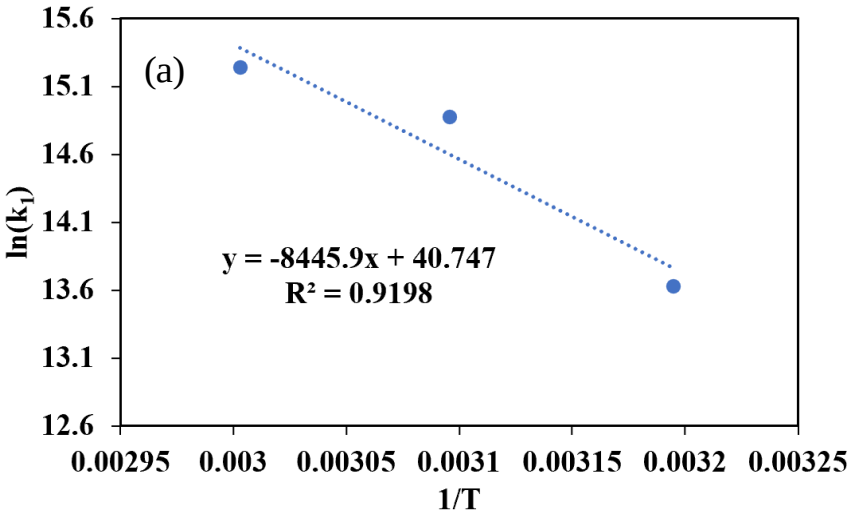
(a)
y = -8445.9x + 40.747
R² = 0.9198
ln(k1)
1/T
15.6
15.1
14.6
14.1
13.6
13.1
12.6
0.00295
0.003
0.00305
0.0031
0.00315
0.0032
0.00325

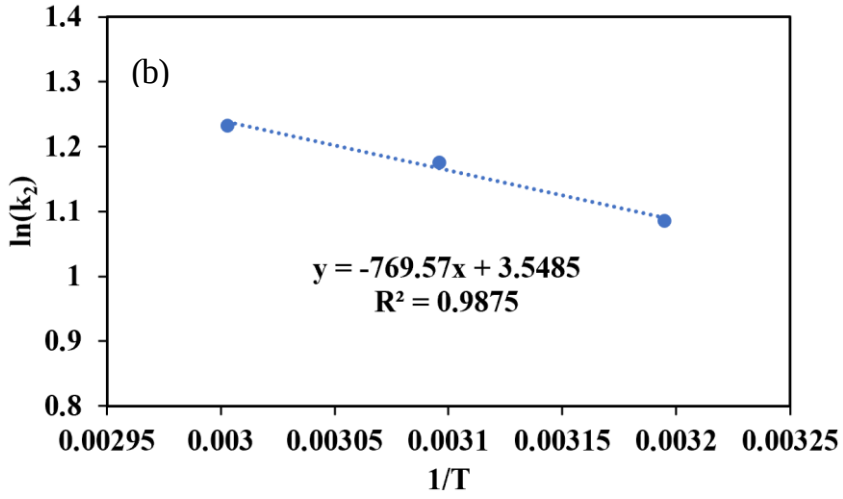
(b)
y = -769.57x + 3.5485
R² = 0.9875
ln(k2)
1/T
1.4
1.3
1.2
1.1
1
0.9
0.8
0.00295
0.003
0.00305
0.0031
0.00315
0.0032
0.00325

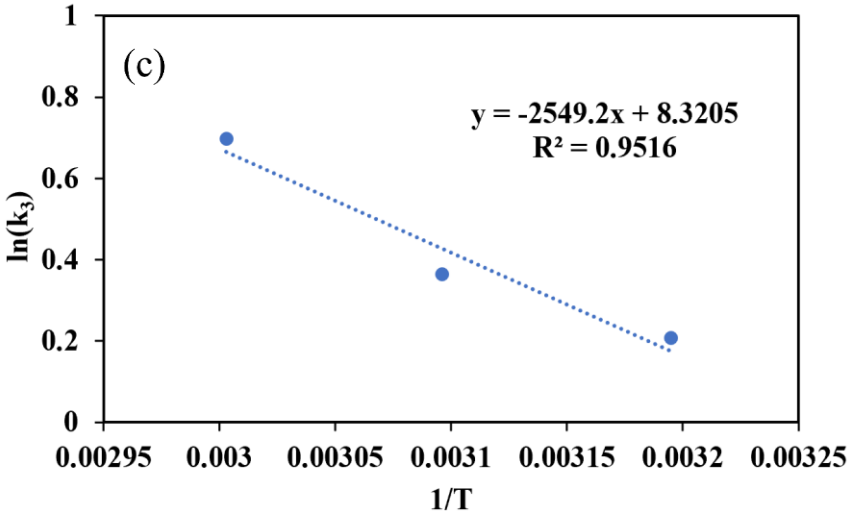
(c)
y = -2549.2x + 8.3205
R² = 0.9516
ln(k3)
1/T
1
0.8
0.6
0.4
0.2
0
0.00295
0.003
0.00305
0.0031
0.00315
0.0032
0.00325

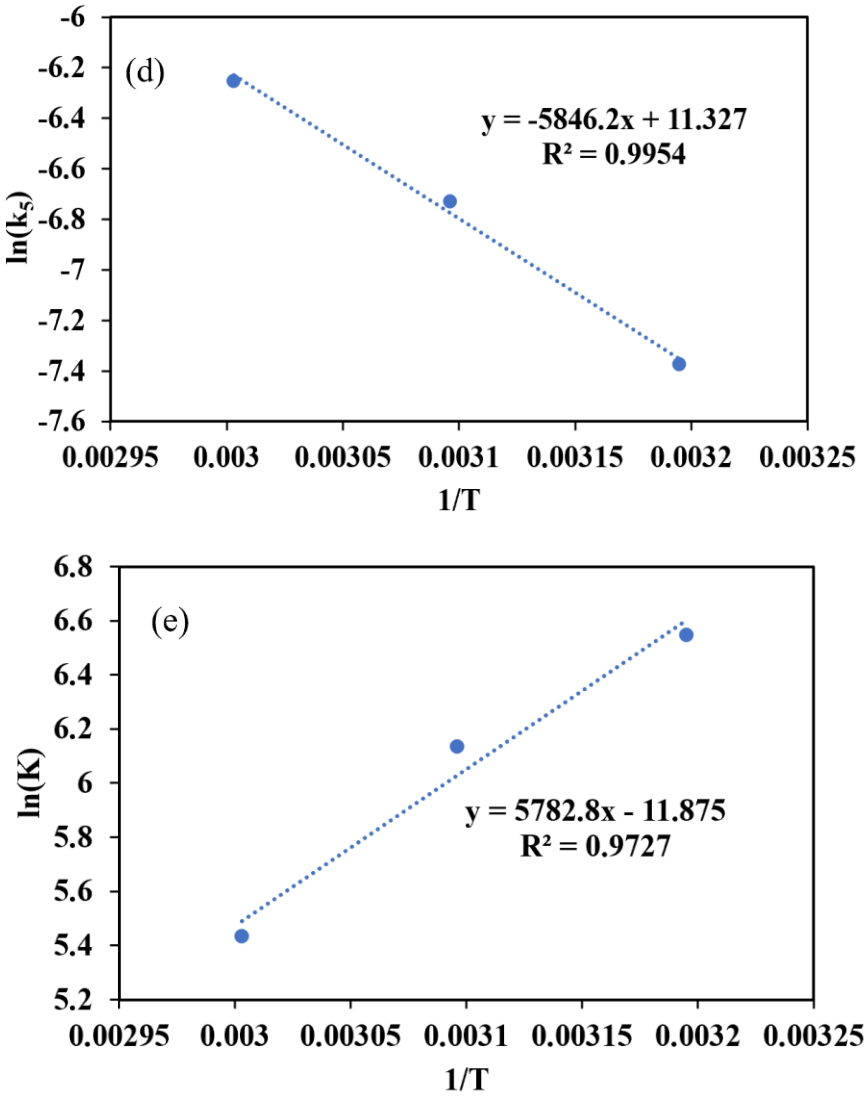

Figure B.2. Arrhenius plots (a) step 1, (b) step 2, (c) step 3, (d) step 5 and (e) Van't Hoff plot for the LHd model for MnO_x/Al_2O_3-I.

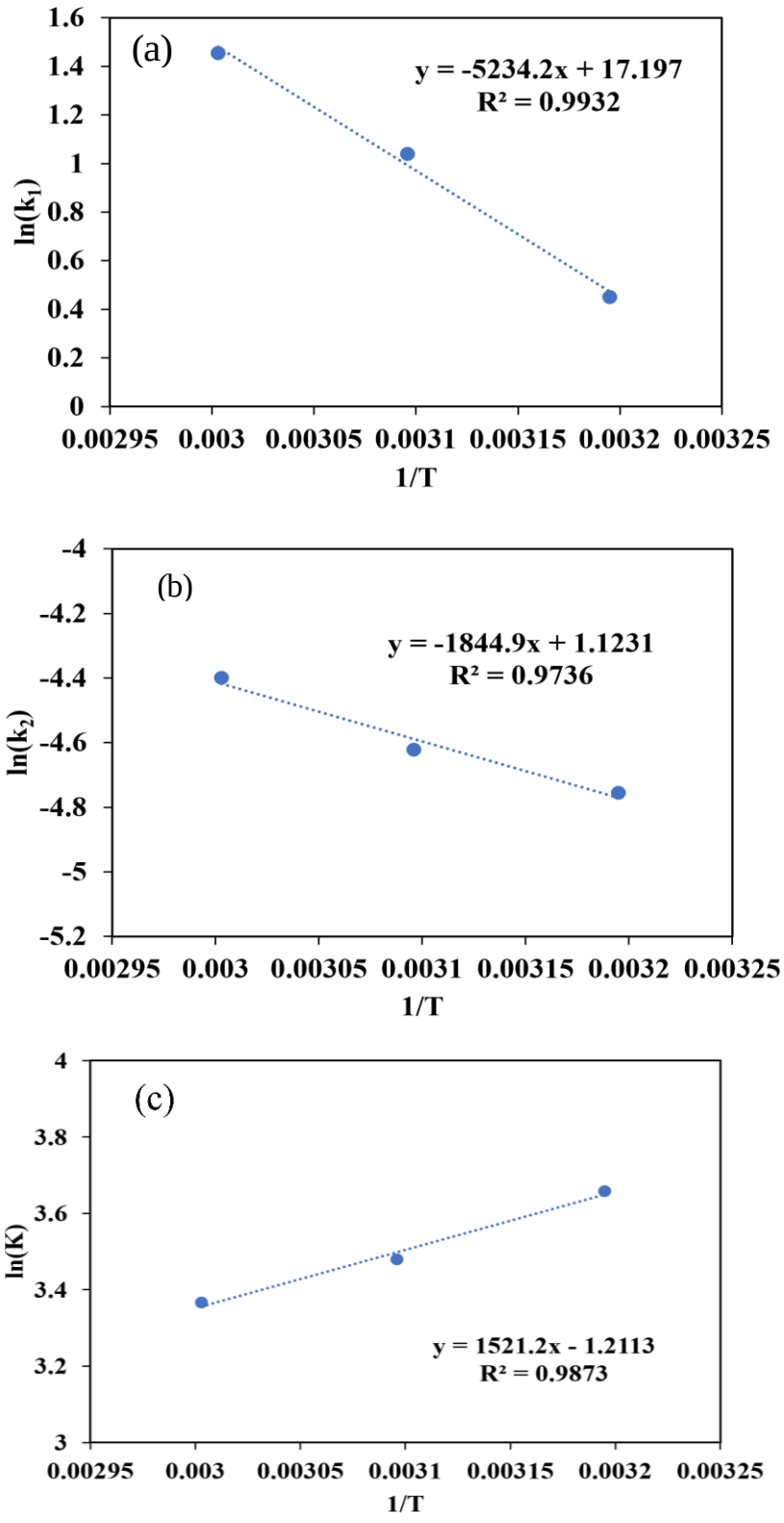

Figure B.3. Arrhenius plots (a) step 1, (b) step 2 and (c) Van't Hoff plot for the LHs model for MnO_x/Al_2O_3-P.

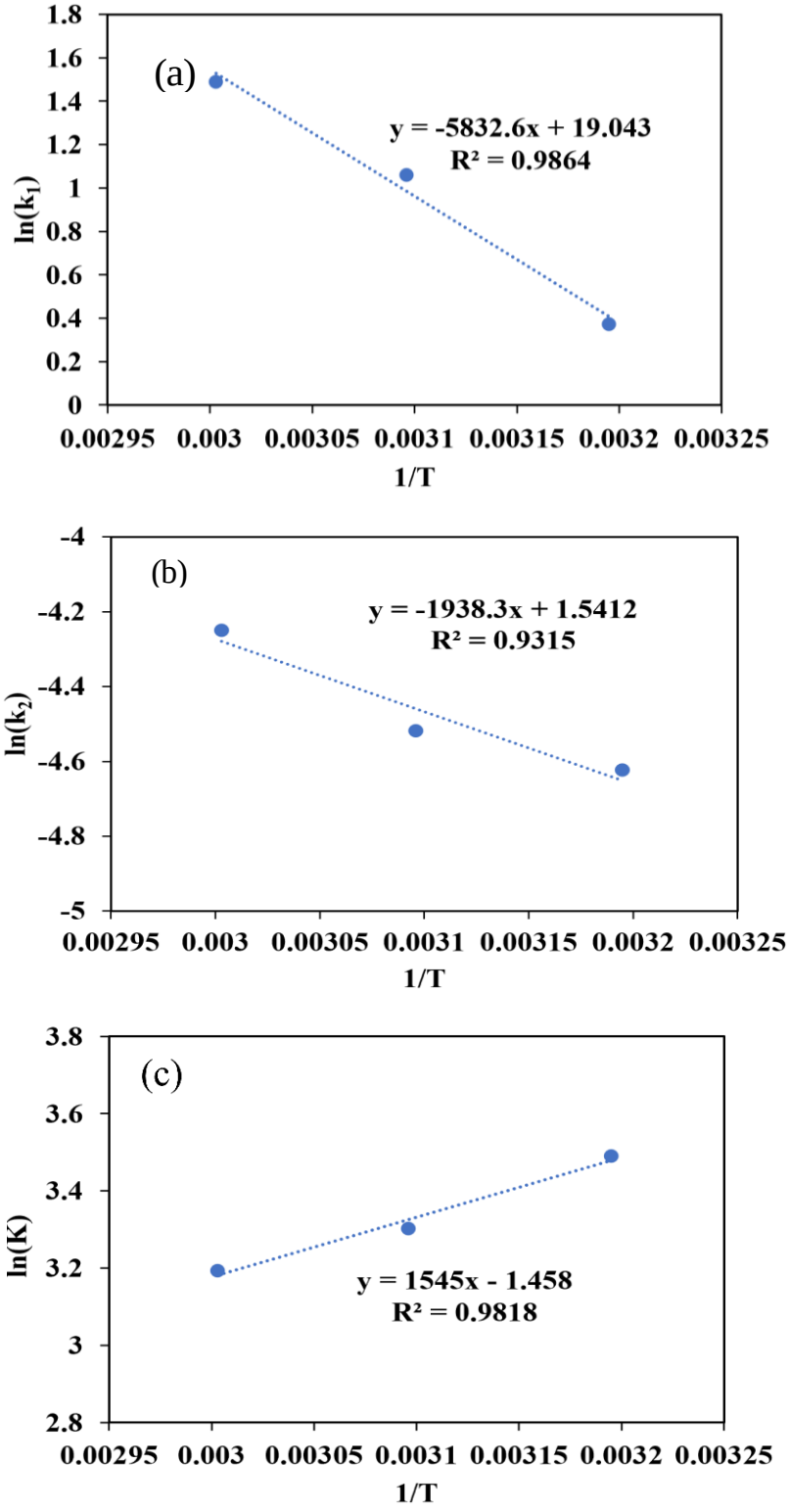

Figure B.4. Arrhenius plots (a)step 1, (b)step 2 and (c)Van't Hoff plot for the LHs model for MnO_x/Al_2O_3-I.

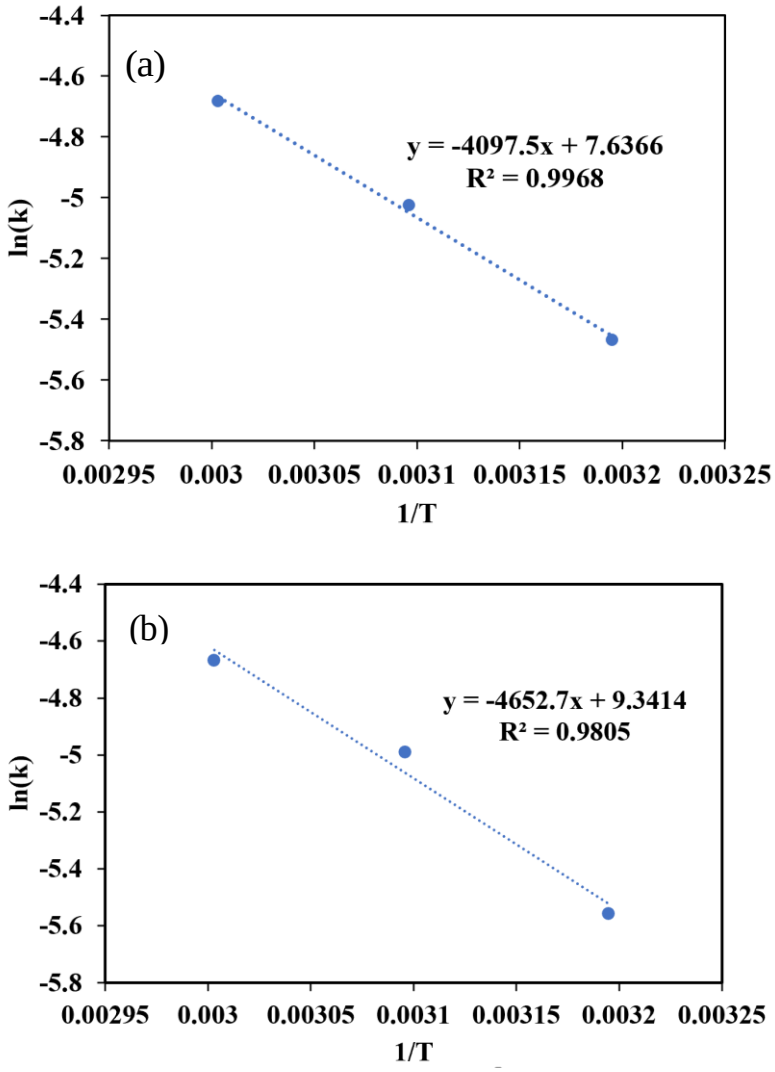

Figure B.5. Arrhenius plots for the PL model (a)MnO_x/Al_2O_3-P and (b)MnO_x/Al_2O_3-I.

Appendix C: Permissions to use the published papers

This Agreement between University of Saskatchewan -- Mehraneh Ghavami ("You") and Springer Nature ("Springer Nature") consists of your license details and the terms and conditions provided by Springer Nature and Copyright Clearance Center.

License Number	5094500988901
License date	Jun 22, 2021
Licensed Content Publisher	Springer Nature
Licensed Content Publication	Frontiers of Chemical Science and Engineering
Licensed Content Title	Room temperature oxidation of acetone by ozone over alumina-supported manganese and cobalt mixed oxides
Licensed Content Author	Mehraneh Ghavami et al
Licensed Content Date	Feb 27, 2020
Type of Use	Thesis/Dissertation
Requestor type	academic/university or research institute
Format	print and electronic
Portion	full article/chapter

Figure C.1. Permission to use the published paper “Room temperature oxidation of acetone by ozone over alumina-supported manganese and cobalt mixed oxides”.

This Agreement between University of Saskatchewan -- Mehraneh Ghavami ("You") and Springer Nature ("Springer Nature") consists of your license details and the terms and conditions provided by Springer Nature and Copyright Clearance Center.

License Number	5094510079672
License date	Jun 22, 2021
Licensed Content Publisher	Springer Nature
Licensed Content Publication	Catalysis Letters
Licensed Content Title	Synthesis of MnOx/Al2O3 Catalyst by Polyol Method and Its Application in Room Temperature Ozonation of Toluene in Air
Licensed Content Author	M. Ghavami et al
Licensed Content Date	Sep 24, 2020
Type of Use	Thesis/Dissertation
Requestor type	academic/university or research institute
Format	print and electronic
Portion	full article/chapter

Figure C.2. Permission to use the published paper "Synthesis of MnO_x/Al_2O_3 Catalyst by Polyol Method and Its Application in Room Temperature Ozonation of Toluene in Air".

This Agreement between University of Saskatchewan -- Mehraneh Ghavami ("You") ar
Springer Nature ("Springer Nature") consists of your license details and the terms and conditions provided by Springer Nature and Copyright Clearance Center.

License Number	5126680289986
License date	Aug 12, 2021
Licensed Content Publisher	Springer Nature
Licensed Content Publication	Reaction Kinetics, Mechanisms and Catalysis
Licensed Content Title	Kinetics and mechanism of catalytic ozonation of acetone in air over MnOx/Al2O3 catalyst
Licensed Content Author	M. Ghavami et al
Licensed Content Date	Jul 16, 2021
Type of Use	Thesis/Dissertation
Requestor type	academic/university or research institute
Format	print and electronic
Portion	full article/chapter

Figure C.3. Permission to use the published paper “Kinetics and mechanism of catalytic ozonation of acetone in air over MnO_x/Al_2O_3 catalyst”.

Thank you for your order!

Dear Ms. Mehraneh Ghavami,

Thank you for placing your order through Copyright Clearance Center's RightsLink® service.

Order Summary

Licensee:	University of Saskatchewan
Order Date:	Jul 8, 2021
Order Number:	5104380292128
Publication:	Building and Environment
Title:	Source apportionment of indoor and outdoor volatile organic compounds at homes in Edmonton, Canada
Type of Use:	reuse in a thesis/dissertation
Order Total:	0.00 CAD

View or print complete details of your order and the publisher's terms and conditions.

Sincerely,

Copyright Clearance Center

Figure C.4. Permission to use Figure 2.1.

Thank you for your order!

Dear Ms. Mehraneh Ghavami,

Thank you for placing your order through Copyright Clearance Center's RightsLink® service.

Order Summary

Licensee:	University of Saskatchewan
Order Date:	Jul 8, 2021
Order Number:	5104390642050
Publication:	Applied Catalysis A: General
Title:	Near-ambient temperature ozone decomposition kinetics on manganese oxide-based catalysts
Type of Use:	reuse in a thesis/dissertation
Order Total:	0.00 CAD

View or print complete details of your order and the publisher's terms and conditions.

Sincerely,

Copyright Clearance Center

Figure C.5. Permission to use Figure 2.4.

Thank you for your order!

Dear Ms. Mehraneh Ghavami,

Thank you for placing your order through Copyright Clearance Center's RightsLink® service.

Order Summary

Licensee:	University of Saskatchewan
Order Date:	Jul 8, 2021
Order Number:	5104390360911
Publication:	CLEAN - Soil, Air, Water
Title:	Plasma-Based Indoor Air Cleaning Technologies: The State of the Art-Review
Type of Use:	Dissertation/Thesis
Order Total:	0.00 CAD

View or print complete details of your order and the publisher's terms and conditions.

Sincerely,

Copyright Clearance Center

Figure C.6. Permission to use Table 2.1.